NASA/TP—2015–216656

Handling Qualities of Large Rotorcraft in Hover and Low Speed

Carlos A. Malpica and Colin R. Theodore
Ames Research Center, Moffett Field, California

Ben Lawrence
San Jose State University Research Foundation
Ames Research Center, Moffett Field, California

Chris L. Blanken
U.S. Army Aviation Development Directorate – AFDD
Aviation & Missile Research, Development & Engineering Center (AMRDEC)
Research, Development and Engineering Command (RDECOM)
Ames Research Center, Moffett Field, California

March 2015

NASA STI Program ... in Profile

Since its founding, NASA has been dedicated to the advancement of aeronautics and space science. The NASA scientific and technical information (STI) program plays a key part in helping NASA maintain this important role.

The NASA STI program operates under the auspices of the Agency Chief Information Officer. It collects, organizes, provides for archiving, and disseminates NASA's STI. The NASA STI program provides access to the NASA Aeronautics and Space Database and its public interface, the NASA Technical Reports Server, thus providing one of the largest collections of aeronautical and space science STI in the world. Results are published in both non-NASA channels and by NASA in the NASA STI Report Series, which includes the following report types:

- TECHNICAL PUBLICATION. Reports of completed research or a major significant phase of research that present the results of NASA Programs and include extensive data or theoretical analysis. Includes compilations of significant scientific and technical data and information deemed to be of continuing reference value. NASA counterpart of peer-reviewed formal professional papers but has less stringent limitations on manuscript length and extent of graphic presentations.

- TECHNICAL MEMORANDUM. Scientific and technical findings that are preliminary or of specialized interest, e.g., quick release reports, working papers, and bibliographies that contain minimal annotation. Does not contain extensive analysis.

- CONTRACTOR REPORT. Scientific and technical findings by NASA-sponsored contractors and grantees.

- CONFERENCE PUBLICATION. Collected papers from scientific and technical conferences, symposia, seminars, or other meetings sponsored or co-sponsored by NASA.

- SPECIAL PUBLICATION. Scientific, technical, or historical information from NASA programs, projects, and missions, often concerned with subjects having substantial public interest.

- TECHNICAL TRANSLATION. English-language translations of foreign scientific and technical material pertinent to NASA's mission.

Specialized services also include organizing and publishing research results, distributing specialized research announcements and feeds, providing information desk and personal search support, and enabling data exchange services.

For more information about the NASA STI program, see the following:

- Access the NASA STI program home page at http://www.sti.nasa.gov

- E-mail your question to help@sti.nasa.gov

- Fax your question to the NASA STI Information Desk at 443-757-5803

- Phone the NASA STI Information Desk at 443-757-5802

- Write to:
  STI Information Desk
  NASA Center for AeroSpace Information
  7115 Standard Drive
  Hanover, MD 21076-1320

NASA/TP—2015–216656

Handling Qualities of Large Rotorcraft in Hover and Low Speed

Carlos A. Malpica and Colin R. Theodore
Ames Research Center, Moffett Field, California

Ben Lawrence
San Jose State University Research Foundation
Ames Research Center, Moffett Field, California

Chris L. Blanken
U.S. Army Aviation Development Directorate – AFDD
Aviation & Missile Research, Development & Engineering Center (AMRDEC)
Research, Development and Engineering Command (RDECOM)
Ames Research Center, Moffett Field, California

National Aeronautics and
Space Administration

Ames Research Center
Moffett Field, CA 94035-1000

March 2015

Available from:

NASA Center for AeroSpace Information
7115 Standard Drive
Hanover, MD 21076-1320
443-757-5802

This report is also available in electronic form at

http://ntrs.nasa.gov

Table of Contents

Nomenclature

Symbol	
a	Airfoil lift curve slope, [rad^{-1}]
a_X	Longitudinal acceleration component in body axes, [ft/s^2]
a_{X_e}	Longitudinal acceleration feedback error in body axes, [ft/s^2]
$\vec{a}$	Acceleration vector of the body axis coordinate system origin, [ft/s^2]
$\mathbf{A}(\rho_k)$	State-space system matrix (as a function of k-th look-up table parameter)
$\mathbf{B}(\rho_k)$	State-space input matrix (as a function of k-th look-up table parameter)
c	Rotor blade chord length, [ft]
d	External disturbance input, generic
$f_2(s)$	Second-order filter in turbulence model
$\vec{F}$	Net force vector acting on aircraft, [lb$_f$]
g	Standard average gravitational acceleration, [$g = 32.1740$ ft/s^2]
$G_{u\beta_{cmd}}(s)$	Transfer function relating the longitudinal velocity response to nacelle tilt actuator control input (including nacelle actuator dynamics), [(ft/s)/deg]
$G_{u\beta_m}(s)$	Transfer function relating the longitudinal velocity response to nacelle tilt angle, [(ft/s)/deg]
$\tilde{G}_{u\beta_m}(s)$	Low-order equivalent transfer function relating the longitudinal velocity response to nacelle tilt angle, [(ft/s)/deg]
$\hat{i}_B$, $\hat{j}_B$, $\hat{k}_B$	Body axis coordinate system unit vectors
I_N	Nacelle/rotor system moment of inertia about its center of mass, [slug·ft^2]
I_{yy}	Aircraft pitching moment of inertia, [slug·ft^2]
$\{I\}$	Aircraft moment of inertia tensor about body axes (static nacelle), [slug·ft^2]
$\{I_{N/F}\}$	Nacelle/rotor system moment of inertia tensor about body axes, [slug·ft^2]
K	Gain or coefficient, generic
K_0, K_1	Tiltrotor turbulence model collective and cyclic scaling coefficients
K_{lat}, K_{lon}, K_{col} and K_{dir}	Aircraft dependent turbulence model scaling coefficients
$K_{\dot{X}}$	Translational rate control input steady-state step response gain, [(ft/s)/in]
K_p	Roll rate feedback control gain, [in/(deg/s)]
$K_u(s)$	Longitudinal velocity feedback controller transfer function, [deg/(ft/s)]
$K_\theta(s)$	Pitch attitude feedback controller transfer function, [in/deg]
K_{D_θ}	Differential pitch attitude (or proportional pitch rate) feedback control gain, [in/(deg/s)]
K_θ	Proportional pitch attitude feedback control gain, [in/deg]

K_ϕ	Proportional roll attitude feedback control gain, [in/deg]
K'_{D_u}	Differential longitudinal velocity (or proportional pitch rate) feedback control gain, [in/(ft/s^2)]
K'_u	Proportional longitudinal velocity feedback control gain, [in/(ft/s)]
L	Rolling moment, [lb$_f$·ft]
ℓ_v	Atmospheric lateral flow field characteristic wave length, [ft]
ℓ_w	Atmospheric vertical flow field characteristic wave length, [ft]
m	Total aircraft mass, [slug]
m_N	Nacelle/rotor system mass, [slug]
M	Pitching moment, [lb$_f$·ft]
M_f	First-order generalized longitudinal flapping moment on the rotor, [rad]
M_B	Main rotor pitching hub moment in body axis coordinates, [lb$_f$·ft]
M_S	Main rotor pitching hub moment in shaft axis coordinates, [lb$_f$·ft]
$\vec{M}$	Net moment vector acting on aircraft, [lb$_f$·ft]
N_b	Number of blades
p	Roll rate, [deg/s]
q	Pitch rate, [deg/s]
q_e	Pitch rate feedback error, [deg/s]
r	Yaw rate, [deg/s]
r_{cmd}	Yaw rate command, [deg/s]
R	Main rotor radius, [ft]
$\vec{r}_{N/F}$	Position vector of the nacelle center of mass in body axis coordinates, [ft]
s	Laplace transform (complex) frequency, [rad/s]
$S(s)$	Closed-loop sensitivity transfer function
t	Time, [s]
T	Main rotor thrust, [lb$_f$]
T_{eq}	First-order TRC command model time constant, [s]
T_{I_θ}	Integral pitch attitude feedback control gain reset time, [s]
$T_{\dot{X}}$, $T_{\dot{Y}}$	Translational rate step response equivalent rise time, [s]
T'_{I_u}	Integral longitudinal velocity feedback control gain reset time, [s]
u	Longitudinal velocity in body axes, [ft/s]
u_{cmd}	Longitudinal velocity command in body axes, [ft/s]
u_e	Longitudinal velocity feedback error in body axes, [ft/s]
u_j	j-th state-space model input

$\mathbf{u}(t)$	State-space model input vector
$\mathbf{u}_0(\rho_k)$	Trim input vector (as a function of k-th look-up table parameter)
$\mathbf{u}_{SP}$	Bare-airframe state-space model input vector
U_0	Trim airspeed longitudinal component in body axes, [ft/s]; Turbulence model flow field mean wind speed parameter, [ft/s]
v	Lateral velocity in body axes, [ft/s]
v_{cmd}	Lateral velocity command in body axes, [ft/s]
V_0	Trim airspeed, [ft/s]
V_∞	Airspeed, [ft/s]
$\vec{V}$	Velocity vector of the body axis coordinate system origin, [ft/s]
w	Vertical (heave) velocity in body axes, [ft/s]
W_n	White noise signal
x	Tiltrotor turbulence model atmospheric scaling exponent
x_1, x_2	Turbulence model atmospheric scaling exponents
x_i	i-th state-space model state variable
x_H	Main rotor hub x-axis position in body axis coordinates, [ft]
x_N	Nacelle/rotor center of mass x-axis position in body axis coordinates, [ft]
x_p	Pilot x-axis position in body axis coordinates (i.e., pilot offset), [ft]
X	Net force longitudinal component in body axes, [lb_f]; Longitudinal position, [ft]
X_0	Net force longitudinal component trim value, [lb_f]
X_B	Main rotor longitudinal hub force in body axis coordinates, [lb_f]
X_H	Main rotor longitudinal hub force in hub axis coordinates, [lb_f]
X_S	Main rotor longitudinal hub force in shaft axis coordinates, [lb_f]
$\mathbf{x}(t)$	State-space model state variable vector
$\mathbf{x}_0(\rho_k)$	State-space model trim state variable vector (as a function of k-th look-up table parameter)
$\mathbf{x}_B$	State-space model rigid body state variable vector
$\mathbf{x}_R$	State-space model rotor state variable vector
$\dot{X}$	Longitudinal translational rate in earth-referenced/inertial coordinates, [ft/s]
$\dot{\mathbf{x}}(t)$	State-space model state variable derivative vector
y_p	Pilot y-axis position in body axis coordinates, [ft]
Y	Net force lateral component in body axes, [lb_f]; Lateral position, [ft]
Y_g	Y-force gravitational force component, [lb_f]
Y_H	Main rotor lateral hub force in hub axis coordinates, [lb_f]

Y_S	Main rotor lateral hub force in shaft axis coordinates, [lb_f]
z	Tiltrotor turbulence model atmospheric scaling exponent
z_H	Main rotor hub z-axis position in body axis coordinates, [ft]
z_N	Nacelle/rotor center of mass z-axis position in body axis coordinates, [ft]
z_p	Pilot z-axis position in body axis coordinates, [ft]
Z	Net force vertical (heave) component in body axes, [lb_f]
Z_B	Main rotor vertical (heave) hub force in body axis coordinates, [lb_f]
Z_H	Main rotor vertical (heave) hub force in hub axis coordinates, [lb_f]
Z_S	Main rotor vertical (heave) hub force in shaft axis coordinates, [lb_f]
α	Tip-path-plane aerodynamic angle of attack, [rad]
$\vec{\alpha}$	Angular acceleration vector of the body axis coordinate system, [rad/s^2]
$\vec{\alpha}_{N/F}$	Relative angular acceleration vector of the nacelle/rotor system, [rad/s^2]
β_{1c}	Longitudinal tip-path-plane orientation/flapping angle, [deg]
β_{1c_S}, β_{1c_A}	Symmetric and anti-symmetric longitudinal tip-path-plane orientation/flapping angle, [deg]
β_{1s}	Lateral tip-path-plane orientation/flapping angle, [deg]
β_{1s_S}, β_{1s_A}	Symmetric and anti-symmetric lateral tip-path-plane orientation/flapping angle, [deg]
β_{cmd}	Nacelle actuator control input, [deg]
β_m	Nacelle, or mast, conversion tilt angle, [deg]
β_{m_0}	Trim nacelle angle, [deg]
$\dot{\beta}_m$	Nacelle, or mast, conversion tilt rate, [deg/s]
$\ddot{\beta}_m$	Nacelle, or mast, conversion tilt acceleration, [deg/s^2]
δ_{col}	Pilot collective stick input, [in]
$\hat{\delta}_{col}$	Collective input to the swashplate servo-actuator control mixer, [in]
$\hat{\delta}_{dir}$	Directional input to the swashplate servo-actuator control mixer, [in]
δ_{lat}	Pilot lateral cyclic stick input, [in]
δ'_{lat}	Pilot lateral cyclic stick input to the roll axis command model after “dead zone” shaping, [in]
$\hat{\delta}_{lat}$	Lateral input to the swashplate servo-actuator control mixer, [in]
δ_{lon}	Pilot longitudinal cyclic stick input, [in]
$\hat{\delta}_{lon}$	Longitudinal input to the swashplate servo-actuator control mixer, [in]
$\hat{\delta}_{lon}^{FB}$	Feedback command to the swashplate servo-actuator control mixer, [in]
δ_{ped}	Pilot pedal input, [in]

δ_{pilot}	Pilot stick input, generic
δ_{TCL}	Pilot Thrust Control Lever input, [in]
ζ	Damping ratio
ζ_{nac}	Damping ratio of the nacelle actuator dynamics
θ	Pitch attitude, [deg]
θ_0	Collective blade pitch angle, [rad]
θ_{1c}	Lateral cyclic blade pitch angle, [rad]
θ_{1c_S}, θ_{1c_A}	Symmetric and anti-symmetric lateral cyclic input, [deg]
θ_{1s}	Longitudinal cyclic blade pitch angle, [rad]
θ_{1s_S}, θ_{1s_A}	Symmetric and anti-symmetric longitudinal cyclic input, [deg]
θ_{cmd}	Pitch attitude command, [deg]
θ_e	Pitch attitude feedback error, [deg/s]
θ_F	Pitch trim attitude, [deg]
θ_{trim}	Reference trim pitch attitude control input, [deg]
θ_{tw}	Linear rotor blade twist angle, [rad]
μ_x	Main rotor advance ratio in-plane component
μ_z	Main rotor advance ratio out-of-plane component
ρ	Air density, [slug/ft^3]
ρ_k	k-th look-up table parameter for quasi-Linear Parameter Varying model
σ_v	Turbulence model wind speed standard deviation in the lateral direction
σ_w	Turbulence model wind speed standard deviation in the vertical direction
τ_{cmd}	Yaw rate command model time delay, [s]; Translational rate command model time delay, [s]
τ_{eq}	Equivalent time delay of the inverse dynamics models, generic, [s]
τ_n	Pitch and roll attitude command model time delay, [s]
τ_p	Phase delay, [s]
τ_{p_X}	Longitudinal position short-term response phase delay, [rad/s]
τ_{ped}	Yaw rate first-order command model time constant, [s]
ϕ	Roll attitude, [deg]
ϕ_F	Roll trim attitude, [deg]
ϕ_{cmd}	Roll attitude command, [deg]
Φ_M	Phase margin, [deg]
ψ	Yaw (heading) attitude, [deg]
ω	Frequency, [rad/s]

ω_{180}	Frequency at which the frequency-response phase is −180 deg, [rad/s]
ω_{BW}	Bandwidth frequency, [rad/s]
$\omega_{BW_{gain}}$	Short-term response gain bandwidth, [rad/s]
$\omega_{BW_{phase}}$	Short-term response phase bandwidth, [rad/s]
ω_{BW_X}	Longitudinal position short-term response bandwidth, [rad/s]
ω_c	Crossover frequency, frequency at which the frequency-response magnitude is 0 dB, [rad/s]
ω_{co}	Cutoff frequency, [rad/s]
ω_n	Pitch and roll attitude command model natural frequency, [rad/s]
ω_{nac}	Nacelle actuator dynamics natural frequency, [rad/s]
Ω	Rotor speed, [rad/s]
$\vec{\omega}$	Angular velocity vector of the body axis coordinate system, [rad/s]
$\vec{\omega}_{N/F}$	Relative angular velocity vector of the nacelle/rotor system, [rad/s]

Abbreviations and Acronyms

ACAH	Attitude Command-Attitude Hold
ADS-33	(U.S. Army) Aeronautical Design Standard–33
AFDD	(U.S. Army) Aeroflightdynamics Directorate
ASMs	Available Seat Miles
ASTI	Advanced Simulation Technology Inc.
ASTOVL	Advanced STOVL
BW	Bandwidth
CAAS	Common Avionics Architecture System
CETI	Control Equivalent Turbulence Input
CG	Center of gravity
CMD	Command
DAFCS	Digital Automatic Flight Control System
DFC	Direct Force Control
DoD	Department of Defense
DRB	Disturbance Rejection Bandwidth
DRP	Disturbance Rejection Peak
FAA	Federal Aviation Administration
FSAA	(NASA Ames) Flight Simulator for Advanced Aircraft
GM	Gain Margin

HQ	Handling Qualities
HQR	Handling Qualities Rating
IAPS	Integrated Aeromechanics/Propulsion Systems
LCTR	Large Civil Tiltrotor
LCTR2	Large Civil Tiltrotor, 2nd generation
LOES	Lower-Order Equivalent System
MTE	Mission Task Element
OLOP	Open-Loop Onset Point
PI	Proportional-Integral
PID	Proportional-Integral-Differential
PIO	Pilot Induced Oscillation
PM	Phase Margin
qLPV	quasi-Linear Parameter Varying
RC	Rate Command
RCHH	Rate Command-Heading Hold
RMS	Root-Mean-Square
RPMs	Revenue Passenger Miles
SISO	Single Input Single Output
STOVL	Short Take-Off and Vertical Landing
TCL	Thrust Control Lever
TRC	Translational Rate Command
UCE	Usable Cue Environment
VMS	(NASA Ames) Vertical Motion Simulator
V/STOL	Vertical/Short Take-Off and Landing

Introduction

According to a number of system studies, large capacity advanced rotorcraft with a capability of high cruise speeds (~350 mph) as well as vertical and/or short take-off and landing (V/STOL) flight could alleviate anticipated air transportation capacity issues by making use of non-primary runways, taxiways, and aprons. These advanced aircraft pose a number of design challenges, as well as unknown issues in the flight control and handling qualities domains. A series of piloted simulation experiments have been conducted on the NASA Ames Research Center Vertical Motion Simulator (VMS) in recent years to systematically investigate the fundamental flight control and handling qualities issues associated with the characteristics of large rotorcraft, including tiltrotors, in hover and low-speed maneuvering.

Need, Mission, and Requirements

Next Generation Air Transportation System (NextGen)

Enabling mobility through the air with sufficient flexibility and affordability is essential to national economic success. Despite recent worldwide economic turmoil, civil aviation still contributed an estimated $728 billion to the U.S. economy, or roughly 5.2 percent of the nation's gross domestic product, in 2009 [1]. The design and deployment of a transformed air transportation system, or Next Generation Air Transportation System (NextGen), was mandated in 2003 in response to: 1) the signs of serious stress the nation's air traffic management system was under as a result of demand levels at the time, and 2) continued expected growth in passenger and cargo traffic demands, and the possible entry into service of new types of aircraft with substantially different operational performance characteristics by 2025. NextGen entails a fundamental transformation in the management and operation of the U.S. airspace system that will be heavily reliant on enhanced system connectivity technologies with the objective of enabling continual system-wide performance improvement capabilities in a way that is *scalable* and *flexible* to adapt to future needs.

The worldwide economic recession that has taken place since the enactment of NextGen has caused projections of air traffic by the 2025 time frame to vary significantly because of the uncertainty surrounding economic recovery projections and the volatility of fuel prices. Downward adjustments of the overall economy in recent years are reflected in slower near-term growth projections for the aviation sector; however aviation is expected to continue to grow over the long run. The 2013 Federal Aviation Administration (FAA) forecast, for instance, calls for U.S. carrier passenger growth over the subsequent 20 years to average 2.2 percent per year, compared to the 2012 forecast growth of 2.6 percent per year. By 2033, U.S. commercial air carriers are projected to fly 1.74 trillion Available Seat Miles (ASMs) and transport 1.15 billion enplaned passengers a total of 1.46 trillion Revenue Passenger Miles (RPMs) [2]. This growth will be underlined in the domestic arena over the entire forecast period (2013–2033) by a faster pace of growth of the regional carriers, relative to their mainline counterparts, with ASMs and RPMs growing at an average annual rate of 3.2 percent and passenger enplanements at 2.2 percent, and increasing aircraft size reflected in the demand for 70- to 90-seat aircraft and retirement of 50-seat regional jets in service.

Various system studies conducted by NASA [3–8] have shown that having a vertical capability at one or both ends of a 300 to 600 nm mission increases airport capacity and that large, advanced technology tiltrotors consistently outpace other configurations in the ability to meet these transportation missions. In references [6–8], particularly, civil tiltrotors show a capability to improve airspace system performance significantly. Advanced technologies will be required to give tiltrotors cost and operational parity with configurations already in use.

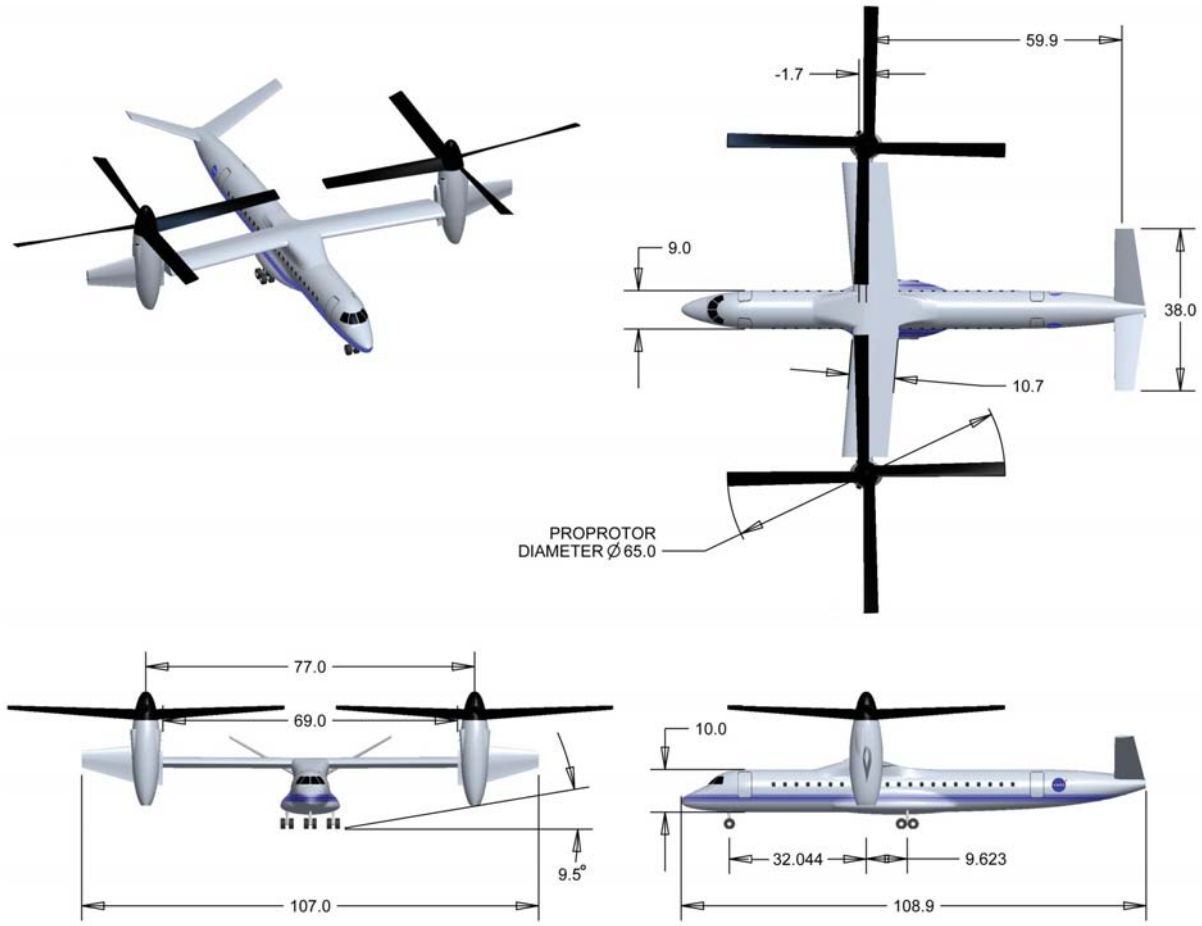

Figure 1. The NASA Large Civil Tiltrotor, LCTR2, baseline version (dimensions in ft).

Performance Targets

NASA has delineated the Large Civil Tiltrotor (LCTR) concept design as the heavy-lift, high-speed rotorcraft configuration with the best potential to meet the technology goals associated with a notional civil mission of operating short-haul regional routes and for substantial impact on the air transportation system [3]. The latest design evolution of the LCTR, the Large Civil Tiltrotor, 2nd generation (LCTR2) configuration, was initially based on aircraft technology projections for a service entry date of 2018, and sized to be representative of equivalent regional jets and turboprops [9]. Designed for a notional civil mission of carrying approximately 90 passengers over a range of at least 1000 nm at a cruise speed of 300 knots, this later LCTR configuration weighs around 100,000 lb, has a 107 ft wingspan, and two tilting nacelles supporting 65 ft diameter rotors. The general aircraft dimensions are shown in Figure 1. The goal of the LCTR2 design studies is to identify research requirements for future tiltrotors. The focus for near-term research is to obtain a realistic assessment of technology requirements and potential benefits.

Technologies Required

There are a number of barrier issues that must be overcome for a vehicle such as the LCTR2. The state of the art will have to be significantly advanced to meet these challenges in a number of technical areas such as Integrated Aeromechanics/Propulsion Systems (IAPS), variable-speed rotor concepts that will enable a 50-percent main rotor speed reduction while retaining propulsion efficiency. This will dictate the use of actively controlled, efficient rotor

systems that simultaneously increase aerodynamic efficiency, control dynamic stall, reduce vibration, and reduce noise while providing a 100-knot speed improvement over current rotorcraft. Also, quieter cabins will be required to reduce interior noise and vibration to a level of regional jets, with minimal weight penalty.

Flight Dynamics and Control Issues

All the aforementioned technologies contribute to the commercial viability of large rotary wing transport systems in a future national airspace, as envisaged by the FAA's NextGen plan. In addition, the LCTR2 payload, range, and speed requirements determine it to be a large vehicle—much larger than any previous VTOL aircraft, bringing a variety of novel issues to the flight control and handling qualities domain, especially in hover and low-speed maneuvering.

The size of rotorcraft such as the LCTR2 poses a number of design challenges. Its demanding operational requirements will mandate unprecedented levels of complexity. In particular, it will likely feature highly nonlinear aerodynamics, and make extensive use of active control, advanced lightweight materials, and advanced propulsion technologies. "Super-Integrated" control concepts are forming the basis of a critical technology that can help meet the wide-ranging targets in performance enhancements, structural loads alleviation, vibration and noise reductions, and stability, control, and handling qualities augmentation, including partial and fully autonomous operations.

The development of both civilian and military rotorcraft typically involves meeting certain sets of specifications and guidelines that cover all phases of design and operation, including environmental, structural, and performance requirements. Within these performance standards are flight control system requirements, which include handling qualities requirements. Design requirements and specifications for civilian rotorcraft include the FAA Airworthiness Standards contained in Part 27 for Normal Category Rotorcraft and in Part 29 for Transport Category Rotorcraft. For military rotorcraft, the handling qualities and flight control system requirements may include criteria from U.S. Army Aeronautical Design Standard-33 (ADS-33E-PRF) [10] and SAE-AS94900 [11], which has now superseded MIL-DTL-9490E [12].

The handling qualities requirements for LCTR2 must also accommodate the envisaged role. This will require precise maneuvering in cluttered terminal area environments, all-weather operations, and operational safety standards comparable or superior to those of current fixed-wing commercial operations with a vehicle that will likely feature a slow control response inherent to its large size.

This Technical Publication presents results that attempt to establish the fundamental relationships between rotorcraft size and handling qualities in the critical hover and low-speed flight regime. This research was conducted through a series of piloted handling qualities experiments on the NASA Ames Vertical Motion Simulator (VMS) and supported by other simulation analyses. Attitude Command-Attitude Hold (ACAH) and Translational Rate Command (TRC) control response types are systematically appraised using methodologies derived from the ADS-33 military rotorcraft handling qualities specification. ADS-33 provides a framework that exceeds any civilian requirements in terms of its ability to precisely quantify handling qualities and provide guidelines for good design. A rotorcraft of the scale and complexity of the LCTR2 concept will certainly need to incorporate such methodologies right from the beginning of its design lifecycle.

In addition to assessing the impact of vehicle size on handling qualities, this document presents analysis of a piloted simulation study that investigates techniques for ameliorating the size-related issues. These include the use of a TRC control law that uses the additional degrees of control available in a tiltrotor such as the nacelles and twin rotors to enable maneuvering in translation with minimal fuselage attitude perturbations. There are technical feasibility questions pertaining to this approach, and the analysis also considers aspects of the control design that maintain the necessary handling qualities levels while minimizing the actuator demands, especially for the large nacelles.

Overview of Experiments

Table 1 presents an overview of the four experiments conducted in the NASA Ames Vertical Motion Simulator (VMS). The initial experiment in the series of handling qualities studies represented the first such evaluation of an LCTR [13]. This study pursued the piloted evaluation of various rotorcraft configurations in hover and low speed with the objective of discerning the handling qualities trade-offs between stability and disturbance rejection characteristics for large rotorcraft. The rotorcraft models considered in this experiment included a medium-lift utility class sized helicopter similar to a UH-60, a heavy-lift cargo class sized helicopter similar to a CH-53K, and a large, ultra-heavy civil tiltrotor.

The second experiment, conducted in 2009 and reported in reference [14], focused exclusively on the LCTR aircraft. The primary objectives of the evaluation were to investigate the effect of pilot station location, relative to the aircraft center of gravity, and attitude response-type requirements on the handling qualities of this type of aircraft. To this effect, the experiment evaluated variations in the pilot station offset of 10, 20, 30, and 40 ft, while keeping the aircraft dynamics invariant, as well as a comprehensive space of short-term attitude and yaw response parameter variations (bandwidth and phase delay).

The third and fourth VMS experiments in the series documented in references [15] and [16], respectively, presented the results of a comprehensive and detailed evaluation of the various design aspects of a Translational Rate Command (TRC) control response on the LCTR2 aircraft. Of particular note is the TRC implementation employed in these experiments, which made use of the rotor nacelle rotations as the primary effectors of longitudinal velocity, and parallel (anti-symmetric) lateral cyclic inputs for lateral velocity control.

Table 1. Summary overview of LCTR experiments conducted in the VMS.

Year	Objective	Aircraft	Control
2008	Evaluate handling qualities impact of reduced stability margin and increased disturbance rejection trade-off	Utility class (H-60), Cargo class (H-53K), LCTR	ACAH
2009	Evaluate short-term response handling qualities requirements and effect of pilot station offset to center of gravity	LCTR	ACAH
2010	Conduct preliminary evaluation of required nacelle actuator limits (rate and position) and attitude/translation response type coordination	LCTR2	ACAH TRC
2011	Evaluate the effect of nacelle actuator bandwidth and ADS-33 TRC requirements on handling qualities	LCTR2	TRC

Simulation Model Development and Experimental Setup

Aircraft Models

As shown in Table 1, four different rotorcraft configurations were employed throughout the various experiments. The primary test subjects of this research were, however, the large civil tiltrotors, and specifically the LCTR2 configuration. Therefore, a significant portion of the discussion in this section refers to the development process of the LCTR2 model. Table 2 summarizes the basic aircraft configuration characteristics of the various models employed in this research. Detailed configuration parameters are shown in Appendix A. All the aircraft simulation models used in the research were based on linear stability derivative state-space models. Linearized bare-airframe models were obtained from high-fidelity blade element simulation models of the four aircraft.

Table 2. Basic aircraft configuration size characteristics.

Aircraft	Gross Weight (lb)	Rotor Diameter (ft)	Class Size
H-60	16,000	53.6	Medium utility
H-53	46,000	79	Heavy cargo
LCTR	140,000	75 (×2)	Ultra-heavy, large tiltrotor
LCTR2	100,000	65 (×2)	Ultra-heavy, large tiltrotor

Linear Model Extraction and Validation

For the single main rotor aircraft models, the H-60 and H-53, single design point (hover) linear models were extracted from the Ames General Helicopter (Gen Hel®) Flight Dynamics Simulation [17] and then reduced to 11 states and decoupled. These models retained the key rotor-body coupling, but dropped the high-frequency modes and off-axis response, thereby allowing a smooth and independent variation in feedback control characteristics in a single axis. This simplification still allowed for realistic attitude disturbance rejection bandwidth (DRB) [18,19] to be achieved with a representative feedback gain, and associated actuator usage, stability margin, and damping ratio. These reduced-order, decoupled (lateral and longitudinal bare-airframe dynamics), 11-state models were then validated against the original linear 25-state Gen Hel model by comparing modes and frequency responses.

For the large (heavy-lift) tiltrotor models, LCTR and LCTR2, the nonlinear Comprehensive Analytical Model of Rotorcraft Aerodynamics and Dynamics program, CAMRAD II® [20,21], was used to generate the high-order linearized systems governing the bare-airframe dynamic responses to rotor inputs. As the experimental requirements for increased fidelity and functionality increased, the real-time piloted simulation LCTR2 model was developed further [22] by using a quasi-Linear Parameter Varying (qLPV) or “stitched” [23] modeling approach that combines multiple linear stability derivative-based state-space models to provide varying model dynamics and trim characteristics for changing flight speed and nacelle angles. The envelope of the model was valid from hover up to medium speeds (0–140 knots) and for nacelle angles between 60 and 95 deg (90 deg being the notional “helicopter” configuration with the mast in the vertical orientation). This model represents “quasi nonlinear” effects through the trim datum and state-space coefficients being a lookup table function of speed and nacelle angle, and the use of nonlinear equations of motion.

Following a process analogous to that of the single hover point models, the high-order linear systems extracted at the various nacelle angle and airspeed datum trim combinations for the

stitched LCTR2 model were reduced. Again, the key rotor-body couplings, including both the lateral and longitudinal rotor degrees of freedom of the low-frequency, or "regressive," flap mode for each rotor were retained. The stitched model reduced-order matrices, however, also retained the lateral-to-longitudinal coupling terms. These were not retained in the previous single point hover models. The resulting reduced-order models therefore consisted of the nine body states,

$$\mathbf{x}_B = [u\ v\ w\ p\ q\ r\ \phi\ \theta\ \psi]^T,$$

and the four low-frequency rotor flap states,

$$\mathbf{x}_R = \left[\beta_{1c_\mathrm{S}}\ \beta_{1s_\mathrm{S}}\ \beta_{1c_\mathrm{A}}\ \beta_{1s_\mathrm{A}}\right]^T.$$

It is shown for the lateral response dynamics of the LCTR2 in Figure 2 that these adequately represent the bare-airframe dynamics beyond the frequency of interest for pilot control, with an accurate match found up to 15 rad/s. The longitudinal axes had similar agreement.

The symmetric and anti-symmetric rotor flapping degrees of freedom describe the combined flapping motion of the individual rotors relative to a vertical plane of symmetry passing through the centerline of the aircraft. Anti-symmetric flapping of the rotors therefore describes a symmetric flapping of the rotors where the flapping motion of the two rotors is unaltered in magnitude but changed in sign. These definitions of the rotor flapping degrees of freedom relate to the individual (left and right) rotors, e.g., for the longitudinal flapping motion, through the coordinate transformations:

$$\beta_{1c_\mathrm{S}} = \frac{1}{2}\left(\beta_{1c_\mathrm{R}} + \beta_{1c_\mathrm{L}}\right) \text{ and } \beta_{1c_\mathrm{A}} = \frac{1}{2}\left(\beta_{1c_\mathrm{R}} - \beta_{1c_\mathrm{L}}\right).$$

For the tiltrotor models in hover, the flight controls employed the six inputs,

$$\mathbf{u}_{SP} = \left[\theta_{0_\mathrm{A}}\ \theta_{1s_\mathrm{S}}\ \theta_{1s_\mathrm{A}}\ \theta_{0_\mathrm{S}}\ \beta_{m_\mathrm{S}}\ \theta_{1c_\mathrm{A}}\right]^T,$$

which are summarized in Table 3, along with the primary axis of control for which they were employed. The swashplate (and nacelle) inputs in Table 3 were defined following the same conventions used for the rotor flapping degrees of freedom, in terms of symmetric and anti-symmetric components. The anti-symmetric collective and longitudinal cyclic inputs are commonly referred to in the literature as the "differential" collective and longitudinal cyclic pitch, respectively. These appellations are used interchangeably herein. Also, unless explicitly indicated, the symmetric components of these swashplate inputs are denoted in this report simply as the "collective" or "longitudinal cyclic" pitch. Similarly, the anti-symmetric lateral cyclic is often labeled "parallel lateral cyclic," or simply, "lateral cyclic." Application of symmetric lateral cyclic would see the inputs for both rotors simultaneously directed either inboard or outboard. The anti-symmetric application would see the inputs applied in a parallel manner, hence the designation.

Table 3. Tiltrotor model inputs.

Swashplate Input	Primary Control Axis
Anti-symmetric collective pitch	Roll
Symmetric longitudinal cyclic pitch	Pitch
Anti-symmetric longitudinal cyclic pitch	Yaw
Symmetric collective pitch	Heave
Symmetric nacelle tilt*	Surge (longitudinal velocity)
Anti-symmetric lateral cyclic pitch	Sway (lateral velocity)

* Direct reorientation of the shaft, used in automatic TRC control.

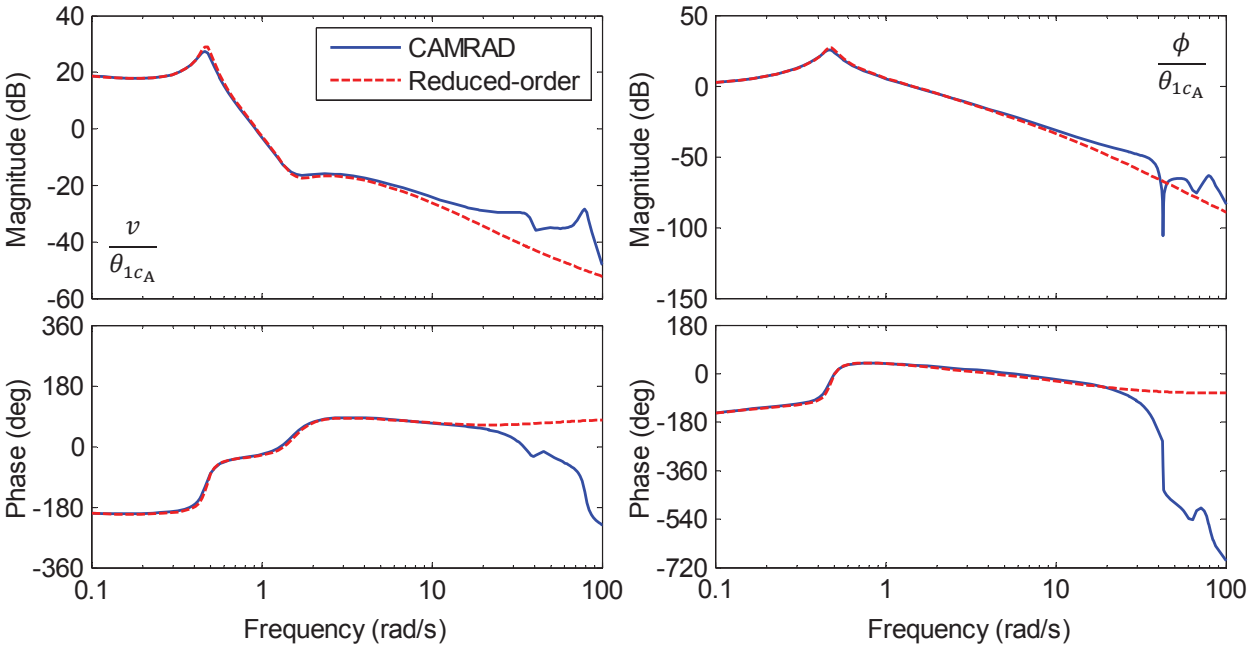

Figure 2. Comparison of frequency responses to anti-symmetric lateral cyclic for the high-order (CAMRAD) and reduced-order models: (a) lateral velocity and (b) roll attitude.

Stitched Model Theory

The qLPV technique consists of "stitching" together multiple stability derivative-based linear state-space models extracted from a range of trimmed flight conditions. The model stability derivatives are interpolated through lookup tables that are functions of the flight states (e.g., flight speed), control inputs, or other configuration parameters. The expression in Eq. (1) illustrates that the formulation is an extension of the standard state-space model [24]:

$$\dot{\mathbf{x}}(t) = \mathbf{A}(\rho_k)\Delta\mathbf{x}(t) + \mathbf{B}(\rho_k)\Delta\mathbf{u}(t) \tag{1}$$

Here, ρ_k are the lookup table independent variable(s) and may vary with time. There is no theoretical limit to how many lookup variables can be used as indicated by the subscript, k. The coefficients of the state and control matrices, $\mathbf{A}$ and $\mathbf{B}$ respectively, are then functions of ρ_k.

The state-space formulation is based on the premise that any dynamics are a small perturbation from a datum, or in the case of flight vehicles, a trim condition. However, the simulation was required to represent more than perturbation effects, including effects such as realistic trim changes in the controls and states with flight condition. Equation (1) is then recast as follows:

$$\dot{\mathbf{x}} = \mathbf{A}(\rho_k)\big(\mathbf{x} - \mathbf{x}_0(\rho_k)\big) + \mathbf{B}(\rho_k)\big(\mathbf{u} - \mathbf{u}_0(\rho_k)\big) \tag{2}$$

Here, $\mathbf{x}_0(\rho_k)$ and $\mathbf{u}_0(\rho_k)$ are respectively the vectors of the trim states and controls at each of the reference conditions, ρ_k, and are also interpolated from lookup tables. In this formulation $\mathbf{x}$ and $\mathbf{u}$ are the absolute values of the states and controls, and the difference between these and the trim values is the perturbation value $\Delta\mathbf{x} = \mathbf{x} - \mathbf{x}_0(\rho_k)$. Note that when the difference is zero, the vehicle has zero resultant accelerations, (i.e., $\dot{\mathbf{x}} = 0$), and therefore will be in trim with the appropriate values of states and controls.

Implementation of the qLPV Technique

Figure 3 illustrates the architecture of the LCTR2 qLPV model. It is first important to point out that the state-space formulation $\mathbf{A}\Delta\mathbf{x} + \mathbf{B}\Delta\mathbf{u}$ is only applied to the aerodynamic propulsive force and moment contributions—i.e., all the linearized gravity force components (e.g., $g\theta$, in nondimensional form) are eliminated from the matrices, as are other inertial stability derivative terms (e.g., $Z'_q = Z'_q - U_0$).

These gravitational and inertial Coriolis effects are accounted for separately in the blocks labeled "Nonlinear Gravitational Forces" and "Integration of Nonlinear Equations of Motion." In the gravitational force subsystem, the equations are the full nonlinear gravitational terms. However, these equations subtract the steady-state force due to gravity as there is no representation of the aerodynamic trim forces in the model to counterbalance. This is achieved by inputting the current absolute Euler angles and the "looked-up" trim Euler angles to this block, computing the terms twice using both angles, and subtracting one from another to get the effective "perturbation" of the nonlinear gravitational forces. For example, for the lateral body axes equation:

$$\frac{\Delta Y_g}{m} = g(cos\,\theta\, sin\,\phi - cos\,\theta_F\, sin\,\phi_F). \tag{3}$$

So, if the aircraft is at the trim Euler angles, the resultant gravitational force is zero.

As shown in Figure 3, the resultant forces and moments due to the aerodynamic and propulsive effects are obtained by multiplying the translational and rotational accelerations by the appropriate mass and inertia terms (which must be consistent with those used at the time of the extraction of the derivatives). These are then summed with the gravitational forces before being reconverted to accelerations for integration via standard Euler nonlinear equations of motion.

The input parameters of the lookup tables are indicated by the dashed lines in Figure 3. For the LCTR2 model, these are the datum (trim) airspeed, V_0, and nacelle angle, β_{m_0}. Airspeed is typically used as a scheduling parameter in qLPV models of aircraft [23,25,26]. However, for a tiltrotor qLPV model, nacelle angle must also be considered in order to realistically capture the

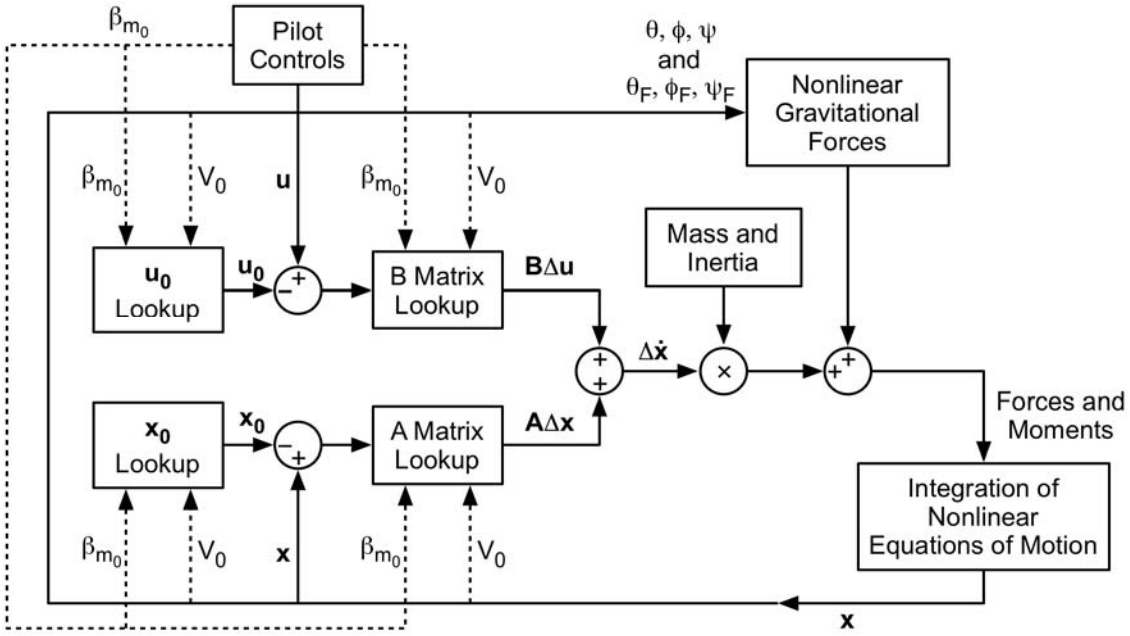

Figure 3. Architecture for LCTR2 qLPV model.

changing dynamics and trim of the aircraft conversion. Another aspect of the qLPV modeling technique that was followed for this model is the application of a low-pass filter on the lookup table scheduling parameters. Reference [23] describes how this approach was applied to the flight speed scheduling parameter, and this technique was followed for this model. A more detailed explanation of the theoretical basis for the model is found in reference [27].

LCTR2 qLPV Model Validation, Verification, and Analysis

In support of the primary development using derivatives from the CAMRAD II nonlinear models, an LCTR2 model was constructed in the FLIGHTLAB® [28] modeling environment to aid the qLPV architecture and dynamic nacelle model validation process. In order to verify the output of the qLPV model, comparisons were made to reduced-order, single point linearized approximations of the high-fidelity, nonlinear CAMRAD II models of the same aircraft. Figures 4 and 5 show frequency response comparisons of the two qLPV models derived from the CAMRAD II and FLIGHTLAB models at hover. Both qLPV models are reduced order (13 states, as is the single point, hover condition linear model derived from CAMRAD II that was included for comparison). The frequency responses are based on linear state-space from models extracted from the qLPV model using state and control input perturbation methods. On the whole, the comparisons are satisfactory within the key region of interest (1–10 rad/s) exhibiting the best agreement for both the rigid-body and rotor responses. These results gave reasonable confidence that conclusions from analysis of the FLIGHTLAB qLPV model would be also applicable to the CAMRAD II–based qLPV model.

Nacelle Modeling

For a tiltrotor, the nacelle is a control as well as a reconfiguration of the aircraft. As such, nacelle motions not only generate forces and moments directly in response to pilot inputs, but they also change the dynamics of the vehicle through the reorientation of the rotors in the aircraft body frame. For the design of the TRC control system that uses the small amplitude nacelle motions for longitudinal control, it was desirable to have a representative model of the coupled nacelle/fuselage dynamics in state-space form that was valid over the frequency range of pilot control. In terms of a state-space modeling approach adopted, however, nacelle effects are not only represented via control derivatives in the $\mathbf{B}$ matrix but also determine different $\mathbf{A}$ matrices for any particular nacelle angle.

The nacelle control derivatives were calculated using a number of high-order models and analytical methods. The analytical terms, based on first principles, offered an independent process that derived the terms from the same model from which other derivatives were extracted. These were compared to the FLIGHTLAB model and an enhanced CAMRAD II model that was also able to represent the nacelle dynamic effects and output them as part of its linearization routines.

Although the analytical process omitted certain effects to make the definition and calculation of the terms more tractable, they provided useful insight into the key physics underpinning the nacelle effects, as well as a dataset to compare to the derivatives computed by the nonlinear simulation models.

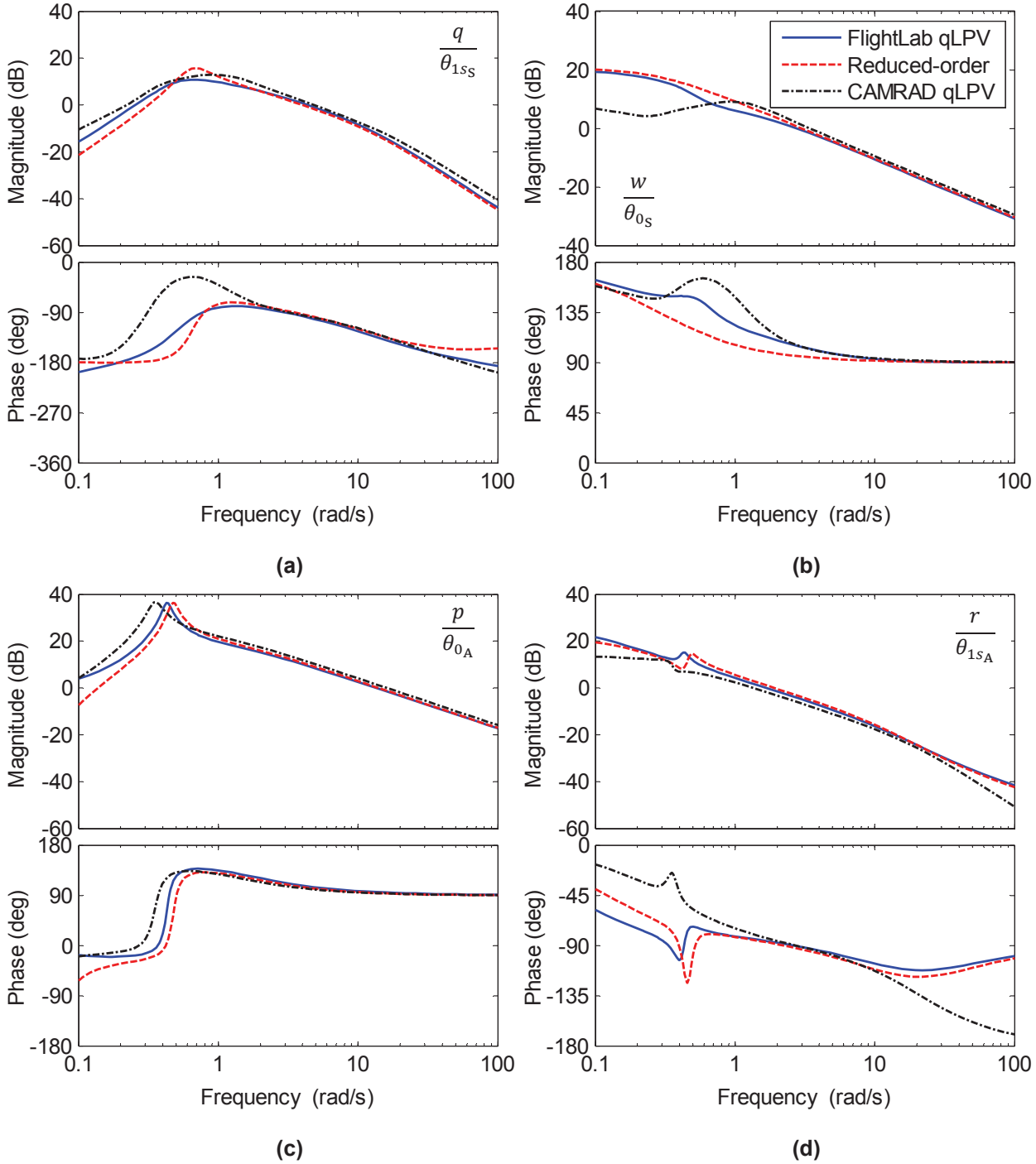

Figure 4. Comparison of the CAMRAD-derived qLPV model (baseline), the CAMRAD reduced-order (13-state) linear model, and the FLIGHTLAB-derived qLPV model (all at hover condition): (a) pitch rate response to symmetric longitudinal cyclic, (b) heave rate response to symmetric collective, (c) roll rate response to anti-symmetric collective, and (d) yaw rate response to anti-symmetric longitudinal cyclic.

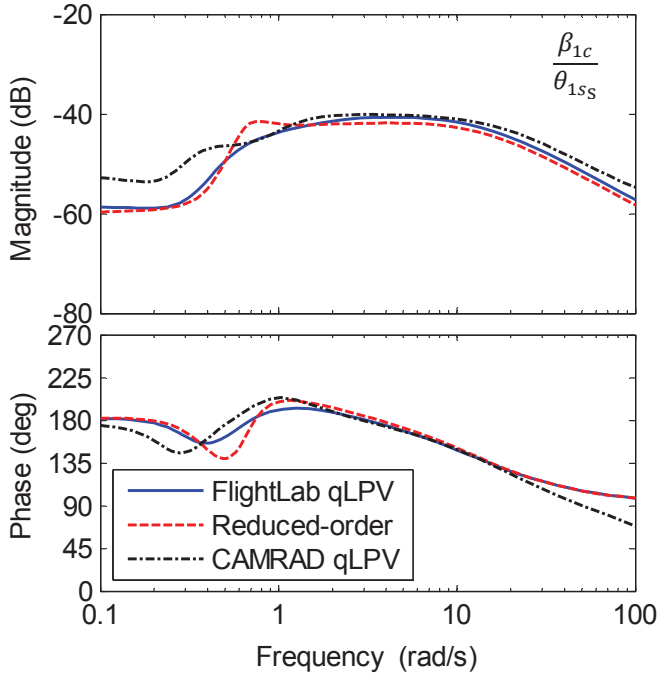

Figure 5. Comparison of the longitudinal rotor flap angle response for the CAMRAD-derived qLPV model (baseline), the CAMRAD reduced-order (13-state) linear model, and the FLIGHTLAB-derived qLPV model (all at hover condition).

Equations of motion. The following expressions, in vector form, define the full nonlinear equations that describe the forces and moments acting on the coupled airframe-nacelle system:

$$\vec{F} = m\vec{a} + m\vec{\omega} \times \vec{V} - m_N \vec{r}_{N/F} \times \vec{\alpha} + m_N \vec{\omega} \times \left(\vec{\omega} \times \vec{r}_{N/F}\right) + 2m_N \vec{\omega} \times \left(\frac{d\vec{r}_{N/F}}{dt}\right)_B + m_N \left(\frac{d^2 \vec{r}_{N/F}}{dt^2}\right)_B \tag{4}$$

and

$$\vec{M} = \{I\}\vec{\alpha} + \vec{\omega} \times (\{I\}\vec{\omega}) + m_N\left[\vec{r}_{N/F} \times \vec{a} + \vec{\omega} \times \left(\vec{r}_{N/F} \times \vec{V}\right)\right] + \left\{I_{N/F}\right\}\vec{\alpha}_{N/F} + \vec{\omega} \times \left(\left\{I_{N/F}\right\}\vec{\omega}_{N/F}\right) - \dot{\beta}_m \left[\frac{d\{I\}}{d\beta_m}\vec{\omega} + m_N \frac{d\vec{r}_{N/F}}{d\beta_m} \times \vec{V} + \frac{d\left\{I_{N/F}\right\}}{d\beta_m}\vec{\omega}_{N/F}\right] \tag{5}$$

where the relative position of the nacelle center of mass with respect to the center of mass of the fuselage is represented by $\vec{r}_{N/F}$, and the relative mast angular velocity and acceleration are

$$\vec{\omega}_{N/F} = \dot{\beta}_m \hat{j}_B \quad \text{and} \quad \vec{\alpha}_{N/F} = \ddot{\beta}_m \hat{j}_B$$

for simplicity.

Equations (4) and (5) show that the forces and moments, $\vec{F}$ and $\vec{M}$ respectively, due to the various aerodynamic, propulsive, and mechanical systems are balanced by the inertial loads generated by the motions of the fuselage and nacelle masses as a total system, as well as mutually relative motions. Note that these expressions have been formulated with the body axis frame of reference fixed at a location that is coincident with the fuselage center of mass. In this

sense, the vectors $\vec{a}$, $\vec{V}$, $\vec{\alpha}$, and $\vec{\omega}$ represent the linear and angular accelerations and velocities at that location. The importance of this distinction is that simulation models typically use a fixed point of reference, and if the expressions were formulated for a reference frame located at the center of gravity of the system as a whole, there would be terms that induce relative rotations of both the fuselage and nacelle systems with respect to that body reference frame. This is not practicable as the stability derivative terms are only compatible with states that are expressed in a fuselage-body-fixed frame.

Figure 6 illustrates the various conventions used herein; note in particular the convention defining a positive nacelle rotation, β_m. The shaft axis coordinate system has its origin at the hub, as shown in Figure 6, and its axes are fixed to the nacelles and rotate with them, but the positive x- and z-axis directions are opposite to the hub axis system. Rotor loads are typically represented in the hub nonrotating coordinate system, but relate to the shaft axes through the linear transformation: $X_H = -X_S$, $Y_H = Y_S$ and $Z_H = -Z_S$.

Nacelle derivatives. The left-hand-side force and moment variations, when expanded as Taylor series and linearized making the small perturbation assumption, are written as linear combinations of the state and control variables. For example, the X-force component variation in the body axis system is written as:

$$\delta X_B = \sum_{i=1}^{n} \frac{\partial X_B}{\partial x_i}\delta x_i + \sum_{j=1}^{p} \frac{\partial X_B}{\partial u_j}\delta u_j + \frac{\partial X_B}{\partial \beta_m}\delta\beta_m + \frac{\partial X_B}{\partial \dot{\beta}_m}\delta\dot{\beta}_m + \frac{\partial X_B}{\partial \ddot{\beta}_m}\delta\ddot{\beta}_m \qquad (6)$$

where $X = X_0 + \delta X$, and x_i and u_j respectively indicate the i-th state and j-th control variables. Similar general expressions can be established for the other body axes forces, moments, and rotor blade modal forcing functions. Significantly, these linearized expansions include the partial derivatives for the nacelle conversion degrees of freedom: β_m, $\dot{\beta}_m$, and $\ddot{\beta}_m$. The derivations that follow illustrate how these derivatives were estimated from first principles.

General analytical model. A general formulation, based on blade element theory, was

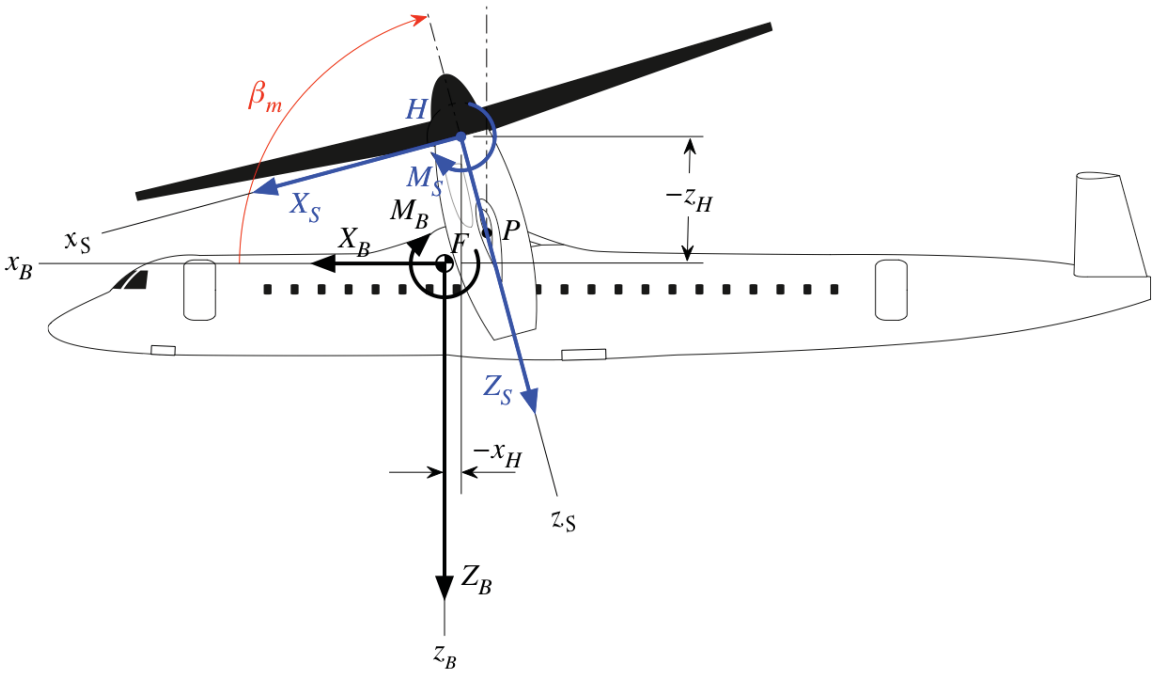

Figure 6. Axes conventions for nacelle longitudinal force and moment derivations.

General analytical model. A general formulation, based on blade element theory, was developed to encompass a broader range of airspeeds and nacelle conversion angles beyond hover. For brevity, only the longitudinal effects are presented, since these are by far the most important for the symmetrical longitudinal nacelle motions. Also, the following derivations are for a single rotor/nacelle combination without loss of generality, so any longitudinal terms are doubled or repeated for a two-rotor system. Rotor and other nacelle forces and moments in the body axes are therefore expressed in terms of the shaft axis reference frame components by means of the linear transformation:

$$X_B = X_S(\beta_m)\sin\beta_m - Z_S(\beta_m)\cos\beta_m \tag{7}$$

$$Z_B = X_S(\beta_m)\cos\beta_m + Z_S(\beta_m)\sin\beta_m \tag{8}$$

and

$$M_B = M_S(\beta_m) - Z_B x_H(\beta_m) + X_B z_H(\beta_m). \tag{9}$$

Note that the forces and moments in the shaft axes can themselves be a function of the nacelle angle. Following the rules of calculus of variations, the variation for the X-force from Eq. (7) results in:

$$\delta X_B = \delta X_S \sin\beta_m - \delta Z_S \cos\beta_m + (X_S\cos\beta_m + Z_S\sin\beta_m)\delta\beta_m. \tag{10}$$

Expressing the shaft-axis force variations δX_S and δZ_S in the first-order Taylor series expansion form of Eq. (6) and substituting into Eq. (10) results in:

$$\begin{aligned}\delta X_B = {} & \left[\sum_{i=1}^{n}\frac{\partial X_S}{\partial x_i}\delta x_i + \sum_{j=1}^{p}\frac{\partial X_S}{\partial u_j}\delta u_j\right]\sin\beta_m - \left[\sum_{i=1}^{n}\frac{\partial Z_S}{\partial x_i}\delta x_i + \sum_{j=1}^{p}\frac{\partial Z_S}{\partial u_j}\delta u_j\right]\cos\beta_m \\ & + \left[\frac{\partial X_S}{\partial\beta_m}\sin\beta_m - \frac{\partial Z_S}{\partial\beta_m}\cos\beta_m + (X_S\cos\beta_m + Z_S\sin\beta_m)\right]\delta\beta_m \\ & + \left[\frac{\partial X_S}{\partial\dot{\beta}_m}\sin\beta_m - \frac{\partial Z_S}{\partial\dot{\beta}_m}\cos\beta_m\right]\delta\dot{\beta}_m \\ & + \left[\frac{\partial X_S}{\partial\ddot{\beta}_m}\sin\beta_m - \frac{\partial Z_S}{\partial\ddot{\beta}_m}\cos\beta_m\right]\delta\ddot{\beta}_m\end{aligned} \tag{11}$$

Comparing Eq. (6) with (11), the partial derivatives with respect to β_m, $\dot{\beta}_m$, and $\ddot{\beta}_m$ in the body axis system are made thus obtaining the expressions for the individual stability derivatives in the shaft axes:

$$\frac{\partial X_B}{\partial\beta_m} = \frac{\partial X_S}{\partial\beta_m}\sin\beta_m - \frac{\partial Z_S}{\partial\beta_m}\cos\beta_m \underline{+(X_S\cos\beta_m + Z_S\sin\beta_m)} \tag{12}$$

$$\frac{\partial X_B}{\partial\dot{\beta}_m} = \frac{\partial X_S}{\partial\dot{\beta}_m}\sin\beta_m - \frac{\partial Z_S}{\partial\dot{\beta}_m}\cos\beta_m \tag{13}$$

$$\frac{\partial X_B}{\partial\ddot{\beta}_m} = \frac{\partial X_S}{\partial\ddot{\beta}_m}\sin\beta_m - \frac{\partial Z_S}{\partial\ddot{\beta}_m}\cos\beta_m \tag{14}$$

Finally, analytic expressions for the calculation of the partial derivative terms on the right-hand side of the previous equations need to be defined. These terms are the change of the rotor forces with respect to the nacelle dynamics. The aerodynamic perturbation forces acting on the nacelle are neglected in this theoretical analysis. Again, focusing on the X-force term, the variation due to a nacelle angle perturbation, β_m, can be approximated from blade element theory. The simplifying assumptions that permit the use of this analytical approach are that the airspeeds are low (incompressible), the angles of attack remain small (within the linear regime), and the rotor speed remains constant. Accordingly, the effects of the reverse flow region are neglected. Other simplifications are to neglect the tip losses and root cut-out. The aerodynamic perturbation forces acting on the nacelle are also neglected in this theoretical analysis. The flapping dynamics are not being considered either. Blade element theory is only employed in the estimation of the integrated aerodynamic forces on the rotor. With all other conditions remaining constant, the formulation treats a nacelle perturbation as analogous to a change in the angle of attack of the rotor. Based on the assumption of uniform constant inflow, the analytical expression of the rotor thrust partial derivative with respect to angle of attack is:

$$\frac{\partial T}{\partial \alpha} = -\frac{N_b \rho a \Omega^2 R^3 c}{2}\left[\left(\mu_x \theta_0 + \frac{\mu_x}{2}\theta_{tw} + \frac{\theta_{1s}}{2}\right)\mu_z - \frac{\mu_x}{2}\right] \tag{15}$$

where μ_x and μ_z are the in- and out-of-plane advance ratio components:

$$\mu_x = \frac{V_\infty}{\Omega R}\cos\alpha \quad \text{and} \quad \mu_z = \frac{V_\infty}{\Omega R}\sin\alpha$$

A similar process can be carried out for the remaining force and moment components. Whereas the expressions for the aerodynamic in-plane rotor forces are more complicated, these are nonlinear functions of order $\mathcal{O}(\varepsilon^2)$ and are largely neglected in this theoretical formulation. Furthermore, if symmetrical flight and rotor symmetry is enforced, the lateral terms become simplified. Making the approximation $Z_S = -T$ and $X_S = -T\beta_{1c}$, and recalling that $\delta\beta_m = -\delta\alpha$ because of the positive direction convention chosen in Figure 6, the partial derivatives of the X and Z rotor forces, in the shaft-axis, are obtained from:

$$\frac{\partial X_S}{\partial \beta_m} = \frac{\partial T}{\partial \alpha}\beta_{1c} \quad \text{and} \quad \frac{\partial Z_S}{\partial \beta_m} = \frac{\partial T}{\partial \alpha} \tag{16}$$

where all the terms in the right-hand side of Eq. (15) can be computed from the trim solution.

It is worth mentioning that for the hover case, this term is zero. As such, the derivative in the body axis system from Eq. (12) simply becomes the underlined term, which is the trim force Z (Eq. (8)). This demonstrates that for small angles at hover, the perturbation forces due to nacelle angle changes are approximated to the quasi-steady reorientation of the rotor trim forces.

The rotor in-plane velocity component generated by the nacelle rate of rotation also causes a variation in the thrust, but this amount is negligible. The effect on the blade flapping dynamics is retained however. The pitching moment reaction to the rotational rate is attributed primarily to the flap-back response of the rotor and thus analogous to the moment induced by the rotor flap dynamics in response to pitch rate of the aircraft, such that:

$$\frac{\partial M_f}{\partial \dot{\beta}_m} = \frac{\partial M_f}{\partial q} \tag{17}$$

Therefore the rotor flapping derivative with respect to nacelle rate can be approximated using the known quantities with respect to body motions by relying on the analogy of nacelle rate to body pitch rate. Because of the peculiarities of the order-reduction method, key force components that were also retained were the longitudinal rotor hub force derivatives with respect to longitudinal flapping rate, $X'_{\dot{\beta}_{1c}}$ and $Z'_{\dot{\beta}_{1c}}$.

Finally, the inertial contributions of the nacelle rotational acceleration are attributed solely to the inertial reactions generated by the mutually relative motions (accelerations) of the nacelle and fuselage masses defined in Eqs. (4) and (5).

First-order approximation in hover. A simplified first-order approximation of the gross effects of nacelle reorientation in hover was very illustrative, comparing favorably with the high-order models. Force and moment variations to a small reorientation, or rotation, of the mast angle were assumed to be caused primarily by the reorientation of the rotor thrust vectors and the position shift of the center of gravity. Therefore the force derivatives are:

$$\frac{X_{\beta_m}}{m} = X'_{\beta_m} \approx -g \tag{18}$$

and

$$\frac{Z_{\beta_m}}{m} = Z'_{\beta_m} \approx g\theta_F \tag{19}$$

where θ_F refers to the pitch trim attitude and g is the gravitational acceleration. Note in particular that these derivatives have been defined such that a forward nacelle rotation, β_m, relative to the vertical position, is defined to be in the negative direction. The pitching moment derivative was therefore approximated as:

$$\frac{M_{\beta_m}}{I_{yy}} = M'_{\beta_m} \approx -g\frac{m_N z_N}{I_{yy}} \tag{20}$$

where m_N is the nacelle mass (including the rotor), and z_N is the center of mass as measured in the body axis frame of reference from the fuselage center of mass (point F in Figure 6). This quantity reflects the effect of the shifting center of gravity of the aircraft. The rotor dynamic reaction to nacelle conversion rate is treated as per Eq. (17). Finally, the longitudinal force and pitching moment derivatives with respect to an angular acceleration of the nacelle are fundamentally defined by the inertial load reactions generated by the relative accelerations of the nacelle in Eqs. (4) and (5), such that:

$$\frac{X_{\ddot{\beta}_m}}{m} = X'_{\ddot{\beta}_m} = -\frac{m_N\, z_N}{m} \tag{21}$$

and

$$\frac{M_{\ddot{\beta}_m}}{I_{yy}} = M'_{\ddot{\beta}_m} = -\frac{I_N + m_N(z_N^2 + x_N^2)}{I_{yy}} \tag{22}$$

Table 4 shows a comparison of the control derivatives extracted from the FLIGHTLAB and CAMRAD II models and the analytical calculations. This example is at the hover condition with the nacelles at the 90 deg (vertical) position. Comparing the bare-airframe frequency response to nacelle oscillation, Figure 7 shows a favorable agreement between the various FLIGHTLAB- and CAMRAD-generated derivatives, and the analytical predictions based on first principles.

Discrepancies between the CAMRAD- and FLIGHTLAB-based models in Figure 7 are attributed to the differences in the rotor flapping dynamics, which are also manifested in the $\dot{\beta}_m$ derivatives.

The agreement between this case and others gave reassurance that the automatic derivative calculation process from FLIGHTLAB was providing reliable results. This validation against the analytical approach led to the use of the FLIGHTLAB automatically generated

Table 4. Comparison of nacelle control derivatives extracted from the FLIGHTLAB and CAMRAD II LCTR2 models, and the analytical techniques (trim: hover, 90 deg nacelle).

	Units	FLIGHTLAB	CAMRAD II	Analytical (massless nacelle)	Analytical (w/nacelle inertia)	First Order
X'_{β_m}	ft/s^2	–34.2	–34.83	–34.86	–34.86	–32.15
Z'_{β_m}	ft/s^2	2.39	1.871	1.88	1.88	1.8
M'_{β_m}	1/s^2	0.0514	0.046	0.048	0.048	0.033
$X'_{\dot{\beta}_m}$	ft/s	1.99	0.553	0.444	0.444	0
$M'_{f_{\dot{\beta}_m}}$	–	1.24	0.953	0.96	0.96	0.955
$X'_{\ddot{\beta}_m}$	ft	0.272	0.351	0.305	0.297	0.313
$M'_{\ddot{\beta}_m}$	–	–0.0139	–0.037*	–0.0265	–0.0429	–0.0273

* The CAMRAD II model featured additional mass located at nacelle pivot (so it only contributed inertia effects to derivatives) but is partly responsible for the higher term.

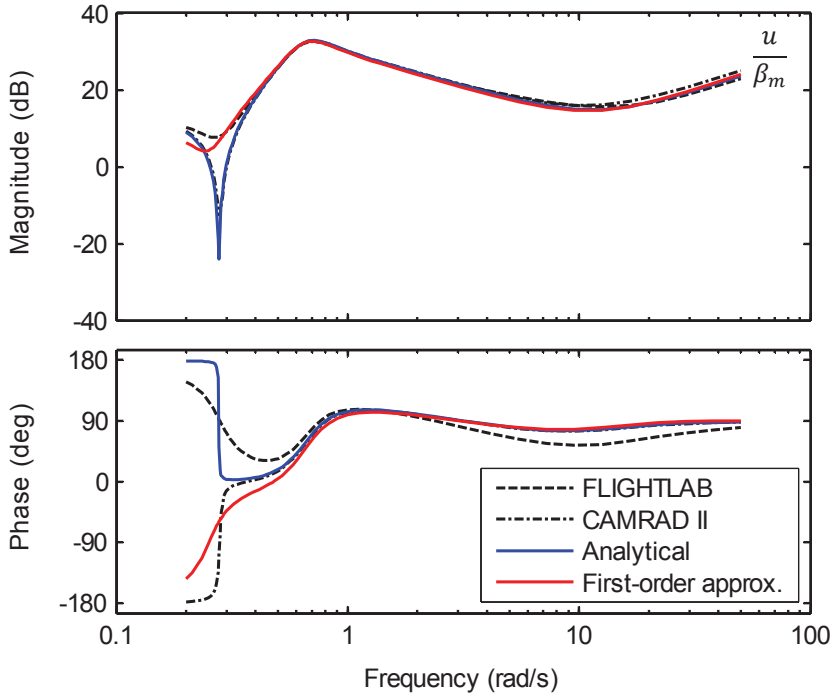

Figure 7. Comparison of bare-airframe frequency responses of aircraft *u* velocity (ft/s) to nacelle angle (rad) from FLIGHTLAB, CAMRAD II, and analytical derivations.

derivatives in the qLPV model employed in the first TRC experiment [15]. These were added as additional columns in the **B** matrix where the coefficients were implemented as functions of lookup tables [22]. Later evolutions of the LCTR2 model, used in reference [16] and developed for the purposes of expanding the speed envelope, employed partial derivatives derived solely from CAMRAD II. In fact, the analytical derivatives were used in the early TRC control law design process. This resulted in a seamless application of the controller to the qLPV model that featured the more complete set of nacelle motion derivatives from the computational models.

Nacelle inertia considerations. In generating the bare-airframe nacelle/rotor model, the inertia of the nacelles themselves was initially neglected. The total mass of the system corresponded to that of the rotor only and the center of mass was located at the rotor hub, with the inertial properties of the rotor blade mass distribution being accounted for via the multibody dynamics formulation used in FLIGHTLAB. This construct was employed in the modeling of the LCTR2 airframe used in the TRC VMS study in reference [15]. This was an obvious simplification, but in the absence of more tangible design data, it represented a sensible starting point for a model that was suitable for flight control system design and handling qualities evaluation. Provided that the ratio of the nacelle to airframe moments of inertia in pitch remains small, this assumption was considered to have a negligible impact on the aircraft flight dynamics.

Concentrating the entire mass of the rotors at the hub results in an unbalanced nacelle system, that is, one in which the aircraft center of gravity moves with the mast conversion angle causing a pitch change of the aircraft. However, this was not expected to have a noticeable effect on the handling qualities for small ranges of motion. Below 10 rad/s, the primary effect on the rigid body dynamics of the airframe from the tilting rotor/nacelle system is the quasi-steady reorientation of the rotor thrust vectors. A simple comparison of the magnitude of the derivatives suggests that inertial effects of angular nacelle acceleration become apparent for nacelle frequencies in the vicinity of 7–8 rad/s but would only begin to dominate the X-force component (i.e., force component along the body x axis) over 10 rad/s, which is on the upper limit of the frequency range of pilot control.

An improvement to the nacelle modeling in CAMRAD II, employed for the study in reference [16], was the inclusion of an estimation of the nacelle mass and inertia due to engine, drivetrain, and airframe contributions (Table 5). This additional moment of inertia in pitch accounted for an extra 1.9 percent of the airframe pitching moment in addition to the current 2.8-percent ratio associated with the rotor inertial properties. The additional mass was located at the nacelle hinge, which was assumed to be the nacelle-only (i.e., minus the rotor) center of mass. As such, this additional nacelle mass made only a second-order contribution to the LCTR2 center of gravity motion when the nacelle was rotated. However, the additional moment of inertia about the hinge did confer an additional effect when the nacelles were moved—the most significant difference being an increased value of the derivative with respect to angular acceleration of the nacelle, $M_{\ddot{\beta}_m}$ (see Table 4).

Table 5. Nacelle inertial properties (mass and principal moments of inertia).

Property	Units	Value
Mass (total lumped parameter)	slug	221.3
Principal moment of inertia about parallel axis to the x_S shaft axis	slug·ft^2	8127.5
Principal moment of inertia about parallel axis to the y_S shaft axis	slug·ft^2	8127.5
Principal moment of inertia about the z_S shaft axis	slug·ft^2	1487.8

Control Law Design

Model-Following Architecture

The flight control system design used an explicit model-following architecture throughout the range of experiments for both attitude and translational rate response type implementations, and for all the rotorcraft types. Shown in Figure 8, the generic control system block diagram of the model-following architecture permitted easy adjustment of the feedback characteristics or the desired response to piloted inputs, while retaining the other constant. In addition to the primary experimental Translational Rate Command (TRC) and Attitude Command-Attitude Hold (ACAH) response types, the control systems also provided yaw and vertical (heave) Rate Command (RC) control response types to pedal and collective stick (or Thrust Control Lever (TCL), in the tiltrotor) inputs, respectively. The feedback controllers consisted of a simple Proportional-Integral-Differential (PID), Single-Input/Single-Output (SISO) design in each of the control axes, allowing for a tractable design and synthesis process.

Attitude Command

The desired response to piloted inputs was determined by the command model transfer function, while the regulator was independently designed to set the disturbance rejection bandwidth (DRB) and associated stability characteristics. This was crucial to the conduct of these experiments, as variations in the feedback path could be examined without significantly impacting the piloted bandwidth of the aircraft, and vice versa. For investigation of the trade-off between stability margins and DRB, the command models (CMD/δ in Figure 8), defined by Eq. (23), were specifically configured to meet ADS-33 Level 1 attitude bandwidth requirements. Also, it was through tuning of the command models that the bandwidth and phase delay variations for the short-term response investigation of the LCTR were achieved. A second-order command model was used in the pitch and roll axes, and a first-order command model was used in the yaw axis. These were independently set based on the general transfer function models:

$$\frac{\phi_{cmd}}{\delta_{lat}}, \frac{\theta_{cmd}}{\delta_{lon}} = \frac{K\omega_n^2 e^{-\tau_n s}}{s^2 + 2\zeta\omega_n s + \omega_n^2}, \quad \frac{r_{cmd}}{\delta_{ped}} = \frac{K e^{-\tau_{cmd} s}}{\tau_{ped} s + 1} \tag{23}$$

The vertical response for all aircraft configurations was augmented with Proportional-Integral (PI)-control on the altitude rate to improve vertical damping and provide a pseudo-Altitude Hold. First-order inverse models, which invert the short-term aircraft response dynamics while

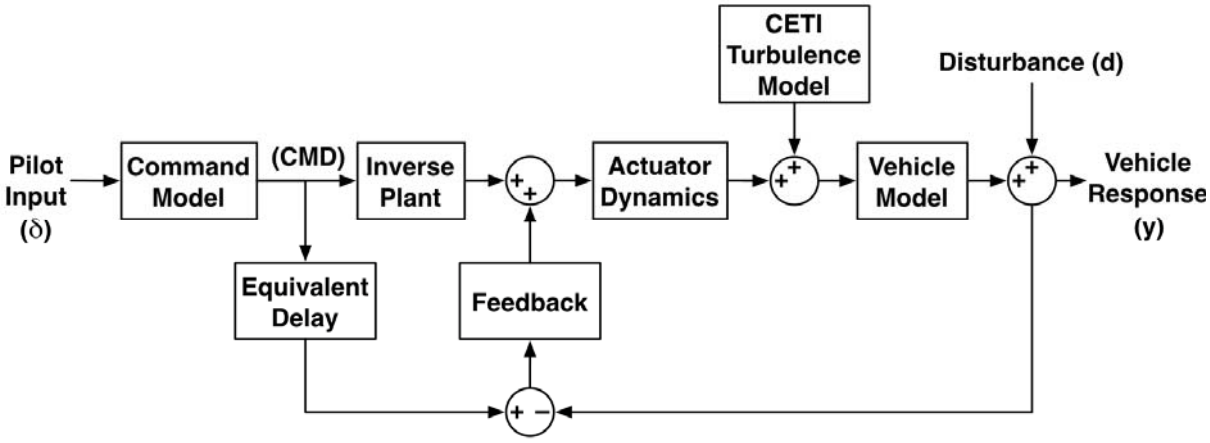

Figure 8. Overview of the generic model-following control system architecture.

ignoring the higher-order rotor and actuator dynamics, were generated for each channel based on simple equivalent-system fits of on-axis angular-rate responses of the 11-state bare-airframe model. For example:

$$\frac{p}{\delta_{lat}} = \frac{L_{\delta_{lat}} e^{-\tau_{eq} s}}{s - L_p} \tag{24}$$

Implementing the inverse of Eq. (24) typically involves the configuration of a (non-causal) time lead (i.e., the inverse of a time delay). Rather, an equivalent time delay block was included on the command output path to the error summer, effectively synchronizing the command signal with the measured aircraft response to avoid overdriving higher-order dynamics (rotor and actuator). The values were determined using an equivalent system match of the forward path response to the command model response.

Because of the deterministic nature of the dynamic models developed of the aircraft for this study, this inversion technique resulted in a near-perfect match between the inverse and aircraft dynamics in the frequency range of interest. This, however, is seldom the case in real aircraft, and so 30 percent uncertainties were introduced into the parameters of the inverse model for the stability margin and DRB trade-off study to simulate mismatch between the expected and actual inversion behavior. Each of the parameters (i.e., the control derivative, the stability derivative, and the time delay), was randomly increased or decreased by the 30-percent uncertainty value. This degraded the otherwise perfect inversion and had the desired effect of exciting the feedback path as would occur in reality. This was crucial to the stability margin and DRB trade-off experiment, as it brought out the differences between the different feedback cases of each configuration.

Translational Rate Command

The model-following architecture was also used in the design of the TRC control system for the LCTR2 [15,16]. This particular TRC implementation, with the longitudinal axis control loops shown in Figure 9, employed parallel (anti-symmetric) lateral cyclic on the two rotors for lateral translational rate control, and nacelle tilt angle for longitudinal control. In the control laws, lateral and longitudinal velocities were compared to the desired vehicle response determined by the command model, and the error was fed back through a simple PID regulator to compute the necessary corrections to the control inputs estimated by the inverse plant model. With the TRC mode engaged, the ACAH control loops were also still active, which enabled deck level, hover

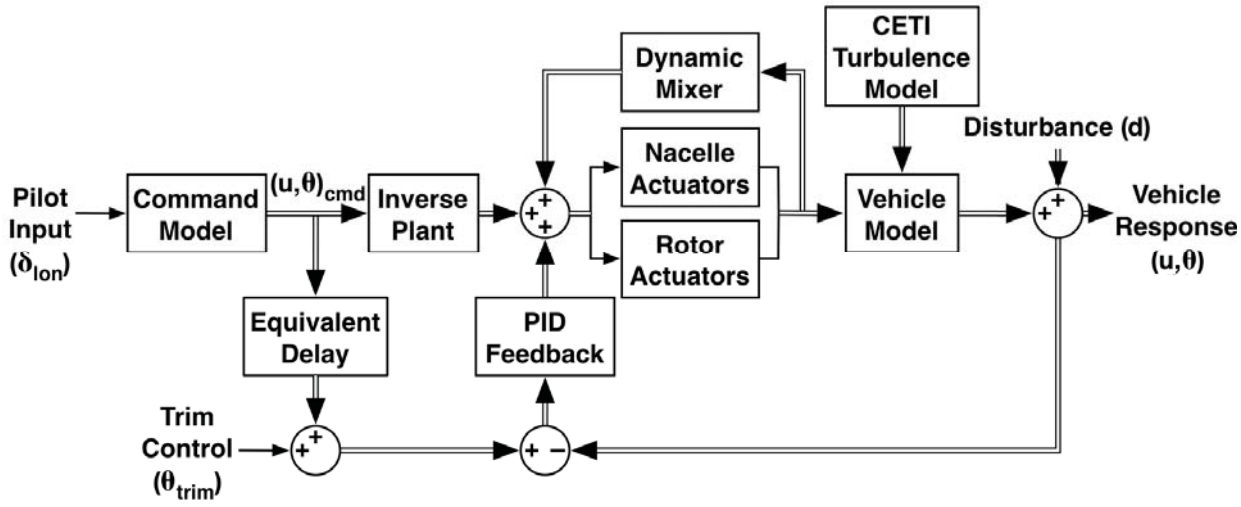

Figure 9. Model-following architecture for longitudinal TRC.

trim attitude regulation by maintaining the attitude command model inputs at zero ($\theta_{cmd} = 0$ in Figure 9). This automatic regulation of the longitudinal cyclic and differential collective was intended to counteract the natural off-axis pitch and roll responses to nacelle and lateral cyclic inputs. Thus, the velocity and attitude loops were closed in parallel. Consequently, the two sets of regulators complemented each other by acting on independent control variables, made possible by the additional control mechanisms available in a tiltrotor aircraft.

The TRC control system command models were designed to provide the first-order qualitative character (i.e., the absence of objectionable pitch and roll oscillations, zero velocity for zero stick displacement, and no noticeable overshoots in the response of translational rate to control inputs) and the equivalent rise-time specifications defined in ADS-33. The simulation results section below discusses these requirements more fully along with their technical background. Additionally, the command models provided experimental control over the variation in translational rate with control deflection. A first-order command model was used in the lateral and longitudinal axes to achieve desired TRC response types. The transfer functions employed were of the general form:

$$\frac{u_{cmd}}{\delta_{lon}}, \frac{v_{cmd}}{\delta_{lat}} = \frac{Ke^{-\tau_{cmd}s}}{T_{eq}s + 1} \tag{25}$$

Here δ_{lon} and δ_{lat} are the longitudinal and lateral pilot inputs, through the center stick, and u_{cmd} and v_{cmd} are the commanded body axes velocities. The commanded response delay and equivalent rise times are defined by the time constants τ_{cmd} and T_{eq}, respectively. The coefficient K sets the steady-state response/control sensitivity gain in (ft/s)/in, where the maximum stick deflection was ±5 inches. These parameters were the subject of experimental assessment and results of their effect on the handling qualities are reported in the simulation results section below. The command model time delays, (τ_{cmd}), were set at a minimal 0.01 s value. The baseline equivalent rise-time specification of 5 s was achieved through the tuning of the command model time constants, T_{eq}, in the lateral and longitudinal translational rate response axes.

The inverse dynamic models of the translational short-term response dynamics for the TRC control system were based on first-order approximations analogous to that defined in Eq. (24), such that:

$$\frac{u}{\delta_{lon}} = \frac{X_{\beta_m}e^{-\tau_{eq}s}}{s - X_u}, \quad \frac{v}{\delta_{lat}} = \frac{Y_{\delta_{lat}}e^{-\tau_{eq}s}}{s - Y_v} \tag{26}$$

Here X_{β_m} and $Y_{\delta_{lat}}$ are the longitudinal and lateral force derivatives with respect to nacelle tilt rotation and rotor lateral cyclic.

Hybrid Attitude/Translational Rate Command Response Type

A “Hybrid” response type in which attitude and translational rate were commanded simultaneously was implemented to investigate the benefits, if any, of providing a blend of both the TRC and ACAH response types. Issues of interest for investigating hybrid response types included: a) the effect of control system implementation on rotor flapping demands, and b) mechanics for transitioning between angular and translational response types. The TRC/ACAH hybrid control mode was only configured in the lateral axis, as it had already been determined that pitching in the longitudinal axis was undesirable. Center stick displacements greater than 1 inch from center with this system would command roll attitude at reduced sensitivity (0.3 of the baseline ACAH command model) in addition to the normal translational lateral rate commanded. The longitudinal axis in this control system implementation retained a TRC response type only as described in the previous section.

Implementation of this hybrid response type was achieved through a simple adaptation of the command model systems of Eqs. (23) and (25). For lateral cyclic stick displacements below 1 inch, the system operated in TRC, commanding lateral translational rates per Eq. (25) and zero roll attitude ($\phi_{cmd} = 0$). For stick displacements greater than 1 inch, the command model blended in non-zero attitude commands, in addition to the translational rates. This was automated as a "dead zone" on the input to the roll axis command model of Eq. (23) such that:

$$\delta'_{lat} = \begin{cases} 0.3(\delta_{lat} + 1), & \delta_{lat} < -1 \\ 0, & -1 \leq \delta_{lat} \leq 1 \\ 0.3(\delta_{lat} - 1), & \delta_{lat} > 1 \end{cases} \tag{27}$$

Crossfeeds for TRC Control Mixing

The control laws featured a number of crossfeed signals, handled in the "Dynamic Mixer" block of Figure 9, that were developed based on piloted simulation experience to reduce the inter-axis coupling of the control mechanisms, and ultimately improve the handling qualities. These included:

- Crossfeed of lateral cyclic pitch to differential collective pitch—to reduce the undesired roll response when lateral TRC commands are made.
- Crossfeed of lateral cyclic pitch to differential longitudinal cyclic pitch—to reduce the undesired yaw response when lateral TRC commands are made.
- Crossfeed of nacelle angular rate to longitudinal cyclic pitch—introduced to minimize a "non-minimum phase" pitch response to nacelle rotational rate commands resulting from longitudinal velocity TRC commands. This simple proportional crossfeed gain of the nacelle angular rate provided an appropriate amount of feedforward lead compensation to counteract the non-minimum phase characteristics of the bare-airframe dynamics. The effect of this crossfeed on the handling qualities is the subject of experimental assessment and detailed analysis presented in the simulation results section and Appendix B.

Cyclic Augmentation

A version of the TRC control laws that was tested featured additional longitudinal cyclic pitch actuation to supplement that of nacelle tilt. This version, referred to as the "longitudinal cyclic augmented TRC" or, simply, the "cyclic-augmented TRC," comprised full PID *feedback control* of the measured longitudinal velocity aircraft output and effected control by means of longitudinal cyclic input in response to the velocity error. This was in addition to the crossfeed of nacelle rate to cyclic described in the previous section. In this context, the longitudinal feedback command $\hat{\delta}_{lon}^{FB}$ to the primary swashplate servo-actuator control units, and ultimately driving the symmetric longitudinal rotor cyclic input, was defined by:

$$\hat{\delta}_{lon}^{FB} = K_\theta \left(1 + \frac{1}{T_{I_\theta} s}\right) \theta_e + K_{D_\theta} q_e + K'_u \left(1 + \frac{1}{T'_{I_u} s}\right) u_e + K'_{D_u} a_{X_e} \tag{28}$$

where the feedback compensation is comprised by the sum of the PID control signals of the pitch attitude error, θ_e, and the longitudinal velocity error, u_e. Actual design of the controller employed the direct measurements of the pitch rate and longitudinal acceleration to determine the error signals, q_e and a_{X_e}, respectively, that were used for the computation of the differential feedback control signals.

This control law was developed as part of a research effort to evaluate alternate techniques that would enable the responsiveness, and thus the handling qualities, of the TRC control laws to be maintained at Level 1 as the primary nacelle actuator bandwidth dynamics were degraded. It is noted that the feedback control law defined by Eq. (28) is fundamentally equivalent to that which results from the classical TRC design problem for conventional helicopters using inner loops for stabilization and attitude control, and outer loops for translational rate control, except the objective here was simply to supplement the primary nacelle tilt actuation. Because the controller still relied on the rotor cyclic for the regulation of pitch, the relative weighing of the PID control actions in Eq. (28) needed to be carefully attuned to avoid competing demands for the rotor cyclic. The control gains for the two cyclic loops were thus set to ensure adequate crossover frequency separation and attitude response damping, and to avoid objectionably abrupt pitch responses.

Actuators

Models of the actuator dynamics were included to correctly account for the handling qualities degradations associated with the effective bandwidths and nonlinear characteristics introduced by the various systems. For the TRC nacelle actuators, a simple second-order servo-actuator dynamic model (29) was assumed for a nacelle angular command:

$$\frac{\beta_m}{\beta_{cmd}} = \frac{\omega_{nac}^2}{s^2 + 2\zeta_{nac}\omega_{nac}s + \omega_{nac}^2} \tag{29}$$

Here, β_m refers to the mast angle, which is used equivalently to the nacelle angle, and ω_{nac} is the natural frequency, or bandwidth, of the nacelle tilting actuator. Nacelle actuator dynamics (i.e., bandwidth) were examined during the experiment. The baseline bandwidth was defined at 8 rad/s, and the nacelle conversion actuators were assumed to be critically damped (ζ_{nac} =1) to avoid natural oscillatory behavior, but still ensure minimum response times. Nacelle rotational conversion position and rate limits were also modeled, and subject to experimental assessment. The angular displacement limits of the nacelle conversion actuator, in the baseline TRC control configuration, were rotation amplitudes of 9 deg forwards and backwards from the 86 deg hover datum position, conferring a 77–95 deg range (zero being the horizontal, airplane mode). The baseline actuator rate limits were established at ±7.5 deg/s.

For the rotor swashplate, high bandwidth (8 Hz) servo-actuator models were included and assumed also to possess simplified second-order dynamic response characteristics, but featured rate limits only. The damping ratio of the second-order dynamics was taken at 0.7. The rate limits were set to ±5 in/s throughout the series of experiments.

Turbulence Modeling

A realistic aircraft response to atmospheric gust disturbances for the various airframes was simulated by means of an empirical approach based on the Control Equivalent Turbulence Input (CETI) model described in references [29,30]. A large enough level of simulated turbulence was desired to impact the handling qualities of the aircraft to allow, primarily, for the evaluation of the trade-off between varying disturbance rejection bandwidth (DRB) and related phase stability margins. Originally developed to meet the needs of simulating the effects of atmospheric turbulence on conventional single main rotor helicopters in hover and low speed, the CETI model was also adopted for use in this investigation and extended for use with a tiltrotor aircraft.

The outputs of the CETI model are turbulence inputs injected into the control system of an aircraft (as shown in Figure 9) operating in calm atmospheric conditions to cause the aircraft to respond as if it were operating in a prescribed level of atmospheric turbulence. For actual use in flight testing, the CETI commands would typically drive the control system servo actuators. The

CETI model inputs in the VMS are specified in the four primary axes of control (roll, pitch, heave, and yaw) and added to the output of the actuators with the appropriate control mixing. The main governing equations shaping the turbulence inputs are presented here in their general form:

$$\frac{\hat{\delta}_{lat}}{W_n} = K_{lat}\sigma_w^{x_1}\sqrt{\frac{U_0}{\pi\ell_w}}\cdot\frac{1}{s+\frac{U_0}{\ell_w}}\cdot f_2(s) \tag{30}$$

$$\frac{\hat{\delta}_{lon}}{W_n} = K_{lon}\sigma_w^{x_1}\sqrt{\frac{U_0}{\pi\ell_w}}\cdot\frac{1}{s+\frac{U_0}{\ell_w}}\cdot f_2(s) \tag{31}$$

$$\frac{\hat{\delta}_{col}}{W_n} = K_{col}\sigma_w^{z}\sqrt{\frac{3U_0}{\pi\ell_w}}\cdot\frac{s+20\frac{U_0}{\ell_w}}{\left(s+.63\frac{U_0}{\ell_w}\right)\left(s+5\frac{U_0}{\ell_w}\right)}\cdot f_2(s) \tag{32}$$

$$\frac{\hat{\delta}_{dir}}{W_n} = K_{dir}\sigma_v^{x_2}\sqrt{\frac{U_0}{\pi\ell_v}}\cdot\frac{1}{s+\frac{U_0}{\ell_v}}\cdot f_2(s) \tag{33}$$

Equations (30–32) govern the gust input shaping that drives the helicopter roll, pitch, and heave simulated responses to a vertical velocity gust field impinging on the *main rotor*. The yaw response, modeled by Eq. (33), is governed by the *tail rotor* thrust response to a lateral velocity field. Empirically derived CETI model configuration parameters include aircraft and atmospheric physical parameters. Aircraft parameters, such as main rotor diameter and blade inertial properties, are used to scale the CETI model between different rotorcraft. These are all reflected in the K_{lat}, K_{lon}, K_{col}, and K_{dir} coefficients. Atmospheric parameters include flow field mean wind speed, U_0, and standard deviation in the lateral and vertical directions, σ_{v} and σ_{w}, respectively, and lateral and vertical wave characteristic lengths, ℓ_v and ℓ_w, also respectively. A second-order low pass filter, $f_2(s)$, is a legacy implementation from flight testing incorporated to prevent unwanted high-frequency commands to the actuators.

Testing in the VMS was conducted in multiple levels of simulated turbulence, ranging from “ambient” to “light” to “moderate,” using the CETI model parameters from Table 6. The model parameters for the “moderate” level of turbulence are based on values used for an in-flight simulation study conducted on the RASCAL helicopter [29]. The “moderate” values of U_0 and σ_{v} were changed slightly for this study so that the RASCAL project pilot flying the H-60 in the VMS rated the turbulence as "moderate.” The parameters for the “light” level of turbulence were set to one-half of the “moderate” values. The “ambient” parameters were selected to provide a very low level of disturbance.

Table 6. Turbulence model configurations.

Turbulence Level	CETI Model Parameters		
	U_0 (ft/s)	σ_{v} (ft/s)	σ_{w} (ft/s)
Moderate	60.0	8.5	6.5
Light	30.0	4.3	3.3
Ambient	13.3	1.9	1.5

Tiltrotor CETI Turbulence Model

The standard CETI model described previously was initially applied to the LCTR and LCTR2 tiltrotor models used in the simulation testing in references [13–15] by applying gust inputs to the bare-airframe pilot control inputs (i.e., the symmetric and anti-symmetric collective and longitudinal cyclic swashplate inputs) because these were the primary mechanisms for heave, roll, pitch, and yaw control. Although adjudged by experimental test pilots to provide a functional representation of aircraft motion in a turbulent flow field, it is limited to these four primary axes of control. The translational response is of a second-order relative to the attitude. For use in evaluating the TRC control response types, it was desirable to have the capability to disturb the lateral and longitudinal translational degrees of freedom directly.

The CETI model was therefore recast to be consistent with rotorcraft configurations of multiple main rotors—for use with the LCTR2 in the simulation experiment in reference [16]—recalling that the helicopter roll, pitch, and heave responses to atmospheric turbulence are heavily dominated by the response of the rotor, that is, the rotor force and moment reactions to a vertical velocity gust field. Thus, the new CETI approach relied on two sets of three equations, Eqs. (34), (35), and (36), one for each rotor, governing the equivalent nonrotating frame blade pitch inputs (i.e., the lateral, longitudinal, and collective pitch inputs) required to generate the simulated aircraft response to atmospheric turbulence:

$$\frac{\theta_{1c}}{W_n} = K_1 \sigma_w^x \sqrt{\frac{U_0}{\pi \ell_w}} \cdot \frac{1}{s + \frac{U_0}{\ell_w}} \cdot f_2(s) \tag{34}$$

$$\frac{\theta_{1s}}{W_n} = K_1 \sigma_w^x \sqrt{\frac{U_0}{\pi \ell_w}} \cdot \frac{1}{s + \frac{U_0}{\ell_w}} \cdot f_2(s) \tag{35}$$

and

$$\frac{\theta_0}{W_n} = K_0 \sigma_w^z \sqrt{\frac{3U_0}{\pi \ell_w}} \cdot \frac{s + 20\frac{U_0}{L_w}}{\left(s + .63\frac{U_0}{\ell_w}\right)\left(s + 5\frac{U_0}{\ell_w}\right)} \cdot f_2(s) \tag{36}$$

Same as in the standard model, ℓ_w is the vertical characteristic wave length, taken here to be equal to the rotor radius; σ_w is the wind speed standard deviation in the vertical direction; K_0 and K_1 are overall scaling coefficients; and x and z are atmospheric scaling exponents.

Extensive tuning of these parameters was performed with the project pilot, until satisfied that the turbulence response felt realistic and overall task workload and difficulty was comparable to the earlier CETI models—while providing disturbances in all six degrees of freedom, and ostensibly, a more representative approach. The results from this process are presented in the following discussion.

Comparison to Standard CETI Model and Discussion

One of the primary differences with the standard approach applied to the LCTR2 was the introduction of coupled responses. That is, the independent collective rotor responses to atmospheric gusts naturally resulted in both heave and roll responses. Similarly, the longitudinal cyclic rotor responses resulted in the coupling of pitch and yaw. Axes were not independently tunable as with the standard CETI model. Only two scaling constants, K_0 and K_1, were available to be tuned, along with the mean wind speed, U_0. The wind speed standard deviation parameter and the related exponents were selected to be consistent with the moderate level of turbulence from Table 6.

The second difference was the capability of the model to generate significantly larger lateral and longitudinal translational disturbances. This is illustrated by the Root-Mean-Square (RMS) values of the velocities shown in Table 7 for the new model configured to match the heave response of the standard CETI implementation ($U_0 = 60$ ft/s). Note, however, the similar attitude and rate RMS values. One further observation from analysis of the LCTR2 turbulence response time histories (not shown) was the tendency for the tiltrotor-specific implementation to drift away from the initial position, while the standard implementation tended to oscillate around, but not deviate from, its initial trim position. This particular behavior of the modified CETI model was considered to be more consistent with the expected response of an attitude-stabilized rotorcraft freely suspended in a turbulent flow field without position hold, and was reflected in the larger RMS values for X and Y positions shown in Table 7. These characteristics, combined, had the effect of inordinately increasing the task difficulty.

After a systematic tuning of the new model by the project pilot, the final configuration parameter set had the scaling constants, K_0 and K_1, and the mean wind speed parameter, U_0, all reduced to one-half of their initial values (i.e., U_0 was set to 30 ft/s (Table 7), K_0 to 0.0192, and K_1 to 0.0616). Table 7 illustrates the significant reduction in amplitude of the longitudinal and lateral velocity RMS, and related attitude and rate disturbances relative to the initial tiltrotor CETI parameter set. Although this final CETI configuration exhibited significantly larger translational disturbances relative to the standard CETI configuration, the overall workload was deemed comparable after factoring the reduced attitudinal disturbances. This was an important experimental aspect in order to retain consistency with prior evaluations. Comments by the evaluation pilot clearly indicated noticeably “higher workload in the lateral axis” for higher parameter gain sets.

Analysis of the auto-spectra from simulation time histories, shown in Figures 10–15, confirmed the reduction of the high-frequency content, compared to the standard CETI approach applied to the LCTR2. Note that in tuning the model, the pilot achieved a near perfect match of the roll and pitch rate auto-spectra over the low-frequency range (below 1 rad/s). The lateral velocity auto-spectrum was also closely approximated over this frequency range, and a slight reduction in the amplitude of the longitudinal velocity was observed. The heave and yaw perturbations both saw noticeable reductions in amplitude across the frequency spectrum. This specific agreement of the pitch and roll attitude rates, for frequencies up to 1 rad/s, suggests the project pilot was most sensitive to these, along with the lateral and longitudinal velocities, while heave and yaw had less impact.

Table 7. Comparison of LCTR2 turbulence response RMS for various CETI models.

State	Units	Standard CETI ($U_0 = 60$ ft/s)	Tiltrotor CETI ($U_0 = 60$ ft/s)	Tiltrotor CETI ($U_0 = 30$ ft/s)
u	ft/s	0.2339	0.5484	0.311
v	ft/s	0.3382	0.7759	0.4438
w	ft/s	0.4575	0.4577	0.1881
p	deg/s	1.7397	1.3163	0.5000
q	deg/s	0.7193	0.7852	0.2817
r	deg/s	0.4186	0.3530	0.1187
ϕ	deg	0.6567	0.6305	0.3205
θ	deg	0.3512	0.4533	0.1649
X	ft	1.5026	12.3	3.283
Y	ft	1.0639	5.861	5.0641

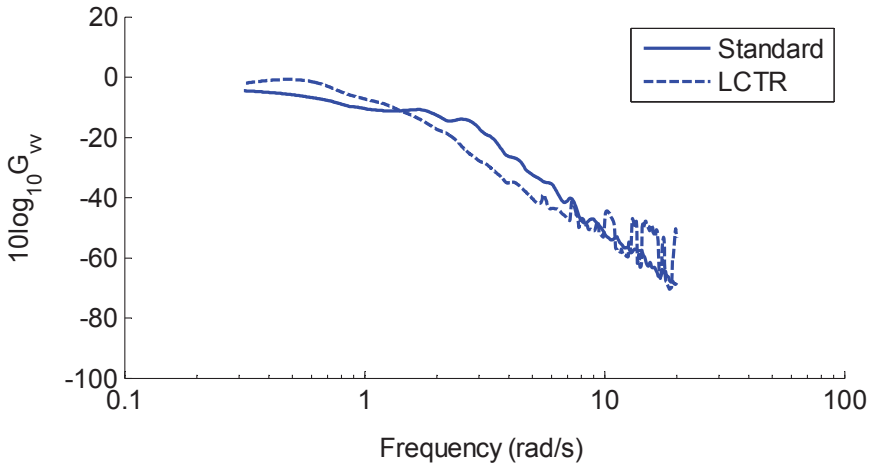

Figure 10. Lateral velocity auto spectrum comparison for the standard and tiltrotor CETI model implementations on the LCTR2 (ACAH).

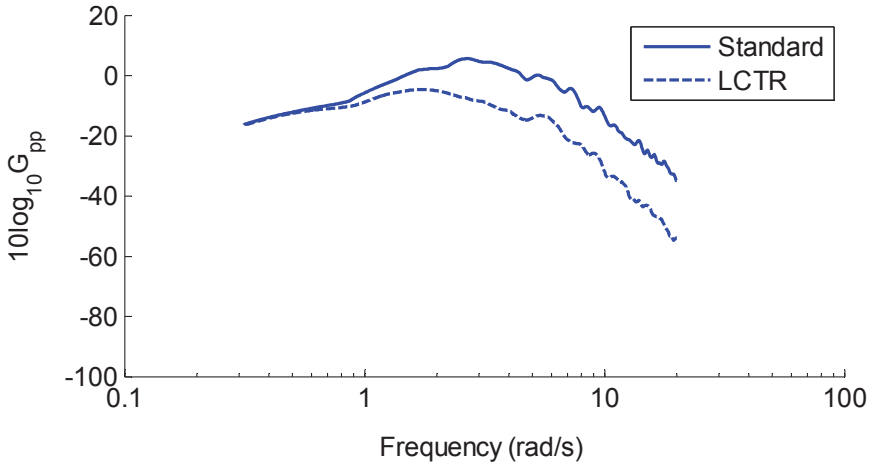

Figure 11. Roll rate auto spectrum comparison for the standard and tiltrotor CETI model implementations on the LCTR2 (ACAH).

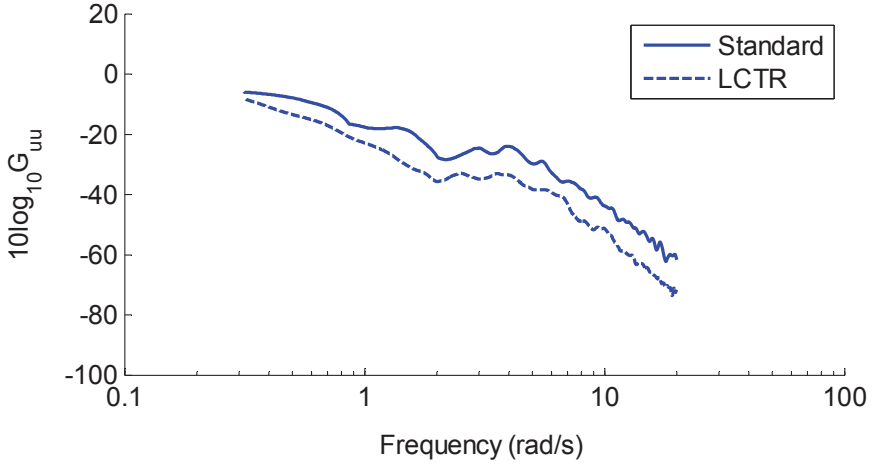

Figure 12. Longitudinal velocity auto spectrum comparison for the standard and tiltrotor CETI model implementations on the LCTR2 (ACAH).

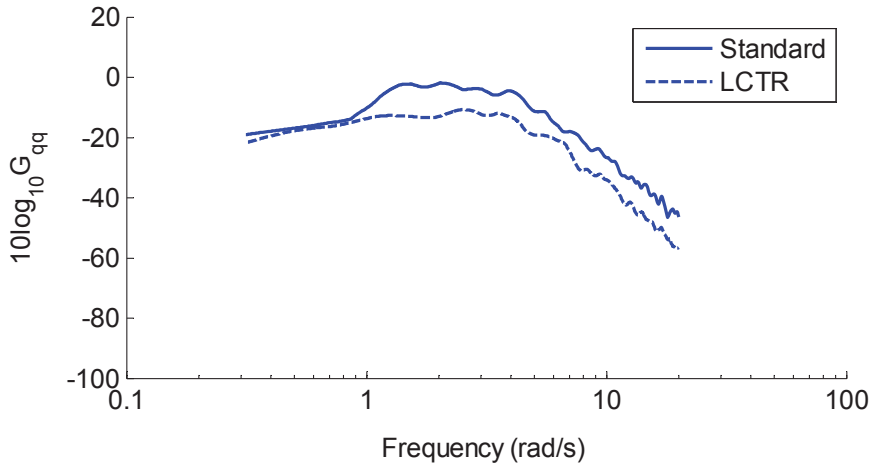

Figure 13. Pitch rate auto spectrum comparison for the standard and tiltrotor CETI model implementations on the LCTR2 (ACAH).

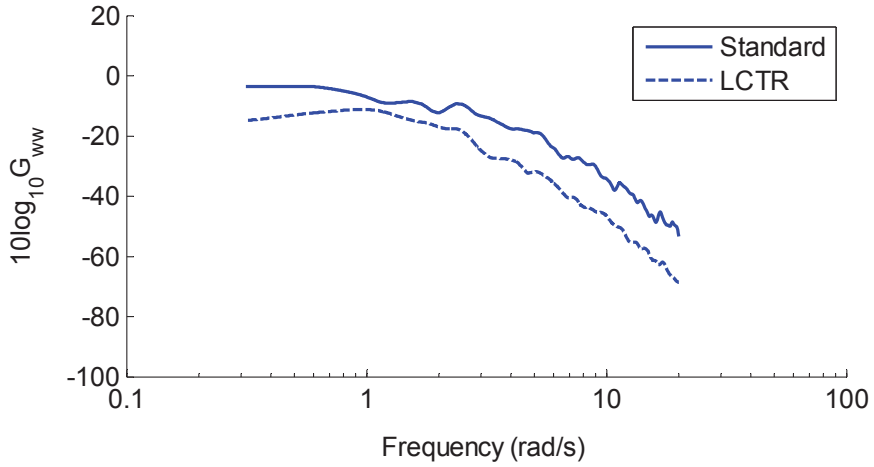

Figure 14. Heave velocity auto spectrum comparison for the standard and tiltrotor CETI model implementations on the LCTR2 (ACAH).

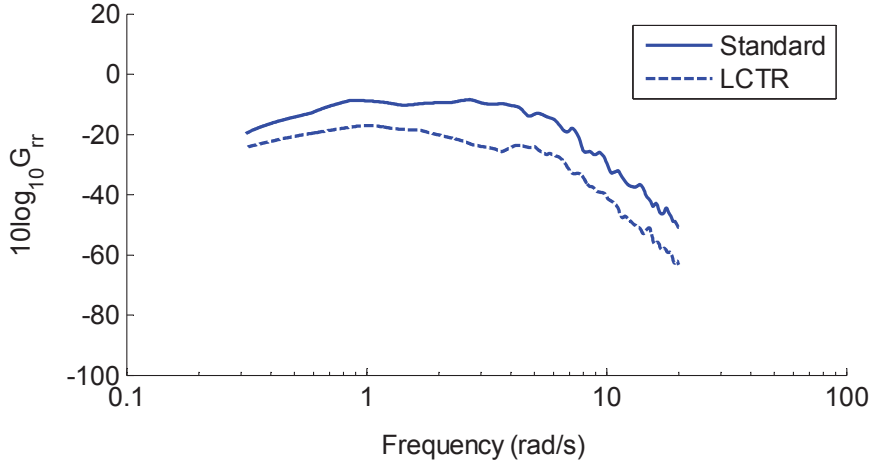

Figure 15. Yaw rate auto spectrum comparison for the standard and tiltrotor CETI model implementations on the LCTR2 (ACAH).

Simulation Facility

The piloted experiments documented in this report were conducted in the NASA Ames Vertical Motion Simulator (VMS) [31], illustrated in Figure 16. The Transport Cab (T-Cab) cockpit was employed for its large (220 deg) field of view as seen in Figure 17. The T-Cab has dual pilot seats mounted in the cab and seven image-presentation "windows" to provide outside imagery. The visual imagery was generated using an 8-channel Rockwell-Collins EPX 5000 Image Generator. The visual delay of this system has been measured as 48 ms. The Moffett Field database is carefully tailored to contain adequate macro-texture (i.e., large objects and lines on the ground) and light cues for the determination of the rotorcraft position and heading with reasonable precision. This visual database was modeled after the flight tests in references [32,33]. Aural cueing is provided to the pilot by an Advanced Simulation Technology Inc. (ASTI) sound generator and cab-mounted speakers. Airspeed and rotor thrust, primarily, are used to model aural fluctuations.

The T-Cab features traditional helicopter center stick and pedal pilot control inceptors for the evaluation pilot position in the right cockpit seat. An experimental tiltrotor Thrust Control Lever (TCL), shown in Figure 18, was used primarily for the vertical rate control. The exception to this was the first experiment [13], in which a conventional collective grip inceptor was used. Pilots could manually adjust the friction coefficient on the TCL to their preference. Main inceptor forces, in terms of gradients, breakouts, damping, and friction are provided by a hydraulic McFadden variable force-feel system. The various force-feel characteristics for the experimental rotorcraft configurations are listed in Table 8. Figure 18 also shows an experimental thumb stick inceptor [15] configured in place of the more conventional thumb wheel used for control of the nacelle position in currently operational tiltrotor aircraft. The thumb stick functioned as a miniature, dual-axis joystick. If released after displacement, it returned back to center using a linear, fixed spring constant. Also shown in Figure 18 is a “rocker switch,” employed to deploy the nacelle to the next stop within a sequence of predetermined discrete angular positions, both in its downward (forward) and upward (backward) motion. The complete functionality of the rocker switch and its experimental use is covered in reference [15].

The primary flight display and the horizontal situation (hover) display, replicating the Army’s Common Avionics Architecture System (CAAS) displays, were provided on the instrument panel. A nacelle position indicator showing current position and direction of motion, and discrete position stops was added to these displays (Figure 19).

Evaluation Tasks and Procedures

For each experiment, the pilots were required to complete sessions to familiarize themselves with the experiment objectives, methodology, Mission Task Elements (MTEs), and baseline control configurations prior to any formal evaluations. During the formal evaluations, the aircraft control input and state data, task performance, and pilot comments were recorded. A questionnaire (included as Appendix C) was used to elicit structured pilot opinion about task aggressiveness versus performance, aircraft characteristics, and pilot workload. The pilots used the Cooper-Harper HQR scale [34], shown in Appendix C (Fig. 86), to provide a subjective evaluation of the configuration for each MTE. Pilots flew each experimental test configuration as many times as required until they felt consistent performance was achieved before formal evaluation. A minimum of three evaluation runs were then performed “for record,” after which pilot comments and ratings were collected. If pilots considered that one of the three runs was anomalous, they were free to execute additional runs to resolve the inconsistency. Task performance displays in the VMS control room presented pilot-vehicle task performance in terms of the desired and adequate standards for each MTE. This information was fed back to the pilot after each maneuver was completed, both during training and formal evaluation.

Table 8. Inceptor force-displacement characteristics.

	Cockpit Control	Rotorcraft Configuration	Gradient (lb/in)	Break-out (lb)	Friction (–)	Damping (–)
Trim Release Disengaged	Longitudinal	H-60	0.7	1.0	0.0	0.2
		H-53	0.5	0.5	0.0	0.3
		LCTR	0.9	1.0	0.0	0.3
		LCTR2	0.9	1.0	0.0	0.3
	Lateral	H-60	0.7	1.0	0.0	0.2
		H-53	0.5	0.5	0.0	0.3
		LCTR	0.7	0.6	0.0	0.2
		LCTR2	0.7	0.6	0.0	0.2
	Pedal	H-60	7.2	8.8	0.25	6.0
		H-53	7.2	8.8	0.5	6.0
		LCTR	1.0	2.0	0.0	0.5
		LCTR2	1.0	2.0	0.0	0.5
	Collective	H-60	1.5	1.0	0.0	0.0
		H-53	1.5	1.0	0.0	0.0
		LCTR	1.5	1.0	0.0	0.0
	TCL	LCTR	0.0	0.0	Selectable*	0.0
		LCTR2	0.0	0.0	Selectable*	0.0
Trim Release Engaged	Longitudinal	H-60	0.0	0.0	0.75	0.0
		H-53	0.0	0.0	0.75	0.0
		LCTR	0.0	0.0	0.3	0.0
		LCTR2	0.0	0.0	0.3	0.0
	Lateral	H-60	0.0	0.0	0.6	0.0
		H-53	0.0	0.0	0.6	0.0
		LCTR	0.0	0.0	0.7/0.3†	0.0
		LCTR2	0.0	0.0	0.3	0.0
	Pedal	H-60	0.0	0.0	0.5	6.0
		H-53	0.0	0.0	0.5	6.0
		LCTR	0.0	0.0	0.75	0.0
		LCTR2	0.0	0.0	0.75	0.0
	Collective	H-60	0.0	0.0	3.7	0.0
		H-53	0.0	0.0	3.7	0.0
		LCTR	0.0	0.0	2.0	0.0
	TCL	LCTR	0.0	0.0	Selectable*	0.0
		LCTR2	0.0	0.0	Selectable*	0.0

† Value was set to 0.3 for the second experiment.
* Default value is 2.4. Pilots were allowed to adjust to their preference.

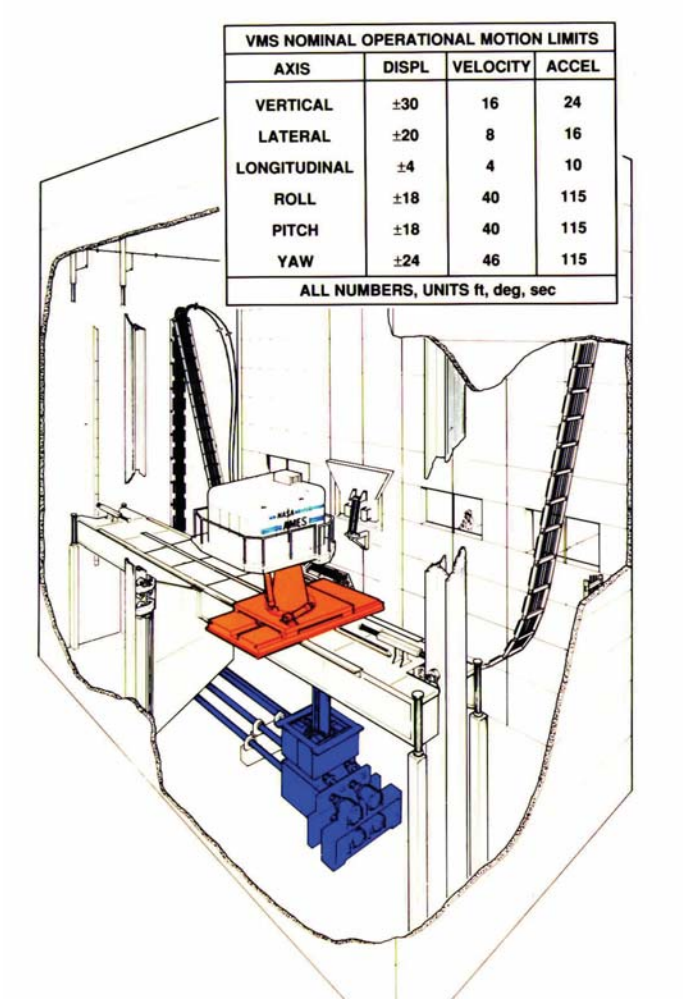

Figure 16. Vertical Motion Simulator (VMS).

Figure 17. VMS two-seat transport cab overview.

Figure 18. Thrust Control Lever Grip. Center rocker switch controls discrete nacelle movement. The thumb stick is a two-axis proportional controller. Used with TRC, the stick provides an alternative to center stick inputs for longitudinal and lateral speed control. In ACAH, the thumb stick controls fore and aft nacelle rate, proportional to control displacement, up to a maximum of 7.5 deg/s.

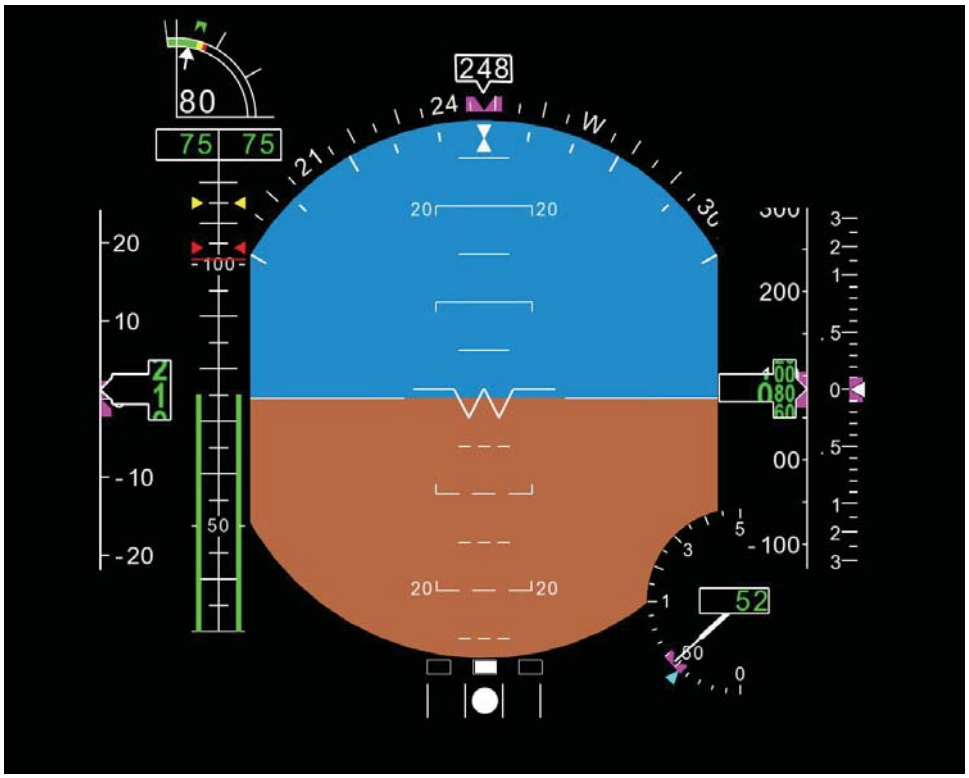

(a)

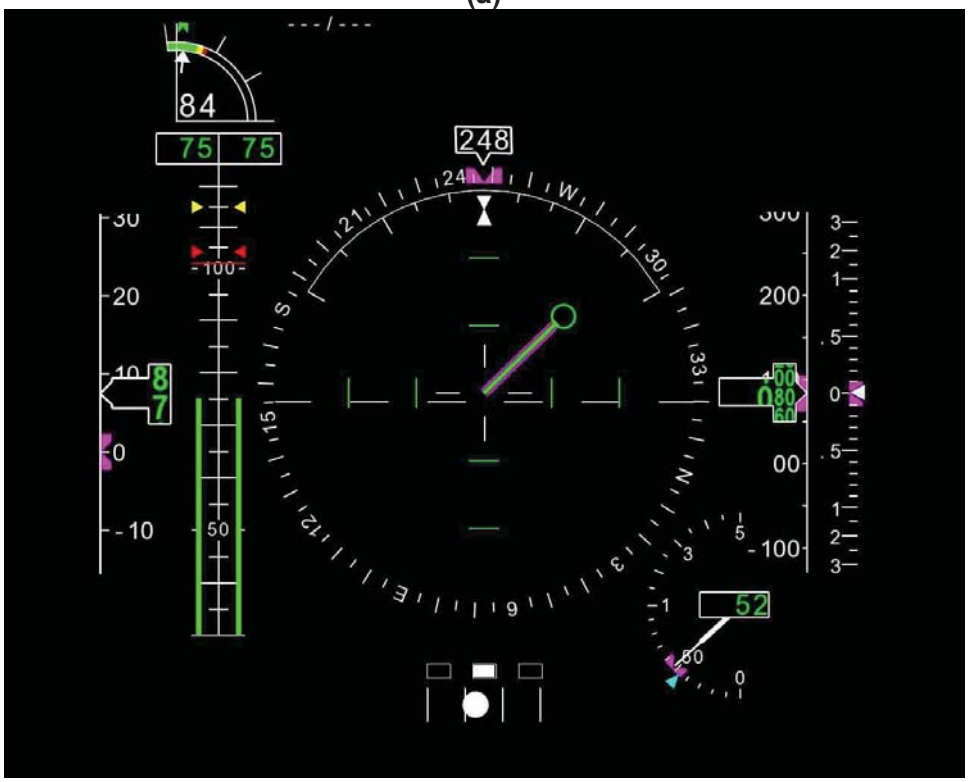

(b)

Figure 19. NASA Ames VMS emulation of the CAAS displays with a nacelle position indicator (top left): (a) Vertical Situation Display, and (b) Horizontal Situation Indicator-Hover page (magenta commanded velocity shows under actual velocity vector when using TRC).

Evaluation Tasks

The evaluation tasks included, or were derived from, a number of the hover and low-speed MTEs from ADS-33. Specifically, these were the Hover, Lateral Reposition, Pirouette, Hovering Turn, and Depart/Abort MTEs. However, the majority of the data were predominantly collected in the Hover and Lateral Reposition MTEs. From early training and initial evaluations, it was found that these two maneuvers, and in particular the Hover MTE, best exposed potential differences in the configurations. The Hovering Turn MTE was employed specifically for the purpose of evaluating the yaw response characteristics for the LCTR. The ADS-33 cargo/utility maneuver performance standards were used in general, except when specifically noted for the LCTR or LCTR2. For these two large tiltrotor models, some refinements to the Hover MTE performance standards were necessary, as it was found during the initial phase of the simulation that the cargo/utility maneuver performance standards were too "tight" and aggressive for this large of an aircraft. The developments towards more acceptable and appropriate standards for this large aircraft are discussed in the following section. The existing cargo/utility performance standards for the Lateral Reposition MTE were found acceptable for the LCTR and LCTR2 configurations and were employed as such in the disturbance rejection bandwidth (DRB) and stability margin trade-off study. Subsequent revisions to the Lateral Reposition MTE were aimed at reducing the speed requirement from 35+ knots to 15+ knots ground speed for use in the assessment of TRC control. Accordingly, completion times were redefined at 25 s for *desired* performance and 30 s for *adequate*. Finally, the LCTR and LCTR2 configurations, with their large offset between the pilot station and the aircraft center of gravity, called for special modifications of the Hovering Turn MTE standards and evaluation procedures, which are also described in the following section.

MTE Development

The LCTR2 configuration, in particular, has a rotor tip-to-tip span on the order of 150 ft plus a number of components (e.g., engine exhaust and tail) exposed to a hypothetical ground strike. The LCTR is a somewhat larger configuration, and future military tiltrotors could likely be even larger. This prompted altitude changes to the evaluation tasks to ensure realistic safety margins for ground clearance. Both the Hover and Lateral Reposition MTE altitudes were raised to 50 ft with consequent reduction noted by the pilots in the visual cues both in field of view and reduced resolution of the ground surface texture.

Furthermore, there was a sense by the evaluation pilots that the ADS-33 cargo/utility Hover MTE performance standards were "disproportionately constraining" for the LCTR, specifically. In particular, the tolerances for the lateral and longitudinal position deviations (±3 ft) and altitude deviations (±2 ft) in the stable hover were considered too "tight" and aggressive. Using the baseline LCTR configuration, several pilots evaluated a range of standards: lateral-longitudinal positions deviations included ±3, ±4, ±5, and ±10 ft. The task altitude deviations were varied proportionately and included ±2, ±3, ±4, and ±6 ft. The ±10 ft was considered too large. The ±5 ft was also considered a little larger than necessary. The pilots ultimately deemed the ±4 ft lateral-longitudinal position deviation and ±3 ft altitude deviation were appropriate for the limits of *desired* performance. *Adequate* position and altitude performance limits were set at double the desired limits, i.e., ±8 ft and ±6 ft, respectively. All other cargo/utility Hover MTE standards remained unchanged for the LCTR configuration. These performance changes effectively reflect a 25-percent increment in the lateral-longitudinal position requirements and a 50-percent increment in the altitude requirements.

The 2008 experiment (see Table 1) pointed to the need for a formal evaluation of yaw response characteristics for large hovering aircraft. A project pilot using a series of 180 deg pedal turns evaluated the yaw axis response for that experiment. For the formal evaluations conducted in the 2009 study, an early effort was the development of a formal yaw evaluation task (MTE definition). The initial yaw evaluation task proposed required a complete, 360 deg

turn about the pilot station. This task was dismissed quickly because of lack of appropriate visual cues. Pilots found the workload in the lateral and longitudinal channels to be extreme, masking the yaw characteristics. A simple pedal hover turn was developed to independently evaluate the yaw-axis response dynamics by modifying the Hovering Turn MTE in ADS-33 for the cargo/utility category to a 90 deg turn (instead of the standard 180 deg) performed with pedal input alone, in turbulence but without steady wind. The lack of wind compensated for the lack of a hover position hold system that likely would be provided for the large aircraft size. The 90 deg heading change was sufficient for the evaluation and well supported by available visual cues. The task performance standards retained the time requirements of the standard cargo/utility MTE: 15 s for *desired*, and 20 s for *adequate* performance. This effectively halved the *desired* maximum yaw rate to 9.5 deg/s, approximately. This rate was consistent with the Limited Agility MTE category in the hover and low speed ADS-33 requirements for large-amplitude attitude changes. Although pilots were able to fly the aircraft more aggressively than this rate, this maneuver was considered to be more appropriate for an aircraft of this size, in terms of the agility required for a civil mission. Final heading capture tolerances were set at ±3 deg, which forced enough aggressiveness and precision from the pilots to evaluate the different issues at hand.

VMS Cabin Orientation

The VMS cabin has the ability to have either its longitudinal or lateral axis be oriented with the motion system's axis of greatest horizontal motion. This allows the engineer to control which axis has a greater range of motion and therefore to confer larger and more sustained acceleration cues. Naturally, for the Lateral Reposition MTE, the primary direction of the maneuver of interest is sideward motion, and thus the cab was oriented with the lateral axis along the beam for evaluation. This was also the orientation for the Hovering Turn MTE. The Hover MTE, however, could be performed with either orientation, since it does not have a dominant axis of motion. In the early piloted experiments, the orientation was restricted to the cab lateral axis aligned with larger horizontal motion axis (denoted crossbeam). Later in the research program, when the LCTR2 TRC control laws were tested, it became apparent that the longitudinal axis of the aircraft response was the critical axis of interest; subsequent Hover MTE evaluations were executed with the VMS cab oriented with the longitudinal aircraft axis along the beam to provide a greater range of longitudinal motion and potentially more compelling cues, thus offering increased simulation fidelity.

Evaluation Pilots

Evaluation test pilots with diverse experience backgrounds were drawn from a variety of government and private organizations including the U.S. Army, the U.S. Navy, the German Army (Wehrtechnische Dienststelle 61, WTD-61), NASA, and rotorcraft industry. A minimum of 5, and up to a maximum of 10 pilots, including the project pilots, participated in each of the piloted experiments for a total of 20 evaluation pilots (see Table 9). All pilots had extensive rotorcraft experience ranging from light utility, single main rotor helicopters to medium and heavy lift tandem helicopters. An emphasis was given to the selection of pilots with significant experience in either large helicopters or tiltrotors. A total of six pilots were highly experienced tiltrotor test pilots. Also, nine evaluation pilots participated in more than one of the experiments (with two participating in all four experiments) and therefore achieved a higher familiarity with the aircraft, simulator, and general experimental procedure and some of the issues associated with it. This provided a level of continuity between the various experiments in the series. Conversely, not all pilots returned, and new pilots contributed to experiments, continually expanding the diverse breadth of backgrounds and piloting techniques to provide a widely representative sampling group. All were experienced test pilots, familiar with the use of the Cooper-Harper Handling Quality Rating scale and the ADS-33 MTE evaluation tasks.

Table 9. Summary of participating evaluation pilots.

Year	Description	Number of Pilots		
		Total	Tiltrotor	Large Rotorcraft
2008	Stability margin and disturbance rejection trade-off investigation	10	3	7
2009	Large rotorcraft short-term response handling qualities requirements study	5	2	4
2010	Low-speed LCTR2 handling qualities investigation	10	2	8
2011	Evaluation of TRC requirements on handling qualities for LCTR2	7	4	5

Simulation Results

Overview

The results presented in this section illustrate the fundamental influence of aircraft size on the handling quality requirements of rotorcraft in hover and low speed. The organization of the results is driven by two fundamental facets: the first centered on the effect of aircraft dynamics and the role of gross weight, and the second on the impact of vestibular and visual cueing associated with pilot station location. The first set of results correspond to the investigation into the effect of rotorcraft size on the flight control system feedback stability and disturbance rejection handling quality requirements for Attitude Command-Attitude Hold (ACAH) type responses. Results for three rotorcraft weight classes are presented: medium, heavy, and ultra-heavy. These were respectively represented by H-60, H-53, and LCTR models. Subsequent results primarily deal with the second aspect of rotorcraft size, the effect of pilot station location and the influence of the response type. These results include those from a comprehensive piloted investigation of the ACAH response type short-term handling quality requirements for the LCTR concept aircraft, as well as the results from a systematic evaluation of a TRC response control system for the LCTR2.

Flight Control Requirements Connected With Large Rotorcraft

The handling quality requirements embodied in the U.S. Army's Aeronautical Design Standard–33 (ADS-33) [10] are the basis for military rotorcraft flight control design in the U.S., such as on the fly-by-wire UH-60MU [33], and internationally on the NH-90 [35]. Key among quantitative requirements are metrics associated with the attitude response to piloted stick inputs such as bandwidth, phase delay, short-term response damping, and quickness. The same requirements effectively translate to the design of civilian aircraft, such as the S-92 helicopter [36]. In addition to providing satisfactory response to piloted inputs, the flight control system must also reject responses due to disturbances and provide for an inherently stable platform with satisfactory margins to address both variations in flight conditions and uncertainties in dynamic response. The current guidance in ADS-33 on disturbance rejection requirements is inadequate and does not include explicit requirements on stability margins. The U.S. Army Aeroflightdynamics Directorate (AFDD) has developed and flight-test validated a disturbance rejection bandwidth (DRB) metric that is directly analogous to the piloted bandwidth metric [37]. Increased DRB, associated with higher feedback levels, is desirable for flight operations in degraded weather and visibility, but is accompanied by reduced stability margins and increased actuator activity [18]. This metric has been found to be well suited to flight control design and flight testing, and proposed criteria values for inclusion in ADS-33 have been published [19]. While ADS-33 has no direct requirements on stability margin, the minimum mid-term control response damping ratio requirement of $\zeta \geq 0.35$ (for modes below the bandwidth frequency) can be interpreted as a 35 deg phase margin requirement for an equivalent second-order system [38].

Refinements to the U.S. Department of Defense (DoD) specification for air vehicle flight control systems, MIL-9490, incorporated in SAE 94900, require a phase/gain margin of not less than 45 deg/6 dB for the worst-case flight condition and at least half these margin levels in the presence of uncertainties of up to 20 percent in the dominant stability and control derivatives. Adequate margins are needed to help ensure that: the flight control system is robust to expected variations in flight condition that are not gain-scheduled (e.g., center of gravity, weight, turn rate, etc.) and modeling uncertainties in the design process—has some margin for future expansion of the flight envelope; and there are no detrimental effects due to flight control hardware degradation over the life of the aircraft. Ensuring adequate stability margins is also beneficial by keeping potentially adverse dynamics associated with rotor/body coupling and coupled structural/flight control response outside of pilots' frequency range, thus preventing a

key potential trigger for pilot-induced oscillations [39]. The current minimum stability margin requirements of SAE 94900 are not well supported with published data. Rather, these are generally based on historical rules of thumb and can be considered conservative. Lower margins might be acceptable and allow for tighter disturbance rejection, but the handling-quality implications are not well understood.

In the CH-47F Digital Automatic Flight Control System (DAFCS) development program [40], good handling qualities were obtained for roll-axis disturbance rejection even though this resulted in reduced stability margins (about 30 deg) as compared to 94900. A waiver for reduced stability margin has also been granted for flight control design of the CH-53K when carrying external loads in order to achieve acceptable feedback loop performance [41]. It is expected that this fundamental trade-off between satisfactory disturbance rejection performance and stability margin will become more acute as rotorcraft increase in size and associated control power becomes more limited. The first set of results and analysis presented in this section attempts to address these considerations and make the link between achievable disturbance rejection, the associated stability margins, and handling qualities.

Response Type Augmentation

Another key aspect of a control law is the short-term response characteristics to pilot commands. The handling qualities requirements set forth in ADS-33 for the fundamental short-term (small amplitude) pitch, roll, and yaw attitude response requirements are well supported for currently flying helicopters ranging in size up to cargo class, but their direct applicability to significantly larger rotorcraft such as the LCTR2 has yet to be established. The two key parameters that guide the small amplitude requirements are the attitude bandwidth and phase delay. Analysis of the results presented subsequently illustrates the impact of rotorcraft size on the applicability of these criteria. In particular, experiments with the LCTR identified handling qualities issues resulting mainly from cockpit locations well ahead of the center of gravity (i.e., point of rotation) and from the impact of the reduced natural response frequencies of a vehicle with much greater moments of inertia.

The link between higher levels of control augmentation for conventional rotorcraft and improved handling qualities for nap-of-the-earth hover and low-speed precision tasks has long been well established, specifically concerning operations in degraded visual environments (DVE). In particular, advantages of Translational Rate Command (TRC) over Rate Command (RC) and Attitude Command-Attitude Hold (ACAH) response types for handling qualities improvements in degraded visual conditions are reported in reference [42]. More recently, advanced control modes with response types other than RC and ACAH have been extensively investigated for cargo class helicopters such as the CH-47F (and MH-47G) [40,43] and CH-53K [44]. These have resulted in improved handling qualities and reduced pilot workload without sacrificing the purported agility of RC. An early piloted simulation study of TRC for a tiltrotor aircraft [45], conducted in the now-retired NASA Ames Flight Simulator for Advanced Aircraft (FSAA) motion platform, investigated actuator authority requirements for the XV-15 stability and control augmentation system (SCAS). The study was the first to exploit the tiltrotor's ability to effect longitudinal and lateral thrust vectoring via the nacelles and parallel lateral cyclic tilting of the rotors. Reduction of large attitude excursions made possible by maneuvering using vectored thrust was a major factor in the handling qualities rating (HQR) improvements in that study. Lastly, this section presents the analysis of results that investigate a form of TRC using nacelle tilt to achieve longitudinal thrust vectoring. In particular, the handling qualities impact of various TRC design parameters, such as the control response specifications (i.e., sensitivities and equivalent rise time) and nacelle tilt actuator characteristics (bandwidth, and position and rate limits) are assessed. Finally, results present design requirements to achieve Level 1 handling qualities in hover with this form of TRC, as well as methods to maintain good handling qualities for degraded nacelle actuator bandwidth values.

Design Trade-offs of DRB vs. Stability Margin

The control design optimization technique using CONDUIT® [46] was used to design families of control law configurations of varying disturbance rejection bandwidth (DRB) and stability margins for each of the three rotorcraft types described previously. Starting from a baseline Level 1 control system, which included 30 percent uncertainties in the inverse model parameters, design margin optimization [18] was used to generate cases of increasing DRB and associated reduced stability margin (and damping ratio). A constant crossover frequency was set to provide adequate model following and performance robustness to uncertainty. In the case

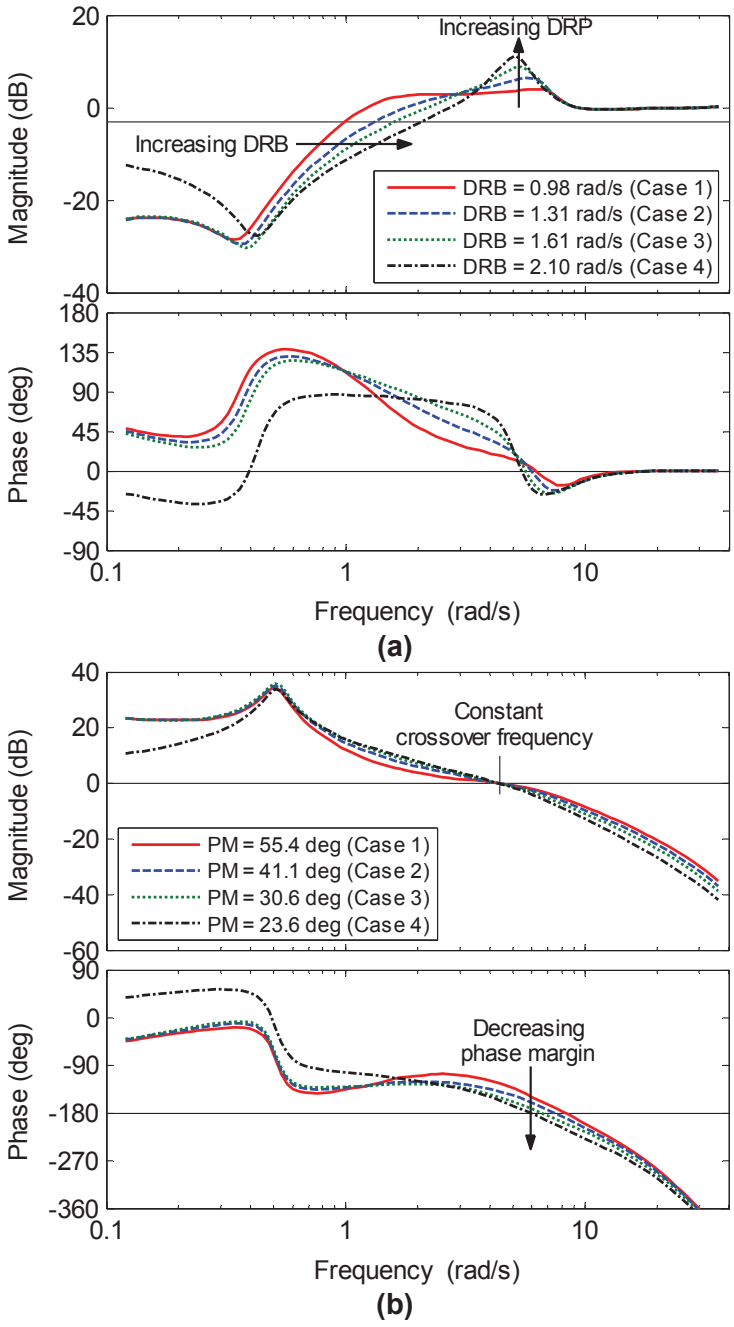

Figure 20. (a) Disturbance rejection and (b) stability margin in the lateral axis for the H-60 family of cases. An increase in DRB [arrow on (a)] is accompanied by a decrease in phase margin [arrow on (b)].

of the H-60 configuration, the baseline design was matched to that used for the UH-60M Upgrade [33]. DRB is defined as the frequency at which the magnitude of the disturbance response (y/d in Figure 8) is –3 dB. Figure 20 shows the lateral axis (a) disturbance rejection frequency response and (b) broken-loop frequency responses for the family of DRB/phase margin cases generated for the H-60. Similar families of cases were generated for the other aircraft models evaluated.

The crossover frequency was held approximately constant for all the cases. Figure 21 shows the associated roll-axis attitude and rate feedback gains for the H-60 family of cases. Increased DRB requires a significant increase in attitude gain and a slight decrease in rate gain. Figure 22 shows the responses of the four H-60 cases to (a) a pilot lateral stick input and (b) a disturbance pulse input, and demonstrates that as the DRB of the aircraft is increased, the response to disturbance is faster. However, because of the decrease in phase margin, the response is more oscillatory as well. This is also seen as an increase in the magnitude peaks in Figure 20(a) for the higher DRB configurations and the oscillatory response leads to increased actuator usage—leading to the possibility of actuator rate saturation, especially in the pitch axis. Figure 23 shows the increased actuator activity associated with increased DRB for the disturbance input shown in Figure 22(b). Note that oscillations are above the piloted bandwidth frequency, confirming that all designs meet the ADS-33 damping requirements for ACAH, i.e., the mid-term response to control inputs ($\zeta \geq 0.35$ below the piloted bandwidth frequency).

Each aircraft configuration had a family of four control laws designed for evaluation that ranged from low DRB/high phase margin (Case 1) to high DRB/low phase margin (Case 4). The piloted bandwidths and broken-loop crossover frequencies of the different cases remained approximately constant. For the different aircraft configurations, Figure 24 shows the variation in phase margin, and Figure 25 shows the variation in damping ratio as the DRB increases for (a) the roll and (b) the pitch axes. Here, the damping ratio was calculated using the logarithmic decrement method based on angular-rate responses to a pulse at disturbance input in each channel. The 45 deg phase margin line is highlighted in Figure 24. Table 10 presents a summary of pitch and roll axes DRBs, stability margins, damping ratio to disturbance and control inputs, and the control input response bandwidths and phase delays for the different aircraft configurations and flight control cases.

Table 10. Aircraft configurations and flight control system characteristics.

Aircraft Configuration	Case	DRB (rad/s)		Stability Margins (deg, dB)		Damping Ratio: Disturbance Input		Damping Ratio: Control Input		Bandwidth (rad/s)		Phase Delay (s)	
		Lat	*Lon*	*Lat*	*Lon*	*Lat*	*Lon*	*Lat*	*Lon*	*Lat*	*Lon*	*Lat*	*Lon*
H-60	1	0.98	0.56	55.4, 5.9	46.4, 9.0	0.58	0.58	1.00	1.00	4.72	3.84	0.144	0.129
	2	1.31	0.76	41.2, 5.5	37.1, 8.6	0.44	0.78	1.00	1.00	4.85	3.82	0.141	0.128
	3	1.62	0.96	30.6, 4.9	30.6, 8.3	0.20	0.38	1.00	1.00	4.86	3.78	0.138	0.126
	4	2.10	1.40	23.6, 3.9	20.4, 7.5	0.15	0.23	0.62	0.63	4.78	3.64	0.133	0.122
H-53	1	0.88	0.53	44.4, 7.0	44.3, 10.4	0.75	0.81	1.00	1.00	2.15	2.17	0.22	0.184
	2	1.03	0.66	37.9, 6.6	38.8, 10.1	0.46	0.87	1.00	1.00	2.25	2.27	0.216	0.184
	3	1.24	0.81	30.4, 5.9	32.5, 9.7	0.28	0.37	1.00	1.00	2.39	2.41	0.212	0.183
	4	1.50	1.04	20.9, 4.7	23.2, 9.0	0.17	0.30	1.00	1.00	2.69	2.62	0.207	0.182
LCTR	1	1.00	0.81	46.6, 9.1	45.5, 10.7	1.00	0.71	1.00	0.77	2.09	2.19	0.154	0.154
	2	1.24	0.98	37.3, 9.4	36.1, 10.6	1.00	1.00	1.00	1.00	2.22	2.14	0.157	0.146
	3	1.42	1.12	30.6, 8.9	30.6, 9.9	0.50	0.50	1.00	1.00	2.27	2.18	0.161	0.144
	4	1.60	1.30	21.7, 9.2	20.4, 10.0	0.25	0.25	1.00	1.00	2.79	2.19	0.159	0.117

Note: when the response is not oscillatory, a damping ratio of $\zeta = 1$ is indicated in the table.

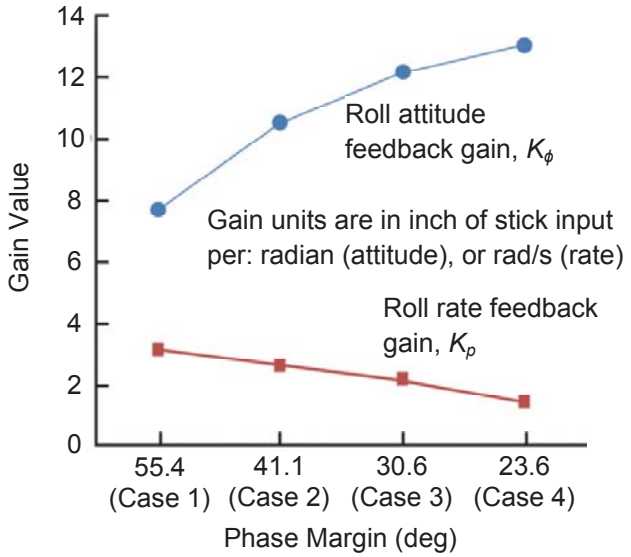

Figure 21. Variations in the roll axis feedback attitude and rate gains for the H-60 family of cases.

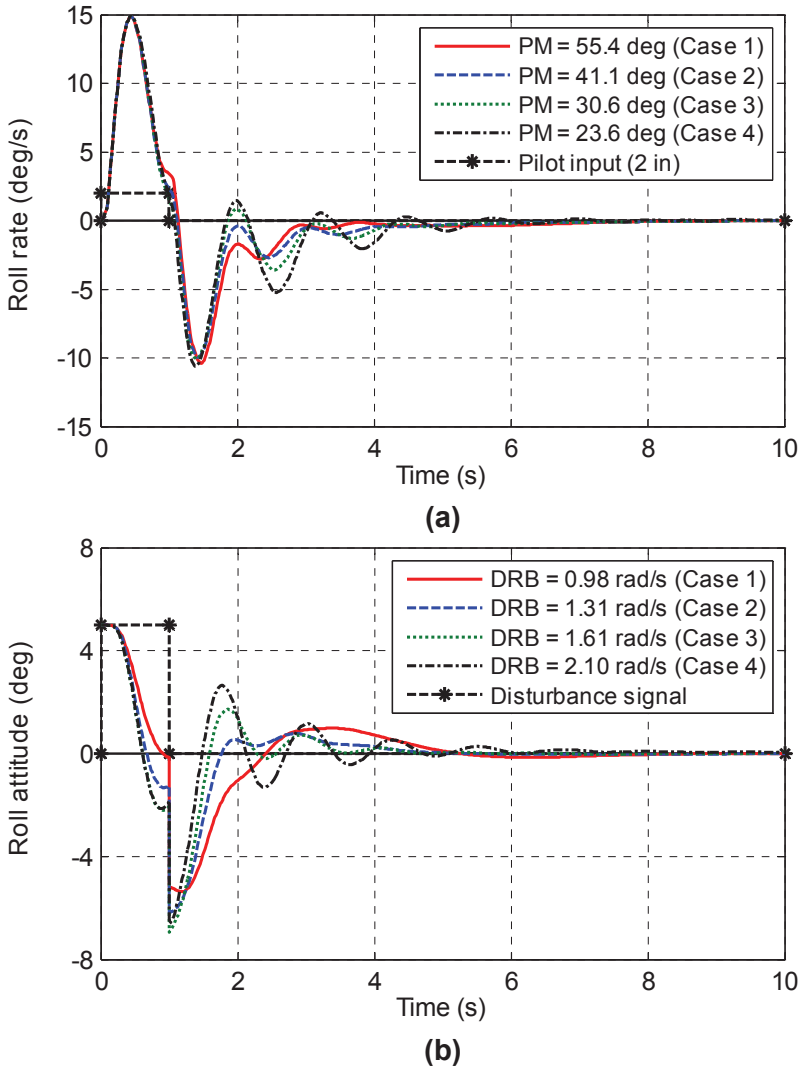

Figure 22. Time histories of (a) a lateral cyclic stick pulse and (b) a disturbance pulse in roll attitude for the H-60 family of cases.

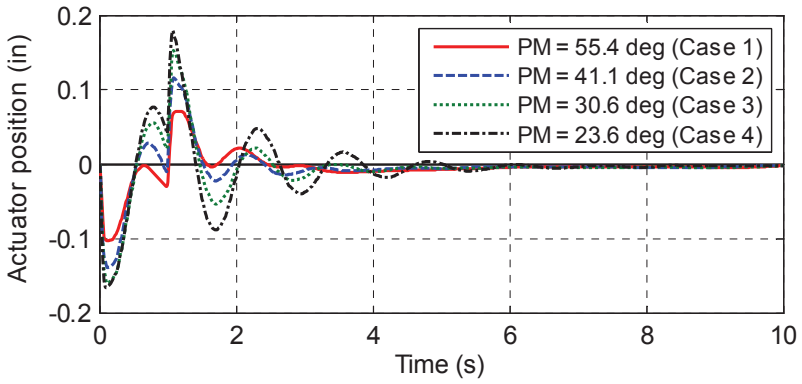

Figure 23. Lateral actuator activity for a 5 deg disturbance pulse input into roll attitude for the H-60 family of cases (actuator position limits are ±2.5 in).

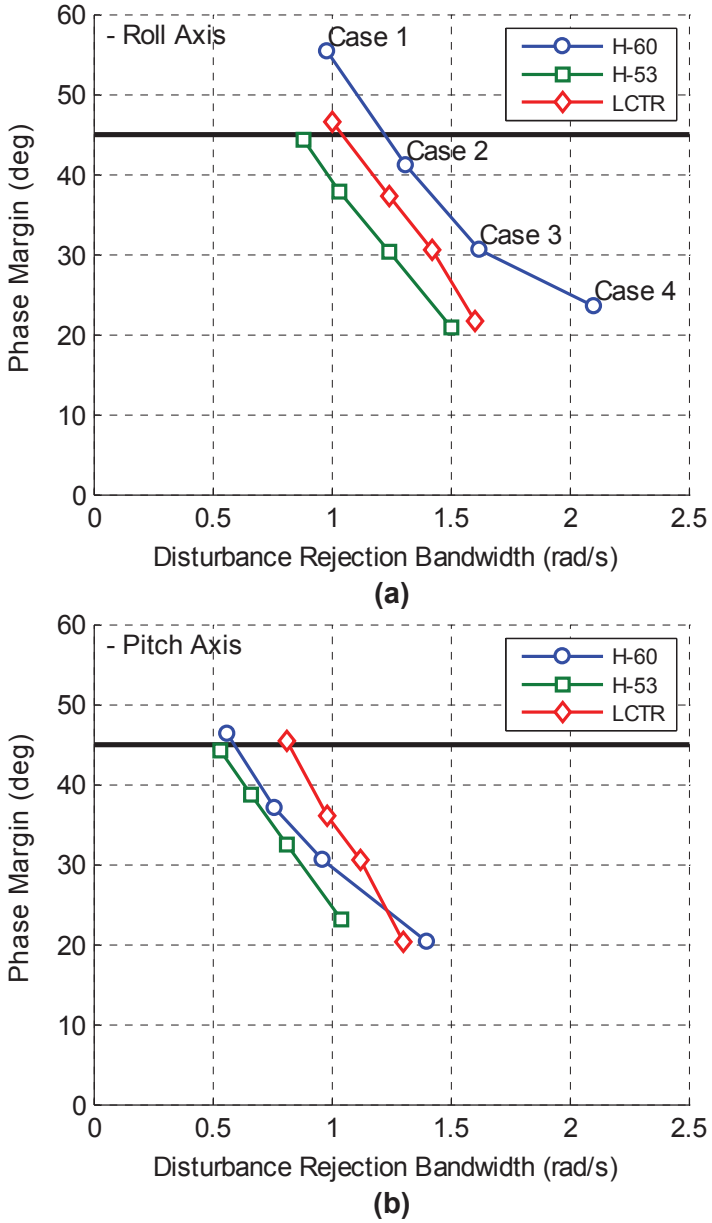

Figure 24. Stability margin vs. disturbance rejection bandwidth of the different aircraft configurations: (a) roll axis and (b) pitch axis.

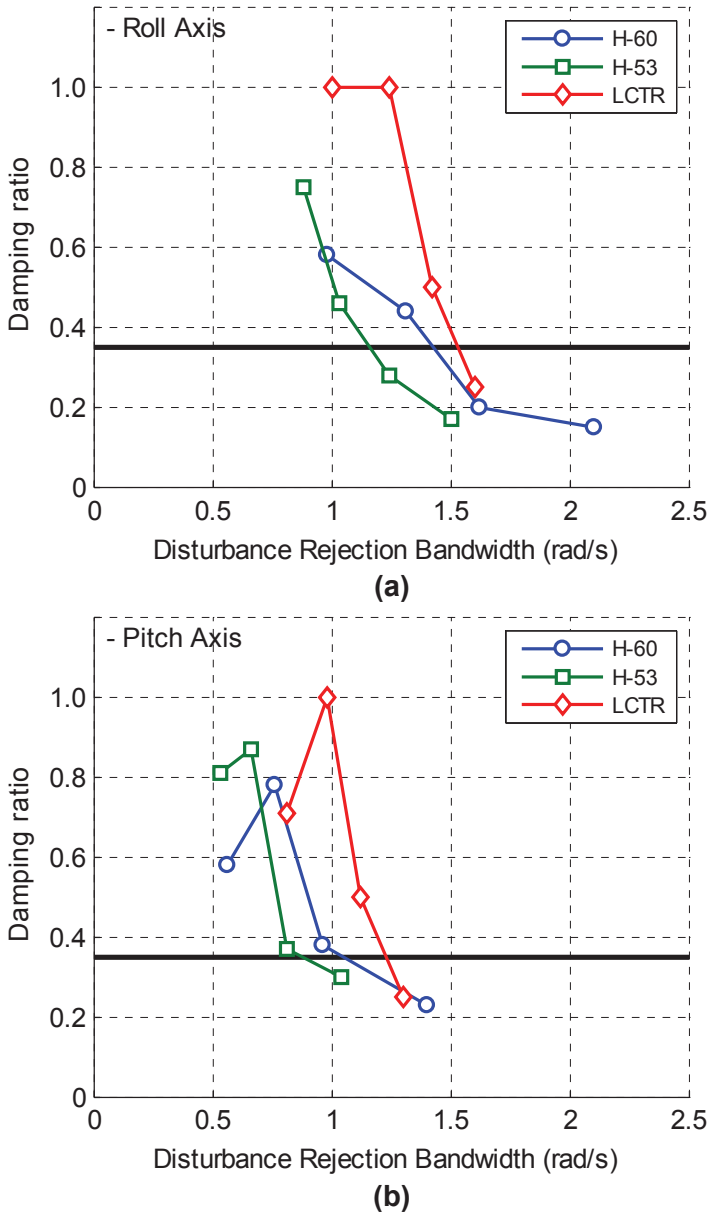

Figure 25. Damping ratio vs. disturbance rejection bandwidth of the different aircraft configurations: (a) roll axis and (b) pitch axis.

Finally, it is important to note from Table 10 that with the exception of the H-53 configuration, which needed the lateral short-term response specifications relaxed to avoid rate-limiting of the actuators, the designs not only meet the mid-term control response damping requirements discussed previously, but also satisfy short-term response bandwidth and phase delay requirements for Level 1. Although the bandwidth of the H-53 configurations was ensured to be greater than 2 rad/s, with the phase delay in the roll axis spanning the 200–220 ms range these configurations lie in the vicinity of the Level 1 handling qualities boundary for Usable Cue Environment (UCE) greater than 1 and/or divided attention operations.

Pilot Evaluations

For the Hover MTE, the averaged HQRs are shown in Figure 26 for the three aircraft configurations as functions of the control system phase margin. The bars represent the 95-percent confidence bands for the data available. The hover task required the pilot to actively

work with the control system through all three phases of the task: the 6–10 knot translation, deceleration, and 30 s station-keeping phase. The task required significant longitudinal, lateral, and heave control activity, while the yaw axis could largely be ignored. Each case was tested in multiple levels of turbulence, ranging from ambient to light to moderate, using the CETI model parameters summarized in Table 6.

The Hover MTE proved to be a Level 1 task in light turbulence that degraded to Level 2 in moderate turbulence for the H-60 and the LCTR aircraft, with little variation of the average HQR shown across the stability margin cases. The H-53 configuration was rated as Level 2 on average, irrespective of the turbulence level, but more importantly, also did not vary significantly with respect to the control system cases. The task performance did not reveal any significant differences either. Results for the LCTR configurations, however, displayed a larger variance in the ratings for each case compared to the H-60 and H-53 configurations. These aspects are discussed in more detail below.

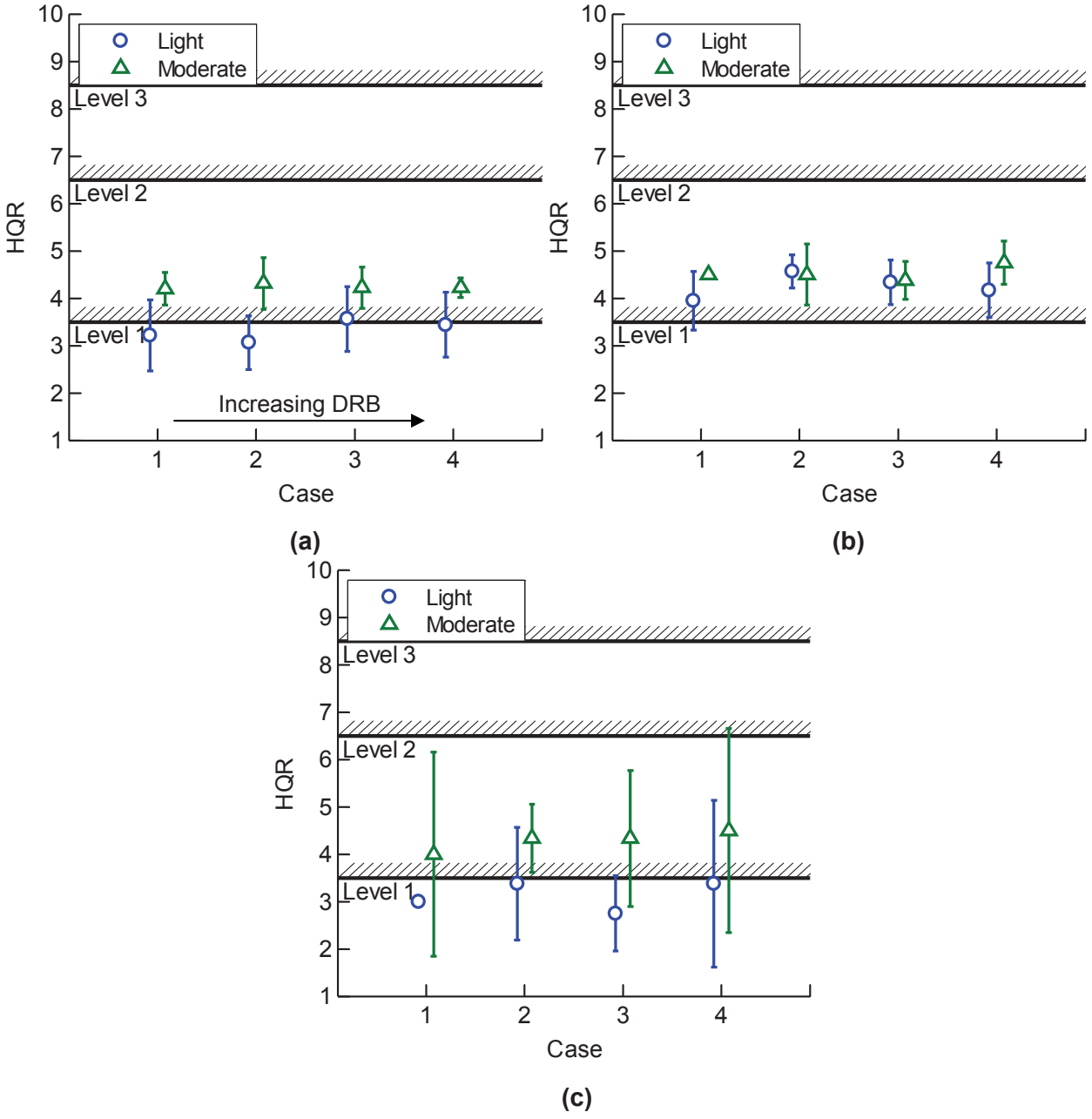

Figure 26. HQRs for Hover MTE: (a) H-60, (b) H-53, and (c) LCTR.

Results for the Lateral Reposition MTE, shown in Figure 27, mirror the trends observed for the Hover MTE evaluations, mainly that: (a) average HQRs show minimal variation across the stability margin cases, and (b) the variance of the ratings for the LCTR configuration is generally larger compared to the other configurations.

Pilot Comments on Aircraft/Task Characteristics

Two of the fundamental aircraft characteristics considered were the *oscillatory* behavior and the *predictability* of the initial aircraft response. In the absence of major differences in the HQRs, it was instructive to distinguish the different control system configurations on the basis of the pilot comments on these aircraft characteristics. Pilot comments on aircraft *oscillations* were broken down into three discrete categories: annoying or slight, objectionable or unacceptable, and propensity to pilot induced oscillation (PIO). Results were plotted in terms of the number of pilots who described a specific configuration as possessing any one of these characteristics, or,

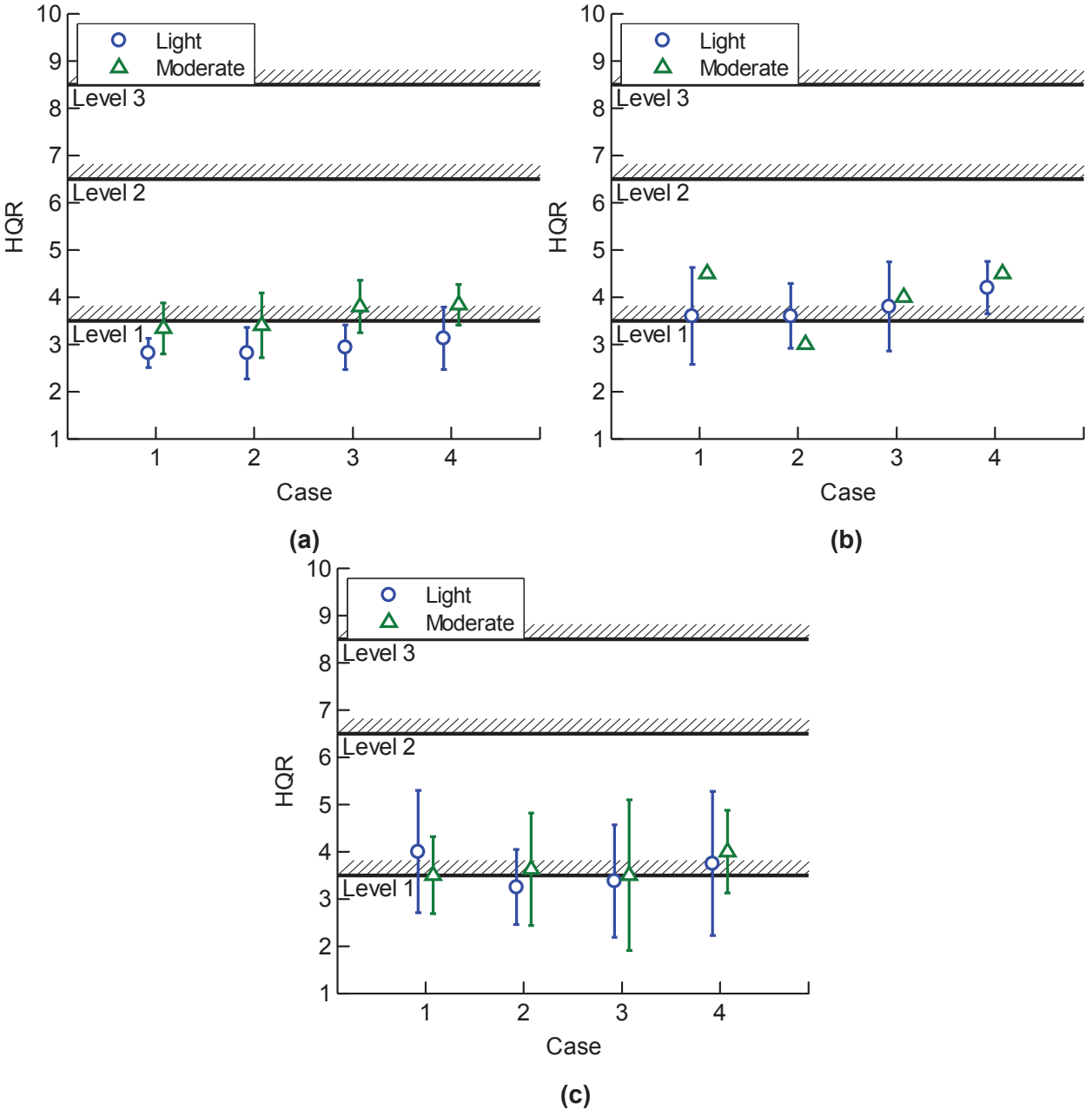

Figure 27. HQRs for Lateral Reposition MTE: (a) H-60, (b) H-53, and (c) LCTR.

alternatively, the number of times a specific configuration was characterized as such by the pilots. Note that pilot judgment represents a measure of the overall oscillatory motion of the aircraft. Pilots often found it difficult to distinguish oscillation of the aircraft induced from its response to external gusts or from oscillation resulting from pilot input. Therefore, it can be argued that pilot perception and associated commentary is an overall indicator of the fundamental trade-off between DRB and stability phase margins. Unless the pilots went hands-off, it was generally difficult for them to isolate the cause or source of the oscillations. Pilot commentary regarding the *predictability* of the initial response was expected to be binary in nature with pilots describing the initial aircraft response as "predictable" on one hand, and "unpredictable" on the other. Pilots were not always able to explicitly commit to one of the two, however. Consequently, cases described as slightly unpredictable, or less predictable (relative to the most predictable of the control system configurations), were classified as "indeterminate" for the purposes of this exercise. These results are presented for the Moderate Turbulence levels; Light Turbulence did not sufficiently excite pilot and control system activity to elicit such marked differences in the comments.

Figure 28 presents a summary of the pilot comments on aircraft oscillations for the H-60 configurations while performing the Hover MTE. Case 1 did not have any objectionable oscillation or PIO comments. Aircraft oscillatory behavior, for the lower stability phase margin cases, was considered objectionable. Case 4 was determined to be highly objectionable by the pilots and clearly the worst configuration, despite the damping ratio of the closed-loop attitude response to *pilot input* for this case being above 0.6 (see Table 10).

Figure 28 also shows the damping ratio of the response due to disturbances for both the pitch and roll axes. For Cases 1 and 2, the disturbance response damping ratios were in the range of 0.45 and higher, in both roll and pitch, whereas for Cases 3 and 4 they were closer to 0.35 and below. For the "highly-objectionable" Case 4, the disturbance response damping ratio saw the extreme low of 0.15 in the roll axis (combined with 0.23 in pitch). Comments confirmed a direct link between gust response damping specifications and mid-term response characteristics of the aircraft, for which oscillation is a prime indicator. The flight tests in reference [37] presented results consistent with those seen here, for disturbance response damping ratios of 0.45 minimum. Additional data, including flight test data, would be needed to

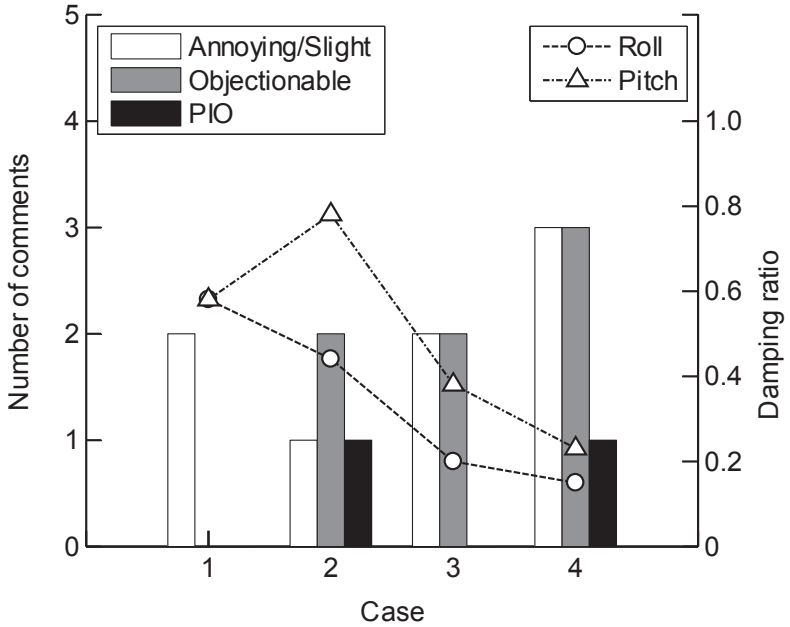

Figure 28. Pilot commentary on aircraft oscillations and damping ratio of system response due to disturbances; H-60 in moderate turbulence.

help support and anchor a mid-term gust response damping ratio criteria, however. The disturbance rejection peak (DRP) magnitude, which was recently proposed as a candidate requirement for ADS-33 in reference [47], effectively addresses the same issue, that is, to ensure good damping of disturbance response.

Pilot reports about the oscillatory nature of the aircraft in the roll axis correlated very well with the quantitative attitude and rate measurements taken during the 30 s stabilized hover portion of the Hover MTE. Figure 29 shows the roll rate Root-Mean-Square (RMS) values for the H-60 for both turbulence levels. For the moderate turbulence level, there is an increase in roll rate RMS as the stability margins decrease, supporting pilot perception of objectionable oscillations.

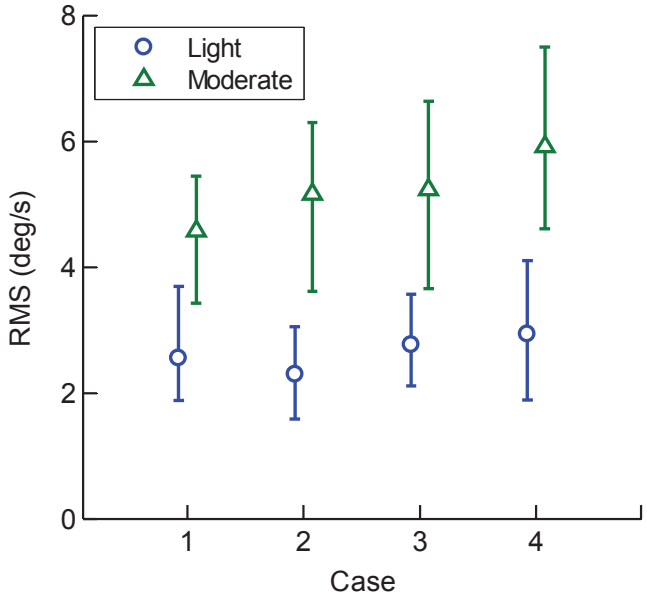

Figure 29. H-60 roll rate RMS during 30 s stabilized hover.

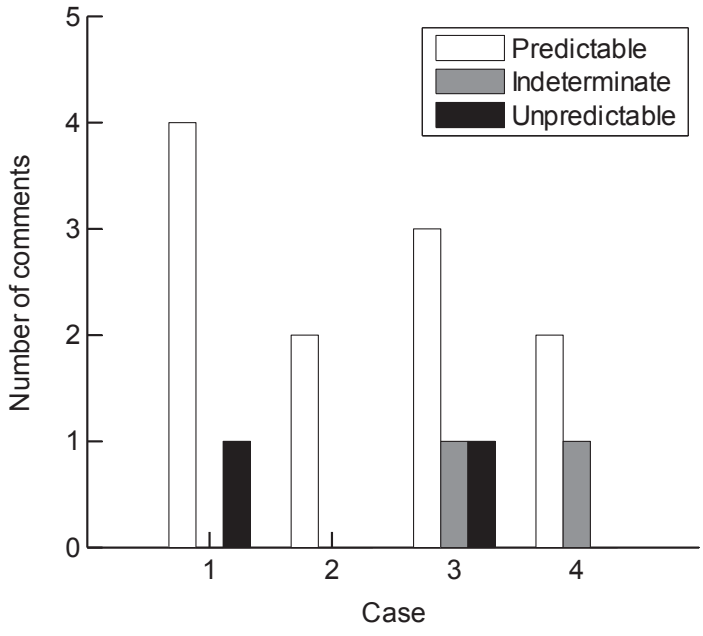

Figure 30. Pilot commentary on predictability of initial aircraft response; H-60 in moderate turbulence.

Pilot perception of the predictability of the initial response of the H-60 helicopter in moderate turbulence is summarized in Figure 30. Although Case 2 had only *predictable* comments (i.e., no negative comments), Case 1 received more favorable comments. The two *unpredictable* comments were from the same pilot, who employed a high gain approach and was consistently more aggressive in controlling the aircraft. Cases labeled as *unpredictable* were also reported to possess *crisp* or *good* response types. A strong argument could be made, based on the overall assessment of oscillation and predictability of the H-60 configuration, that the nominal stability phase margins (Case 1) rendered desired characteristics (i.e., the best trade-off between DRB

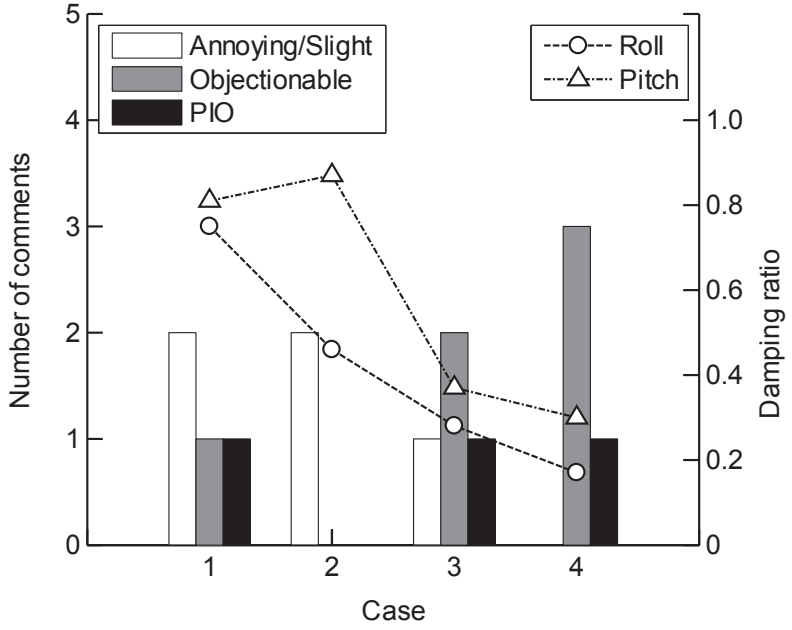

Figure 31. Pilot commentary on aircraft oscillations and damping ratio of system response due to disturbances; H-53 in moderate turbulence.

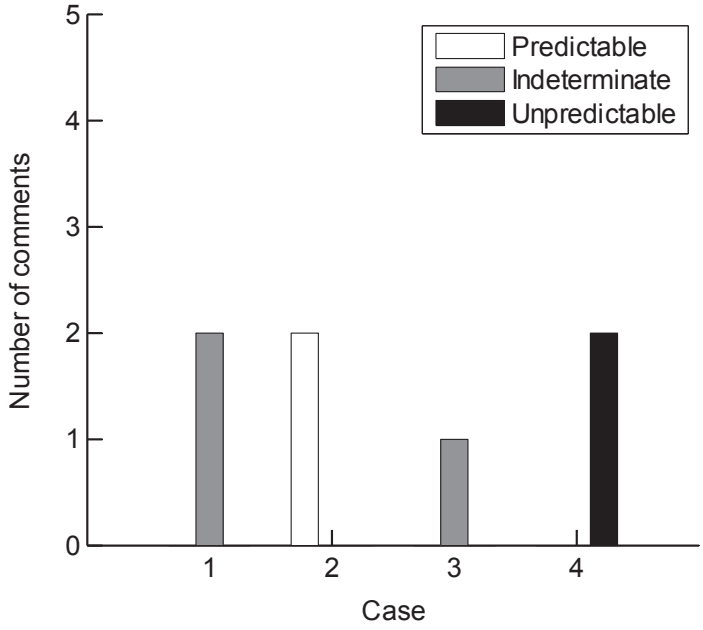

Figure 32. Pilot commentary on predictability of initial aircraft response; H-53 in moderate turbulence.

and stability), while Case 4 was unacceptable on the basis of its objectionable oscillation and PIO propensity. Similar results were observed in the flight tests in reference [37].

Figure 31 summarizes pilot appraisal of the oscillatory behavior of an H-53 class helicopter in moderate turbulence while performing the Hover MTE. Four pilots in total rated this configuration. The bar graph shows Case 1 was characterized as objectionably oscillatory by one pilot, while Case 2 elicited no such comments. One pilot also reported slight oscillations for Case 1 when attempting very tight hover position control. These were classified as "Pilot Induced Oscillations," but they were not objectionable, nor was the aircraft particularly prone to PIO in a precision task such as this one. In terms of the predictability of the initial response, Figure 32 shows Case 2 stood out as the preferred H-53 configuration, while Case 4 was the worst. Together, the oscillation and predictability elements make a strong argument that Case 2, with the higher DRB (which corresponds to ~38 deg of phase margin), has a preference over Case 1 for this class of aircraft. However, similar to the H-60 configuration, the phase margin for Case 4 was determined to be too low, resulting in the incipient handling qualities cliff indicated by the objectionable oscillatory characteristics and PIO propensity, as well as the unfavorable assessment of predictability. Roll rate RMS shown in Figure 33 supports pilot comments for Case 4, but Cases 1–3 were found to exhibit comparable oscillation rates and thus did not fully support pilot perception. If anything, Case 1 was the least oscillatory (slightly) of the four cases, even less than Case 2 and Case 3 during the hover portion of the maneuver.

The damping ratio for the response to gust disturbances is also shown in Figure 31. For the H-53 configuration, these results show that when the damping ratio of the lateral response (to gust disturbances, in this case) dropped approximately below 0.35, the resulting aircraft oscillations were deemed by the pilots to be worse, or objectionable, compared to the other cases. This result is consistent with damping ratio limits specified in the ADS-33 mid-term response to control input requirements.

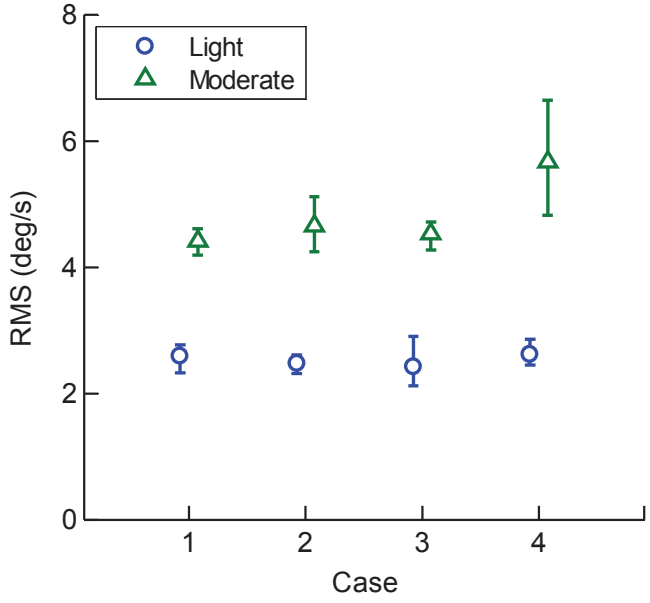

Figure 33. H-53 roll rate RMS during 30 s stabilized hover.

Station Keeping Performance With Increasing Turbulence

The RMS value of the aircraft position error (i.e., the distance between the pilot station and the hover reference point in ft) for the stable hover portion of the Hover MTE with light and moderate turbulence is shown for the H-60 in Figure 34 and for the H-53 in Figure 35. The average value for each case and turbulence level is shown as a marker, and the vertical bars represent the maximum and minimum values. As the level of turbulence increases from light to moderate, the H-60 lateral and longitudinal data show an increasing trend in the mean RMS position error for all cases. For the H-53, in Figure 35(b), this trend is only slightly apparent in

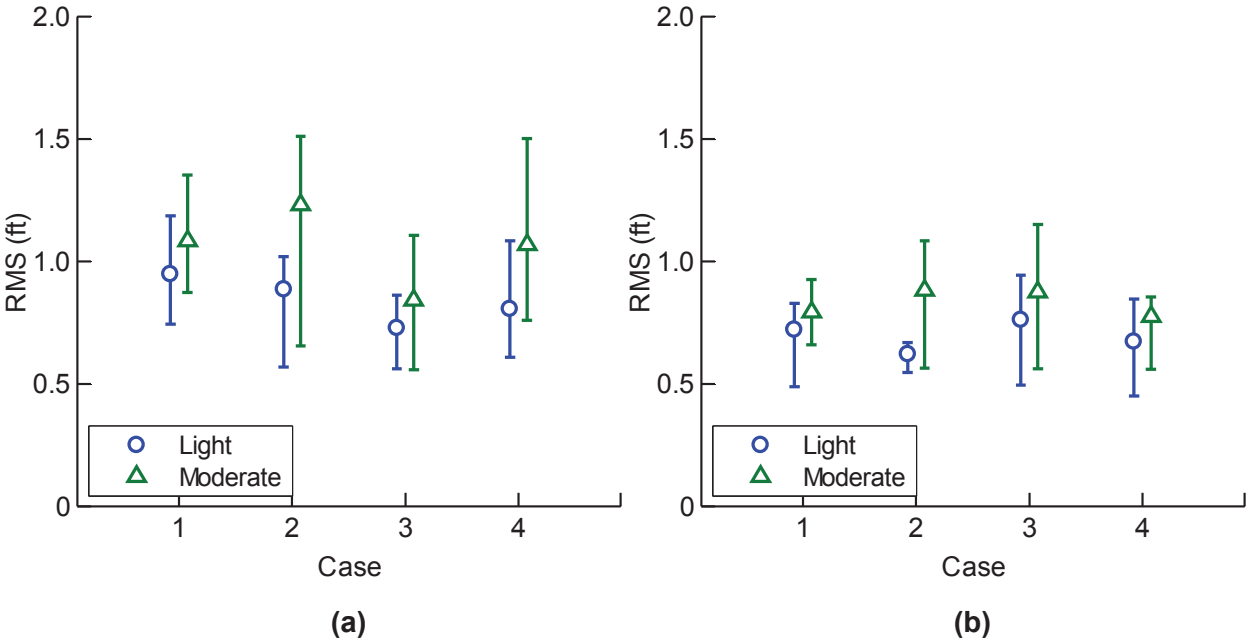

Figure 34. H-60 position error RMS during 30 s stabilized hover: (a) longitudinal and (b) lateral.

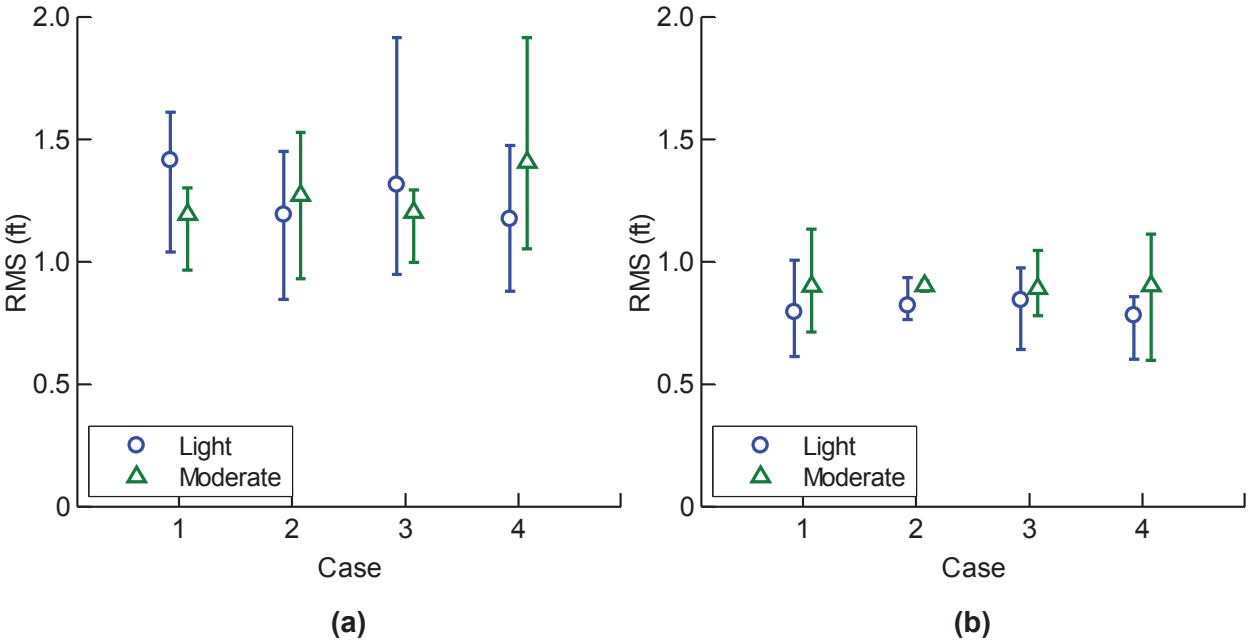

Figure 35. H-53 position error RMS during 30 s stabilized hover: (a) longitudinal and (b) lateral.

the lateral position error data and inconclusive for the longitudinal position. The trends in these data correlate well with the handling qualities ratings (HQRs) shown in Figure 26, where the H-60 showed degradation in handling qualities of about one full rating for all cases as the turbulence level increased, and the H-53 ratings remained about the same for both levels of turbulence. For the moderate level of turbulence, the highest level tested, the data does not show a decreasing trend in the RMS position error as the DRB increases. In fact, Figures 34 and 35 show that the position error for Case 1 (lowest DRB) was approximately the same or less than the position error for Case 4 (highest DRB). In addition, Figures 29 and 33 show that the highest aircraft roll rates were associated with Case 4 in moderate turbulence, and pilot comments indicated that this combination was unacceptable because of objectionable aircraft oscillation and PIO propensity. While a minimum DRB is required to reject atmospheric turbulence, these results show that there may also be an upper limit, beyond which increasing the DRB does not improve station keeping performance but lowers stability and damping, and can result in unacceptable oscillations when the aircraft is subjected to atmospheric turbulence. This is direct evidence of the trade-off between the DRB and the stability margins (as shown in Figure 24).

DRB and DRP Limits

Information from the testing of the varying levels of disturbance rejection bandwidth (DRB) with the different rotorcraft types was used to validate the DRB table in the ADS-33 Test Guide [19] and provide more data towards proposing Level 1 criteria boundaries. Since the effect of the DRB is strongest in turbulent conditions, where the rejection for disturbances is most needed, only the data sets from moderate turbulence were considered. DRB is a measure of the speed at which the control system can reject disturbances. This should be directly related to the standard deviation of the attitude excursions during a stabilized hover in turbulence if the pilot was out of the loop. However, since the pilot was in the loop, they provided additional disturbance rejection to minimize attitude excursions (at an increased workload), especially when the control laws exhibited low DRB. Therefore, it was important to consider a combination of the attitude RMS data during the Hover MTE maneuver (30 s stable portion), as well as pilot comments. These data were used to support ADS-33 Test Guide values for satisfactory pitch and roll DRB.

Pilot comments summarized in Figure 36 suggested the differences in the gust response of the aircraft were perceptible to the pilot. Correlation with the attitude RMS data, however, was generally low across the three lower DRB cases because of the pilot being in the loop to compensate for deficiencies in the disturbance rejection. The strongest correlation was for the H-60 configuration, in the pitch axis, with the pitch RMS data showing a notable (22.4-percent or 0.35 deg) monotonic reduction in the measured average pitch RMS for design cases 1 through 3. For the H-60 in particular, this was hypothesized to be because the pilots were compelled to be more attentive to the roll axis (and in the loop making corrections), because of the overall stability margin and effective disturbance response damping being significantly lower in roll than in pitch for similar phase margins. In contrast, average roll attitude RMS data for the three control cases were not quantifiably different (less than 4 percent difference, or 0.07 deg, from the average RMS midpoint). The highest DRB cases for all aircraft showed an increase in attitude RMS, not from the increased DRB, but because of the low stability margin and effective damping (0.15 and 0.17 in roll for the H-60 and H-53, respectively).

Pilot comments in Figure 36 also illustrate the correlation between the disturbance rejection peak (DRP) magnitude and the degradation of the mid-term response characteristics. The 5 and 5.4 dB boundary lines for the DRP data were effectively anchored by the H-53 test points in both pitch and roll, with the higher DRP values of the H-60 eliciting oscillations that were characterized to some degree as objectionable.

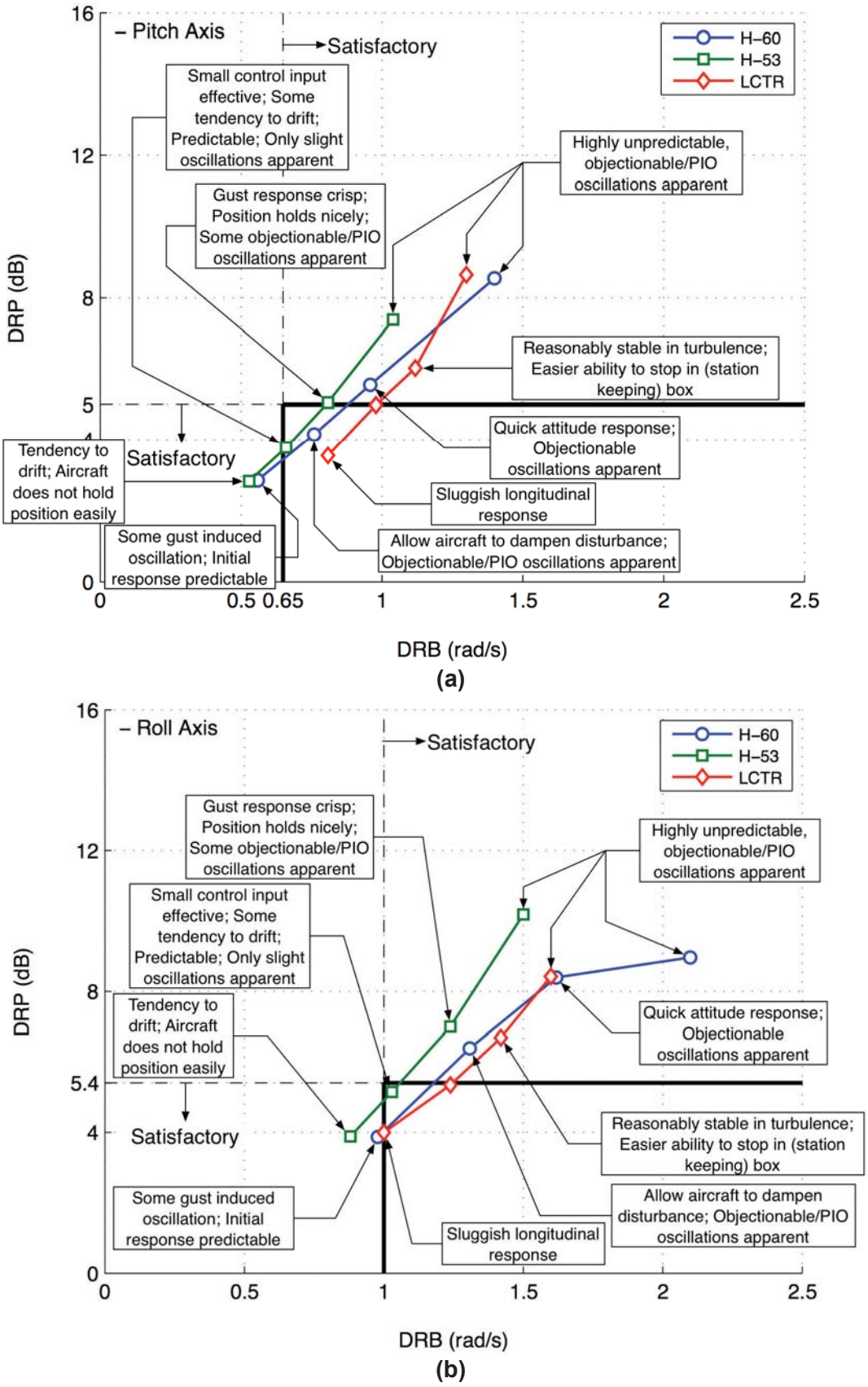

Figure 36. Proposed boundaries for attitude DRB and DRP: (a) pitch and (b) roll.

Extensive recent experience with the RASCAL JUH-60A [48] has since validated the proposed boundaries of Figure 36, supporting the requirements proposed in reference [47] for satisfactory pitch and roll DRB and DRP (Table 11). The results from the VMS show slightly higher minimum frequencies for the boundaries in the pitch and roll axes, but close to the ADS-33 Test Guide values.

DRB for Large Civil Tiltrotor

The unique characteristics of this aircraft warranted a separate discussion. Four pilots evaluated the LCTR in the DRB tests. Three of these pilots had tiltrotor flight experience. The large aircraft size, with a long moment arm between the aircraft center of gravity and the cockpit, produced the most significant result differences compared to the more conventional, single main rotor helicopters in this investigation. The impact of the long moment arm to the cockpit was immediately seen as heave motion at the cockpit due to aircraft pitch attitude changes and abrupt side-force due to yaw. The yaw-axis impact was somewhat dealt with by tuning provided by one pilot. This provided the yaw bandwidth, which was reduced compared to the original design, used for the rest of the evaluations. The heave motion at the cockpit due to pitch led to altered pilot control techniques. In general, pilots sought to minimize their use of pitch attitude for longitudinal position control, relying on aircraft stabilization to do most of the longitudinal station keeping for both evaluation tasks. The precision hover task required pitch movement to initiate and terminate the inbound translation to the station keeping point. Pilots compensated by using thrust control simultaneously with pitch control, keeping the cockpit at a constant height above ground.

The LCTR was regarded in general as being more stable in turbulence, or less easily disturbed by turbulence, compared to the single main rotor helicopter configurations investigated. This was attributed to the LCTR possessing higher effective damping and DRB for the same stability margins. DRB values for the four LCTR control law cases were all above the minimum limits suggested in Table 11. In common with the helicopter configurations investigated, the HQRs for the Hover MTE with the LCTR were relatively insensitive to the primary control system characteristic variations, as seen in Figures 26(c) and 27(c). However, the pilot comments supporting those choices do show differences. Table 12 lists selected pilot comments illustrative of the four control configurations.

Table 11. Comparison of proposed disturbance rejection criteria boundaries.

Control Axis	Satisfactory DRB – rad/s		Satisfactory DRP – dB	
	ADS-33 Test Guide	VMS	Reference [47]	VMS
Roll	0.9	1.0	5.0	5.4
Pitch	0.5	0.65	5.0	5.0

Table 12. Selected pilot comments for LCTR.

Case	Hover MTE Pilot Comments
1	Desired performance achieved but can be inconsistent. Pilot in control loop leads to higher workload. Sluggish in longitudinal axis.
2	Desired performance achieved (one pilot). On border of desired performance. Cautious control strategy used (another pilot). Moderate pilot compensation—heave with pitch.
3	Adequate performance. Reasonably stable in turbulence. Easier ability to stop in (station keeping) box. Workload still high. By far, best looking configuration.
4	Working hard. Oscillation apparent. Large collective reactions required. On edge (of controllability) when pilot gets into control loop.

The Case 1 control responses were regarded as providing a sluggish aircraft, with the pilot having to work hard at getting the desired maneuver performance. Cases 2 and 3 were assessed as having crisper control response, being more predictable, and being more stable in turbulence. For this larger aircraft, the pilots preferred Cases 2 and 3 over Case 1. These preferred Cases 2 and 3 possess higher effective damping (with Case 3 exhibiting a disturbance damping ratio of 0.5 in both pitch and roll) for the same stability margins, compared to the smaller helicopter configurations investigated. Recall that Case 1 was the preferred configuration for the H-60 helicopter, and Case 2 for the H-53. Therefore, a trend of pilot preference toward reducing stability margins for increasing aircraft size could be discerned, to the extent that larger aircraft gross weight correlated with improved mid-term gust response characteristics. Again, Case 4, with low stability margins, had apparent oscillations and could be easily upset with the pilot active in the control loop, and pilots sensed an incipient cliff. At 0.25, in both pitch and roll, the damping ratio of the response to disturbance inputs for the LCTR Case 4 was also below the 0.35 damping ratio limits specified in the ADS-33 mid-term response to control input requirements. The aggregate results for all three aircraft show a consistent relationship between the perceived oscillation of the aircraft and the mid-term gust response characteristics.

Effect of Pilot Longitudinal Position Offset in ACAH

Although piloted evaluation results reported in the previous section suggested the LCTR handling qualities in light atmospheric turbulence to be Level 1, the specific characteristics associated with the long lever arm rendered the flying qualities unacceptable, imposing practical operational constraints in the context of commercial transport and all-weather operations. The abnormalities in the reported pilot control techniques raise fundamental questions about the influence of pilot location in the aircraft on the handling qualities of the aircraft in hover (and low speed). To investigate how the pilot offset from the center of gravity affects handling qualities, a piloted simulation experiment was conducted in the VMS where the pilot station position on the LCTR simulation was varied to locations 10, 20, 30, and 40 ft forward of the center of gravity, while retaining constant vehicle dynamics. This is, of course, in consideration of the center of gravity being the fundamental instantaneous center of rotation of the aircraft in hover. The 10 ft configuration was chosen to provide comparable results with existing utility-class helicopters, on which much of the current testing for ADS-33 requirements is based. Importantly, while the vehicle response dynamics were not changed, the visual scenes and motion responses of the cab changed consistently with the pilot station position. The study was also conducted with a moderate level of atmospheric turbulence, with attention to the purported mission requirements that demand safe commercial transport in all-weather operations.

The results presented in this section include those from evaluations performed in modified versions of the ADS-33 Hover and Hovering Turn MTEs discussed previously. The evaluations of the pitch and roll response dynamics were done for pilot offsets of 10 and 40 ft only, but for six different combinations of bandwidth and phase delay. Performed in the Hover MTE exclusively, results from these evaluations show an interdependency of the handling qualities between the pitch and roll short-term response bandwidth and phase delay requirements and the pilot offset. Results from the Hovering Turn MTE evaluation of the yaw axis requirements (~2.7 rad/s bandwidth and ~0.19 s of phase delay) for locations 10, 20, 30, and 40 ft forward of the center of gravity are also presented.

Control System Design Considerations

Stability margins of approximately 38 deg and 12 dB, in both the longitudinal and lateral axes, were selected for this investigation. This fixed the inner-loop feedback gains of the attitude control law for the pitch and roll axes. While these values did not meet the MIL-9490 requirements (now in SAE 94900), they were considered acceptable based on the stability

margin and DRB trade-off analysis findings reported previously. The stability margins for the yaw axis were also set at approximately 38 deg and 12 dB. The corresponding DRBs associated with these feedback gains were approximately 0.8 rad/s in the pitch axis, 1 rad/s in roll, and 0.7 rad/s in yaw.

Variations in the response bandwidth and phase delay were all performed via changes in the command model, and thus achieved independently of the feedback loop control gains (see Figure 8). Note that an additional 48 ms are included in the computation of the bandwidth and phase delay to account for stick-to-visual delay. The response types implemented in the command model are ACAH in pitch and roll, and Rate Command-Heading Hold (RCHH) in yaw.

Finally, it is important to note that all evaluations were conducted with fixed control response sensitivities in all axes. The attitude sensitivity gains, 11.5 deg/in in both pitch and roll, were selected to be the same as in the prior experiment for consistency, ensuring also that the controller forces were acceptable to pilots during steady-state translation. Similarly, the yaw (rate) control sensitivity gain was set at 8.6 (deg/s)/in.

Evaluations in the Hover MTE of the 10 ft Baseline Offset

HQR results for pitch and roll bandwidth and phase delay combinations, set by command model variations, for the 10 ft cockpit offset are shown in Figure 37 to be in general agreement with the ADS-33 short-term response design requirements. The Level 1 and 2 ratings in the Level 2 and 3 regions, respectively, occurring for the two high-phase delay cases despite the increased task altitude and moderate turbulence, are explained because of the relaxation of the Hover MTE position maintenance performance requirements. As anticipated, the low-bandwidth configuration shown (with 0.73 rad/s in both pitch and roll) resulted in major control deficiencies, which, in an extreme case, produced a marginally uncontrollable aircraft, reflected by the HQR 9 assigned. In this case, the pilots required maximum control inceptor displacement just to maintain control of the aircraft, much less to adequately perform the task. Increasing the roll bandwidth up to 1.23 rad/s (and pitch to 1.35 rad/s) provided marked improvements, but was still found to possess fairly objectionable handling qualities, as indicated by the Level 2 rating assigned. The pilots consistently indicated *extensive* compensation was required to achieve *adequate* performance with this configuration, mainly because of sluggishness in the response and an overall lack of controllability.

Comparison Between 10 and 40 ft Offsets in the Hover MTE

The six configurations, defined *approximately* by nominal 1.8 (low) and 2.3 rad/s (high) bandwidth and 0.16 (low), 0.22 (mid), and 0.28 s (high) phase delay values, were evaluated for comparison using a 40 ft pilot offset configuration. Pilot offset location had a noticeable effect on pitch (and roll, as a combined case) handling qualities (Figs. 38 and 39), with the 40 ft case only achieving Level 2 handling qualities. The main deficiencies in the handling qualities were primarily in the longitudinal axis, with the ability to compensate for longitudinal drift through control of pitch attitude deteriorating because of an objectionable heave coupling. Importantly, the evaluations confirmed a fundamental difference in the nature of the control technique required from the pilots, mainly that the heave motion at the cockpit due to pitch response led to altered pilot control techniques attempting to minimize the impact. The precision hover task required pitch movement to initiate and terminate the inbound translation to the station keeping point. The pilots reported choosing to minimize pitch inputs to reduce the coupling to height control, and compensated by using thrust control simultaneously with pitch control, keeping the cockpit at a constant height above ground. The tiltrotor pilots noted they would ordinarily use nacelle movement for longitudinal acceleration and positioning, an option not available with the simple math model employed. Similarly, use of parallel lateral cyclic control was suggested for flat maneuver control of such a large aircraft.

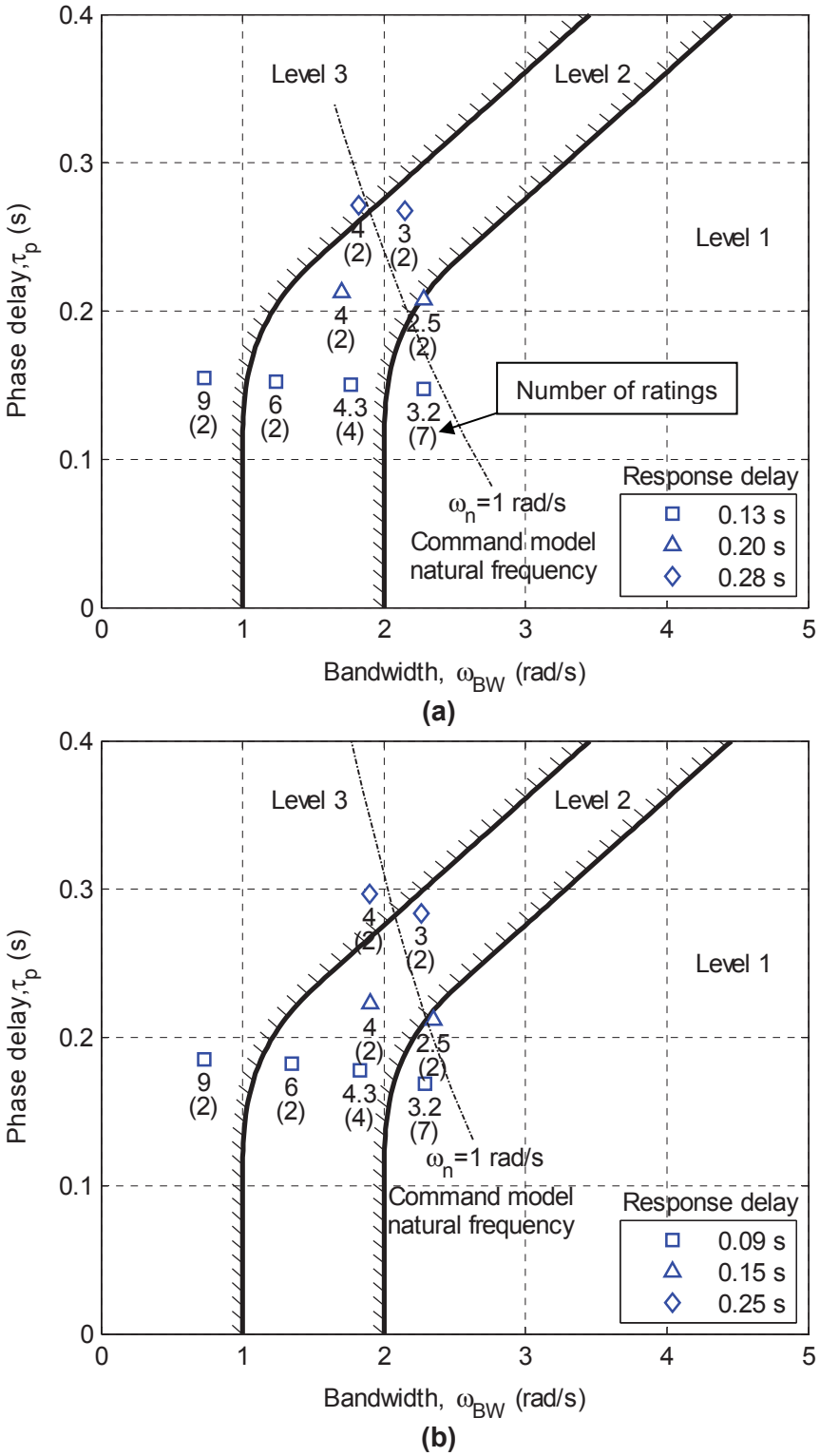

Figure 37. Average HQRs in Hover MTE for a 10 ft pilot offset: (a) roll and (b) pitch.

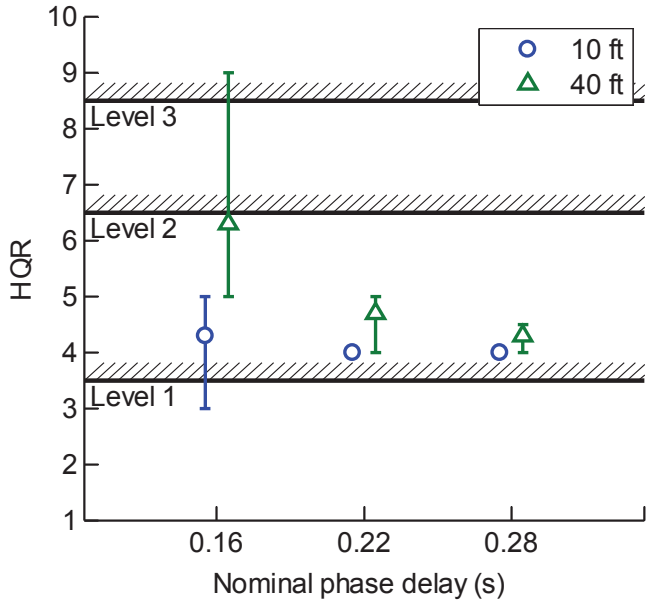

Figure 38. Comparison of HQRs for 10 and 40 ft pilot offsets (1.8 rad/s nominal bandwidth, Hover MTE).

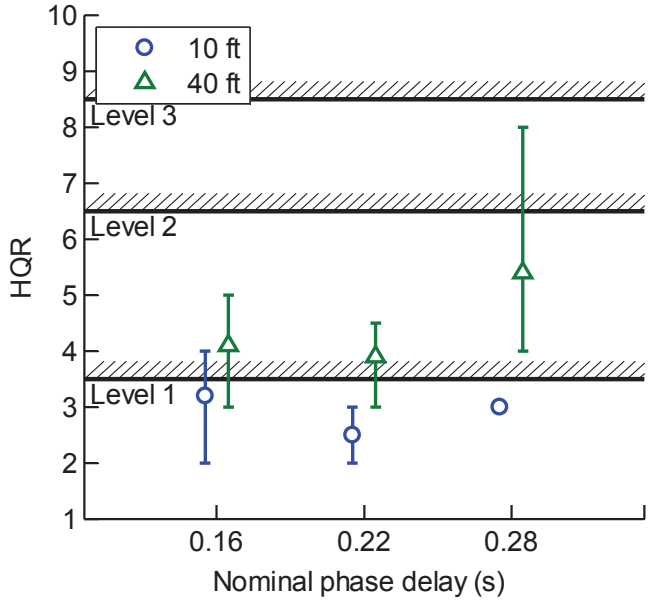

Figure 39. Comparison of HQRs for 10 and 40 ft pilot offsets (2.3 rad/s nominal bandwidth, Hover MTE).

A one to one-and-a-half HQR deterioration was observed, on average, for the 40 ft pilot offset case, when compared to the 10 ft pilot offset. The smallest increase on the average HQR was 0.3 and 2.4 the largest. Intriguingly, the largest differences in the ratings were seen in the combined low bandwidth/low phase delay and the high bandwidth/high phase delay "corner" configurations, suggesting the best handling qualities for the 40 ft case are for a command model natural frequency of 0.8 to 1 rad/s. As seen in Figure 38 for the 40 ft case, there is a highly atypical decreasing tendency of the HQRs for increasing values of phase delay, not patently manifested in the 10 ft cases, where the sluggishness of the attitude response of

the lowest phase delay case was consistently identified by the evaluation pilots as a major deficiency contributing significantly to the workload of managing the coupled pitch and height control demands. The handling qualities improvements with the increasing phase delay can be explained in context with the increasing quickness of response afforded by the increasing natural frequency of the command model. Because of the way the command model natural frequency and time delay parameters map into the bandwidth and phase delay plane, at a constant bandwidth, the increasing phase delay is matched to an increasing natural frequency of the command model (see Table 13). Similarly, the highest bandwidth and phase delay configuration in Figure 39 possessed the highest natural frequency (1.33 rad/s in pitch and 1.25 rad/s in roll). At this end of the spectrum, pilots reported the quickness of response of the aircraft to be excessive and difficult to predict. Pilots also reported the degradation in the handling qualities to be accompanied by objectionable ride qualities with sudden or jerky cockpit motions in response to aggressive attitude changes.

Spectral Analysis Comparison of Pilot Input from the Hover MTE Evaluations

The general trends observed are of increasing average longitudinal pilot input cutoff frequencies with both bandwidth (Figure 40) and phase delay (Figure 41), with only subtle differences between the two pilot offsets, suggesting the pilots largely flew to the task demands or aircraft dynamics. Pilot cutoff frequency, determined from spectral analysis of the inceptor position time histories (during the 30 s precision hover hold subtask in this instance) is a measure of pilot operating frequency, and considered a good estimate of pilot crossover frequency for pilot-in-the-loop tasks [27,49]. Error bars in these data denote the standard deviation of the cutoff frequency for all the pilots. Based on the average cutoff frequency estimates, task bandwidth (in pitch) is surmised to be at, or below, the installed bandwidth for all control and pilot offset cases. Incidentally, for the 10 ft offset in Figure 40, the task and installed bandwidths are very close on the low nominal bandwidth (1.8 rad/s) control configuration, compared to the higher 2.3 rad/s bandwidth, where pilots appear to operate with substantial margins. This result is consistent with the assigned handling qualities shown in Figure 37 for the two highest phase delay control cases and helps to explain the observed insensitivity of the HQRs to the value of the phase delay. This reduced task bandwidth is explained in relation to the relaxed hover maintenance performance requirements that were employed, compared to the standard Hover MTE requirements for the cargo/utility class.

The increasing cutoff frequency trends of Figures 40 and 41 are matched to progressive reductions in the magnitude of the longitudinal pitch control RMS shown in Figures 42 and 43, for increases of both bandwidth and phase delay. Thus, the pilots evidently adapted their compensation activity to a higher frequency but smaller amplitude shaping of the inceptor input for the higher bandwidth and phase delay control configurations. This was true for both pilot offset positions, however. Significantly, Figures 42 and 43 show an approximate 13–29 percent increment across the board in the mean longitudinal cyclic control input RMS when the pilot was positioned at a 40 ft offset. This is contrary to the reported pilot perception of minimizing pitch control, and is actually an indication of increased compensation activity. This increase is

Table 13. Command model natural frequency and time delay parameters for nominal bandwidth and phase delay cases (pitch).

Nominal Phase Delay Case	Natural Frequency (rad/s)		Time Delay (s)
	Low Bandwidth	High Bandwidth	
Low	0.45	0.8	0.09
Mid	0.6	1.07	0.15
High	0.8	1.33	0.25

accompanied by a two-fold (over 100 percent) increment in the thrust, or "collective," control lever adjustments for the larger offset (Figs. 44 and 45), a result indicative of increased control activity in the heave control axis associated with the pitch-heave coupling experienced at the pilot station with the longer lever arm.

Of particular interest at this point is the comparison of pilot control activity metrics for the lowest and the highest bandwidth and phase delay combinations for the two pilot offsets, where the HQR differences were largest (Fig. 38 and 39). A slight reduction in the longitudinal input cutoff frequencies for the 40 ft offset is seen in Figure 41, relative to the 10 ft offset case. This could indicate a further reduction in the pilot operating frequency in response to the deficiencies

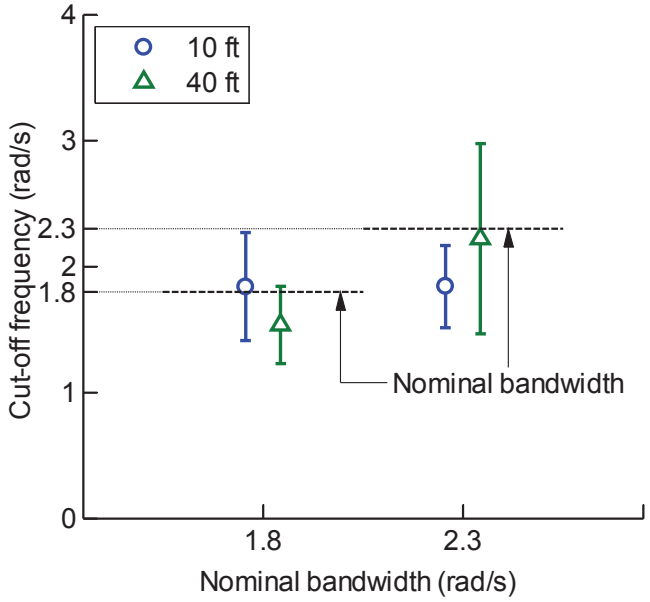

Figure 40. Comparison of longitudinal pilot input cutoff frequencies for 10 and 40 ft pilot offsets (0.28 s nominal phase delay, Hover MTE).

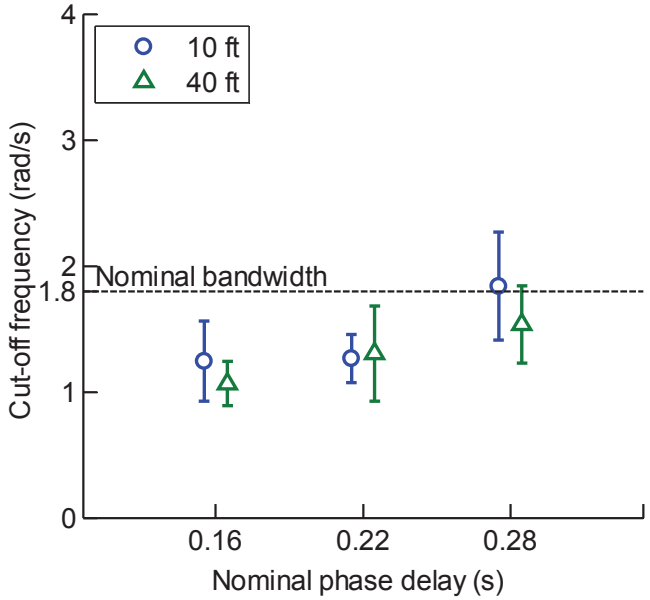

Figure 41. Comparison of longitudinal pilot input cutoff frequencies for 10 and 40 ft pilot offsets (1.8 rad/s nominal bandwidth, Hover MTE).

identified with the increased coupling of the pitch and heave control activity associated with the increased pilot station offset, but this result is somewhat inconclusive. Apart from the RMS increment seen in the longitudinal input time histories, common to all 40 ft short-term response configurations, there are no quantifiably significant differences in the piloted control input activity in the pitch axis between the two pilot offsets for this particular configuration. It is inferred from this that the pilots effectively operate at a fundamental limit imposed by the aircraft dynamics, rather than as a consequence of the increased station offset. The large HQR increase is thus attributed to a disproportionate increase of the workload and the reported deterioration of the precision hover task performance associated with having to manage the coupled pitch and height control axes for the slower response dynamics.

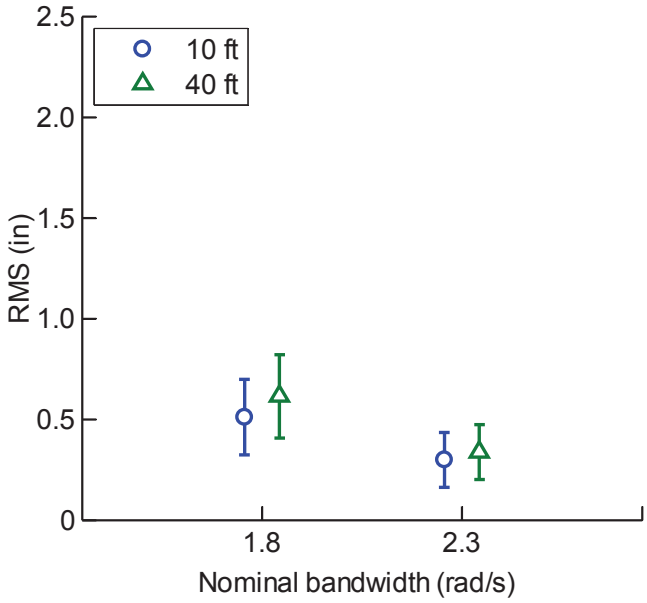

Figure 42. Comparison of longitudinal pilot input RMS for 10 and 40 ft pilot offsets (0.28 s nominal phase delay, Hover MTE).

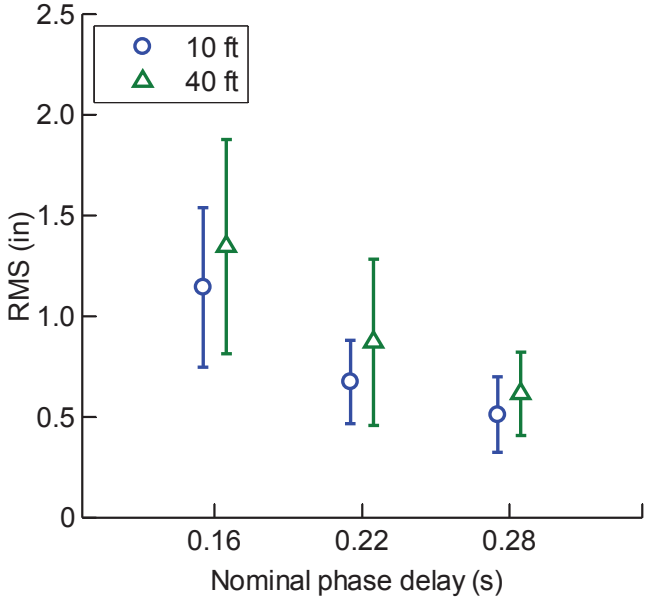

Figure 43. Comparison of longitudinal pilot input RMS for 10 and 40 ft pilot offsets (1.8 rad/s nominal bandwidth, Hover MTE).

On the other hand, the average cutoff frequency for the highest bandwidth and phase delay configuration in Figure 40 is about 0.5 rad/s higher and the standard deviation about twice as large for the 40 ft pilot offset. This result highly suggests a handling qualities difference between the two pilot station offsets, reflected in the pilots compensating at higher frequencies as a result of deficiencies in the aircraft. The “quick,” “jerky,” and “unpredictable” response of the aircraft that was reported by the evaluation pilots was bound to result in the pilots having to apply more corrective inputs than desired. The effect of biodynamic feedback cannot be discounted either, with a few pilots explicitly mentioning this problem. The larger standard deviation band is consistent with the reports of unpredictability of the initial response, suggesting a broader range of piloted operating frequencies was employed by the different pilots.

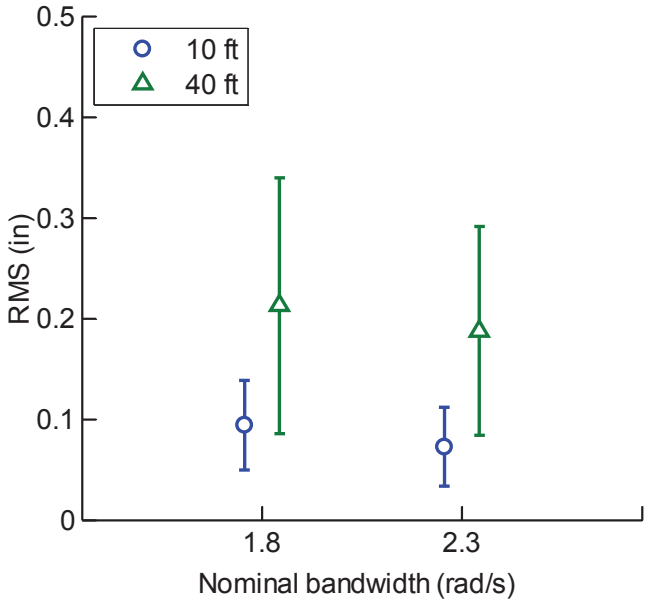

Figure 44. Comparison of TCL pilot input RMS for 10 and 40 ft pilot offsets (0.28 s nominal phase delay, Hover MTE).

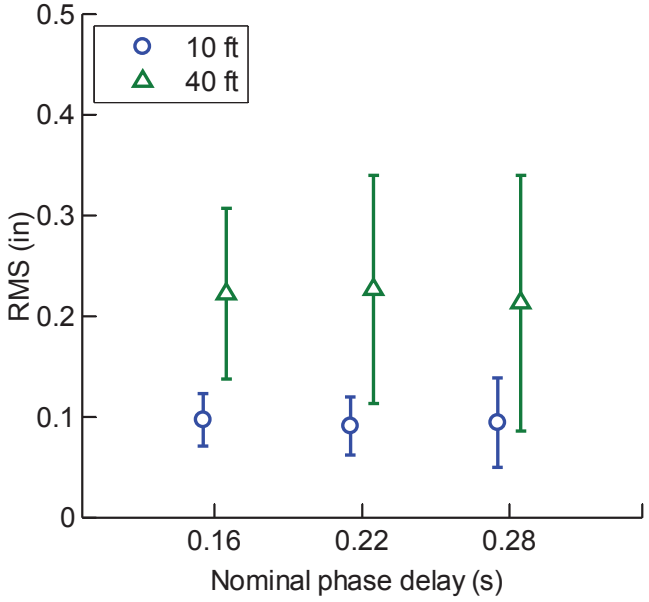

Figure 45. Comparison of TCL pilot input RMS for 10 and 40 ft pilot offsets (1.8 rad/s nominal bandwidth, Hover MTE).

Effect of Pilot Offset on Yaw Handling Qualities

The yaw axis handling evaluations were conducted in a hover turn task with the LCTR model configured to meet the Level 1 ADS-33 bandwidth requirements and response sensitivities. For pilot offsets of 30 ft and greater, yaw maneuvering conferred large, sudden, lateral accelerations, or side-forces, at the pilot station, which severely interfered with the ability of the pilot to capture a precise heading. Figure 46 shows an increase of two full handling qualities ratings (HQRs) in the pedal turn task (including an HQR of 10) when increasing the pilot offset between 20 and 30 ft, for the configuration defined by ~2.7 rad/s bandwidth and ~0.19 s of phase delay. Results suggest bandwidth requirements should be relaxed or pilot control input response sensitivity reduced.

Naturally, the pilot offset distance amplifies the lateral pilot station accelerations, and their time rate of change—customarily referred to as "jerk." As the lateral pilot station motions become increasingly amplified by the increased offset, pilots tend to slow down the maneuver by reducing the maximum rates generated, consequently compromising the overall task performance. Figure 47 exemplifies the control technique adjustments that pilots underwent for the increasing pilot offsets. The 10 and 20 ft offset distances allowed aggressive execution of the maneuver without exciting the large amplitude lateral jerk seen with the 40 ft offset. All four pilot-offset configurations, having the same bandwidth, exhibited similar high-frequency jerks in the response when the pilot attempted the heading capture maneuver. The reductions in the control (pedal) amplitude made the maneuver more tolerable to the pilot.

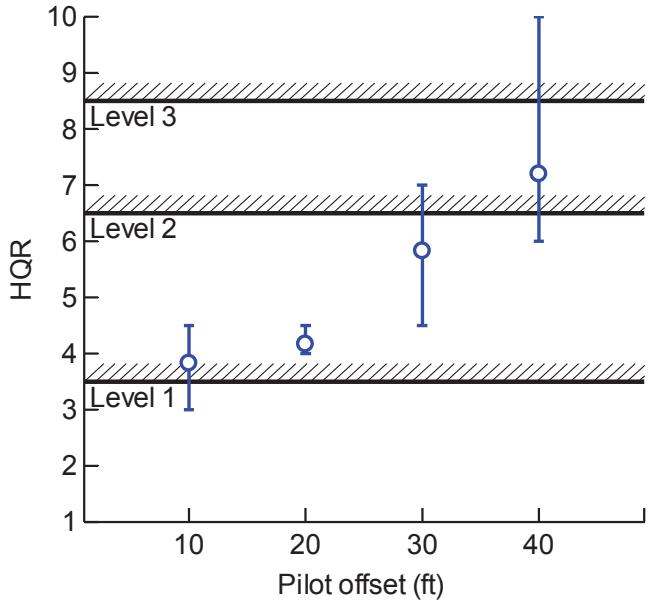

Figure 46. Effect of cockpit position on HQR scores for high yaw response bandwidth (Hovering Turn MTE).

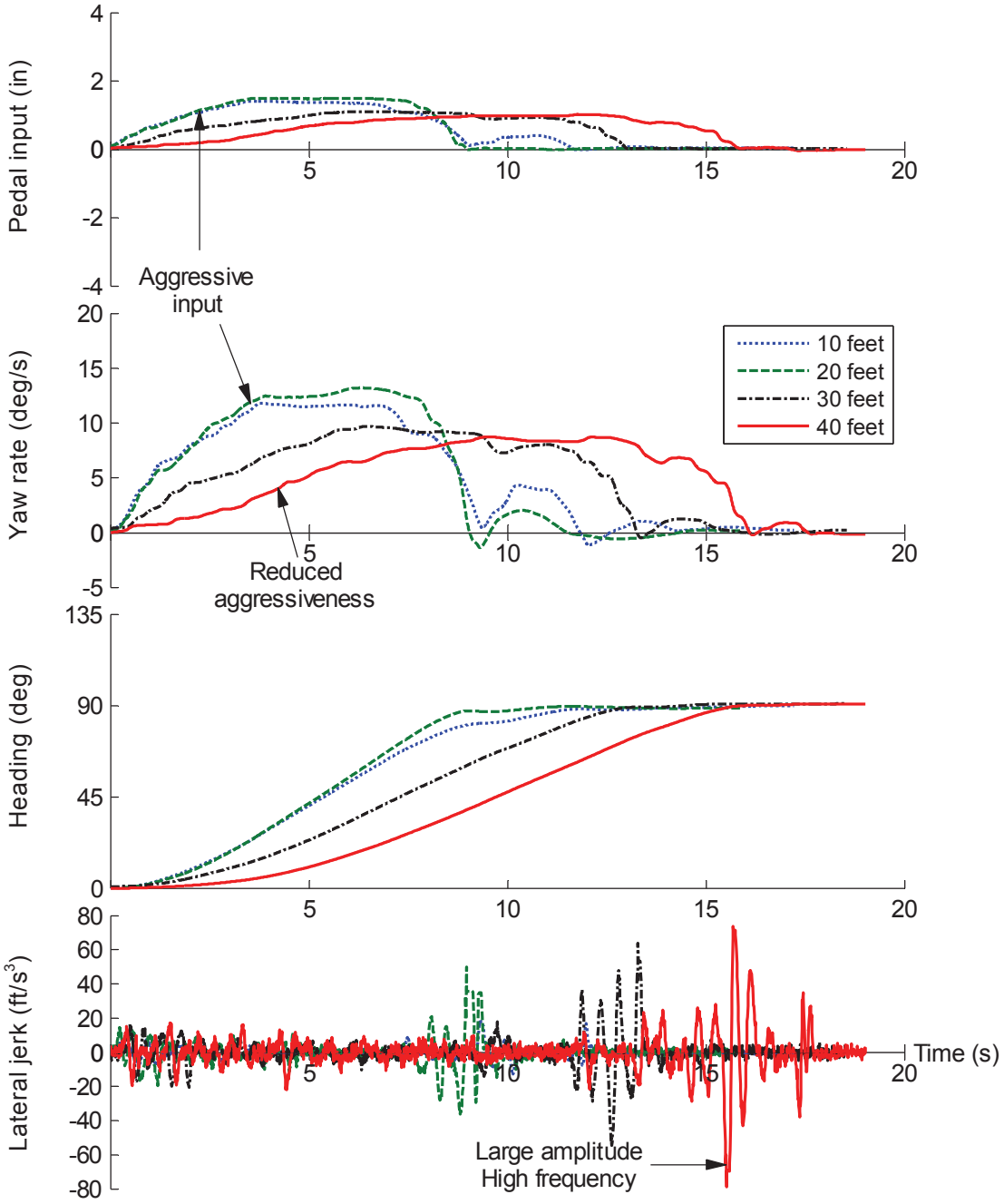

Figure 47. Effect of pilot offset for high bandwidth response on hover turn maneuvers.

Short-Term Attitude Response Requirements for Large Rotorcraft

The previous analysis showed adverse fundamental aspects related to the position of the pilot station ahead of the center of gravity that have a significant effect on the handling qualities of a rotorcraft in hover; and that the usual approach of the ADS-33 standard that more bandwidth leads to improved hover handling qualities might not be appropriate for rotorcraft with large pilot offsets such as the LCTR. With that in mind, this section focuses on the study of pitch, roll, and yaw (heading) short-term attitude response hover handling qualities requirements for LCTR-sized rotorcraft configurations, which may differ from those currently established in ADS-33. Families of bandwidth and phase delay combinations were used for assessment and

the results are shown in this section. The results for the pitch and roll short-term attitude response requirements are presented first, followed by those for yaw. Cooper-Harper handling qualities ratings (HQRs) are presented in conjunction with pilot commentary within an overall discussion, highlighting handling and ride qualities issues associated with the LCTR size and configuration. A quantitative assessment of pilot control techniques, including crossover frequencies, completes the analysis.

Experimental Considerations

Using the model-following flight control architecture described above, the response bandwidth and phase delay were varied for the pitch, roll, and yaw axes through changes to the command model parameters. An additional 47–48 ms are included in the computation of the bandwidth and phase delay to account for stick-to-visual delay. In addition to the natural time delays in the bare-airframe and other systems, a small amount of extra phase delay is produced because of mismatch in the closed-loop and command responses introduced by model uncertainty. Therefore, even if zero time delay is commanded, there is a minimum value of phase delay present in addition to that of the visual system. In the following analysis, references to the natural frequency and time delay refer to the command model parameters; because of the model-following architecture these can still be considered approximately representative of the vehicle response within the effective frequency range of the control system. Finally, large differences in the attitude bandwidth or phase delay metrics between pitch and roll axes led to the pilots objecting to disharmony of control. Therefore, the pitch and roll attitude short-term response characteristics could not be evaluated completely independently of each other, and consequently every pitch bandwidth and phase delay point is paired to another harmonizing value in roll.

For consistency with the prior analysis above, the same feedback and controller characteristics were retained. Accordingly, the inner-loop feedback gains were kept constant, ensuring a single combination of stability margins, approximately 38 deg and 12 dB in all three axes, throughout the investigation. Also, the control response sensitivities (all axes) were fixed throughout the experiment, ensuring all control system configurations had identical low-frequency gains, independent of the natural frequency or time constant. These characteristics ensured controller forces were acceptable to pilots during steady-state translation. While this has no impact on the bandwidth and phase delay values, it can play a potentially significant role in the handling qualities of the aircraft for pilot-in-the-loop maneuvering. The sensitivity gains were set at 11.5 deg/in for both pitch and roll, and 8.6 deg/s/in for yaw.

Finally, evaluation maneuvers consisted of the modified variants of the ADS-33 Hover and Hovering Turn MTEs discussed earlier, and were flown with a “moderate” amount of simulated atmospheric turbulence via the CETI model using the parameters shown in Table 6.

Pilot Evaluations of LCTR Short-Term Pitch and Roll Response in Hover MTE

As previously ascertained, the main handling qualities deficiencies in the hover for the LCTR were identified primarily in the longitudinal axis, with the ability to compensate for longitudinal drift through control of pitch attitude deteriorating because of the objectionable coupling of pitch and heave motion associated with the location of the cockpit relative to the center of gravity of the aircraft. A severe degradation of ride and handling qualities for high-frequency bandwidths is contrary to the experience with current utility-type rotorcraft. Pilots found the aircraft handling qualities to be very sensitive to pilot control aggressiveness, especially in the longitudinal axis. This was due to both an objectionable sensitivity to control (characterized by a disproportionate amplitude and quickness of the response to pilot input), and a high propensity to rate-limit the actuators. Combined, these characteristics yielded an unpredictable aircraft response, both initial and mid-term. In practice, this behavior increased the difficulty of cancelling out aircraft position drift and necessitated a heightened visual cue pattern scan frequency to ascertain the hover position. As such, both of the “measurable” handling qualities factors, performance and

workload, were directly impacted. Only by substantially decreasing their control gains were some of the pilots able to effect the precise maneuvering necessary to achieve desired task performance. This situation was not representative of an average pilot using normal control technique. Compounding these handling qualities issues, pilots complained in general about an uncomfortable roughness of ride, and this often factored decisively in the rating process.

The HQRs drew a fairly consistent image of the piloted short-term pitch and roll attitude response preferences for this class of aircraft. Average ratings for the pitch bandwidth and phase delay test point pairs in the Hover MTE are shown in Figure 48, overlaid on the hover and low-speed ADS-33 requirements for *All Other MTEs and Usable Cue Environment (UCE) greater than 1*. The annotated average HQRs show that, using an ACAH response type in moderate turbulence, Level 1 handling qualities were not consistently attainable for an aircraft of this class with the pilot station located approximately 40 ft ahead of the center of gravity. Furthermore, Figure 48 shows that better HQRs tend to align with the command model constant 1 rad/s natural frequency contour below 250 ms of phase delay. It is suspected that increasing delay along this line will result in increasingly worse handling qualities in a manner that is qualitatively consistent with the current specifications. Increasing HQR gradients tend to point outward from this 1 rad/s constant line, towards both higher and lower frequencies, in directions roughly orthogonal to the constant frequency lines. This result suggests, incidentally, a strong correlation between the handling qualities and the natural frequency of the approximate second-order attitude response of the aircraft to pilot input, confirming the observations from the preceding section.

The Open-Loop Onset Point (OLOP) design criteria [50], often used in fixed-wing flight control system design and tested for use with rotorcraft in reference [13], is also shown in Figure 48. The OLOP criteria is a frequency-domain linear metric employed to predict PIO phenomena based on the onset condition of nonlinear behavior such as actuator rate-limiting. Based on the actuator and control system implementation tested, this criteria suggests the presence of an intrinsic upper bandwidth limit for acceptable handling qualities.

Because of the pairing of pitch and roll short-term response characteristics, these same trends were naturally observed in Figure 49 for the roll bandwidth and phase delay as well—mainly the clustering of the better configurations around the 1 rad/s line and below 250 ms of phase delay into a characteristic “thumbprint” pattern. Overall, there was a general inability to achieve Level 1 handling qualities in the Hover MTE.

The preponderant influence of the command model natural frequency on the ratings is further evidenced by the approximate loci of the HQR 6.5 contour lines suggested by the data in Figures 48 and 49. These contour lines separating the Level 2 and Level 3 ratings in the low-frequency region for the particular test correspond roughly to natural frequencies of about 0.6 rad/s for roll, and in between 0.4–0.5 rad/s for pitch. At lower frequencies, configurations were deemed too sluggish in response to pilot input, with PIO tendencies, and consistently resulted in intolerable workloads and adequate performance not being achieved.

Figure 50 illustrates the strong correlation between the natural frequency of the command model and the average HQRs for the LCTR with the nominal ~40 ft pilot offset. Configurations with pitch attitude natural frequencies below 0.4 rad/s (0.6 rad/s in roll) were all found to possess Level 3 qualities. Better HQRs were found between 0.8 and 1.2 rad/s, but not Level 1, and the average rating scores tended to rise with further increases of the natural frequency. Plotting results in this fashion concealed the effect of delay in the response. Differences in the average HQR for configurations with similar natural frequencies, however, generally correlated with differences in the response delay. The effect of command delay was inferred from subtleties in pilot evaluation, where the main differences were in the degree of severity of the perceived deficiencies in the initial response qualities, with task performance not compromised as strongly in the low time delay cases. The most notable effect of delay was in the three cases

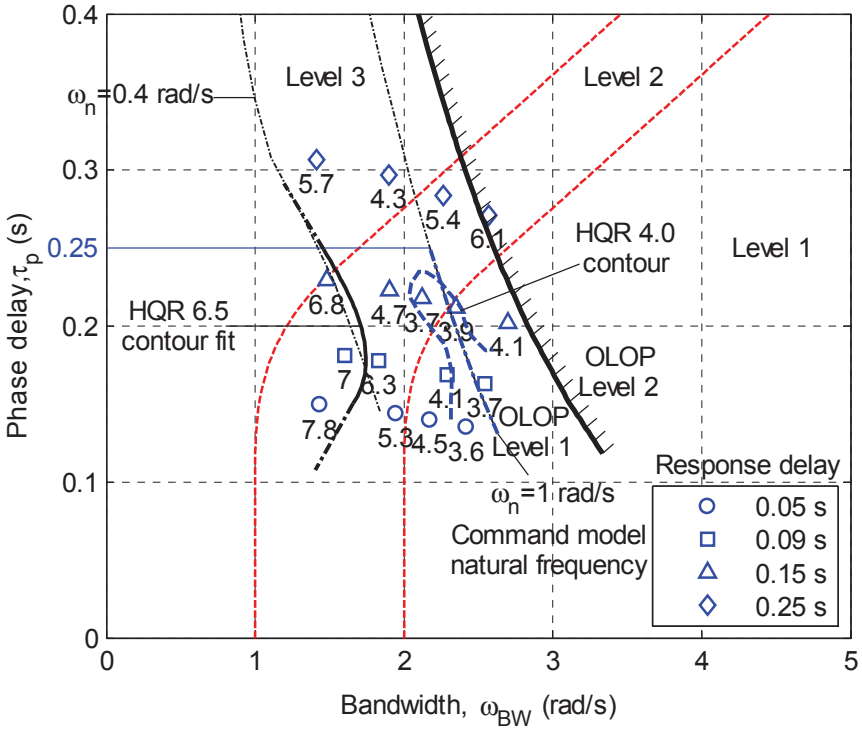

Figure 48. Short-term pitch response handling qualities evaluations for a 40 ft pilot offset in moderate turbulence.

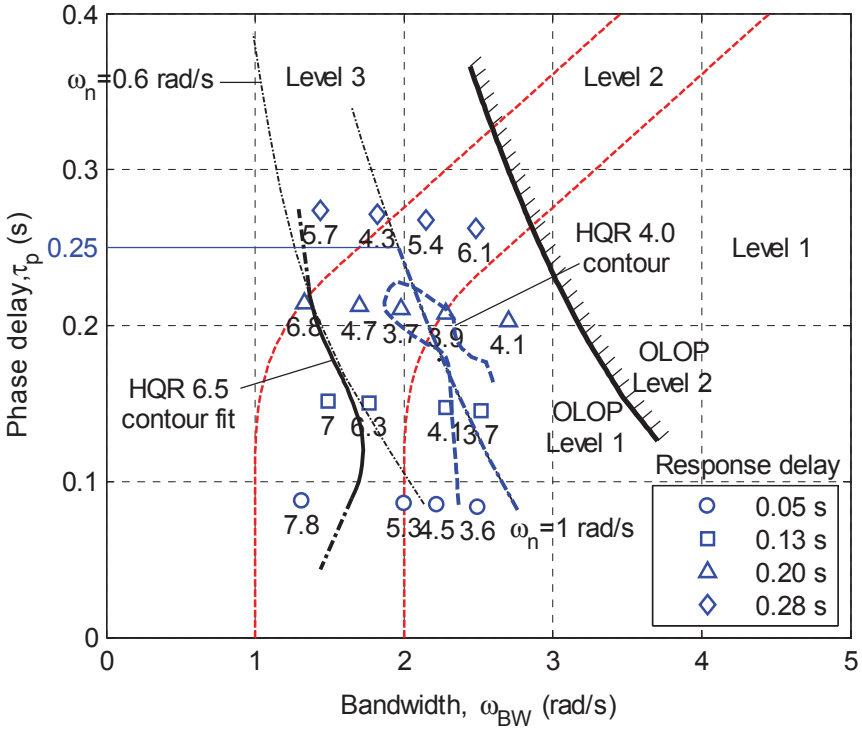

Figure 49. Short-term roll response handling qualities evaluations for a 40 ft pilot offset in moderate turbulence.

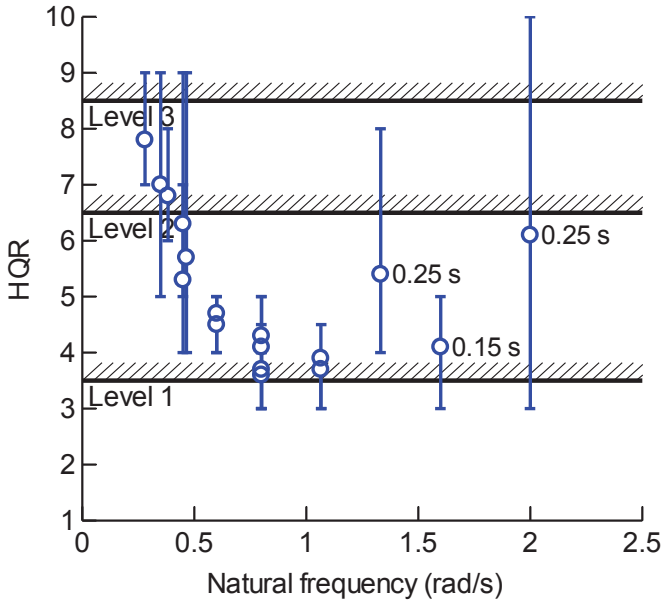

Figure 50. Correlation of pitch natural frequency of the commanded second-order response with average Cooper-Harper HQRs for 40 ft pilot offset.

with natural frequencies greater than 1.2 rad/s. Task performance was significantly compromised in the 0.25 s delay cases, when compared to the 0.15 s delay case. The general objections to the handling qualities for these three configurations, however, were all related to a reduced predictability of the initial response. Pilots observed a “sudden,” “large,” or “sharp” response to small control input, particularly in the pitch/heave axes, which made it difficult to correct for drift without inducing a “jerky,” “choppy,” or ”rough” ride quality. For the two higher frequency configurations, actuator saturation was recognized as a further deficiency. Occasional instances of biodynamic feedback in pitch resulting from the “objectionable oscillations and cockpit motions” were also identified.

Overall, the primary differentiator of the pilot ratings seemed to be associated with the quickness, or lack thereof (i.e., sluggishness), of the initial aircraft response. Quickness refers to how rapidly a pilot can achieve a change in attitude from one steady-state condition to another. These qualities are intrinsically related to response characteristics such as the peak attitude rate (and acceleration) to a step or impulse input, for example, and are therefore fundamentally governed by the natural response dynamics (natural frequency and damping). Crucially, these would be characteristic of the attitude response to small- or moderate-amplitude discrete-like control inputs typical of pilot control behavior in the type of maneuvering required by the task. Therefore, inasmuch as these are perceived by the pilot, this would perhaps explain the strong dependency of the ratings on the natural frequency, in contrast to the bandwidth. Incidentally, typical time delays would have only a small impact in this type of maneuvering. Bandwidth is an effective measure of the small-amplitude, short-term attitude response characteristics to pilot input that accounts for all natural dynamics and time delays in the vehicle response. Specifically, it offers a meaningful way of quantifying the control precision in tight compensatory pilot-in-the-loop tracking tasks. If the vehicle response dynamics to pilot input were of approximate second-order form, then bandwidth would be directly related to the natural frequency. Time delays, however, introduce significant variation in the bandwidth for a given natural frequency, thus blurring the relationship between the two parameters, especially for higher natural frequencies.

Spectral Analysis of Piloted Input

The pilot cutoff frequency for this analysis was determined from the spectral analysis of the inceptor position time histories during the 30 s precision hover hold subtask. The pilot control input cutoff frequencies are plotted against the pitch and roll attitude response bandwidths in Figure 51. Bars are one standard deviation. Two key observations are possible from these results. The first is that there did not appear to be a clear, unique functional relationship between the cutoff frequencies and the bandwidth, as indicated by the spread in the *average* cutoff frequency values. The pilots generally appeared to employ higher frequency of control for

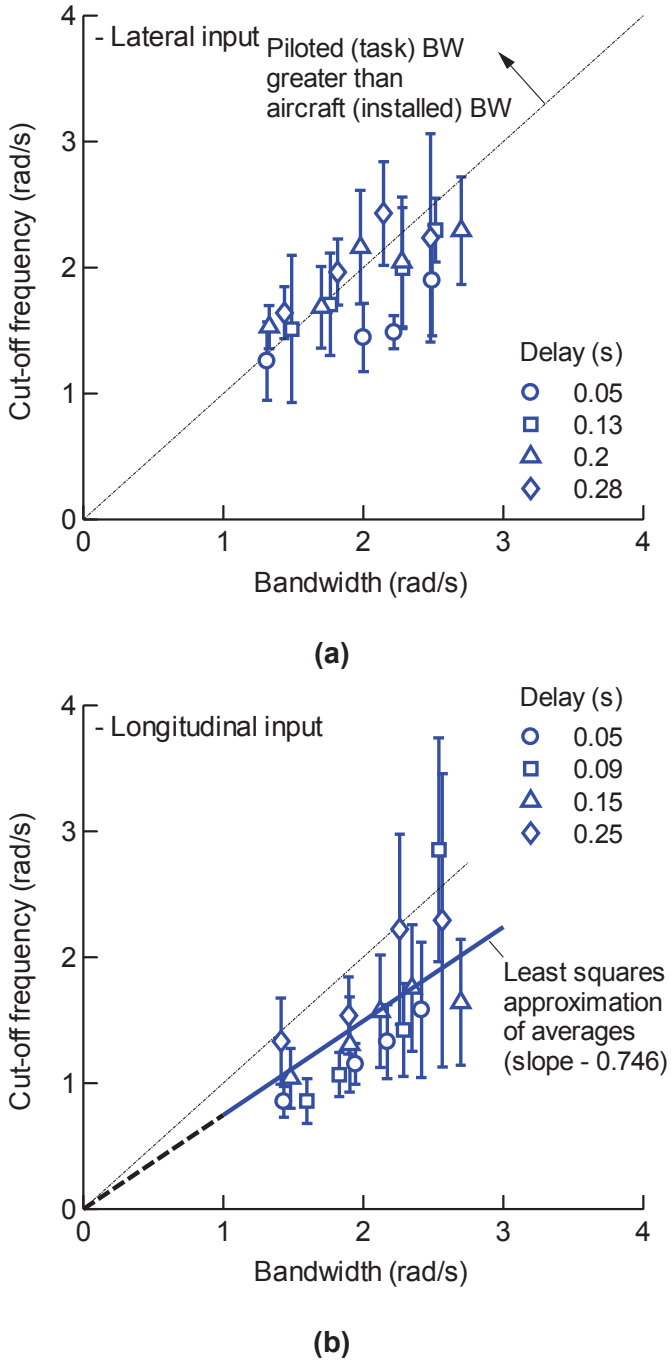

Figure 51. Relationship between pilot input cutoff frequencies and aircraft short-term attitude response bandwidth for Hover MTE: (a) lateral axis and (b) longitudinal axis.

the configurations having higher time delay, also suggesting a strong dependency on the later, or equivalently, the phase delay. The second observation is that if cutoff frequency is accepted as a measure of the task bandwidth, then the installed bandwidth in the longitudinal, or pitch, axis generally exceeded the task requirements on the pilot. These results were consistent with those shown in Figures 40 and 41. In contrast, pilot control activity in the lateral axis was more often at the limit of the available aircraft bandwidth.

With the exception of a few outliers in pitch, Figure 52 suggests there is a strong relationship between cutoff frequency and natural frequency of the second-order equivalent attitude

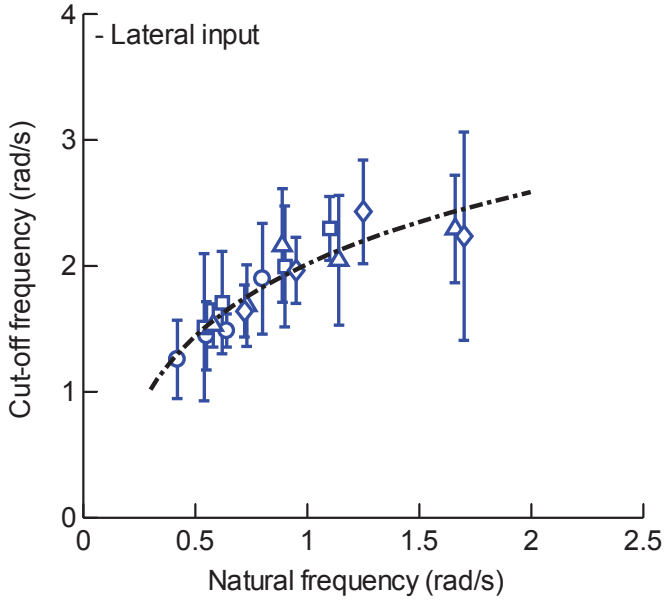

(a)

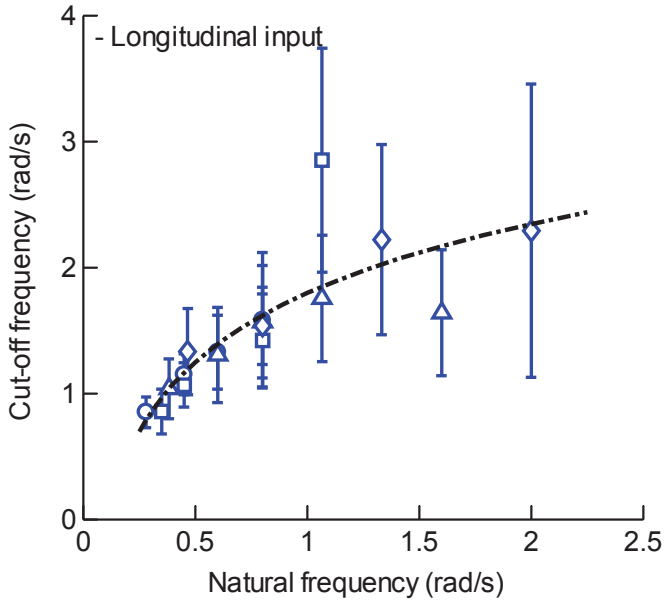

(b)

Figure 52. Relationship between pilot input cutoff frequencies and aircraft second-order response dynamics for Hover MTE: (a) lateral axis and (b) longitudinal axis.

response dynamics. Pilot operating frequency increases as a direct function of increasing quickness of vehicle response. Certainly, higher frequency inputs were allowed by, and perhaps also driven by, task demands on the pilot loop closure for the quicker attitude responses. Conversely, more sluggish vehicle responses manifested a reduction in the frequency of compensation of the pilots.

Consistent with results shown previously, pilot input amplitude, as measured by the inceptor displacement RMS, is shown in Figure 53 to decrease exponentially with the natural frequency of the response. This result confirms the shift to a high frequency and low amplitude control

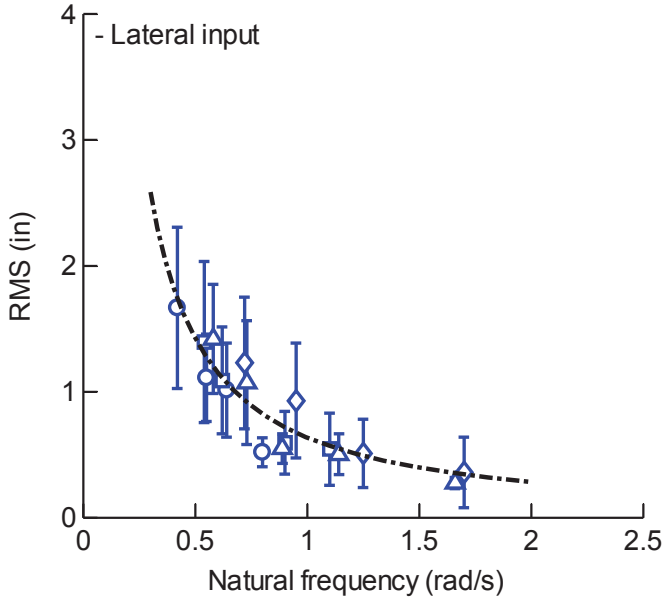

(a)

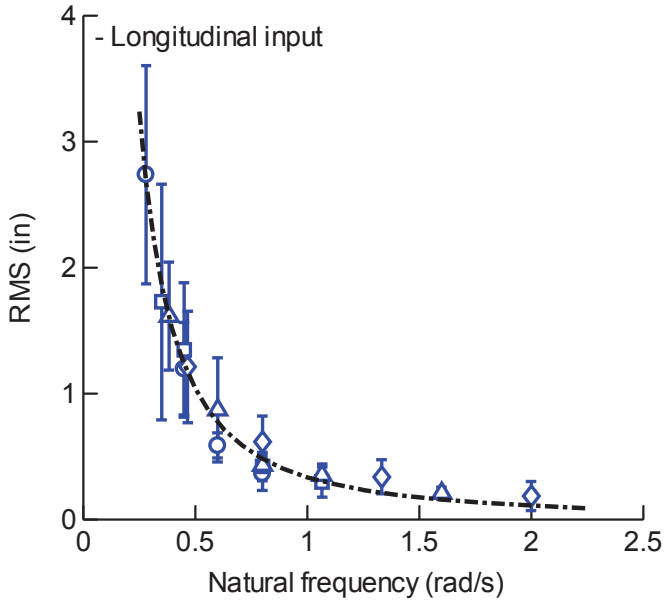

(b)

Figure 53. Relationship between pilot input RMS and aircraft second-order response dynamics for Hover MTE: (a) lateral axis and (b) longitudinal axis.

compensation strategy for the higher response frequency. As a corollary to this result, for the low-frequency attitude responses, it can be inferred that the pilots tend to "over-drive" the aircraft to compensate for the slow response. As indicated by the results from the previous section, this is not a unique characteristic of the extended (i.e., 40 ft) pilot offset location. Rather, it confirms a normal compensation technique adaptation of the pilot in line with the classical crossover model [51].

The significance of the results in Figures 52 and 53 is they confirmed a direct link between the second-order command model system natural frequency parameter and quantifiable metrics of pilot compensation, independent of time delay. This key result suggests pilot compensation frequency was inherently governed by the aircraft equivalent second-order natural dynamics. Effectively, it could be argued that task bandwidth was set by the aircraft natural response dynamics, mainly the natural frequency. As the command model second-order natural frequency increased, pilots appeared to become more comfortable with increasing the frequency of their inputs. This trend was naturally limited by the objectionable flying/ride qualities that emerged for higher bandwidth configurations, where it eventually exceeded the compensation ability of the pilot, in particular when coupled with large delays.

The grouping of better HQRs near 2.1 rad/s in Figure 54(a) suggests pilots consistently preferred the vehicle roll dynamics that allowed them to operate at this frequency. Pilots appeared to be more tentative in pitch, with the mean longitudinal control cutoff frequency for these optimal control system configurations dropping to about 1.6 rad/s (Figure 54(b)). In general, operating at higher frequencies excited objectionable deficiencies in the aircraft response qualities, especially with large added delay. One particular case stands out in Figure 54(b) as an exception where pilots, on average, used a higher crossover frequency of about 2.85 rad/s, yet rated this configuration to have borderline Level 1–Level 2 handling qualities. However, a large standard deviation of 0.89 rad/s in the longitudinal control cutoff frequency, along with a 1.72 rad/s minimum and 4.27 rad/s maximum, indicate significant variability in the control techniques. Reviewing pilot comments, it is evident that ride quality, though described as "very rough," was not weighed into the HQR score for this particular configuration. Pilots indicated they could operate the aircraft with continuous, but small amplitude, control inputs. This is consistent with the quantitative pilot input cutoff frequency measurements. While pilots disliked the ride qualities of the aircraft, they liked the fact that the particular control system allowed them, under the appropriate control technique, to achieve reasonable accuracy in task performance.

Pilot Evaluations of LCTR Short-Term Yaw Response in Hovering Turn MTE

Analysis of the effect of pilot offset on the yaw handling qualities presented above showed that Level 1 handling qualities requirements in hover might not be applicable to vehicles where the pilot station is 30 ft, or farther, from the center of rotation of the aircraft. The analysis presented here focuses on the evaluation of yaw short-term response requirements for an LCTR configuration. The results in this section are from two separate assessments of the LCTR.

Early assessments of the LCTR aircraft found that the initial design yaw bandwidth, based on the ADS-33 requirements, was extremely obtrusive to the pilot, and therefore, disruptive of the normal execution of the experiment. This process provided some insight into the adequate amount of control authority required for this type of aircraft. There are two basic elements that define overall yaw control authority: first, the control power or maximum yaw rate, and second, the precision required in capturing a target heading. The first element is not in question in this case, because it was generally possible to reach maximum yaw rates up to about 27.5 deg/s with the yaw-rate command system implemented. This surpasses the ADS-33 Level 1 minimum achievable yaw rate for Moderate Agility. With the pilot sitting almost 40 ft ahead of the center of gravity, it became apparent that bandwidth requirements for future large rotorcraft of this type would need to be balanced from a human factors and ride quality perspective. The

bandwidth is closely related to the angular yaw acceleration, and at the large longitudinal offset location the pilot was subjected to highly objectionable peak lateral accelerations in excess of 0.6 g. Current ADS-33 bandwidth requirements are minimums and are unbounded on the high side. The current exercise illustrates the potential necessity to curtail or modify current requirements, to account for aircraft size. The maneuver performed in this yaw bandwidth investigation loosely resembled the Hovering Turn MTE specified in ADS-33. No restrictions were placed on the aggressiveness and agility of the maneuver. The maneuver consisted of the pilot aligning the aircraft along the runway centerline, at an arbitrary altitude, and then executing 180 or 360 deg turns in an attempt to recapture the aircraft-runway alignment. Phase delay

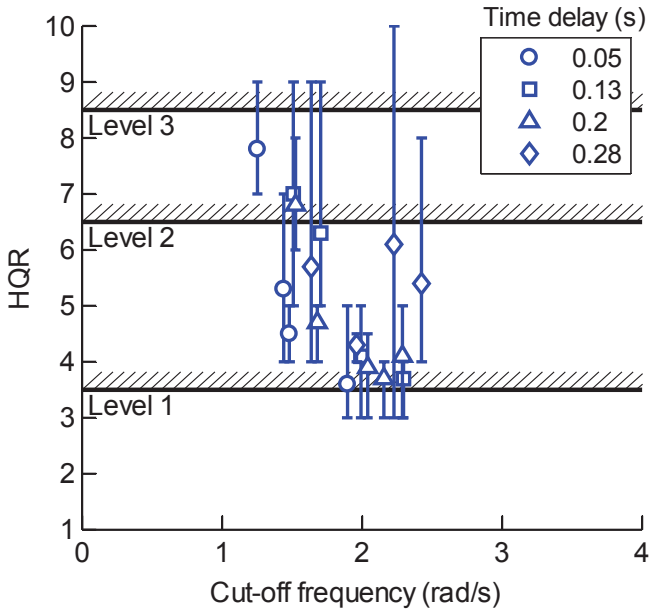

(a)

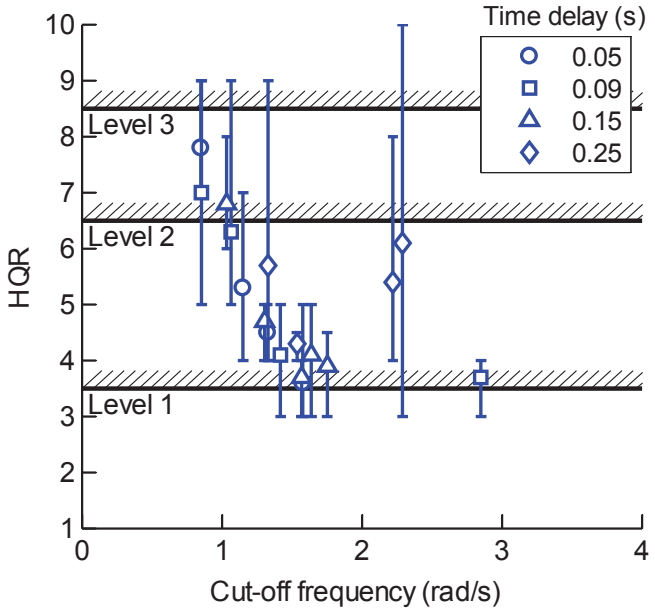

(b)

Figure 54. Correlation of HQRs with pilot cutoff frequency: (a) lateral axis and (b) longitudinal axis.

values for all control system configurations were around 0.15 s, placing the ADS-33 yaw bandwidth requirements approximately at 0.5 rad/s for the Level 2 minimum and 2 rad/s for the Level 1 minimum. The original design was set at 2 rad/s, with the intent that the design point be on the Level 1 boundary.

Figure 55 summarizes the pilot commentary for the different bandwidth and phase delay design points tested. The configurations that nominally fell within the ADS-33 Level 3 handling qualities region (for *All Other MTEs*) were, not surprisingly, found to be lacking in terms of yaw bandwidth. However, design points that should theoretically possess Level 2 properties were unexpectedly characterized as having a major deficiency. The design points at 1.5 and 2 rad/s were reported to have very degraded characteristics. The latter 2 rad/s configuration, in particular, being the initial design bandwidth, was immediately considered unacceptable by pilots upon going into motion with this configuration. Response to pedal inputs for the three control system configurations with bandwidth values under 0.5 rad/s was described by the pilot as being too sluggish. All of these configurations required some level of pilot shaping of the pedal inputs in order to capture the desired heading accurately. In particular, the lowest bandwidth case, i.e., 0.1 rad/s, was deficient in the ability to capture a desired heading, and highly prone to PIO, as well. Additionally, a larger pedal input was required in order to achieve the desired initial response (understood as yaw rate). Pilot comments seem to support the assertion that yaw performance is not adequate enough for these cases to be considered to have Level 2 handling qualities; the 0.5 rad/s case was considered to be equivalent to a borderline Level 2/Level 3 situation.

Yaw response bandwidths of 0.8, 1, and 1.5 rad/s possessed markedly quicker response characteristics, and therefore tended, up to a point, to lead to more predictable configurations. The 0.8 rad/s point was deemed to be the best compromise value by the project test pilot. A second pilot confirmed this as the best trade-off. At higher bandwidth values (i.e., 1 through 2 rad/s), the effects of the large distance between pilot station and axis of rotation manifested a sharpness of the response that was characterized as a major deficiency, with controllability even put into question for the initial design configuration of 2 rad/s.

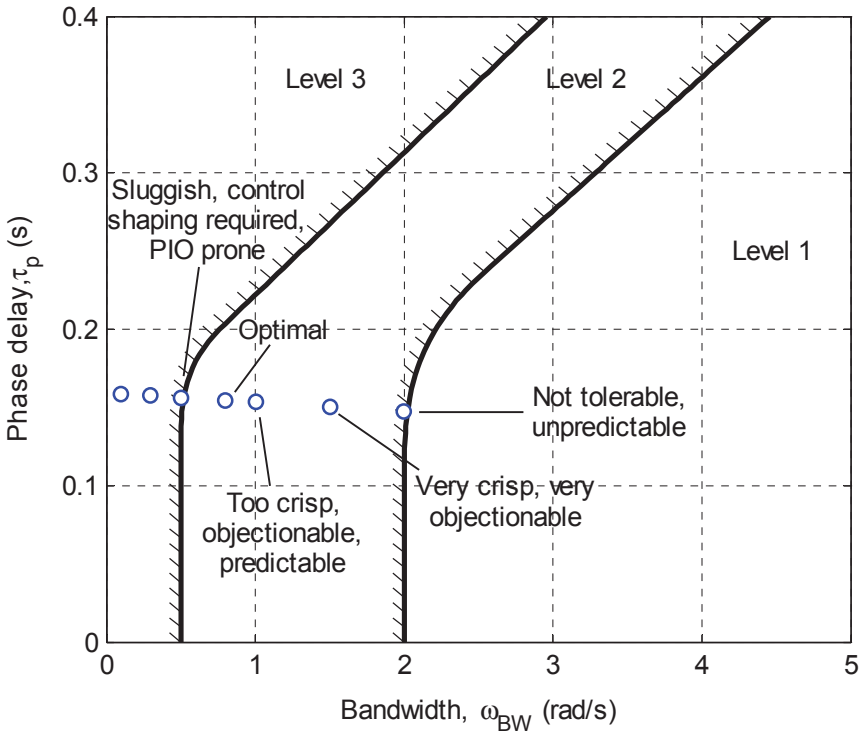

Figure 55. Pilot commentary for LCTR yaw bandwidth and phase delay design points.

After this initial exploratory phase of the yaw characteristics, the simple pedal hover turn task that was developed from the ADS-33 Hovering Turn MTE was employed for the subsequent evaluations. Regarding the task itself, it is noted that although pilots were able to push for much higher aggressiveness than needed, the task was considered representative of an actual mission an aircraft of this size would be required to perform. Based on this Hovering Turn MTE, the average HQR scores shown in Figure 56 indicate there is a broad yaw axis bandwidth range where the aircraft will prove satisfactory. HQR 3.5 and 6.5 contour lines for the surface interpolation of the average HQRs demarcate the Level1, Level 2, and Level 3 handling qualities regions for the available data.

A minimum bandwidth of 0.25 rad/s was required to generate satisfactory yaw control for precise heading capture maneuvers. The HQR surface interpolation contour line distinguishing the Level 1 and Level 2 ratings correlates approximately with the first-order yaw rate command model 3.6 s time constant (τ_{ped}) isoline, highlighting that, at these timescales, the handling qualities are largely insensitive to delay. Below these frequencies, the yaw response becomes unsatisfactory for precision capture of a desired heading. It is expected that yaw control will eventually be lost in the limit when bandwidth approaches zero, as the time to build up desired rates becomes excessive and meeting the performance metrics impossible. A Level 3 boundary was not identified, but extrapolation would put it below 0.1 rad/s. It is noted that while the current ADS-33 short-term yaw response boundaries are not supported for the yaw task defined for this experiment, the same trends are observed for bandwidths less than 1 rad/s, mainly that increasing yaw bandwidth results in improving handling qualities.

The size of the LCTR presents issues when configured for high yaw bandwidths not anticipated in the current ADS-33 specifications. As indicated by the contour boundary lines, degradation into Level 2 of the short-term response handling qualities was observed for bandwidth and phase delay pairs beyond a line defined approximately by rate response time constants in the order of 0.45–0.5 s. Increasing the quickness of response further to response time constants of 0.1 s or less resulted in major control deficiencies that put the aircraft with the ~40 ft pilot offset, squarely in Level 3 handling qualities. Delay in the response has significant

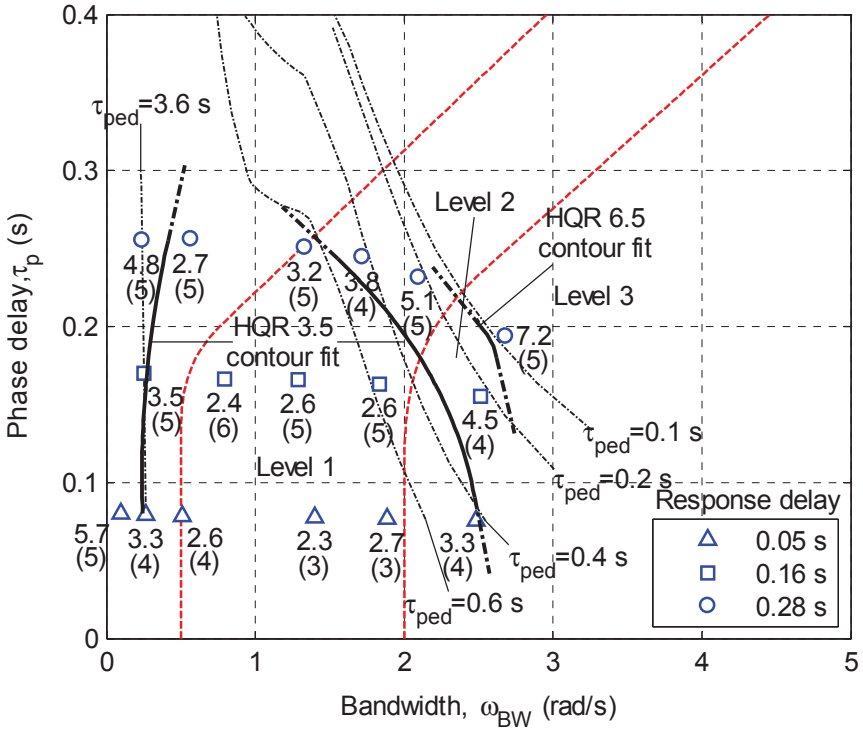

Figure 56. Short-term yaw response handling qualities evaluations for a 40 ft pilot offset.

impact on the handling qualities at bandwidths over 1.5 rad/s. All three configurations with bandwidths between 2.5 and 2.7 rad/s jumped one full handling qualities Level for every 110–120 ms of time delay added to the commanded response dynamics. Pilots consistently described the extreme (i.e., Level 3) case as having a highly unpredictable initial response to input.

A contributing factor to the degraded handling qualities, and likely to the general sense of unpredictability of the initial yaw response, for these configurations commanding fast yaw rate dynamics, was related to a degraded ability of the control system to track aggressive pilot commanded responses because of increased actuator rate saturation.

It is further suspected that some of the issues with the predictability of the response are related to a fundamental distortion of the initial response, where pilots observed a “sudden” or “sharp,” but somewhat delayed response occurring sometime after application of the input. Several pilots identified this type of characteristic response, where they would apply an input expecting an immediate response, which would then occur very suddenly a fraction of a second later. This would be the case where the time scales associated with the dynamics, or the dynamic response, are of the same order of magnitude as the time delay. Take a first-order rate response time constant of 0.4 s or lower, for example. A time delay in the order of 0.1–0.25 s represents a comparable time scale resulting in the type of distorted initial response characteristic discussed above. This discussion is somewhat academic, of course, because the evaluations in the Hovering Turn MTE have confirmed there is no practical need to design the yaw control axis to such high bandwidths for these types of large rotorcraft.

Analogous to the results from the pitch and roll short-term response evaluations discussed previously, where the HQRs showed a close dependency to the second-order command model natural frequency, results shown in Figure 57 from the yaw-axis evaluations in the Hovering Turn MTE illustrate the direct impact of the command model first-order yaw rate response time constant on the handling qualities. Major handling qualities improvements are shown in Figure 57 for a very modest increase in the time constant reciprocal. Also, the HQRs degrade again for the increasing response quickness, crossing the Level 1 handling qualities boundary for a first-order rate response reciprocal of 2.5 s^{-1} (i.e., 0.4 s time constant), according to the deficiencies and issues discussed above. The better handling qualities seem to be found between 0.5 and 1.5 s^{-1}, independent of the time delay.

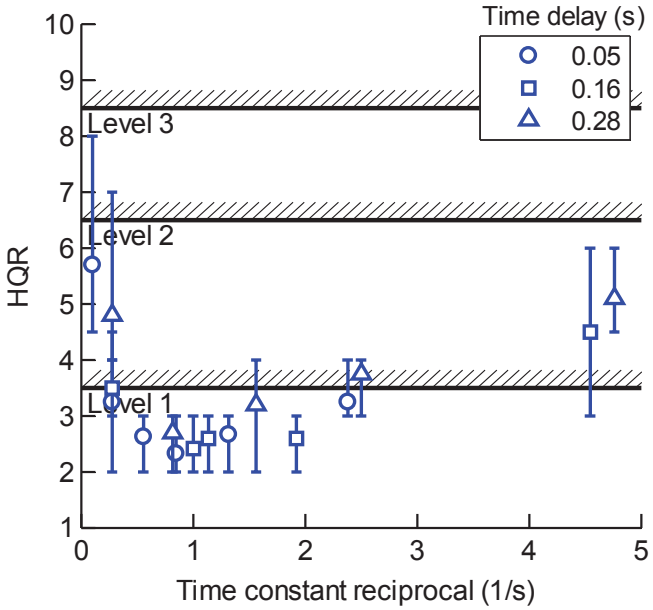

Figure 57. Correlation of average HQRs with reciprocals of the time constants of the commanded first-order rate response for a 40 ft offset.

Handling Qualities for Large Tiltrotor Using Translational Rate Command

Rationale of Investigation

The experimental results from the piloted simulations presented in the previous sections have demonstrated how an ACAH response type was insufficient to confer Level 1 handling qualities for a large tiltrotor in the Hover and Lateral Reposition Mission Task Elements (MTEs). The primary issues were related to the objectionable motion induced at the pilot station because of the offset location from the center of gravity when rotating. Using a Translational Rate Command (TRC) control that eliminated the need to pitch or roll to maneuver was a natural progression. Furthermore, the tiltrotor configuration offers a solution that enables TRC without attitude changes, which helicopters cannot provide. This section presents analysis of results from further piloted simulations that apply a form of TRC, described above, that makes particular use of the tiltrotor control devices to enable maneuvering in translation with almost no angular (attitude) motion. This is achieved by using nacelle tilt to effect longitudinal translation and lateral rotor cyclic tilt for lateral translation. These were designed to act in conjunction with the conventional use of longitudinal cyclic and differential rotor thrust on the left and right rotors to regulate and maintain the pitch and roll attitude at the nominal “deck-level” datum position.

The control law was designed to the TRC criteria specified in ADS-33, and although there is no requirement to apply the military-focused ADS-33 specifications to the civilian LCTR2, it is considered the de-facto design standard for rotorcraft handling qualities and therefore a good basis for the control law design. This section also presents a brief description of the current criteria and background information, and an alternative short-term position response frequency-domain characterization proposed in this investigation.

ADS-33 TRC requirements. The ADS-33 TRC design criterion consists of two quantitative parameters, an equivalent rise time and a steady-state stick to control response sensitivity. Further criteria specify “a qualitative first-order appearance” of the translational rate response to a step controller input is required [10]:

- The pitch and roll attitudes shall not exhibit objectionable overshoots in response to a step cockpit controller input.
- Zero cockpit control force and deflection shall correspond to zero translational rate with respect to fixed objects, or to the landing point on a moving ship.
- There shall be no noticeable overshoots in the response of translational rate to control inputs. The gradient of translational rate with control input shall be smooth and continuous.

The ADS-33 criteria encompass a significant amount of research in their foundation, and it is useful to review this body of work to understand how they were established and also to compare the earlier analysis to results in this section.

ADS-33 criteria definition. The ADS-33 design criteria is built on data from a variety of sources, including some of the important work described in references [52,53,54] that contributed largely to the criteria selection. In particular, this work led to the established respective minimum and maximum rise times of 2.5 and 5 s that are recommended for the desired first-order translational response. The reason for a maximum limit is intuitive; if the rise time is too long, the aircraft response will be too sluggish for precise maneuvering. The cause for the minimum rise time is less obvious, but it is fundamentally linked to an implementation of TRC where an inner attitude loop is enclosed by an outer translational motion loop, and the translation is caused by changing the attitude of the aircraft. A minimum rise time is a compromise between achieving a quick enough translational response and mitigating abrupt attitude changes that would be induced by a high-bandwidth TRC response.

The other key TRC requirement in ADS-33 is the “Control Response,” which is the steady-state translational velocity response per unit stick. Again, reference [52] was the key source for establishing the boundaries. They consist of an upper and lower limit for a nonlinear shaping of

the control sensitivity in ft/s/in. The shaping confers reduced control sensitivity between 3 and 6 ft/s/in for speeds of up to ~10 knots and higher sensitivity for larger velocity commands.

The supporting data for the ADS-33 TRC criteria were a number of experimental analyses of TRC conducted in flight test, and in motion- and fixed-base simulation, on a variety of platforms including the X-22A ducted fan V/STOL aircraft [54,55,56], the AV-8B jet aircraft [57], and the XV-15 tiltrotor [45,58], as well as other generic types. Studies in references [54,55] reported on an in-flight simulation experiment using the X-22A variable stability aircraft. Highlights included the use of an inner/outer loop-style TRC control law using attitude changes. The experiment examined equivalent translational response rise times in the range of 1.5 to 4 s, and variation of the control response sensitivity in the range of 3 to 12 ft/s/in. Similar conclusions to reference [52] were arrived at, in that pilots did not like the attitude changes that came with this form of TRC.

Reference [54] describes how different pilots reacted to attitude changes in TRC. The results from the experiment were used to create a TRC handling qualities criterion that was reappraised in an analysis in reference [56]. The purpose of this follow-up study was to validate the use of fixed-base simulation for the prediction of the X-22A in-flight simulation TRC handling qualities. A key premise of the paper was that TRC criteria based on correlating regions of cross-plots of the equivalent rise time and the control/response sensitivity parameter (linear constant) were inconsistent in predicting the piloted handling qualities.

The alternate criteria in reference [56] used a frequency-domain approach of regions of predicted Level 1 and Level 2 handling qualities on a Bode plot of the translational velocity response to stick input. The envelopes were applied to both the magnitude and phase plots of the frequency response, and the different regions of the plot were annotated to indicate possible handling qualities problems if a system frequency response curve entered that region.

The study in reference [56] showed that this frequency-domain approach was superior in predicting the handling qualities, especially when used in conjunction with a secondary criterion that included a measure of the magnitude and abruptness of the attitude response. The paper reported that this attitude sensitivity aspect was an area of “critical concern” for pilots.

This secondary criterion was based on a similar sensitivity criterion from a study in reference [58] that investigated TRC using an XV-15 simulation. In this work, the TRC system sensitivity, stiffness, and damping were varied parametrically using simplified linear models. Here, the stiffness was akin to the rise-time parameter as it effectively determined the quickness of the response and, as it was an attitude-based TRC, it also consequently governed the magnitude and abruptness of the attitude response. Again, optimum values for the translational response sensitivity and stiffness featured a trade-off between fine control and attaining adequate translational response in gross maneuvering, as well as between having low enough time constants to provide precise, responsive control without large or abrupt attitude changes. The pilots preferred a TRC response that was more first-order in nature with less oscillations and overshoots in the velocity.

Reference [53] highlights the importance of this first-order characteristic that describes the use of Lower-Order Equivalent System (LOES) models to characterize the TRC response. Reference [53] reports that better handling qualities were obtained where the translational response fit well to a first-order form such as in Eq. (37). In Eq. (37) $\dot{X}$ represents the translational rate, δ_{pilot} is the pilot stick input, and $K_{\dot{X}}$ and $T_{\dot{X}}$ are the control response sensitivity and equivalent rise time, respectively. Degraded handling qualities were reported in reference [53] when the aircraft response characteristics required a third-order form to capture higher-order dynamics (i.e., the attitude dynamics were significantly affecting the TRC response). This reinforced the observation that these configurations are unacceptable because of the excessive attitude responses.

$$\frac{\dot{X}}{\delta_{pilot}} = \frac{K_{\dot{X}}}{T_{\dot{X}}s + 1} \tag{37}$$

The study in reference [53] also assesses the equivalent rise time and steady-state velocity response sensitivity of the TRC control laws. Their analysis (based on results from reference [45]), is in alignment with the others reported in that they identified an optimum rise time for handling qualities in the 2.5 to 5 s range. For the sensitivity characteristics, there was a general complaint that the maximum speed attainable (~24 knots) in TRC was too low. However, one interesting observation made is that a trend of higher control sensitivity for attitude-based TRC can be accepted when the rise time increased, i.e., when more sluggish. The hypothesis derived from this observation was that the pilot ratings somewhat aligned with curves of constant attitude change per unit stick in TRC (this ratio being a function of both the rise time and sensitivity).

The underpinning aspect of all of this previous evidence was that attitude-based TRC was used, and that some characteristics of that approach bring limitations. This is a point not completely disregarded in the literature, as references [53,57] both discuss the possibilities of TRC using Direct Force Control (DFC) through forms of thrust vectoring. An analysis of DFC-based response types is presented in reference [59], which compares acceleration and translational rate response types using both DFC and attitude-based approaches. The study in reference [57] reports on a fixed-base simulation study based on the AV-8B aircraft. It highlights how DFC decouples the attitude response from the translational response and how the experiment compared TRC based on attitude changes, DFC, and a combination of the two. A key result was that the pilots liked the attitude-only TRC systems the least and unanimously preferred the DFC systems. The HQRs recorded in the experiment were plotted against the criteria from both the previous Calspan X-22A [54] and the Systems Technology, Inc. (STI) XV-15-based studies [53]. The ratings for the attitude TRC did not match well with either criteria, predominantly because the ratings were mostly connected with the attitude changing aspect, something that the rise-time vs. steady-state velocity sensitivity criteria do not explicitly cover. When the DFC ratings were compared, much better correlation was achieved, particularly with the Calspan boundaries.

Another important experimental result achieved using the DFC-based TRC was that increasingly better HQRs were obtained with increasingly quicker (shorter) rise times. Rise times down to 0.7 s were examined, which conferred Level 1 (HQR ≤ 3) ratings. This is an important result, as the 2.5 s minimum acceptable level reported in a number of the attitude-based TRC studies (and ADS-33) was no longer appropriate because the attitude changes were no longer a factor.

This conclusion of the superiority of DFC TRC response type is not, however, universal. The study in reference [53] also briefly discusses DFC vs. attitude TRC and states, “There is some evidence that complete decoupling between attitude and horizontal translation is not necessarily superior.” It goes on to refer to the study in reference [59] and another using the X-14A V/STOL aircraft. Reference [59] reports that the prime reason that the DFC-based TRC was rated worse was because of negative ride quality effects caused by the generation of “non-gravitational” reaction forces acting on the pilot when maneuvering. It is important to note that the study in reference [59] featured motion cueing as opposed to the fixed-base simulation in reference [57]. Another study of TRC using DFC is a simulation experiment in the NASA VMS of an Advanced STOVL (ASTOVL) aircraft [60,61]. This study has a number of useful parallels with the current research in this paper, i.e., it is a motion-based study in the NASA VMS, and it features an analysis of a hovering vehicle using a DFC form of TRC (in the longitudinal axis). The discussion of the performance of the TRC control law focused much more on frequency-domain parameters such as bandwidth and phase delay.

For longitudinal control, the results in references [60,61] showed that bandwidths (based on the −45 deg phase margin frequency from the translational velocity to stick input frequency response) of between 0.4 and 0.9 rad/s conferred consistently satisfactory handling qualities, whereas values below 0.22 rad/s and above 1.1 rad/s were only adequate. The authors refer to the ADS-33 rise-time criteria of 2.5 and 5 s and compute that for an equivalent first-order

response, these equate to bandwidths of 0.4 and 0.2 rad/s respectively. The authors note that the 0.2 rad/s value agrees well with their results while, at the other end of the range, their results indicate an ability to accept much quicker (higher bandwidth/short rise-time) TRC response with acceptable handling qualities. This discrepancy is attributed to “differences in implementation of the longitudinal velocity command systems,” which alludes to the previously discussed issues connected with attitude-based TRC. Another insight brought to the fore was through the use of the phase delay parameter, which highlighted that delays as high as 0.78 s could be tolerated before the handling qualities degraded to adequate. It was reported that the pilots could sense the delay but were able to compensate without too much effort until the delays became extreme. The authors suggested the Level 1–2 boundary based on phase delay is in the region of 0.4–0.6 s.

Some of the TRC research literature presented has included tiltrotors, which are of particular relevance to the current research. However, the tiltrotor research has not reported any experimentation with the DFC form of TRC using nacelle tilt to vector the thrust (for longitudinal translation). The only mention of such an approach was a consideration in reference [45] to implement a “mast-angle controller” for the XV-15 simulation. This proposed development was abandoned when it became apparent that, as a consequence of the limited performance of the nacelle actuators, the system would possess a very low u/δ_{lon} bandwidth of around 0.7 rad/s, although it is not apparent which measure of bandwidth was used.

The key issues of how the ADS-33 TRC criteria were established have been discussed, as well as the implementation-specific aspects that underpin them. It has been shown that there are a number of useful similarities in the body of work in the literature to the current LCTR2 research. However, there are a number of aspects of the LCTR2 control architecture that are unaddressed in the current literature that require new research, including the influence of nacelle actuation characteristics on this form of nacelle-based TRC and its impact on large tiltrotor handling qualities.

Short-term position response characterization of nacelle-based TRC. As described in the preceding discussion, the TRC response characteristics have been defined and specified using a mixture of qualitative descriptions and quantitative time- and frequency-domain response criteria. The research presented in the following sections shows that the current ADS-33 criteria does not satisfactorily predict the handling qualities for the TRC control laws developed for the LCTR2 configuration. It also shows that response delays due to actuator dynamics, as well as implementation-specific aspects, mean that although a particular configuration meets the Level 1 Handling Qualities (HQ) requirements, other factors affecting the slope of the frequency response phase curve at high frequencies lead to degraded handling qualities. Frequency-domain characterization using parameters such as bandwidth and phase delay is a robust way of defining response characteristics for good handling qualities using rate and attitude response types, and in most cases supersedes the use of time-domain parameters in up-to-date rotary and fixed-wing HQ requirements. For the TRC response, the longitudinal axis (the equivalent inceptor/response variable pairs would be appropriate for the lateral case) could be potentially characterized either by the u/δ_{lon} or the X/δ_{lon} frequency response, an extension of the definitions employed in ADS-33 for attitude responses applied to the translational response. While u/δ_{lon} at first may seem a more natural representation of the aircraft TRC response, neither the gain or phase bandwidth definitions are representative of pilot-in-the-loop operating frequencies for position regulation tasks, according to the discussion above. Herein, the X/δ_{lon} frequency response was chosen to characterize the TRC response, for the different experimental variants, as it was deemed to be a more suitable characterization for pilot-in-the-loop position control tasks, paralleling the approach by Franklin et al. [61] presented previously. Sections below, which consider the TRC control laws, demonstrate that the combination of X/δ_{lon} phase delay and bandwidth correlate well with the piloted handling qualities and, therefore, offer useful metrics for future TRC design specifications.

Figures 58 and 59 show the relationship of the closed-loop X/δ_{lon} frequency response phase bandwidth and delay values for the linearized model with the TRC control law command model equivalent rise times set at 2.5 and 5 s, and various nacelle actuator natural frequencies. Also shown are the phase bandwidth and delay for the cyclic-augmented control law, described above, which uses a 3 rad/s bandwidth nacelle actuator, and the corresponding lateral response

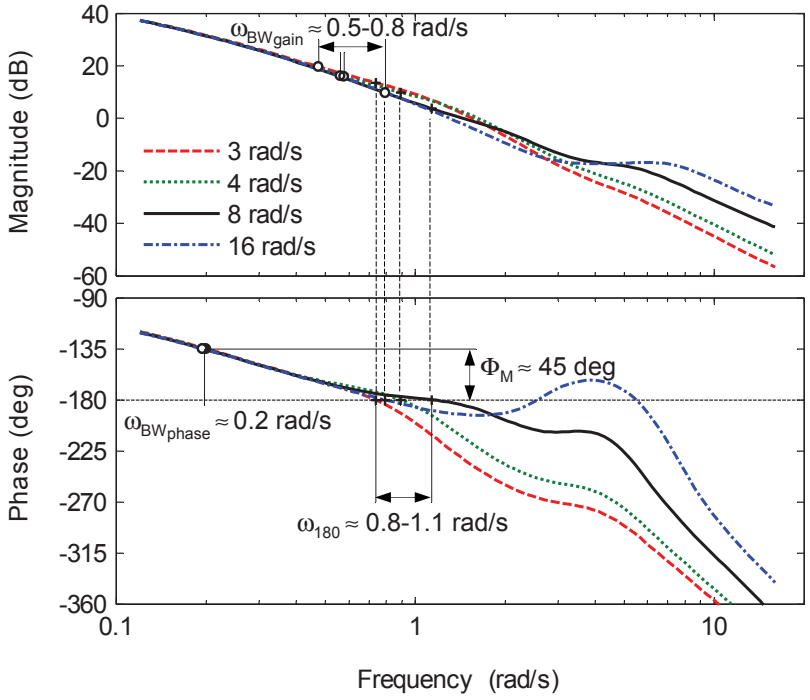

Figure 58. Closed-loop X/δ_{lon} frequency response for varying actuator bandwidth (5 s equivalent rise time).

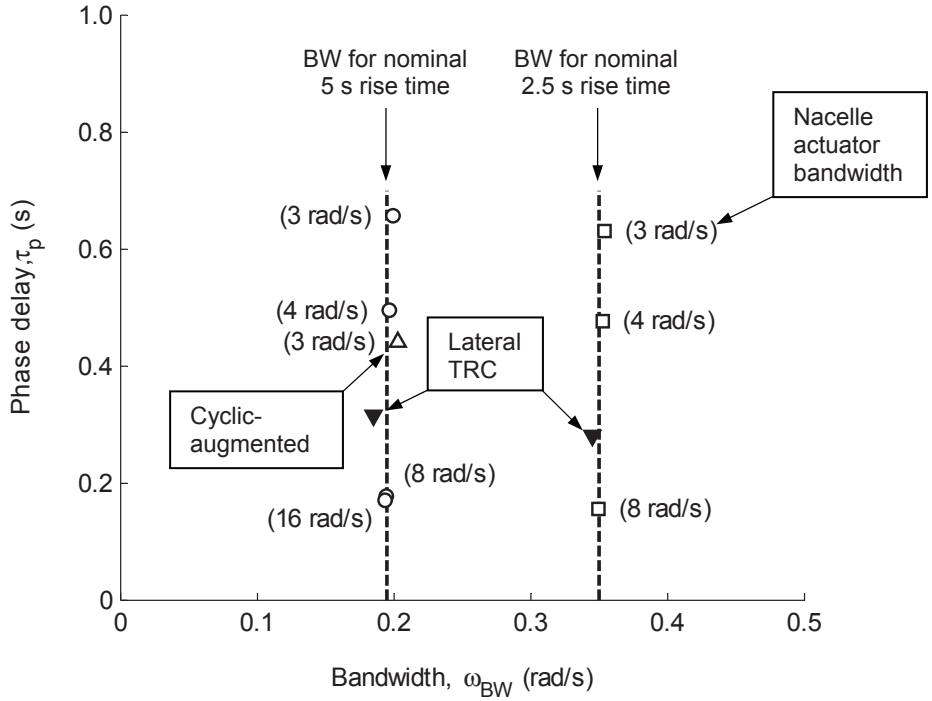

Figure 59. Closed-loop X/δ_{lon} bandwidth and phase delay for experimental TRC configurations.

specification based on the Y/δ_{lat} transfer function. The latter illustrates the typical phase delays attainable with rotor-effected TRC.

Equivalent rise time has a fundamental relationship with the phase bandwidth, $\omega_{BW_{\text{phase}}}$, as defined from the Bode plot of the X/δ_{lon} transfer function shown in Figure 58, but has much less effect on the phase delay, τ_{p_X}. The cases with equivalent rise time of 5 s shown in Figure 58 all had a nominal phase bandwidth of approximately 0.2 rad/s, whereas the 2.5 s equivalent rise time conferred a phase bandwidth closer to 0.36 rad/s (Figure 59). The actuator bandwidth, conversely, predominantly influenced the phase delay. The 3 rad/s actuator, for example, confers a phase delay in the order of 650 ms, but its bandwidth is basically unaffected. A progressive reduction in the phase delay is shown for increasing actuator bandwidths, down to about 200 ms for the 8 and 16 rad/s actuator configurations. The 16 rad/s actuator configuration displays a prominent phase recovery in Figure 58 but conveys minimal phase delay improvements over the 8 rad/s actuator configuration (Figure 59). These issues are further discussed below. Finally, the cyclic-augmented configuration confers a 200 ms phase delay reduction over the baseline configuration with the 3 rad/s actuator. Phase bandwidth was still led by the equivalent rise time and was accordingly close to 0.2 rad/s for this configuration.

Figures 60 and 61 use the qLPV LCTR2 model with nonlinear actuators and show the results of changing the nacelle actuator rate limits on the X/δ_{lon} short-term dynamic response

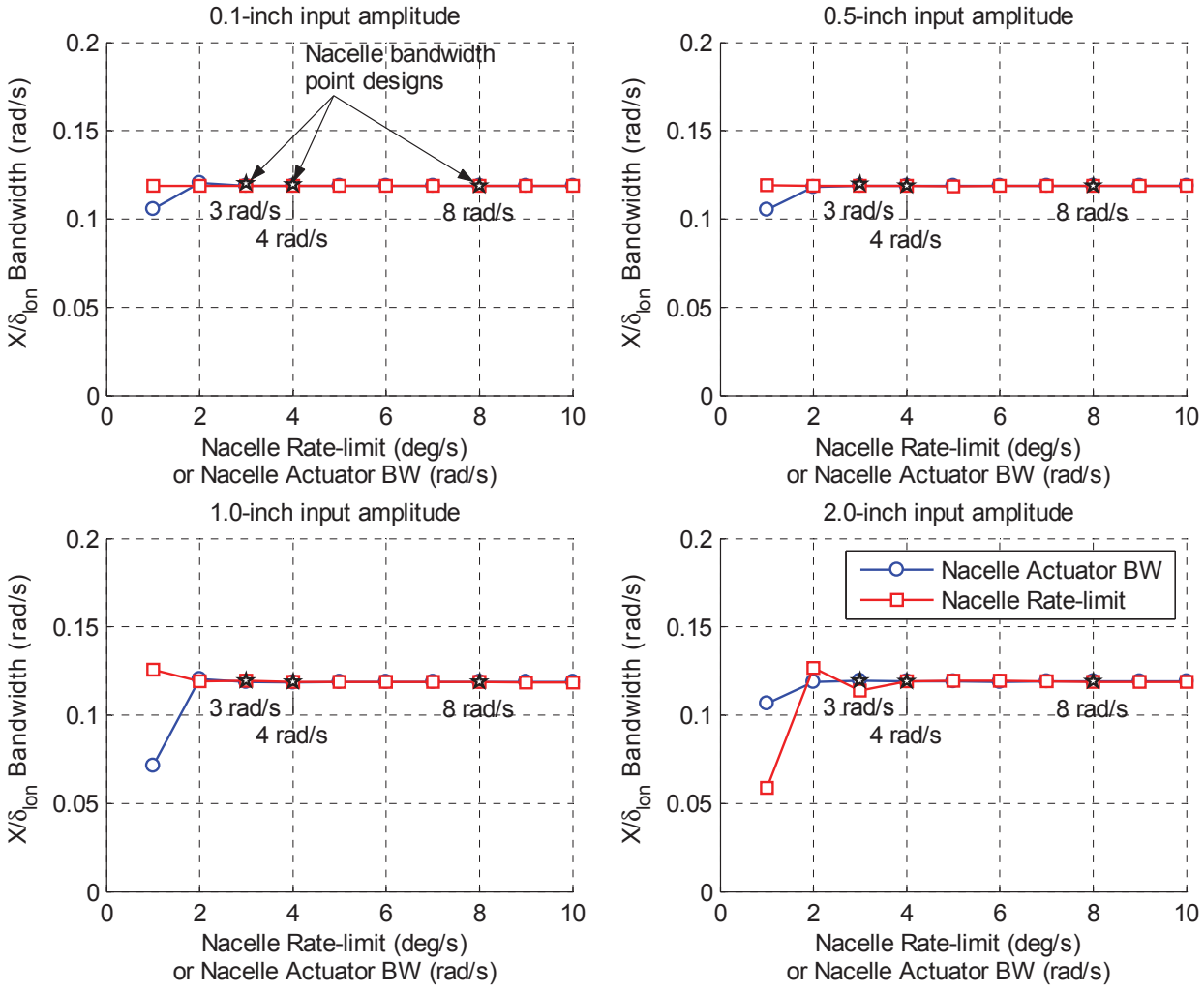

Figure 60. X/δ_{lon} bandwidth from varying amplitude frequency sweeps for varying nacelle actuator rate limits and bandwidths (10 (ft/s)/in control/response sensitivity).

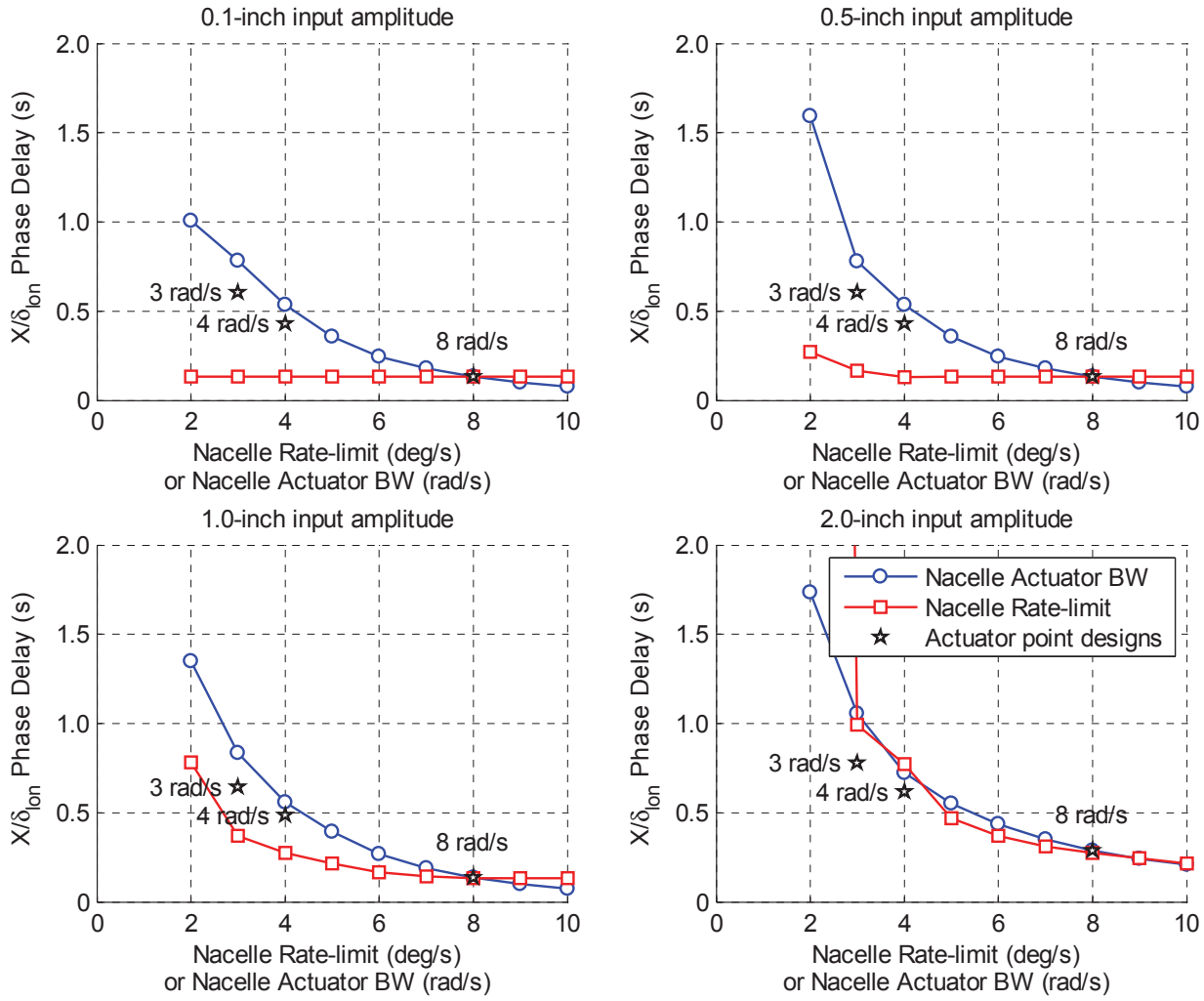

Figure 61. X/δ_{lon} phase delay from varying amplitude frequency sweeps for varying nacelle actuator rate limits and bandwidths (10 (ft/s)/in control/response sensitivity).

parameters: bandwidth, ω_{BW_X}, and phase delay, τ_{p_X}, and compares it to the effect of varying the nacelle bandwidth by independently sweeping over a range of nacelle actuator natural frequencies or rate limits. These were computed using frequency sweeps at four different input amplitudes of the longitudinal stick input, δ_{lon}, shown in each of the subplots. The sweeps were performed on the baseline configuration (8 rad/s bandwidth, 7.5 deg/s rate limit) with one of the two parameters held constant at these values while the other was varied. On each of the charts the 3, 4, and 8 rad/s point design configurations from the piloted experiment are also plotted for comparison; the key difference between these cases and the sweep results is that their control law gains have been optimized for a specific combination of actuator bandwidth and rate-limit point designs.

The effect on the longitudinal position response bandwidth shown in Figure 60 is minimal from either parameter variation except at very low actuator bandwidth or rate limits, where there are some variations. The longitudinal position response phase delay results for the same rate-limit and bandwidth variations are shown in Figure 61. Here there are continuous trends of increasing delay with both bandwidth and rate limit, with both trends showing differing amounts of sensitivity to the input amplitude. At low amplitudes the rate limit does not influence the phase delay until it gets very low, whereas bandwidth has an effect at all amplitudes. As the amplitude

increases, the effect of the variation in the two parameters becomes almost indistinguishable for the range examined, despite the rate-limiting being a nonlinear discontinuity and the bandwidth being entirely a linear dynamic parameter. It is also useful to note that the experimental point designs all have smaller phase delays than the sweep analysis points, implying that the optimization of the TRC gains appears to bring some noticeable benefit. Further discussion of results from the effects in Figures 60 and 61 are provided in subsequent sections.

Overview of results. The handling qualities of various LCTR2 TRC control configurations encompassing variations of the nacelle actuation rate limit and natural frequency, and other design aspects of the control law, are assessed. TRC configurations are compared against each other and to the best-performing ACAH in the Lateral Reposition and Hover MTEs in further piloted simulation experiments in the NASA Ames Vertical Motion Simulator (VMS). The TRC discussion concludes with analysis of a "cyclic-augmented TRC" design that uses additional longitudinal cyclic inputs as part of the TRC control law to address concerns that only lower nacelle actuator bandwidths may be possible to alleviate the demand on the primary nacelle actuators to create the translational response. Results show that the TRC control system design did not confer *consistent* Level 1 handling qualities. This study called for the fundamental review of the ADS-33 design criteria to understand their relationship with the handling qualities with this type of TRC control law configuration, and ultimately identify design characteristics conducive to Level 1 handling qualities.

The second-order nacelle actuator dynamics was commonly fixed with a value of 8 rad/s for the natural frequency/bandwidth. This was identified as a potentially unfeasibly high value for such a large actuator. Therefore, further research was also required to investigate the handling qualities trends when reducing this actuator bandwidth. This analysis, reported below, sought to identify the minimum bandwidth required to maintain Level 1 handling qualities with this type of TRC control system.

Small non-minimum phase pitch changes in response to longitudinal stick inputs were found to negatively impact the handling qualities of this TRC control system design. Depending on the actuator rate limits, the aircraft response had a coupled pitch motion that was counterintuitive in direction sense and often obtrusive. Reducing rate limits reduced this problem but at the cost of degrading the overall TRC response quickness (or bandwidth). The discussion below describes the results of varying rate limit on the initial TRC control laws.

Further experimentation showed that handling qualities improvements could be achieved by simply reducing the tendency to pitch in TRC mode. This was achieved by developing a TRC control law that incorporated a crossfeed signal between nacelle rate and longitudinal cyclic. The intent was to achieve a "purer" response, i.e., translational motion only with no coupled attitude perturbations. Better ride qualities were not the only advantage of this system. The flight dynamics aspects of this improvement are discussed in detail further below. Analysis of the influence of rotor longitudinal flapping dynamics, nacelle actuator limits, and piloted input amplitude showed that the crossfeed-improved TRC not only reduced the pitching response to almost zero, but also improved the TRC position response phase delay characteristics. Appendix B describes how the key effect of this crossfeed gain was to reduce the tendency for the rotor flapping to lag behind the nacelle rotations.

Finally, the analysis reported below sought to investigate techniques to maintain the Level 1 handling qualities at lower nacelle actuator bandwidths, i.e., second-order dynamics and (equivalently) rate limits, through additional control law modifications.

Improvement of LCTR2 Handling Qualities With TRC

Results for select ACAH and TRC configurations chosen for comparison in the Lateral Reposition and Hover MTEs are presented in this section. When selecting the LCTR2 short-term attitude response characteristics for comparison, care was taken to ensure sensible ride qualities, thus precluding higher bandwidth control response configurations. A methodical verification of various configurations was conducted with the project pilot prior to the

commencement of the experiment. This process confirmed the trends from previous experiences, i.e., that higher response bandwidths result in negative ride qualities. The comparison ACAH therefore represents the best trade-off between handling and ride qualities.

The TRC control system used the conventional center stick controller. The inceptor gradient and break-out force-feel characteristics were configured for ACAH at 0.9 lb/in and 1 lb in the longitudinal direction and 0.7 lb/in and 0.6 lb in the lateral direction. Given these force-feel characteristics, center stick TRC control sensitivities were adjusted to provide the best-expected task performance with acceptable forces for the required inceptor displacements. The evaluation maneuver had constraints for this center stick TRC implementation that required a minimum translational velocity of 25 ft/s (~15 knots). Only directly proportional variations in translational rate with control deflection were investigated (i.e., constant sensitivity gains).

Lateral Reposition MTE. Piloted evaluations in the Lateral Reposition MTE showed that significant handling qualities improvements were conferred with TRC, when compared to the ACAH and "Hybrid" response types (Figure 62). The TRC configuration in Figure 62 employed a 15 ft/s/in sensitivity and a 5 s rise time. As shown, this configuration was consistently rated HQR 2–3. In contrast, ACAH was mostly rated HQR 4 (with a few HQR 3 marks and one HQR 6). Finally, the Hybrid mode fell somewhere in between the TRC and the ACAH response types in terms of their handling qualities (most configurations were rated HQR 3). Recall that the "Hybrid" system was mechanized such that a center stick displacement greater than 1 inch from center would command roll attitude at a 3.45 deg/in sensitivity (0.3 of the baseline ACAH command model) in addition to the normal translational lateral rate commanded. Within this 1-inch displacement range, the system behaved identically to the TRC control system.

Unsurprisingly, the experimental observations suggested that longitudinal position control with the ACAH response type was challenging because of the pitch/heave coupling of pilot control activity associated with the significantly forward position of the pilot station. A survey of the pilot evaluation comments indicated that high workload in the longitudinal axis and altitude maintenance were contributing reasons for the elevated handling qualities ratings (HQRs) assigned to the ACAH mode. Moreover, the high bank angles associated with the ACAH configuration in the Lateral Reposition MTE were a major cause of performance degradation, initiating a sequence of events, to include the loss of usable visual cues, which significantly

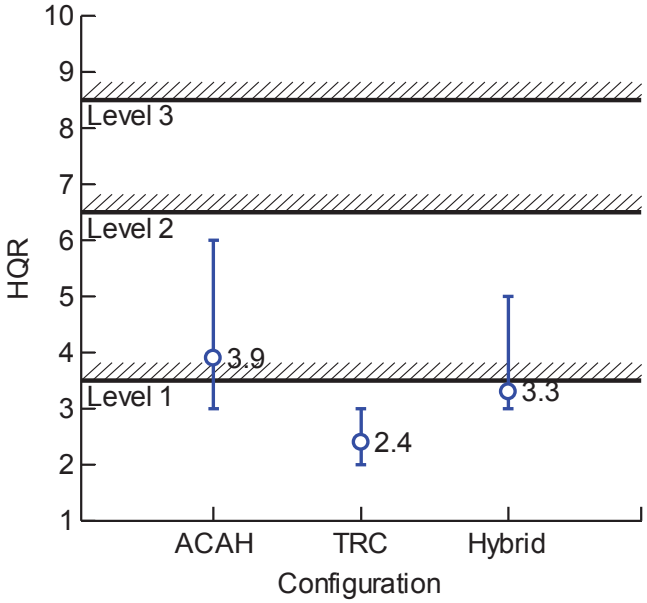

Figure 62. Comparison of the HQRs for the ACAH, TRC, and Hybrid response type control configurations in the Lateral Reposition MTE.

increased the pilot workload. Pilots tended to lose sight of the longitudinal position cueing, especially during the deceleration when commanding large bank angles to arrest the lateral rates at the hover point. Additionally, a tendency to pitch up could cause the pilots to lose the lateral position cue.

It should be noted that the absence of an Altitude Hold mode contributed to a tendency to "balloon," or gain altitude easily, during the deceleration phase of the maneuver. When decelerating aggressively the control system would see the sudden change in the body z-axis velocity component as an un-commanded sink rate. Differences in the commanded and actual rates, if not adjusted quickly by the pilot, would result in the control system increasing power rather suddenly. This, in conjunction with the sudden change in aerodynamic angle of attack, naturally caused the aircraft to climb.

By reducing the bank angle changes, the TRC control response, and to a lesser degree the Hybrid response type, conferred notable improvements to the handling qualities in the Lateral Reposition MTE. Without the large bank angle changes, pilots did not lose sight of the runway as readily. Also the aircraft did not experience significant changes in altitude, such that the power/altitude maintenance did not require attention. Minimization of pitch attitude changes also curtailed the compelling pitch/heave perception issues associated with the center of gravity offset. Pilots described the lack of bank as "odd," but agreed it was possibly the right way to fly this type of aircraft, and the HQRs confirmed their preference and better performance. Less significantly, compared to ACAH, the TRC and Hybrid configurations required larger lateral input. Pilots often mentioned that stick forces generated with these configurations were a little high. With the Hybrid mode, some of the issues related to the high bank angles, such as the loss of visual cues and the power management requirements, were lessened, but not entirely eliminated. Also, the Hybrid mode was not without its own faults, and issues with the phasing in and out of the bank angle felt somewhat unpredictable to two of the evaluation pilots.

Hover MTE. Ratings comparing select ACAH and TRC configurations in the Hover MTE are shown in Figure 63. It shows drastic improvements in the average ratings for the two TRC configurations (5.2 for ACAH, 2.1 for a TRC variant with 8 rad/s bandwidth nacelle actuators, and 2.8 for the so-called "cyclic-augmented" TRC). The TRC results presented in Figure 63 are for a 10 ft/s/in sensitivity and a 5 s first-order response equivalent rise time. These results illustrate the substantial, potential handling qualities improvements that are attainable with a

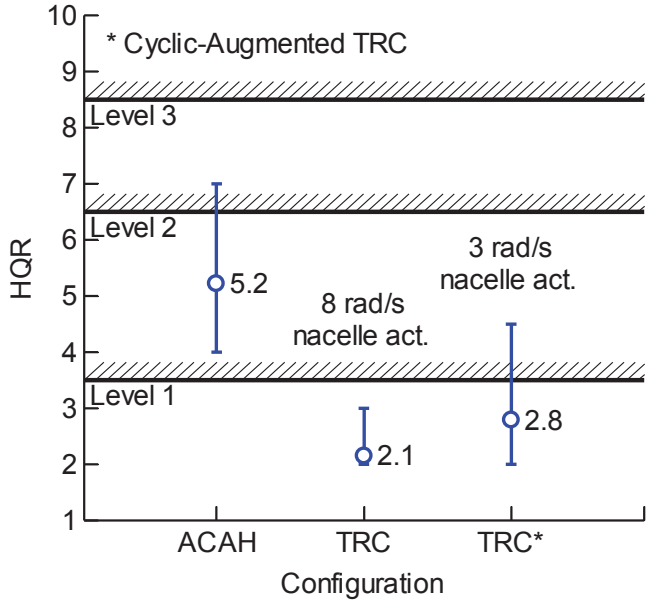

Figure 63. Comparison of LCTR2 handling qualities for select TRC implementations relative to ACAH in the Hover MTE.

Table 14. TRC response parameters.

Control sensitivity ((ft/s)/in)	Nominal rise time (s)
15	5.0
10*	5.0*
5	5.0
15	2.5
10	2.5
5	2.5

* Baseline

TRC response type, provided necessary nacelle actuator bandwidth is installed, and how good handling qualities can be retained by quickening of the TRC response via rotor cyclic inputs with a reduced nacelle bandwidth. The cyclic-augmented TRC control law generated a sharp longitudinal cyclic pulse in response to the velocity command generated by the pilot. This provided the crucial initial longitudinal acceleration desired for the short-term TRC response quickening. As the pitch attitude built up, and once the nacelle actuator caught up with the command, the controller would effectively resume the attitude regulation role removing the initial cyclic input.

The outcome of a systematic analysis of the ADS-33 TRC design criteria and various fundamental design aspects of the nacelle actuators, encompassing a range of control sensitivity, equivalent rise time, and nacelle actuator bandwidth and saturation limit variants, led to the result that handling qualities improvements for the various TRC versions were generally not as definitive as those shown in Figure 63. Many of these results are shown in the subsequent discussions. An average improvement of the ratings suggested a general increased weighting of the HQRs towards Level 1 with the TRC configurations, compared to ACAH. However, a handling qualities cliff was exposed, evidenced by the fact that a number of pilots rated the handling qualities with TRC to be either worse or equal to those with ACAH control mode. This is the focus of discussion further below. Consequently, minimum and maximum ratings for the various TRC versions conferred a range of ratings, a range equivalent or even greater than that for ACAH.

Despite the variability in the TRC HQRs, on closure of the velocity feedback loops, all TRC configurations showed a notable reduction in the turbulence-generated motion of the aircraft. Once pilots had stabilized in the hover, workload ceased being a major factor, and pilots reported the aircraft appeared to reject turbulence very effectively. The critical sub-phase of the maneuver was consistently observed to be the deceleration into the hover, which appeared in some occasions to drive aggressive pilot compensation and thus expose the handling qualities cliff.

Effect of Control Sensitivity and Equivalent Rise Time

The control sensitivity and equivalent rise time parameters are the focus of this section. These parameters define the fundamental behavior of the TRC response and form the core of the ADS-33 HQ specifications for TRC as described in the rationale of investigation section. In the control law for the LCTR2 nacelle-based TRC, these parameters were used directly in the model-following command model blocks to specify the desired first-order response type, which the aircraft then attempted to track as closely as possible via the feedback control loops.

Table 14 lists the TRC control system parameters tested, including the control/response sensitivity gradients and nominal equivalent rise times. The baseline TRC control system case consisted of a 10 (ft/s)/in control/response sensitivity, a 5 s equivalent rise time, and a 0.0735 in/(deg/s) nacelle rate to longitudinal cyclic crossfeed. This control system also employed high

bandwidth actuators (8 rad/s) to avoid cutoff of control inputs. Additional control system gain sets basically enforce variations in the control/response parameter and the equivalent rise time.

Summarized in Figure 64, HQRs for the varying control/response sensitivity and equivalent rise-time cases highlight two salient results: first, that 10 (ft/s)/in was the preferred sensitivity, and second, that the increased phase bandwidth associated with the 2.5 s rise time conferred only a slight improvement in the HQRs over the 5 s cases. Consequently, the experimental baseline design conferred the best handling qualities of the range of configurations selected.

Pilots generally indicated that the high stick sensitivity value resulted in the aircraft response being “too jerky.” High control sensitivity also made this configuration much more susceptible to rate-limiting. On the other hand, low stick control sensitivity elicited complaints that excessively large inputs were required. The control sensitivity did, however, offer an added protection against rate-limiting of the nacelle actuators. In interpreting these results, it is important to note that while the control/response sensitivity was varied, the control stick force gradient was left invariant. The potential effect of this parameter should not be discounted when establishing overarching conclusions about the control sensitivity, since it has a direct effect on the forces and thus the dynamic response of the stick. The differences between the VMS and flight motion cueing may also need to be considered before reaching a final conclusion on the appropriate control sensitivities.

A X/δ_{lon} phase bandwidth improvement from just below 0.2 rad/s to 0.36 rad/s due to a smaller rise time did not appear to confer significant improvements in the handling qualities, although it did appear to improve the worst case scenarios. The reduced rise time did convey to the pilots a slight sense of increased quickness in the response when decelerating, and thus improved the ability to decelerate within the required time constraints.

A more detailed analysis of the piloted evaluations indicates that three pilots rated the 15 ft/s/in (high) sensitivity, 5 s rise time case in Level 2 (HQR 5/4/4). Comments from these pilots about the deficiencies pointed to, first, a tendency to over-control in the longitudinal axis, and second, a sharp lateral response. In particular, two of the pilots, and importantly, the pilot who rated the aircraft configuration HQR 5, indicated a tendency to over-control in the longitudinal axis; this became apparent during the deceleration and hover stabilization phase of

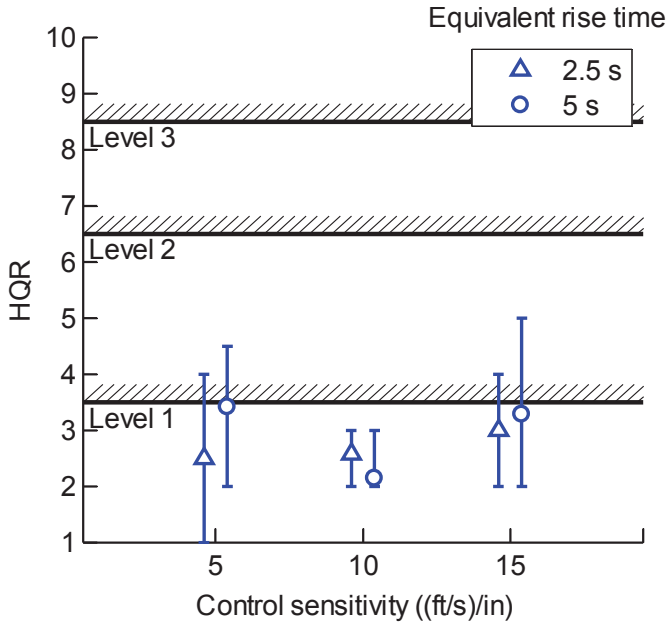

Figure 64. HQRs for varying equivalent rise times and steady-state control response sensitivities (8 rad/s actuator).

the maneuver. Other comments pointed to a very sharp lateral response, to the point of feeling disharmonious with the longitudinal response, but this did not necessarily intimate there was a deficiency in the longitudinal axis per se.

This disharmony observation was even more prevalent for the 15 ft/s/in sensitivity, which, when combined with the 2.5 s equivalent rise time, was greatly exacerbating the sharpness of the initial response. This configuration was often described as “uncomfortable,” and pilots consistently felt they could not be aggressive with it because of the “choppy” nature of the response. A “noticeable and distracting” strong heave perception described as “objectionable” was also reported by some pilots. This configuration, however, presented no tendency to over-control as the 5 s rise time/15 ft/s/in sensitivity case did, which made it perform quite well, especially in the deceleration and hover stabilization phase. The lower rise time fundamentally allowed pilots to achieve desired precision in capturing the hover position simply by releasing the stick and bringing back to center, or with very minimal required input reversal to stop.

The opposite (low) end of the control sensitivity range saw deficiencies in the aircraft characteristics of a different nature. The main objectionable characteristics were all derived from the fact that pilots now had to employ larger displacements, both steady and dynamic, in order to get a response of the aircraft. Associated with the large displacements were large forces, since stick force gradients were left unchanged for all configurations. Steady displacements were uncomfortable because of the large forces being sustained for prolonged periods of time, but these did not necessarily have an impact on the handling qualities. More importantly, in dynamic situations this combination of displacement and force gave the aircraft response a “false sense of sluggishness,” almost as if the aircraft felt “heavier.” This frequently induced some pilots to increase their aggressiveness in order to achieve the desired deceleration performance requirements. It also made velocity maintenance more difficult for some pilots. None of these issues were significantly improved by using the lower equivalent rise time, although this did slightly improve the ability to capture a stable hover.

Nacelle Bandwidth Effects

Another key parameter assessed was the nacelle actuator bandwidth, characterized by the natural frequency of the second-order actuator dynamics. Four values of natural frequency were chosen, summarized in Table 15. The selection of these values was driven by the experimental handling qualities and flight control requirements. A rigid wing structure was assumed, and any potential structural implications were disregarded at this stage. A preliminary assessment in piloted simulation with the experimental project pilot suggested that a 3 rad/s bandwidth represented the lowest practicable value for the baseline TRC control system design used in this research. Lower bandwidths led to severe controllability issues. A baseline damping ratio of 1 was chosen to ensure the quickest nacelle response for a given bandwidth, but without displaying any natural oscillatory behavior.

Table 15. Nacelle actuator configurations.

Bandwidth (rad/s)	**Rate Limits** (deg/s)
3	5.0
4	5.0
8	7.5
16	7.5

Control implications of nacelle actuator bandwidth. Inclusion of nacelle-tilt actuator dynamics with increasingly higher actuation bandwidth (natural frequency) may cause potentially undesirable excitations of higher frequency dynamics in the longitudinal velocity open-loop response. This impacts the stability margin characteristics, as well as the closed-loop end-to-end response. Excitations in the pitch response are also expected because of the coupled nature of the longitudinal dynamics, leading to a range of handling and ride qualities issues that may impact the control system feedback design. While only the rigid body fuselage dynamics have been considered in this study, airframe structural modes have been recently found to impact the various aspects of control system design [62], making these considerations increasingly relevant.

Stability and performance design trade-off. Given a constant crossover frequency, an increment in the actuator bandwidth directly translates into an increase of the phase stability margin and the open-loop −180 deg phase crossover frequency. This is, of course, assuming the actuator bandwidth is greater than the open-loop crossover frequency. In this particular problem, this was also accompanied by a slight reduction of the gain margins. A control system design optimization, again using CONDUIT [46], was performed for each actuator natural frequency value to determine a set of feedback gains that would ensure 45 deg stability phase margins in both the lateral and longitudinal translational axes, and 38 deg stability phase margins in the pitch and roll axes, as per the findings of the investigation of stability margins for large rotorcraft presented previously. The optimization strategy was to maximize the disturbance rejection bandwidth (DRB) in the longitudinal translational axis for a given set of actuator dynamics, while minimizing the margins to the allowable extent (Figure 65).

Open-loop frequency responses shown in Figure 66 corresponding to the 4, 8, and 16 rad/s nacelle actuator bandwidth configurations illustrate the gain margin reduction trend and also the increasing values of the open-loop crossover frequency. This positive crossover frequency trend was indicative of the closed-loop performance improvements of the velocity feedback regulator, such as tracking performance and disturbance rejection, that were afforded by increasing the nacelle actuator bandwidth. Incidentally, note that additional lead compensation is required to improve tracking of the command model output beyond these open-loop crossover frequencies.

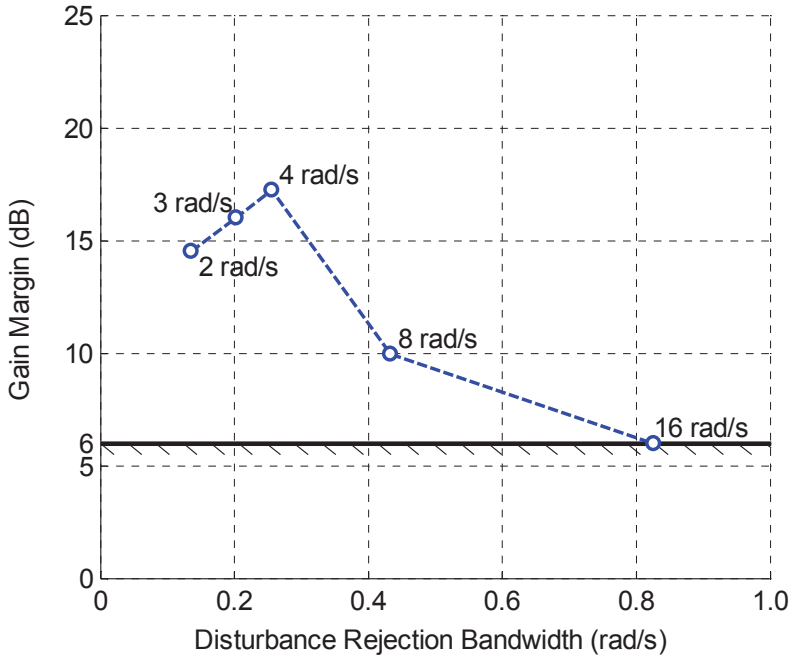

Figure 65. Longitudinal velocity disturbance rejection bandwidth and gain margin feedback characteristics for varying actuator bandwidths.

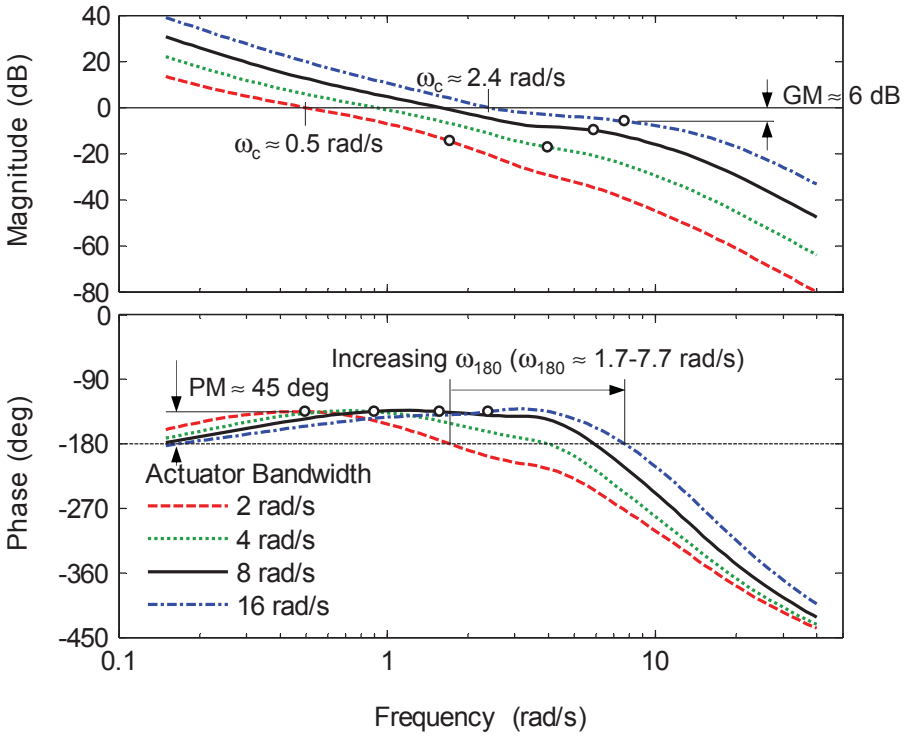

Figure 66. Velocity open-loop frequency response for varying actuator bandwidth.

Model-following performance. In this model-following control system, the required additional lead compensation was provided by the feedforward controller. The overall influence of the nacelle actuator bandwidth on the command model-following performance, with the added lead compensation of the feedforward inverse model controller, is illustrated in Figure 67, which shows the frequency responses of the closed-loop transfer function relating the longitudinal velocity to the velocity command (u_{cmd} in Figure 9) for the various configurations. Inspection of the frequency responses in Figure 67 suggested that a configuration using the 2 rad/s bandwidth actuator would track the command model output in a satisfactory manner at frequencies below 0.8 rad/s (defined by the point where the response phase is 45 deg off the commanded input). This configuration was ultimately deemed unacceptable on preliminary assessment by the project pilot. Instead, a configuration using a 3 rad/s actuator, offering a model-following bandwidth of 1.2 rad/s, was tested. By comparison, the configuration using the 4 rad/s actuator had a model-following bandwidth of 1.5 rad/s, and this increased to 4.8 rad/s for the configuration with an 8 rad/s actuator bandwidth.

The differences in the frequency-response magnitude (and phase) at the higher excitation frequencies for the various nacelle actuator bandwidths were attributed mainly to unmodeled actuator dynamics in the inverse model used in the feedforward control. To understand the impact of these unmodeled dynamics it was instructive to look at the analytical expression of the transfer function of the frequency responses in Figure 67. Comprising the feedforward controller inverse model dynamics in addition to those of the closed-loop feedback controller, this transfer function can be expressed, generally, as:

$$\frac{u}{u_{cmd}} = \frac{G_{u\beta_{cmd}}(s)\tilde{G}^{-1}_{u\beta_m}(s)}{1 + K_u(s)G_{u\beta_{cmd}}(s)} + \frac{K_u(s)G_{u\beta_{cmd}}(s)e^{-\tau_{eq}s}}{1 + K_u(s)G_{u\beta_{cmd}}(s)} \tag{38}$$

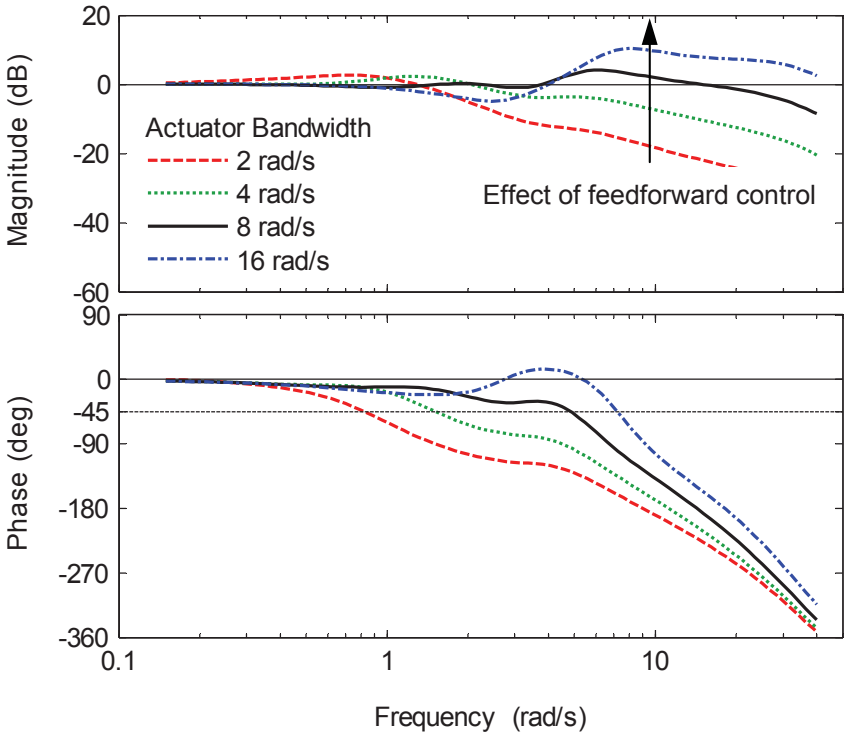

Figure 67. Closed-loop u/u_{cmd} frequency response for varying actuator bandwidth.

Here, the transfer function $\tilde{G}_{u\beta_m}^{-1}(s)e^{\tau_{eq}s}$ represents the inverse model dynamics of Eq. (26). Barring the $e^{-\tau_{eq}s}$ factor that arises from the equivalent time delay of the dynamic inverse model implementation, the transfer function of the feedforward controller effectively approximates the closed-loop sensitivity transfer function:

$$S(s) = \frac{1}{1 + K_u(s)G_{u\beta_{cmd}}(s)},$$

hence, providing the lead compensation necessary to improve the tracking performance for input frequencies above the open-loop crossover frequency. The nacelle actuator dynamics were not accounted for in the inverse model. Therefore, they were not adequately eliminated from the feedforward controller and thus reflect in the frequency responses of Figure 67 at these higher frequencies.

Incidentally, the frequency responses in Figure 67 approximate the theoretical pure time delay response behavior expected of the model-following control system architecture. The closest approximation, for a τ_{eq} of 0.293 s, was achieved with the 8 rad/s configuration, because the bare-airframe dynamics for this actuator configuration were more accurately modeled by the approximation of Eq. (26). Indeed, if a perfect inversion of the dynamics were attainable, such that:

$$G_{u\beta_{cmd}}(s)\tilde{G}_{u\beta_m}^{-1}(s)e^{\tau_{eq}s} = 1,$$

then the transfer function of Eq. (38) would simplify to the pure time delay transfer function $e^{-\tau_{eq}s}$, independent of nacelle actuator bandwidth. A corollary to this result is that the theoretical model-following performance is a function only of the equivalent time delay, τ_{eq}. Presumably some amount of delay would still be required in the approximation of the bare-airframe dynamics, but what this value of τ_{eq} would be in this scenario is unclear.

This was a key result, suggesting that a more sophisticated feedforward control system may achieve improved model-following performance, even with low-bandwidth actuators. This is a largely hypothetical question, beyond the scope of this study, however. The current approach offered a conservative, tractable control system design approach suitable for investigating these fundamental handling qualities issues.

Effect on short-term TRC response characterization. From an experimental standpoint, the more important effect of the nacelle actuator dynamics on the phase characteristics of Figure 67 was the effect on the phase delay of the position response to pilot input. This was illustrated by the longitudinal position response X/δ_{lon} Bode plot in Figure 58 for the four primary actuator configurations. Incidentally, the closed-loop response for the 16 rad/s actuator configuration had a marked phase recovery due to the extra lead compensation afforded by the feedforward controller. Despite this recovery, the 16 rad/s actuator bandwidth did not confer significant phase delay reductions over the 8 rad/s case, suggesting no further advantage is gained by increasing the actuator bandwidth.

It is further noted that the −180 deg phase curve crossover point for the closed-loop X/δ_{lon} response shown in Figure 58 was between 0.74 and 1.1 rad/s, with values monotonically increasing as a function of actuator bandwidth, except for the 16 rad/s actuator case displaying a crossover at 0.8 rad/s. This later result was attributed to a slight resonance near the open-loop −180 deg phase crossover frequency causing the phase curve to dip between 0.5 and 2.6 rad/s. However, since phase delay was small, the particular characteristics of the TRC configuration with the 16 rad/s actuator were considered minor issues.

The differences in this frequency where the phase was −180 deg were simply a function of the small variations in the closed-loop frequency responses of Figure 67 below 2 rad/s. The general existence and approximate location of this crossing, however, was considered an inherent characteristic of TRC control, and fundamentally independent of the nacelle actuator bandwidth. While a pure first-order velocity response yielded an undefined −180 deg phase crossing, additional phase in the frequency response, due to the added dynamics and delays in the control system, ensured the longitudinal position response X/δ_{lon} phase was −180 deg for a frequency between the phase bandwidths of the TRC command model bandwidth and the model-following control system (defined by the frequency such that the phase is −45 deg). Based on the ideal transfer function response (with a τ_{eq} of 0.293 s), this point was predicted to be 1.15 rad/s for the 2.5 s equivalent first-order TRC response time, and 0.82 rad/s for the 5 s case, which was consistent with the phase curves shown in Figure 58. In ideal settings this frequency could be stretched out to 2–2.5 rad/s (perfect inversion and equivalent time delays lower than 0.1 s), but for representative second-order approximations of the closed-loop model-following transfer function and time delays this −180 deg phase crossing would normally be expected to be in the 0.5 to 1.2 rad/s range.

Significantly, for the TRC control system design as a whole, these values are well within the frequency range of pilot control and may be a possible indication of limited control margins being available to the pilots. This characteristic also highlights the impact of the shape of the phase curve beyond the −180 deg crossover frequency, which the phase delay tries to represent. Should pilots be required to operate beyond the installed bandwidth, particularly for the low actuator bandwidth cases, this would easily lead them to be out of phase with the desired position response, and consequently at risk of entering PIO.

Disturbance rejection. Based on the control system optimization strategy that was adopted, it was expected that configurations with higher actuator bandwidth would possess improved rejection of atmospheric turbulence disturbances. Spectral analysis of the aircraft response, in a turbulent atmospheric field, shown in Figure 68 suggested marked horizontal motion reductions in the longitudinal axis with the higher actuator bandwidths. For example, below 1 rad/s there was an approximate 17 dB reduction in the auto-spectra of the longitudinal velocity between the 3 and 16 rad/s actuators. In terms of the RMS of the longitudinal position, this translated into an 80-percent reduction down from ~0.2 to 0.04 ft. This was consistent with the progressive

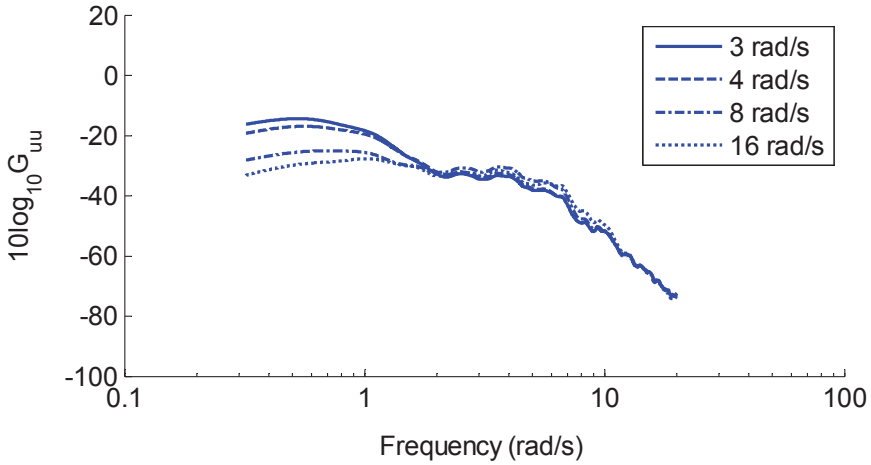

Figure 68. Auto-spectrum comparison of the turbulence response for varying nacelle actuator bandwidths: longitudinal velocity (units of u are in ft/s).

increase of DRB in the longitudinal translational axis afforded by the higher actuator bandwidths, as shown in Figure 65.

Pitch coupling aspects of high crossover frequency design. A physical coupling of the pitch and velocity control loop dynamics, for the configuration with the 16 rad/s actuator, was hinted at by the approximate match between the open-loop crossover frequencies, at 2.4 rad/s, in both control loops (Figure 69). By comparison, the open-loop crossover frequencies for the TRC control system with the 8 rad/s bandwidth actuator were 3.4 and 1.6 rad/s in the pitch attitude and longitudinal velocity loops, respectively. The remaining TRC configurations were ensured to

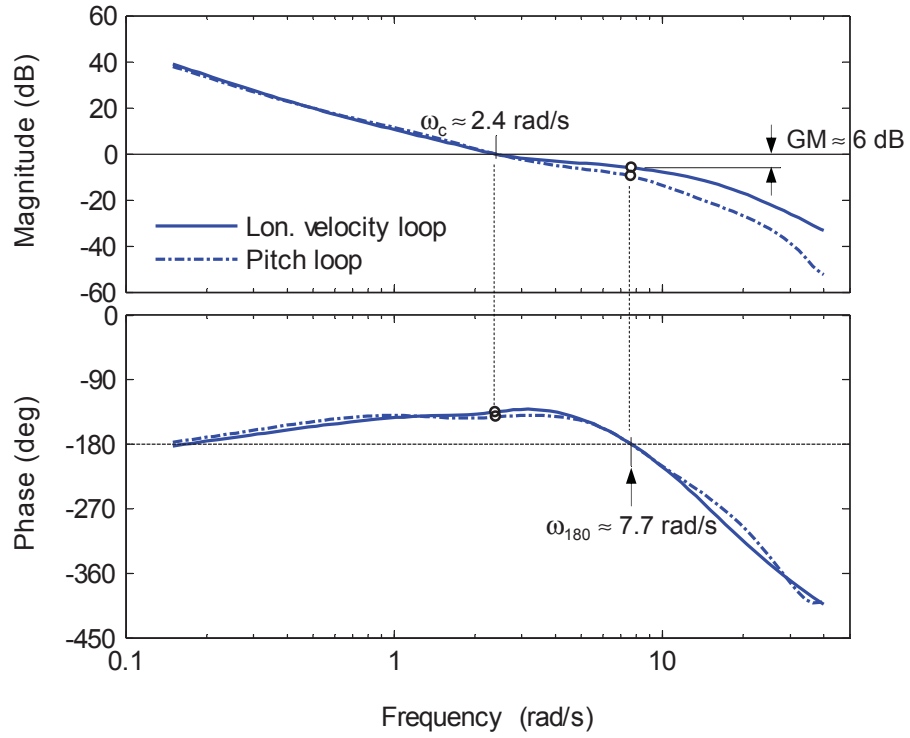

Figure 69. Open-loop frequency responses for the configuration with 16 rad/s actuator bandwidth.

have even larger crossover frequency separations by factors of 3.5 or greater, and importantly, retained approximately the same pitch loop crossover frequencies (~3.4 rad/s). Naturally, this higher crossover frequency (1 rad/s difference) was associated with better pitch disturbance rejection characteristics, and would be expected to exhibit less pitch motion in response to turbulence or pilot input disturbances.

Incidentally, spacing of the open-loop crossover frequencies had not been seen as a critical design aspect for this form of TRC, since the two loops relied on independent actuation mechanisms. Indeed, results of the piloted evaluations presented below show this to be only a very minor, although perceptible, deficiency from a handling qualities perspective.

This coupling of the pitch and velocity control loops resulted, however, in measureable off-axis pitch motions in response to both atmospheric turbulence and pilot input. In Figure 70, for example, the configuration with the 16 rad/s actuator was noticeably more active in pitch as it reacted to atmospheric turbulence. This behavior extended to the piloted input response. Inspection of Figure 71 indicates the pitch response is roughly 3.5 dB higher magnitude for input frequencies below 1 rad/s. This long-term response characteristic of the closed-loop TRC

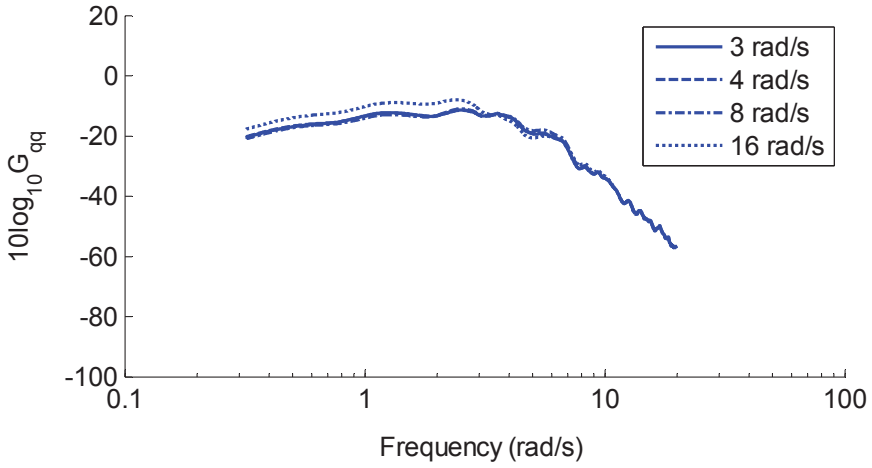

Figure 70. Auto-spectrum comparison of the turbulence response for varying nacelle actuator bandwidths: pitch rate (units of q in rad/s).

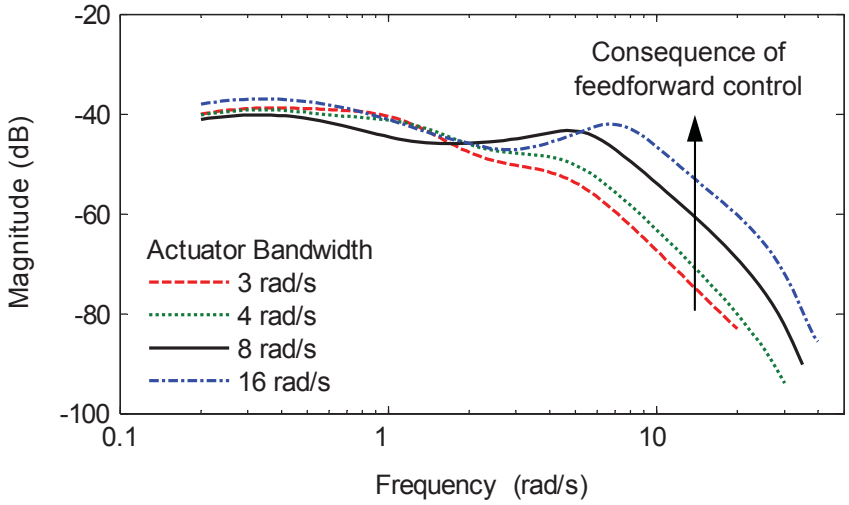

Figure 71. Closed-loop θ/δ_{lon} frequency-response magnitude for varying nacelle actuator bandwidths (5 s rise time).

system with the 16 rad/s nacelle actuator bandwidth was attributed to the coupling of the nacelle-actuated velocity feedback loop and the rotor-actuated attitude feedback loop, and is shown from the piloted evaluations discussed below to be a perceptible aspect of this control system.

A further consequence of this off-axis coupling was the dependency of the pitch response on the nacelle actuator bandwidth. As shown by the θ/δ_{lon} Bode diagram in Figure 71, this configuration in particular also exhibited a distinct pitch response magnitude increase above the 3 rad/s point, noticeably exceeding the magnitude of the 8 rad/s bandwidth case for input frequencies greater than 5 rad/s. These off-axis pitch responses were attributed to the excitation of higher frequency dynamics by the feedforward control, and were accompanied, accordingly, by notably higher frequency angular nacelle accelerations (and corresponding pitching moments due to the torque reactions) in response to pilot input. With these response dynamics being within the frequency range of pilot control, they would also likely generate a series of ride qualities issues at high frequency if disturbed by the pilot, through off-axis couplings in addition to the primary longitudinal control axis response issues.

Piloted evaluations in the Hover MTE and rate-limiting considerations. The handling qualities ratings (HQRs) shown in Figure 72 for the baseline TRC implementation indicate that with nacelle-only actuation (i.e., no cyclic augmentation) Level 1 handling qualities are possible with actuator bandwidths greater than 4 rad/s. The phase delay for the 4 rad/s case was in the order of 480–500 ms. With this in consideration, the results in Figure 72 indicate there is a good correlation of the handling qualities with the X/δ_{lon} phase delay, with the 480–500 ms of the 4 rad/s actuator configuration conferring borderline Level 1–2 handling qualities, on average, for a TRC phase bandwidth of 0.2 rad/s. These results are consistent with those of Franklin et al. [61], which proposed a Level 1–2 boundary at 0.4–0.6 s for a similar (non-attitude based) TRC response type implementation.

Note that although the 3 and 4 rad/s actuators had lower rate limits than the 8 and 16 rad/s actuator configurations, rate-limiting was carefully monitored throughout the experiment and was not judged to be a major factor in the piloted experiments. As suggested by Figure 73, these lower bandwidth configurations would have only experienced gradual degradation of the effective phase delay for control amplitudes (in terms of RMS) up to 1 in. Rate-limiting certainly compounded the problems encountered when very large control inputs were required by the pilot, but it was never the precipitator of the initial handling qualities problem, which was a fundamental phase delay due to the low actuator bandwidth.

As shown in Figure 60, the effect on the longitudinal position response bandwidth is minimal from either parameter variation except at very low actuator bandwidth or rate limit, where there are some variations. The value of the bandwidth is already a very low frequency and is essentially governed by the translational response rise time, which was 5 s for the cases shown.

The results for the phase delay of the X/δ_{lon} response in Figure 61 are more informative. The nonlinear trends with input amplitude varied from configuration to configuration. Figure 73 illustrates the variation of the longitudinal position response phase delay with longitudinal stick amplitude represented in RMS of the sinusoidal input used in the automated frequency sweeps. For the lower bandwidth cases (3 and 4 rad/s), the phase delay starts at higher values at small amplitudes and increases almost immediately with increased RMS input. The higher actuator bandwidth cases (8 and 16 rad/s) have much lower minimum phase delays at low input and actually maintain that value constant up until a given input amplitude after which there is a rapid rise in the phase delay. The trend appears to be that the breakpoint for the rising phase delay is at higher amplitudes for higher actuator bandwidth but with a more aggressive increase.

The response lag in the longitudinal axis associated with the actuator bandwidth of 3 rad/s was consistently deemed by the evaluation pilots to be excessive and PIO conducive. Phase delay was in the order of 650 ms (Figure 59). This configuration was rated Level 2 by all evaluating pilots (Figure 72). The handling qualities improved significantly with the 4 rad/s actuator, with the perceived response lag being less objectionable, but still problematic when subjected to aggressive control. Comments generally pointed to mid-term or residual oscillations, particularly after an aggressive deceleration, which implies that pilots could not relax after achieving a stable hover. The initial response was not crisp, but was still predictable. This amounted to an inability to be aggressive with the aircraft, but allowed for desired performance to be achieved if employing a low gain control technique. Consistent with these comments, HQR scores indicate borderline Level 1–2 handling qualities were conferred with this configuration.

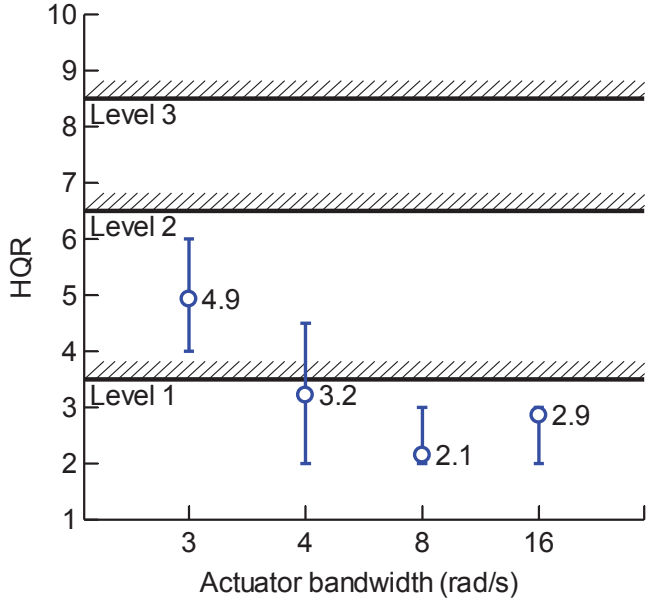

Figure 72. HQRs for varying actuator bandwidth configurations (5 s rise time).

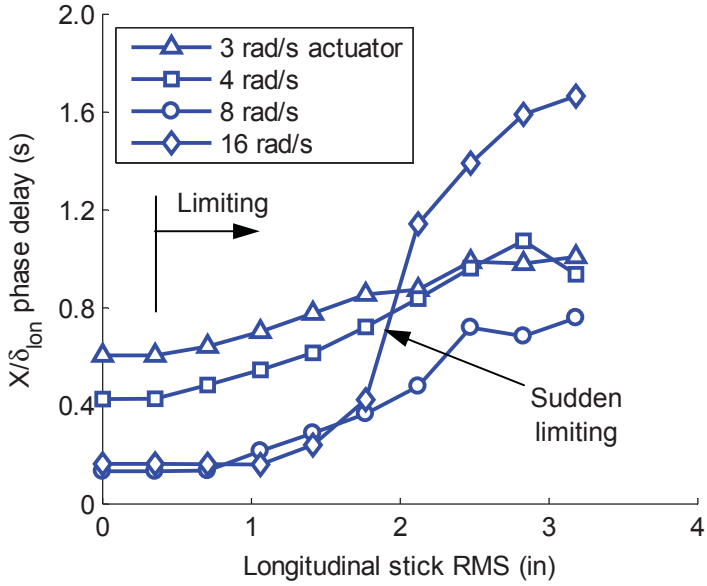

Figure 73. X/δ_{lon} phase delay for varying frequency sweep amplitude.

The higher bandwidth actuators (8 and 16 rad/s), conferring low phase delay values (under 200 ms for both), consistently gave “very predictable” and “crisp” responding qualities, offering “very good speed control” with “precise and low workload hover stabilization.” Only passing mentions of a slight tendency to oscillate longitudinally from aggressive deceleration attempts were made by one pilot. Most pilots indicated that these configurations were quite insensitive to aggressiveness.

Although rated as conferring Level 1 handling qualities, the 16 rad/s actuator unexpectedly conferred slightly degraded handling qualities compared to the 8 rad/s actuator. Consistent with the analysis documented previously showing the increased off-axis pitch responses (Figs. 68 and 69), this configuration was persistently felt by the pilots to be notably more active in the pitch axis in response to both turbulence gusts and pilot inputs. In line with this assessment, the pilots indicated the presence of noticeable heave accelerations due to pitch that affected the compensation required. The 3.5 dB difference in the pitch response for input frequencies below 1 rad/s, indicated by the θ/δ_{lon} Bode diagram shown in Figure 69, implied that the rate and amplitude of oscillation would be about 50 percent larger for a given size of input. It is noted that while the amplitude of oscillation may be small, for a pilot station located 32 ft in front of the center of rotation, even a fraction of a degree of pitch results in a perceptible vertical displacement of the cockpit. This is consistent with pilot evaluation comments. Other issues reported in the piloted evaluations were also attributable to the high gain feedback design and manifested primarily in ride quality deficiencies: a “snappy” response, large lateral accelerations, etc.

Nacelle Rate-Limit Effects

Although a nonlinear phenomenon, actuator rate-limiting is seen from the short-term position response characterization discussion presented previously, to have a similar effect on the X/δ_{lon} characteristics to that of actuator bandwidth. Specific fundamental underlying aspects of this nonlinearity are further examined in this and subsequent sections.

HQRs for evaluations in the Hover MTE of four nacelle conversion actuator rate limits for a control sensitivity of 15 (ft/s)/in, and zero nacelle rate to longitudinal cyclic crossfeed, are shown in Figure 74. Error bars indicate the maximum and minimum values. This control sensitivity was not optimal, as seen from the results of Figure 64, which explains the average Level 2 ratings. Indeed, this higher sensitivity tended to exacerbate the effects of these nonlinearities. Also, absence of the nacelle rate to longitudinal cyclic crossfeed, the purpose of which is to eliminate small “non-minimum phase” pitch attitude changes with this TRC system, was an important aspect, and its effect will be discussed further below. As such, the results suggest that 10 deg/s was found consistently to be the least objectionable of the nacelle actuator rate-limit configurations. Lower rate limits (5 and 7.5 deg/s) were too restrictive of pilot input and resulted in PIO more frequently. The 5 deg/s rate limit in particular was rated at least one HQR higher than the others. The 7.5 deg/s rate limit did confer the lowest individual rating, however. Interestingly, the 12.5 deg/s rate limit, which was expected to be less restrictive and receive better ratings, was found to possess unsatisfactory deficiencies due to “obtrusive pitch perturbations” and was thus awarded Level 3 ratings. This pitch response is directly tied to the “non-minimum phase” pitch attitude changes associated with nacelle rate. Looking at this configuration more closely, the control system was observed to command nacelle rates near the 12.5 deg/s limit, but frequently without reaching the rate limit.

The interconnected factors of nacelle rate limit and coupled pitching led to conflicting trends for the HQRs for the various TRC rate-limit configurations—both increasing and decreasing the rate limit could cause a reduction in HQR. For some of the TRC configurations the non-minimum phase pitch response appeared only to be a minor “nuisance” factor, especially as several pilots did not comment or notice it at all as the amount of pitching is dependent on the pilot input magnitude—something that was somewhat dependent on pilot technique. Some pilots did comment on the perceivable aforementioned “opposite sense” pitching that would occur with any longitudinal stick input. The scenarios where it became more obvious were where a PIO occurred, with a large amount of fore-aft motions, large stick inputs, and the nacelle actuators reaching their limits.

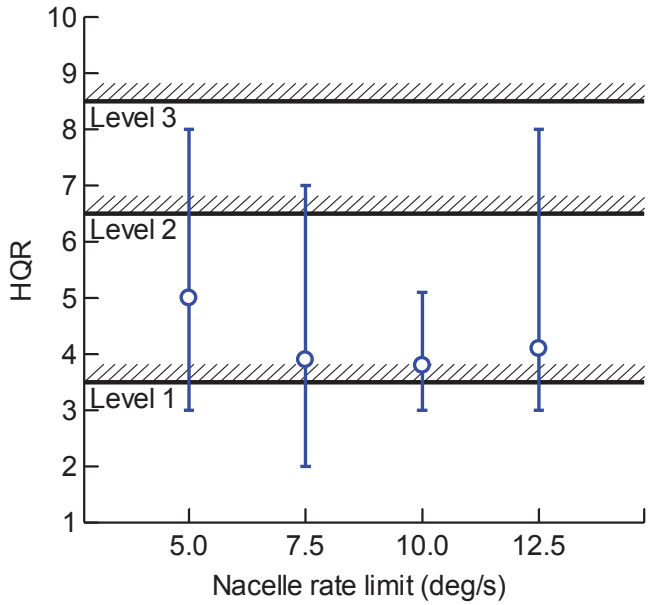

Figure 74. HQRs for varying nacelle actuator rate limits in the Hover MTE (5 s rise time and 8 rad/s actuator bandwidth).

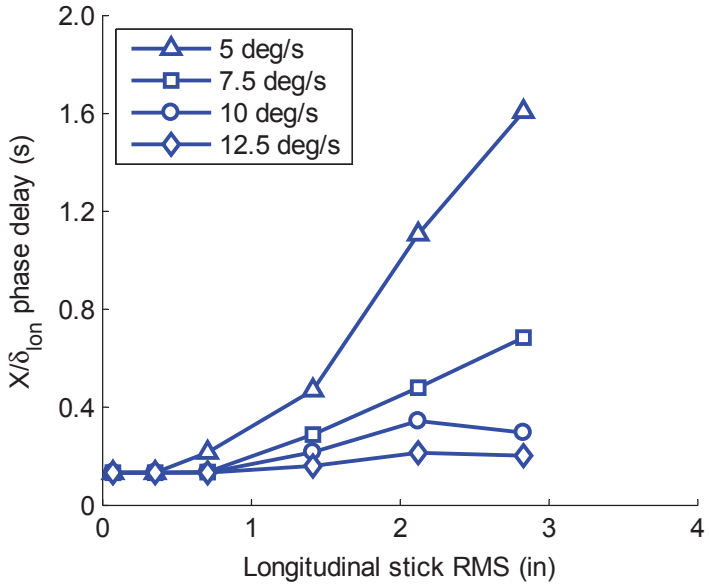

Figure 75. Nonlinear phase delay effect of rate limits for varying pilot control input.

Notwithstanding the pitch coupling effects, the relationship of the rate limit on the TRC handling qualities can mostly be explained using the results in Figure 75. Here the X/δ_{lon} phase delay is compared for the four nacelle actuator rate-limit configurations tested in the piloted simulation. At small pilot input RMS values, the systems are effectively linear, and there is no perceivable difference in the phase delay. However, for larger RMS inputs, the rate-limiting effect becomes prevalent, with the lower rate-limit cases exhibiting an earlier phase delay increase "breakpoint" as well as a steeper gradient. The X/δ_{lon} phase delay strongly correlated with the HQRs for the Hover MTE for TRC control. A high phase delay value alone is poor, but a strong dependency of worsening phase delay on the pilot input amplitude leads to a highly nonlinear and negative control characteristic. If the input amplitude can be kept small, then the poor handling qualities are "avoided." This is the core reason for the handling qualities cliff; if the input is too large, a large amount of delay is experienced and thus likely to increase the pilot gain to compensate, induce further large inputs, and exacerbate the problem. This HQ cliff is borne out by the ratings shown in Figure 74 where the different rate-limit cases showed a high degree of variability, even when the pitch attitude issues connected with rotor flapping were eliminated by the crossfeed (see section below).

Application of Open-Loop Onset Point (OLOP) design criteria. The correlation of the degradation of the handling qualities with reduced rate limit described in the previous section is not an unexpected outcome, albeit in a novel application of nacelle-actuated TRC. What is useful is to determine how to predict limiting in such a control architecture where rate-limiting might impact the handling qualities. The OLOP design criteria [50] was used in this case to predict the potential handling qualities impact associated with rate-limiting of the nacelle actuator. Figure 76 shows the effect of the experimental nacelle rate limits on the OLOP phase and amplitude criteria assuming a maximum control input amplitude of 1 in. The extra margins offered by the larger rate limits are clearly illustrated. For comparison, Figure 76 also illustrates the effect of pilot maximum input amplitude on the OLOP criteria. Center stick maximum displacement range was ±5 in, allowing the handling qualities impact of piloted input frequency and amplitude to be freely evaluated.

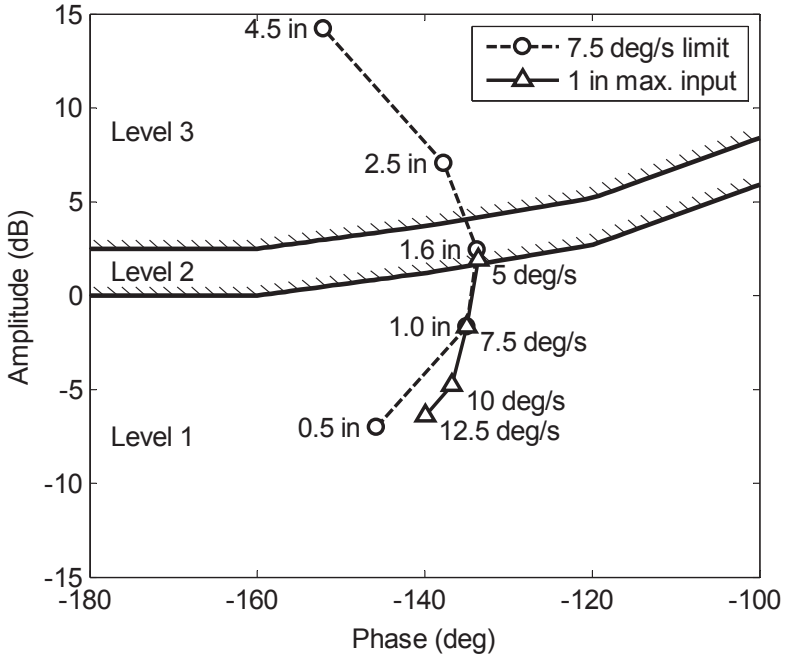

Figure 76. OLOP specifications for varying nacelle rate limits (15 ft/s/in sensitivity and 1.0 in maximum pilot input).

OLOP uses linear analysis to predict the onset of rate-limiting; typically the input to compute the result is the maximum input but in some respects that determines an unrealistic scenario. Figure 76 shows that increasing the input to 2.5 in from the nominal 1 in used for the 7.5 deg/s rate-limit case pushes the result into Level 3 handling qualities. This somewhat correlates with the result in Figure 75 where the same case at an equivalent RMS amplitude has a phase delay of around 0.6 s, which exceeds the Level 1 HQR boundary values proposed in the summary and discussion section below.

Effect of Crossfeed

In the previous section it was shown that for the TRC control law without the nacelle rate to longitudinal cyclic crossfeed, relatively subtle variations in nacelle actuator dynamics, and how aggressively the pilot flew, led to a large variability in the handling qualities. A non-minimum phase pitch response was most evident in the 12.5 deg/s rate-limit case shown in Figure 74 because of the larger nacelle rates commanded by the TRC control system. Pilot comments for this configuration consistently mentioned the presence of a notable pitch oscillation accompanied by what was described as an unsettling heaving motion. While this oscillation was described as annoying, or bothersome, it did not appear to compromise the ability to meet the targeted performance standards. A few evaluation comments hinted to a quick pitch reversal in response to rapid input, and more interestingly, indicated that this pitch motion could be cueing them on to a false sense of aircraft response because the pitch response was opposite to the expected response pilot control input (e.g., nose-up pitch for a forward stick displacement). It was purported that this opposite pitch response to pilot input may have falsely cued the pilots into overcorrecting after an initial input. Additionally, this pitch oscillation appeared to affect the altitude maintenance because of the presence of an obvious heave motion perception at the pilot station.

The analysis in Appendix B illustrates the mechanics that cause this non-minimum phase response characteristic and the beneficial effect of the crossfeed. The oscillations were induced by the angular rate of the nacelles causing rotor flapping opposite to their rotation through the air, which in turn generated pitching moments on the aircraft body. To compound matters, these pitching moments are opposite in sense to the pilot input, i.e., stick forward commanded a forward rotation of the nacelles to accelerate forward and the rotors flap aft in response and cause a nose-up pitch. The larger the allowable nacelle rate, the larger the pitch disturbances became.

Figures 64 and 72 also show that the relatively simple crossfeed gain improved all the configurations, becoming less sensitive to a variety of pilot techniques and aggression levels and, in some instances, virtually eliminating the PIO tendency that had previously existed. This was a major factor in the large spread in the HQRs in Figure 74. The crossfeed is able to minimize the lagging effects on the longitudinal velocity of both rotor flap-back to nacelle rate and the subsequent pitching motions by effectively keeping the rotor disc plane perpendicular to the nacelle/shaft axis (Appendix B). The resulting effect of the crossfeed is well illustrated in Figure 77. It shows the same X/δ_{lon} phase delay with pilot input RMS in Figure 75, but compares the rate-limit configurations with and without the crossfeed improvement. The solid (black) lines indicate the cases without crossfeed, and the effect of adding the crossfeed is indicated by the dashed (blue) lines. The main effect is an overall downward shift in the curves to lower phase delays. At small amplitudes, the difference is small, but as the RMS increases, inferring larger amplitude nacelle rates (and thus more rotor flapping), the crossfeed effect becomes more significant. At RMS amplitudes of 1 in and above, the phase delay reduction is in the order of 30 ms up to 100–150 ms for the lower rate-limit configurations. This across-the-board improvement was reflected in the HQRs. Also the worse (low rate-limit) configurations were improved more than the higher rate-limit cases—bringing them all closer together in performance.

The OLOP criterion shown in Figure 78 similarly predicts an improvement in the handling qualities from the addition of the crossfeed. The predicted improvement is fairly small and is indicated by the curve shifting to a location such that any given input amplitude point is moved further toward the Level 1 handling qualities region. This is likely the equivalent of the small delta observed in the X/δ_{lon} phase delay curves for small RMS amplitudes where the system is effectively linear.

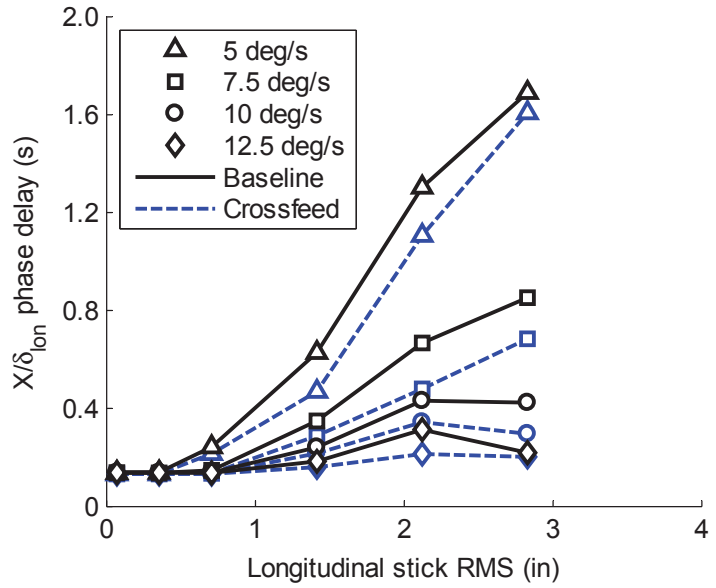

Figure 77. Effect of crossfeed on nonlinear phase delay of rate limits for varying pilot control input.

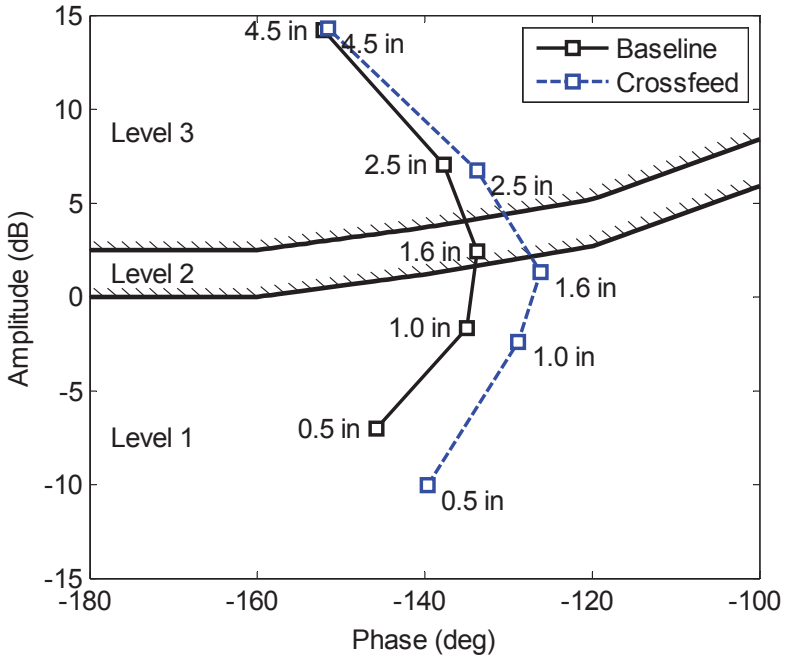

Figure 78. Effect of crossfeed on OLOP specifications for TRC control (15 ft/s/in control sensitivity and ±7.5 deg/s rate limits).

Cyclic Augmentation—Response Quickening

The analysis of the results from the previous sections has established the necessary levels of nacelle actuator bandwidth required for Level 1 handling qualities to be achieved with this particular implementation of the TRC control. Whether these Level 1 handling qualities can be maintained for reduced actuator bandwidths by introducing other control mechanisms remains unanswered. It would be advantageous if additional longitudinal bandwidth or "quickening" of the longitudinal velocity response could be achieved through other methods to reduce the nacelle bandwidth requirements. TRC response augmentation by employing longitudinal rotor cyclic actuation in addition to nacelle actuation was a scheme tested.

The longitudinal cyclic rotor actuation "augmentation" in addition to nacelle actuation was demonstrated to confer significant handling qualities improvements to the equivalent nacelle actuation-only bandwidth cases, specifically the lower 3 rad/s actuator case, shown in Figure 79. All three cases shown were identically configured with the nacelle rate to cyclic crossfeed. The results for these three control cases are that the small increase in phase bandwidth and reduction in phase delay attained with the case with the lower 2.5 s equivalent rise time, but nacelle-only actuation, did not confer a significant improvement in the handling qualities (see Figure 59). By comparison, referring to Figure 59, the phase delay improvement of the cyclic-augmented control system to the baseline 3 rad/s case was in the order of 200 ms (down to ~450 from 650 ms), resulting in a marked improvement in HQRs. With all other parameters remaining unchanged, this again indicated a strong correlation of the phase delay with the handling qualities. Although the cyclic-augmented configuration only used a 5 s rise time and thus had a lower bandwidth than the 2.5 s rise-time case, its bandwidth was sufficient (following the ADS-33 criteria definition), and crucially it had better phase delay characteristics as very little noticeable lag in the response was apparent. As such, the initial response was generally considered to be predictable and speed control easy. Only two pilots observed a slight amount of lag in the response, but considered it to be manageable and definitely not conducive to PIO. Again these issues all point to the reduced phase delay being the cause for the handling qualities improvements.

Also playing a potentially beneficial role, as illustrated by the analysis of the qLPV and nonlinear actuator model used in the pilot experiments in Figure 80, the system overall phase delay is not only lower than both unaugmented cases, but notably, the rise in phase delay with amplitude is also eliminated. The vehicle dynamics effectively "appear" much more "linear" with no changes in response characteristics with changing pilot input amplitude—a significantly improved handling qualities characteristic.

In summary, these results suggest that while high by ACAH standards, a phase delay requirement of around 450 ms or lower in the context of this TRC implementation would be sufficient to achieve desired precision in the Hover MTE, a result that tracks the TRC research results published in reference [61].

It was recognized that the cyclic augmentation approach would reintroduce a certain amount of pitching motion, which although now in the right directional sense (i.e., pitch forward for forward stick input), might bring back undesirable vertical accelerations for crew and passengers. Only one pilot out of seven rated this cyclic-augmented control system Level 2 for this reason. Trying to compensate for a perceived heave motion was not conducive to good handling qualities, forcing the pilot to have to stay out of the loop. While other pilots commented on this coupling, none felt it was problematic other than being a ride quality annoyance. This is, however, a consideration that needs to be taken into account if designing these types of control systems—that is, potential large pitching moments may be generated when using longitudinal cyclic for velocity control.

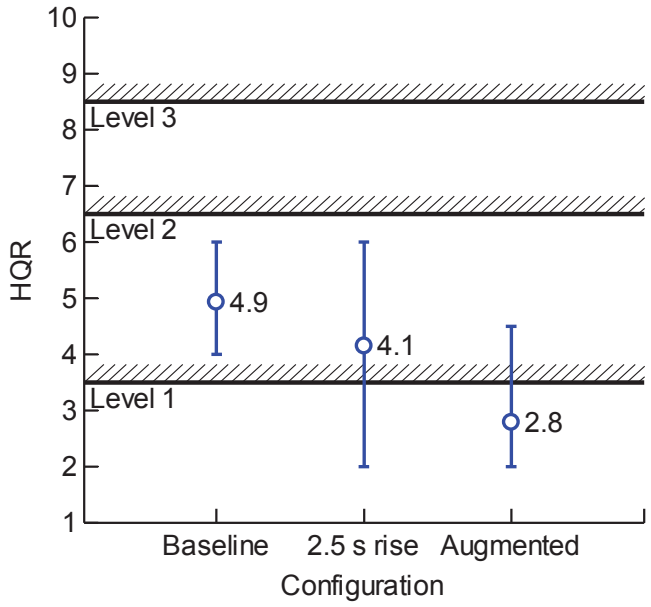

Figure 79. HQRs for baseline 2.5 s rise time and rotor cyclic augmented configurations (3 rad/s actuator).

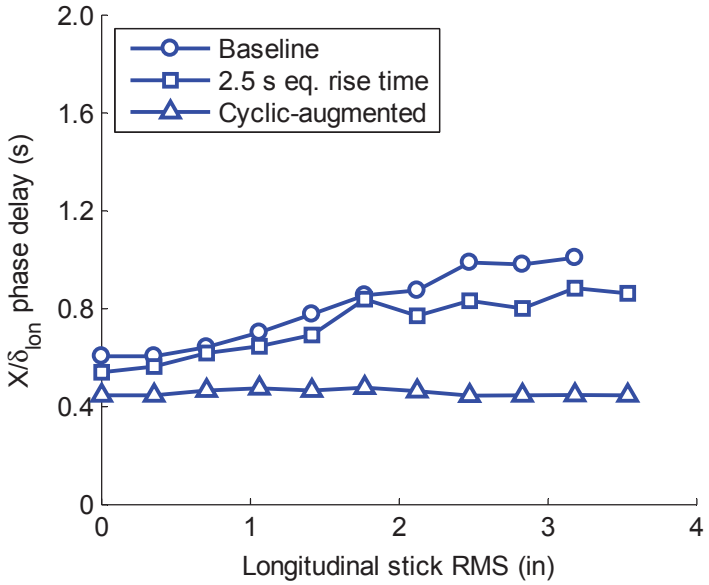

Figure 80. X/δ_{lon} phase delay for varying frequency sweep amplitude (3 rad/s actuator).

Analysis of Pilot Input Control Activity

Figure 81 shows the computed pilot control input cutoff frequencies and root mean square (RMS) for a large proportion of the cases discussed in the sections above. These were computed from time histories of the longitudinal control stick displacements over the entire Hover MTE maneuver. As previously stated, the pilot cutoff frequency, determined from the spectral analysis of the inceptor position time histories, is used as an approximate measure of pilot operating frequency and considered a good estimate of the pilot crossover frequency for pilot-in-the-loop tasks [27]. Additionally, the RMS of the piloted inputs is a statistical measure of the magnitude of control input during the maneuver.

The results suggest that low phase delay control cases (higher nacelle actuator bandwidth) (Figure 81(a) and (b)) generally allowed pilots to operate in a more closely clustered frequency range, roughly between 0.2 and 0.6 rad/s, but possibly lower. High phase delay control cases often resulted in high RMS control input at frequencies closer to 0.8 through 1 rad/s. The later cases would have clearly had the pilots operating at, or near, the −180 deg phase crossover point (Figure 58), which is entirely consistent with the reported PIO tendencies.

Because of the series of events it could trigger if not executed correctly, the critical sub-phase of the overall maneuver was consistently indicated by the evaluation pilots to be the deceleration from a steady velocity translation into a stable hover within the desired time and position performance criteria. It was reported that a poorly executed deceleration would force the pilot to get into the loop to correct for excursions outside of the desired performance criteria. This is an important consideration because, with TRC, position regulatory tasks such as the steady speed ingress and hover hold sub-elements of the Hover MTE may not require high installed control bandwidth. The deceleration sub-element, however, could easily require control bandwidths over 1 rad/s.

A clear correlation between control sensitivity and equivalent rise time (or phase bandwidth), and the cutoff frequency and RMS data can be seen in Figure 81(c). The data show that low control sensitivity (indicated by the circle symbols) elicited larger amplitude but lower frequency control inputs. High, and in a few instances, medium sensitivities led to higher operating frequencies and consequently resulted in a tendency to over-control as documented above (e.g., gain set 15/5, which refers to a 15 ft/s/in control sensitivity and a 5 s equivalent first-order rise time).

The effect of a lower (quicker) equivalent rise time generally resulted in lower overall cutoff frequencies. The exceptions were where it led to a tendency to over-control when combined with the medium- and high-control sensitivities. This can be explained in conjunction with the result, above, that lower rise times typically allowed for easier transitions into a stable hover without the need to over-drive the controller.

Extending this discussion into the frequency-domain, the implication is that higher X/δ_{lon} phase bandwidth generally allowed the pilots to operate with lower natural control “gains” (as reflected by the cutoff and RMS data) in order to meet the desired deceleration performance requirements. This seems to imply a fundamental inverse relationship between installed phase bandwidth and required pilot operating frequency, suggesting the lower bandwidth cases were over-driven by the pilots to achieve *desired* performance.

Pilot longitudinal stick input frequency and magnitude data computed for the overall MTE maneuver may obscure specific events happening at distinct moments in time. When computed for the 30 s the pilot is required to hold the hover position following the enunciation that a stable hover had been reached, the pilot cutoff frequencies and RMS shown in Figure 82 confirm there can be significant residual pilot control activity in the 0.8 to 1.2 rad/s frequency range. Also very minimal pilot control activity, as characterized by an RMS below the neighborhood of 0.4 in is observed, which is a consequence of an improved ability to reject the “moderate” turbulence disturbances and hold position with the TRC. High cutoff frequency values are meaningless in this context, as these are the result of the mathematical characterization of a signal with

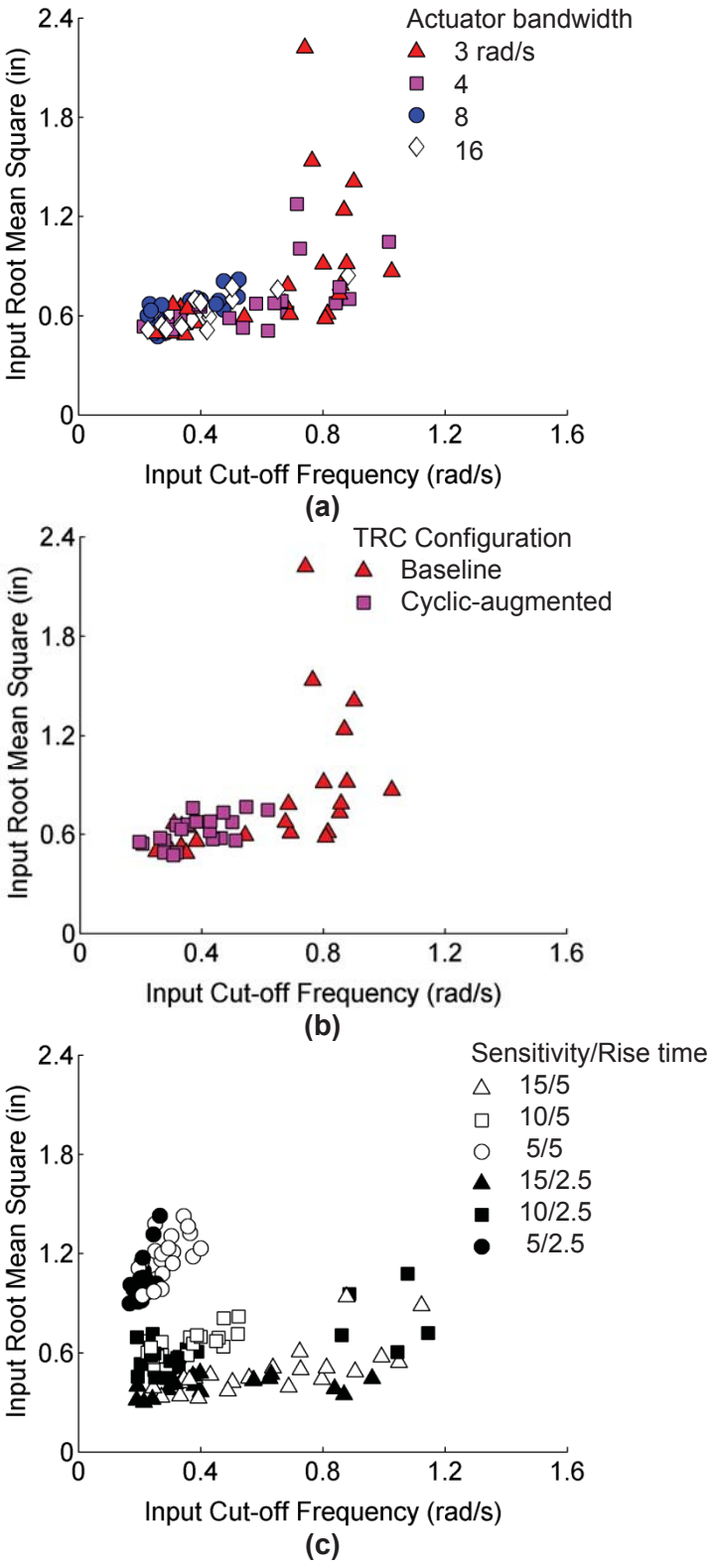

Figure 81. Longitudinal pilot control activity for entire maneuver: (a) baseline, varying actuator bandwidth; (b) cyclic-augmented (3 rad/s actuator); and (c) varying equivalent rise times and control response sensitivities (8 rad/s actuator).

minimal energy (flat auto spectra). However, seen in conjunction with the RMS, they indicate that pilots were effectively staying out of the loop.

Figure 82 shows that the pilot control activity strongly correlates with the HQRs, where the Cooper-Harper ratings are seen on average to increase dramatically with the amplitude of pilot control inputs. These events consistently corresponded to the TRC configurations possessing high phase delay values. Results in Figure 83 further demonstrate this relationship, where several cases—all essentially with ADS-33 Level 1 rise-time characteristics (or bandwidth)—showed a monotonic increase in the average HQR resulted as a consequence of the increasing phase delay.

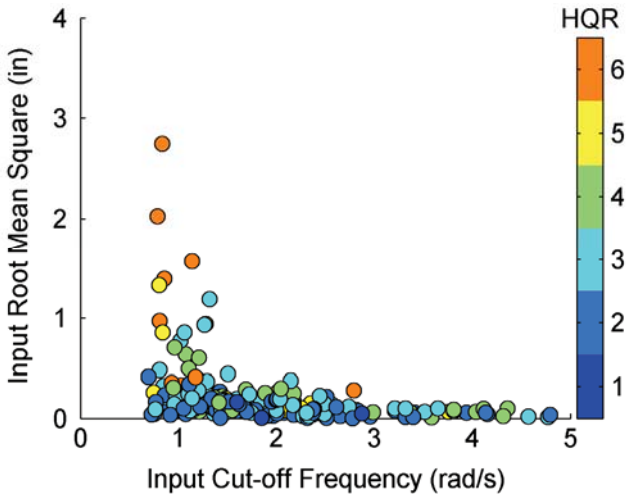

Figure 82. Longitudinal pilot control activity for the 30 s hover hold sub-task (all configurations).

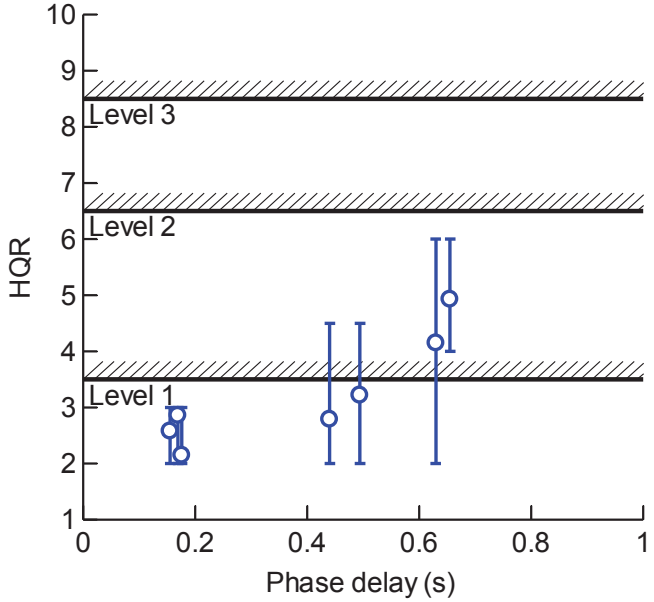

Figure 83. Effect of short-term position response phase delay on handling qualities.

Longitudinal axis time histories and auto-spectra analysis shown in Figure 84 highlight the different nature of the control inputs in these two distinct regions in Figure 82. These correspond to two different runs by the same pilot flying the same sensitivity and rise-time configuration, with the 3 rad/s actuator. Assigned an HQR 6 by the pilot, this configuration exhibited widely different performance in each run. Run A demonstrates a situation where the pilot executed everything perfectly, remaining within desired parameters, and therefore did not need to get in the loop after arresting the initial translational rate. The control compensation employed by the pilot after stabilizing is characterized by infrequent pulse type corrections. This type of time history displays very little energy in its auto-spectrum (Figure 84(c)). Deficiencies with this configuration are illustrated by Run B where, in this case, the same pilot remains in the loop nearly 11 s after indicating a stable hover had been achieved. Examination of the control input and aircraft position time histories during this initial time period suggests significant compensation occurred around 1 rad/s, and the spectral analysis confirms this. Importantly, it is noted that the position response is nearly 180 deg out of phase with the input, clearly indicative of a PIO. This result confirmed the analysis of the X/δ_{lon} frequency response (Figure 58).

As phase delay for other configurations was reduced (to less than 200 ms), this propensity to get out of phase during the stabilization was also diminished, a characteristic that was corroborated by the pilot evaluations, as discussed previously. In terms of the pilot input frequency and magnitude characterization, configurations with lower phase delay show consistently low control RMS values in Figure 82, which is strongly indicative of pilots employing minimal compensation.

A final observation from these results is they support the piloted evaluations that indicated that very little compensation was generally required to hold position after stabilizing the aircraft, particularly for phase delays lower than 450 ms. These results highlight one of the most significant benefits of TRC, that the higher augmentation it confers translates into very low workload for position maintenance tasks.

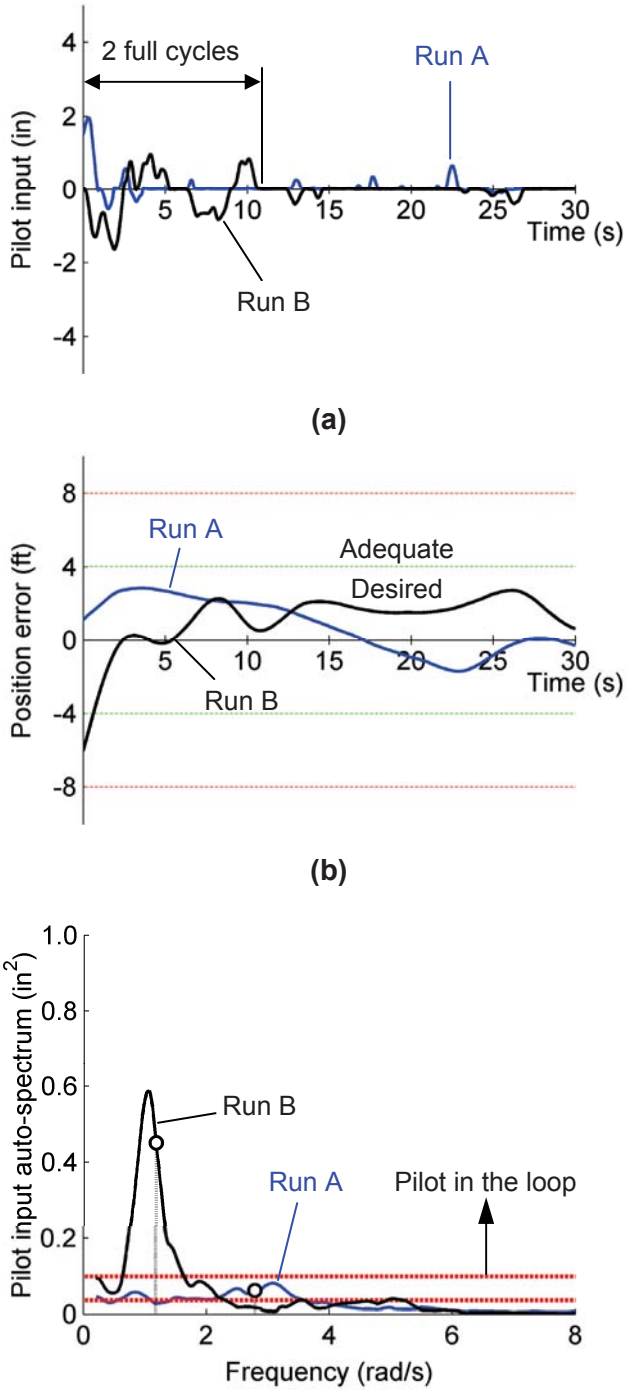

Figure 84. Comparison of different compensation levels in hover hold sub-task (3 rad/s actuator, same pilot): (a) longitudinal input time history, (b) longitudinal position error time history, and (c) longitudinal input spectral analysis (red lines indicate proposed levels where pilot can be considered to be actively in the control loop).

Summary and Discussion

Handling Qualities of Large Rotorcraft With ACAH

The analysis above showed that implications of the large vehicle size are notable and have two key aspects. First, the large size of the vehicle confers high mass and moments of inertia that introduce increased delay to the response of the vehicle to both pilot inputs and external disturbances alike—an aspect that factors into the pilot workload required to stabilize the aircraft and reject disturbances in hover and low-speed maneuvering. The trade-offs between disturbance rejection bandwidth (DRB) and closed-loop stability (characterized by the phase margin) were examined. The balance shifted to a preference for increased DRB and reduced phase margin as the vehicle size increased—this was attributed to the aforementioned workload issues, where for the larger vehicles, pilots preferred the increased automatic rejection disturbances—allowing them to "keep out of loop" and not have to work as hard or make as many corrective inputs to stabilize the aircraft attitude or position.

Underlying all these outcomes was the second key factor—that part of the reason pilots wanted to minimize their control inputs was to keep attitude disturbances, particularly in pitch, to a minimum. The reason was that the conventionally located cockpit at the front of the aircraft, some 40 ft from the center of rotation at the center of gravity, led to a number of motion-related ride and handling qualities issues. Pitching the aircraft created heave motion at the cockpit, and yaw created sideward accelerations. Such responses would not be conducive to passenger acceptance. These factors were investigated further through a comprehensive analysis of the short-term attitude response requirements in hover and low-speed maneuvering for a selection of rotorcraft of different sizes. The analysis also included a specific study on the effect of the pilot offset in isolation, and showed that by simply changing the offset location, and thus modifying the motion and visual cues presented to the pilot, a vehicle with the same dynamics would get progressively better HQRs with decreasing longitudinal offset location. The levels of attitude bandwidth in particular, were "too hot" at the 30 to 40 ft offset location and above. Following the ADS-33 recommendations for Level 1 HQs for cargo/utility class helicopters caused pilots difficulties when trying to perform hovering tasks using attitude control. Reducing the bandwidth of the attitude response ameliorated the problem somewhat, but ultimately the handling qualities for the modified Hover MTE remained Level 2 at best.

There is an open question about the direct applicability of the ADS-33 Hover MTE to the civilian role envisaged for an LCTR2 type rotorcraft. The experimental assessments in this report made some allowance for this by increasing the size of the *desired* and *adequate* hover performance box; however the standard ADS-33 time-to-stabilize requirements were maintained. These could possibly still be overly demanding and require unnecessary maneuvering urgency, but certainly the established ADS-33 values were a natural place to start, and leaving them unchanged provided opportunity for comparison to previous experimentation. If the stabilize time was relaxed, perhaps in conjunction with further precision relaxations, then Level 1 hover and low-speed handling qualities may be achievable with an attitude command response type. Safety is paramount to the civilian role, and handling qualities play an important part. For an LCTR2 type aircraft to be viable it must be able to operate in a cluttered terminal area environment, and be responsive to ATC requirements and commands as well as be operational in all weather conditions. This later point highlights the reasoning for testing in "moderate" levels of turbulence. An argument can be made that the perhaps artificially high MTE demands somewhat push the aircraft limits that would be required in scenarios of high stress or emergency.

Other solutions to the attitude-linked problems could also be proposed, for example, locating the pilot closer to the center of rotation. This would certainly alleviate the motion-related issues but brings a host of other issues such as locating the pilot in a position with adequate field of view without resorting to cameras and/or other sensors, not to mention that the unsatisfactory

motion issues still remain for any passengers substantially offset from the center of gravity. One might also argue that a vehicle such as LCTR2 should feature significant automation, thus piloted HQs might be somewhat outmoded. This is likely to be true but not entirely; the handling qualities for redundant/failsafe modes still need to be satisfactory, and the fundamental work to establish minimum-level requirements for good handling qualities also needs to be carried out to prevent overdesigning and adding unnecessary complexity and cost to the design.

Design Feasibility of Nacelle Tilt and TRC Handling Qualities Design Criteria

Considering the various challenges and issues connected with the ACAH approach, the use of the nacelles in the TRC scheme is an attractive solution from a handling qualities and flight control perspective. The results presented previously have shown that, whereas rigid body dynamics of the aircraft have been considered, a control law can be devised to confer Level 1 handling qualities using such a scheme. The process of designing and assessing the control law led to a reappraisal of the current state of the art of ADS-33 TRC specifications. Meeting the current criteria did not necessarily confer Level 1 handling qualities, and this outcome led to investigation into finding additional techniques to characterize the TRC response. Frequency-domain parameters such as bandwidth and phase delay were applied to the translational response. The analysis showed that the existing equivalent rise-time criteria range from 2.5 to 5 s was equivalent to a X/δ_{lon} (or Y/δ_{lat}) bandwidth of approximately 0.2 to 0.4 rad/s. It was found, however, that meeting this criterion alone was insufficient, but as is typical in a number of short-term attitude response HQ criteria, combining it with a phase delay criterion led to a much better prediction of the handling qualities. Figure 83 (repeated here for convenience) demonstrates a monotonic increase in average HQR was achieved with increasing phase delay, while essentially all cases met the ADS-33 Level 1 rise-time (or bandwidth) characteristics.

The fact that this is not in the existing criteria is somewhat a consequence of the difference in the implementation of TRC in the configurations used to define ADS-33. These were predominately based on inner/outer loop TRC control laws where the translational motion was created by attitude changes of the aircraft. Ultimately, this form of TRC is driven by the rotor, whose control actuator bandwidths and rate limits are typically much higher than those of the nacelle actuator in the TRC used for LCTR2, and so large phase delay issues were not likely to be encountered. This is exemplified by the lateral short-term response characterization, which

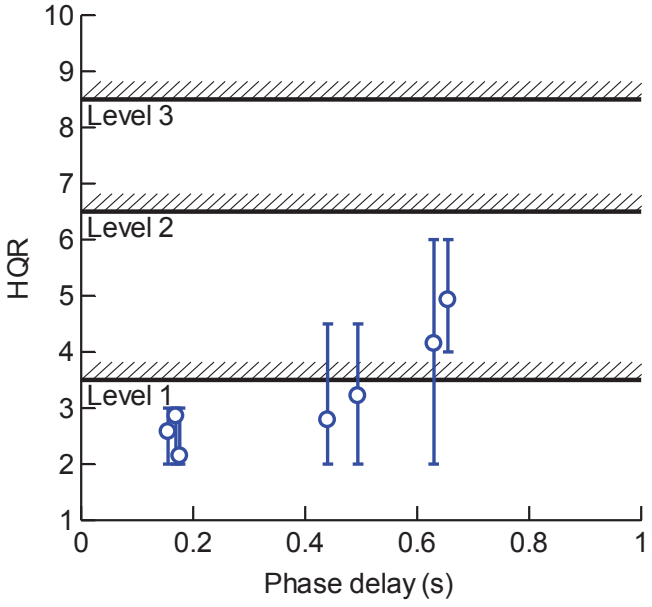

Figure 83. Effect of short-term position response phase delay on handling qualities.

exhibited a phase delay of approximately 0.3 s. As such, the incorporation of the phase delay criteria would be an augmentation of the existing equivalent rise time rather than replacement—albeit that parameter would be converted to its frequency-domain counterpart, bandwidth. Figure 85 shows how proposed TRC handling qualities criteria boundaries using X/δ_{lon} bandwidth and phase delay would look with some tentative values included based on the research presented previously.

There are a number of aspects of Figure 85 to be described: first, the low bandwidth boundary is directly retained from ADS-33 where the upper rise-time limit of 5 s is converted to its equivalent frequency-domain value. There is no evidence to demand a change in this value, and it sets the minimum bandwidth to protect against slow or sluggish response characteristics. The top part of the boundary box is more tentative, but it establishes the boundary based on the phase delay results in this report. The bold part of the line represents a small segment where the confidence is somewhat higher, but whether the boundary would be a constant value or perhaps more relaxed with increasing bandwidth capability cannot be determined; the precedent of the ADS-33 attitude command response criteria show such a trend. The final boundary is an upper limit to the bandwidth requirement; this boundary was not explored in the analysis in this report but is extrapolated from the results in reference [61] and others discussed previously. This boundary exceeds the current ADS-33 levels but, as was discussed in the rationale of investigation, this upper boundary was somewhat overly restrictive as it was based on a particular implementation of TRC that was reliant on the use of attitude changes to generate the translational motion. In attitude-based TRC, beyond a certain TRC bandwidth (or below a certain rise time) the attitude changes required to confer the required response become very large and abrupt, and objectionable to the pilot. However, not all forms of TRC need adhere to this, as demonstrated in the form of the nacelle-tilt-based TRC. Therefore, increased bandwidth can be acceptable if not actually advantageous. However, research in the literature shows there does appear to be a point where the translational response itself can become too abrupt and objectionable—accordingly a boundary as is anticipated in reference [61] is shown.

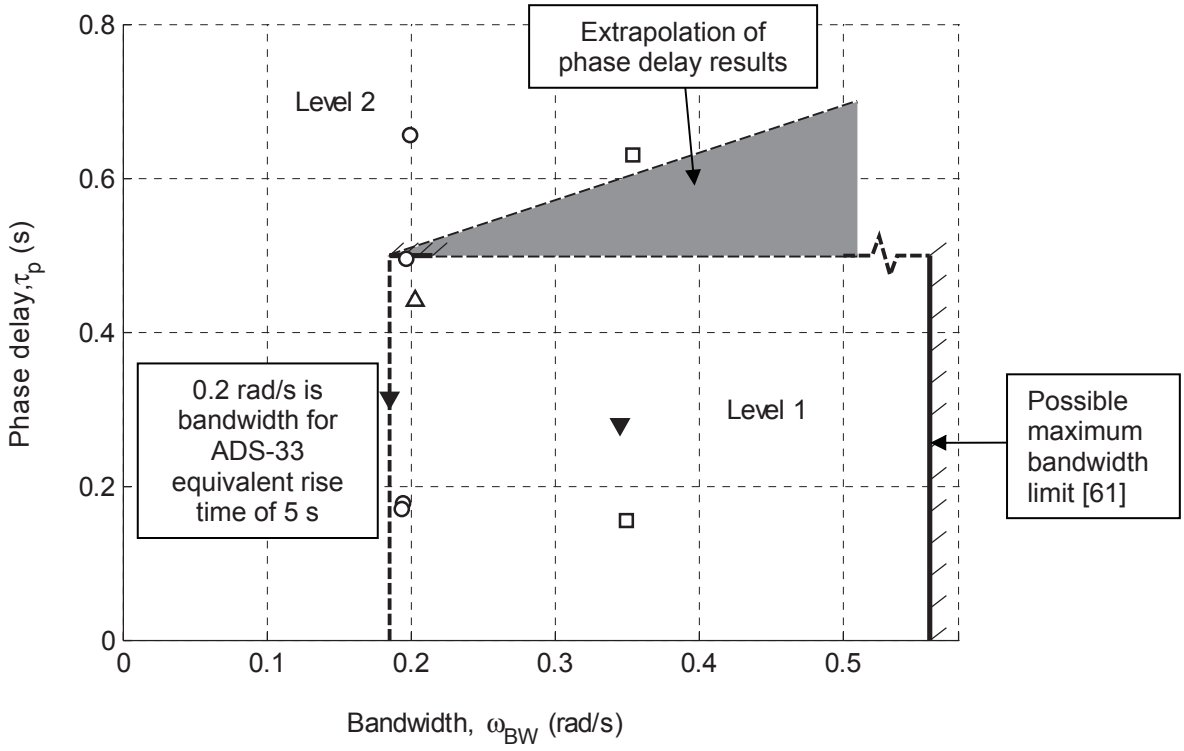

Figure 85. Proposed short-term position response handling qualities criteria for TRC.

Metrics Used—Applicability to Other TRC Implementations

The proposed boundaries should be applicable to any hovering aircraft using TRC; the combined bandwidth and phase delay criteria are generic response characterizations independent of any implementation architecture. Similar issues could be conceived for a compound type rotorcraft with a fixed main rotor(s). Using some form of auxiliary propulsive force to provide the translational motion, sufficient bandwidth of response in the propulsive system (i.e., an engine, propeller, jet, or fan) needs to be provided to ensure phase delay issues are avoided.

A supplementary, supporting, criterion regarding the motion induced at the pilot station and/or other cabin locations (more of a cabin ride quality issue) is also required. This issue was partially accounted for implicitly in the current ADS-33 TRC specifications by virtue of the lower rise time (high bandwidth) guiding against abrupt attitude changes in attitude-based TRC, but what is actually needed is a criterion that directly addresses the issue of motion at the cockpit, such as heave due to pitching, and/or side force due to yaw rates/accelerations.

Modeling Limitations and Requirements

The analysis in this report has shown the fundamental feasibility of a nacelle-based TRC in achieving Level 1 handling qualities in hover and low-speed maneuvering using low-to-moderate fidelity flight dynamics models featuring rigid body dynamics, rigid blade flapping dynamics, and basic cross-couplings. These models cannot consider the structural dynamics that might be a significant issue for a vehicle like LCTR2, especially considering that the two large nacelles will be actuated at relatively high frequency at the end of the slender flexible wings. In references [62,63] a detailed analysis of various control aspects of structural flexibility using a high-fidelity LCTR2 comprehensive model is presented. Moreover, structural strength issues might not be the only factor. Aeroelastic couplings may also impact the handling qualities, especially as the large scale of the LCTR2 confers structural natural frequencies closer to those important for pilot and flight control systems. Increased fidelity modeling is required to determine the structural modes and to decide whether further investigations are necessary to investigate the aeroelastic consequences (if any) on the handling qualities and flight control. The models also had limited aerodynamic modeling, with no dynamic inflow or wake modeling or ground effects. It can only be speculated what impact these effects have on the TRC handling qualities without further research.

Conclusions

Rotorcraft configurations of increasing size and gross weight exhibited a preferable trade-off between disturbance rejection bandwidth (DRB) and stability margin allowing for relaxed attitude feedback phase margins in hover and low speed. Relaxation of the design phase margins must be tempered by an acceptable allowance for margin degradation due to airframe wear and uncertainty.

- For all aircraft configurations evaluated, the low phase margin cases (20–23 deg) were unanimously rated as oscillatory, PIO-prone, and objectionable with a handling quality cliff potentially present. This is in spite of the fact that the Cooper-Harper Handling Qualities Ratings (HQRs) for the range of cases were remarkably the same, being either Level 1 or barely into the Level 2 region.
- For the representative medium-lift helicopter, the H-60, the current recommended stability margins in SAE 94900 (i.e., 45 deg and 6 dB), were preferred by the pilots over the lower stability margin/higher DRB cases. Maintaining these margins may allow for acceptable degradation due to uncertainty and wear and would be consistent with SAE 94900 requirements.
- For the representative heavy-lift helicopter, the H-53, the pilots preferred a higher DRB/lower stability margin configuration (roughly 38 deg of phase margin). Extra care must be taken to assess the influence of variability when nominal flight control gains start with reduced margins.
- For the generic ultra-heavy tiltrotor configuration, the LCTR, the pilot preference included not only a 36 deg phase margin case but also an even higher DRB/lower stability margin configuration (roughly 31 deg). Degradations due to uncertainty and wear become even more critical because of the reduced margin starting point.
- The ADS-33 mid-term response-to-control damping ratio requirement of 0.35 can be applied to the disturbance-response damping ratio. Disturbance-response damping ratios less than 0.35, associated with the low phase margin cases, resulted in highly objectionable oscillations for all three aircraft configurations evaluated.
- The pilot comments on the disturbance response of the aircraft correlated well to the DRB guidelines provided in the ADS-33 Test Guide. The comments indicate that the pitch DRB guidelines should be increased slightly from 0.5 to 0.65 rad/s, which correlates well with recent UH-60 flight tests. The roll DRB guidelines should be increased slightly from 0.9 to 1 rad/s.
- The comments also indicate good agreement with the DRP guidelines proposed in reference [47]. The pitch DRP maximum 5 dB value is consistent. The roll DRP guidelines should be increased slightly from 5 dB to 5.4 dB.

The long lever arm of the cockpit, ahead of the center of gravity, in the very large tiltrotor configurations examined created significant heave coupling with pitch. Similarly, yaw axis accelerations can produce substantial side-force at the cockpit, mandating a reduction in the Level 1 yaw bandwidth requirements. In addition, a revision of a subset of ADS-33 MTE maneuvers resulted in modifications of their performance requirements. The lateral and longitudinal position tolerances for the ADS-33 Hover MTE needed to be increased to better fit the vehicle size, and the Hovering Turn MTE was adjusted to be consistent with the Limited Agility MTE category. The Lateral Reposition MTE standards remained unchanged and were satisfactory for this large vehicle.

- An ACAH response type for the precise hover control of an aircraft with a large (i.e., greater than 30 ft) pilot offset from the center of gravity achieved Level 2 handling qualities, at best, when operating in “moderate turbulence” environmental conditions.
- At such large pilot offsets from the center of gravity, aircraft dynamics exhibiting a high bandwidth attitude response in all axes—over 1.2 rad/s pitch and roll commanded response natural frequencies and under 0.5 s yaw rate commanded response time

constants—displayed objectionable impulsive load factors at the pilot station (a ride qualities issue) and unpredictable aircraft response (a handling qualities issue).

- Configurations with low bandwidth attitude response generally exhibited a lack of control authority in all axes, with sluggish aircraft response lending itself to excessive workload, and PIO tendencies in the face of large amplitude aggressive control techniques.
- Natural frequency of the response appears to have a fundamental impact on the aircraft HQRs for this size of aircraft, probably because it relates to the cockpit accelerations directly. Proposed boundaries therefore tend to follow the constant natural frequency lines.
- A broad range of acceptable yaw bandwidths was identified based on the proposed heading capture evaluation maneuver. Relaxation of the Level 1 yaw bandwidth requirement from 2 rad/s to 0.25 rad/s helped account for the large pilot offset from the center of gravity.

TRC response types with minimal attitude response were unanimously preferred over the attitude-based ACAH, enabling Level 1 handling qualities for large tiltrotor aircraft in hover, even in turbulent ambient conditions. However, the enforcement of ADS-33 TRC requirements, while necessary, was not sufficient to ensure the Level 1 handling qualities were conferred. The various actuator dynamics, control crossfeeds, and feedback aspects of the design have varying effects on the longitudinal short-term position response phase delay. If excessive, this delay results in objectionable oscillatory characteristics in the longitudinal translational axis, with tendencies to PIO, and a handling quality cliff potentially present.

- TRC using a form of longitudinal and lateral thrust vectoring, by using nacelle tilt and parallel lateral cyclic, was a viable method of providing precise position control in hover and low speed, as evaluated in revised Hover and Lateral Reposition MTEs.
- A frequency-domain characterization of the closed-loop TRC short-term position response measured X/δ_{lon}. In the context of this minimal-attitude TRC implementation, this response is a strong candidate handling qualities design metric, correlating well with the ratings. For all the configurations evaluated, the Level 1 handling qualities boundary is around 0.4–0.5 s of phase delay.
- For the controller force gradients evaluated, an optimal 10 ft/s/in control/response gradient was found to confer Level 1 handling qualities consistently. Higher (15 ft/s/in) and lower (5 ft/s/in) gradients conferred a broader handling qualities range, including Level 2. While based on piloted simulation, these results agree qualitatively with ADS-33 but suggest slightly higher gradients are needed.
- Equivalent rise times of 2.5 and 5 s conferred Level 1 handling qualities.
- Nacelle actuator bandwidths greater than 4 rad/s were required to consistently ensure Level 1 handling qualities for the baseline nacelle-only TRC implementation.
- Although a nonlinear phenomenon, nacelle rate limits have a similar effect on the TRC response phase delay equivalent and are interrelated to that of the actuator bandwidth. Actuator rate limits above ±5 deg/s were required for the Level 1 handling qualities to be attainable.
- A simple nacelle rate to longitudinal cyclic crossfeed in the control conferred significant improvements in the handling qualities of this TRC implementation. This crossfeed reduced non-minimum phase pitch responses to almost zero and improved the longitudinal TRC velocity system bandwidth. This was also seen as a reduction in the position response phase delay.
- Augmentation of the nacelle-only TRC through the use of longitudinal cyclic actuation was a viable solution for reducing nacelle actuator bandwidth requirements by providing: (1) a reduction in longitudinal response phase delay, and (2) nacelle rate-limiting prevention.

Appendix A—Aircraft Model Parameters

Table A–1. H-60 aircraft model parameters.

Flight Condition	Speed	Hover	ft/s
	Altitude	100.0	ft
Rotor Parameters	Tail rotor radius	5.5	ft
	Main rotor radius	26.8	ft
	Main rotor chord	1.7	ft
	Solidity	0.082	--
	Number of blades	4	--
	Main rotor speed	27	rad/s
	Tip speed	724	ft/s
Aircraft Configuration	Weight	16,000	lb
	Fuselage station (pilots)	229	in
	Butt line (pilots)	±24	in
	Water line (pilots)	257	in
	Fuselage station (CG)	359.4	in
	Butt line (CG)	0	in
	Water line (CG)	243.8	in
	x_p (CG to pilot)	10.87	ft
	y_p (CG to pilot)	2.00	ft
	z_p (CG to pilot)	–1.10	ft
	I_{xx}	5,451	slug·ft^2
	I_{xz}	1,882	slug·ft^2
	I_{yy}	41,323	slug·ft^2
	I_{zz}	29,437	slug·ft^2
Hover Trim Values	ϕ	–4 (–0.07)	deg (rad)
	θ	4 (0.07)	deg (rad)
	Lateral cyclic (±5)	–0.5	in
	Longitudinal cyclic (±5)	0.5	in
	Pedals (±2.69)	–0.3	in
	Collective (0–10)	5	in

Table A–2. H-53 aircraft model parameters.

Flight Condition	Speed	Hover	ft/s
	Altitude	100.0	ft
Rotor Parameters	Tail rotor radius	9.4	ft
	Main rotor radius	39.5	ft
	Main rotor chord	2.57	ft
	Solidity	0.145	--
	Number of blades	7	--
	Main rotor speed	18.53	rad/s
	Tip speed	732	ft/s
Aircraft Configuration	Weight	46,000	lb
	Fuselage station (pilots)	131	in
	Butt line (pilots)	±30	in
	Water line (pilots)	168	in
	Fuselage station (CG)	355.0	in
	Butt line (CG)	0	in
	Water line (CG)	162.3	in
	x_p (CG to pilot)	18.67	ft
	y_p (CG to pilot)	2.50	ft
	z_p (CG to pilot)	–0.47	ft
	I_{xx}	60,539	slug·ft^2
	I_{yy}	296,694	slug·ft^2
	I_{zz}	275,834	slug·ft^2
	I_{xz}	23,343	slug·ft^2
Hover Trim Values	ϕ	–2.7 (–0.05)	deg (rad)
	θ	4.9 (0.09)	deg (rad)
	Lateral cyclic (±5)	0.3	in
	Longitudinal cyclic (±5)	0.25	in
	Pedals (±2.69)	–0.2	in
	Collective (0–10)	6.7	in

Table A–3. LCTR aircraft model parameters.

Flight Condition	Speed	Hover	ft/s
	Altitude	100.0	ft
Rotor Parameters	Main rotor radius	37.5	ft
	Main rotor chord	3.57	ft
	Solidity	0.12	--
	Number of blades	4	--
	Main rotor speed	20	rad/s
	Tip speed	750	ft/s
Aircraft Configuration	Weight	142,708	lb
	Fuselage station (pilots)	305	in
	Butt line (pilots)	±28	in
	Water line (pilots)	360	in
	Fuselage station (CG)	771.2	in
	Butt line (CG)	0.0	in
	Water line (CG)	333.9	in
	x_p (CG to pilot)	38.85	ft
	y_p (CG to pilot)	2.33	ft
	z_p (CG to pilot)	–2.18	ft
	I_{xx}	2,981,688	slug·ft^2
	I_{xz}	28,930	slug·ft^2
	I_{yy}	1,265,420	slug·ft^2
	I_{zz}	3,553,061	slug·ft^2
Hover Trim Values	ϕ	0 (0)	deg (rad)
	θ	–4.28 (–0.0747)	deg (rad)
	Lateral cyclic (±5)	0	in
	Longitudinal cyclic (±5)	0	in
	Pedals (±2.69)	0	in
	Collective (0–10)	7	in

Table A–4. LCTR2 aircraft model parameters.

Flight Condition	Speed	0–236.3	ft/s
	Altitude	100.0	ft
Rotor Parameters	Main rotor radius	32.5	ft
	Main rotor chord	3.395	ft
	Solidity	0.133	--
	Number of blades	4	--
	Main rotor speed	20	rad/s
	Tip speed	650	ft/s
Aircraft Configuration	Weight	103,695	lb
	Fuselage station (pilots)	111	in
	Butt line (pilots)	±24	in
	Water line (pilots)	136.1	in
	Fuselage station (CG)	495	in
	Butt line (CG)	0	in
	Water line (CG)	182.1	in
	x_p (CG to pilot)	32.0	ft
	y_p (CG to pilot)	2.0	ft
	z_p (CG to pilot)	3.83	ft
	I_{xx}	1,540,000	slug·ft^2
	I_{xz}	30,500	slug·ft^2
	I_{yy}	975,000	slug·ft^2
	I_{zz}	2,280,000	slug·ft^2
Hover Trim Values (86 deg nacelle)	ϕ	0 (0)	deg (rad)
	θ	0.79 (0.0138)	deg (rad)
	Lateral cyclic (±5)	1.3832	in
	Longitudinal cyclic (±5)	0	in
	Pedals (±2.69)	0	in
	Collective (0–10)	6.2520	in

Appendix B—Flight Dynamics Aspects of the Nacelle Rate to Longitudinal Cyclic Crossfeed

Use of a one-degree-of-freedom linear perturbation model of the longitudinal motion in TRC provides insight into the flight dynamics mechanisms behind how the crossfeed improved the longitudinal TRC handling qualities [64]. There are a number of simplifying assumptions to the model, including that rotor flapping and airframe pitching is primarily only disturbed by nacelle inputs and that because of the primary attitude control loop, other pitch disturbances can be considered negligible when considering the longitudinal motion. As such, the equation of the motion, expressed in Laplace form is:

$$su = X'_u u + X'_{\beta_m}\beta_m + X'_{\beta_{1c}}\beta_{1c} - g\theta \tag{39}$$

Here, the main influencing factors on the longitudinal body-axis acceleration are the change in body-axis forward speed, nacelle angle, rotor flap angle, and aircraft pitch attitude.

The equation of motion for the rotor flap is dependent on nacelle angular rate, aircraft pitch rate, and the crossfeed gain, K, which inputs an amount of longitudinal cyclic proportional to the nacelle rate:

$$s\beta_{1c} = M'_{f_{\dot{\beta}_m}} s\beta_m + M'_{f_q} q + M'_{f_{\theta_{1s}}}\theta_{1s} \tag{40}$$

where $\theta_{1s} = Ks\beta_m$. Therefore:

$$s\beta_{1c} = M'_{f_{\dot{\beta}_m}} s\beta_m + M'_{f_q} q + M'_{f_{\theta_{1s}}} Ks\beta_m \tag{41}$$

Dividing by s and rearranging:

$$\beta_{1c} = \left(KM'_{f_{\theta_{1s}}} + M'_{f_{\dot{\beta}_m}}\right)\beta_m + M'_{f_q}\theta \tag{42}$$

where $q \approx s\theta$. Substituting Eq. (42) into Eq. (39):

$$su = X'_u u + X'_{\beta_m}\beta_m + X'_{\beta_{1c}}\left(KM'_{f_{\theta_{1s}}} + M'_{f_{\dot{\beta}_m}}\right)\beta_m + X'_{\beta_{1c}}M'_{f_q}\theta - g\theta \tag{43}$$

The simplified pitch equation for hover assumes the dominant effect is rotor flapping:

$$sq \approx s^2\theta \approx M'_{\beta_{1c}}\beta_{1c} \tag{44}$$

Also substituting for β_{1c} from Eq. (42) here gives:

$$s^2\theta = M'_{\beta_{1c}}\left(KM'_{f_{\theta_{1s}}} + M'_{f_{\dot{\beta}_m}}\right)\beta_m + M'_{\beta_{1c}}M'_{f_q}\theta \tag{45}$$

Solving Eq. (45) for the pitch attitude:

$$\theta = \frac{M'_{\beta_{1c}}\left(KM'_{f_{\theta_{1s}}} + M'_{f_{\dot{\beta}_m}}\right)\beta_m}{s^2 - M'_{\beta_{1c}}M'_{f_q}} \tag{46}$$

Then substituting Eq. (46) into Eq. (43) gives:

$$su = X'_u u + X'_{\beta_m}\beta_m + X'_{\beta_{1c}}\left(KM'_{f_{\theta_{1s}}} + M'_{f_{\dot{\beta}_m}}\right)\beta_m + \left(X'_{\beta_{1c}}M'_{f_q} - g\right)\frac{M'_{\beta_{1c}}\left(KM'_{f_{\theta_{1s}}} + M'_{f_{\dot{\beta}_m}}\right)\beta_m}{s^2 - M'_{\beta_{1c}}M'_{f_q}} \tag{47}$$

Equation (47) shows the influence that the crossfeed gain, K, has on the longitudinal dynamics. The convention is that the nacelle tilt angle, β_m, is negative for a forward rotation, so that the product of $X'_{\beta_{1c}}\left(KM'_{f_{\theta_{1s}}} + M'_{f_{\dot{\beta}_m}}\right)\beta_m$ produces a negative longitudinal acceleration when K is zero and the nacelles are rotated forward. This shows the retarding influence of $X'_{\beta_{1c}}$, which is the longitudinal acceleration due to rotor flapping. This effect is linked directly to the flapping response to nacelle motion—when the rotors flap back against the nacelle tilt rate, the rotor thrust tilts accordingly. This means that the nacelle tilt responding to pilot commands has to work harder against the flap-back-induced thrust tilt. Selecting crossfeed gain K such that $KM'_{f_{\theta_{1s}}} + M'_{f_{\dot{\beta}_m}} = 0$ eliminates this opposing acceleration effect.

The same effect is seen for the final term of Eq. (47), which represents the longitudinal acceleration due to pitch attitude in terms of the rotor flapping and nacelle dynamics derivatives. The mechanism is that the opposite sense pitching moment induced by the moving nacelles causes the aircraft to tilt in the XZ-plane. In the body fixed frame, a gravitational component in the aircraft longitudinal axis manifests, whereas in the Earth frame it is equivalent to the trim Z-axis force being tilted aft. In either frame of reference this action "robs" the aircraft of some of the X-axis acceleration that it is trying to generate by tilting the nacelle—resulting in the nacelle having to rotate further/faster in order to achieve the commanded acceleration. Cancelling this term using the crossfeed gain eliminates this lagging effect, resulting in a simplified longitudinal set of dynamics, $su = X'_u u + X'_{\beta_m}\beta_m$. In summary, the crossfeed is able to minimize the lagging effects on the longitudinal velocity of both rotor flap back to nacelle rate and the subsequent pitching motions by effectively keeping the rotor disc plane perpendicular to the nacelle/shaft axis (Figure 86).

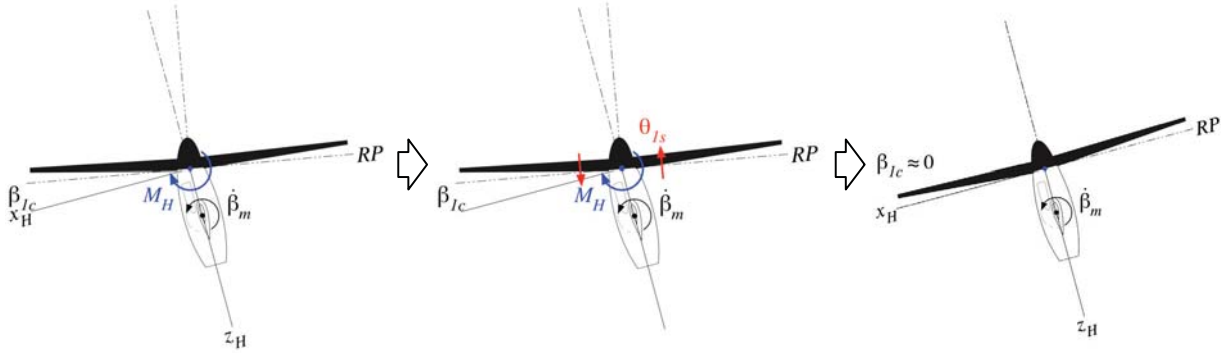

Nacelle rotates and rotor tip-path plane lags behind hub plane

Crossfeed inputs longitudinal cyclic proportional to nacelle rate

Tip-path plane maintained close to perpendicular to shaft axis; flap does not lag behind nacelle or induce pitching

Figure 86. Crossfeed mechanism minimizing nacelle-rate-induced flap and pitch.

Appendix C—Pilot Questionnaire

Task Performance

1. Describe ability to meet DESIRED / ADEQUATE performance standards.

2. Describe aggressiveness / precision with which task is performed.

   a) Assess level of aggressiveness employed:

Limited								Unlimited
1	2	3	4	5	6	7	8	9

   b) Assess level of precision obtainable:

Low								High
1	2	3	4	5	6	7	8	9

3. If trying for DESIRED performance resulted in unacceptable oscillations, did decreasing your goal to ADEQUATE performance alleviate the problem?

Aircraft Characteristics

4. Describe any objectionable controller force characteristics.

5. Describe predictability of initial aircraft response.

6. Describe any mid- to long-term response problems.

7. Describe any objectionable oscillations or tendency to overshoot.

8. Describe any nonlinearity of response.

9. Describe any problems with harmony of pitch and roll, speed control, with height control, and with heading hold/turn coordination. For TRC response types, describe any problems with harmony of pitch and longitudinal translation.

Demands on the Pilot

10. Describe overall control strategy in performing the task (cues used, scan, etc.).

11. Describe any control compensation you had to make to account for deficiencies in the aircraft.

12. Describe any modifications you had to make to what you would consider “normal” control technique in order to make the aircraft behave the way you wanted.

MISC.

13. Please comment on anything else that may have influenced you.

Assign HANDLING QUALITIES RATING for overall task.

14. Using the Cooper-Harper rating scale, please highlight your decision-making process and adjectives that are best suited in the context of the task. If assigned HQR is Level 2, briefly summarize any deficiencies that make this configuration unsuitable for normal accomplishment of this task.

15. What was the critical sub-phase of the task (e.g., entry, steady-state, exit) or major determining factor in the overall Handling Quality Rating (HQR).

16. Please comment on the appropriateness of the MTE maneuvers, test course, and performance standards to check for the ability to perform task in context of rotorcraft's mission.

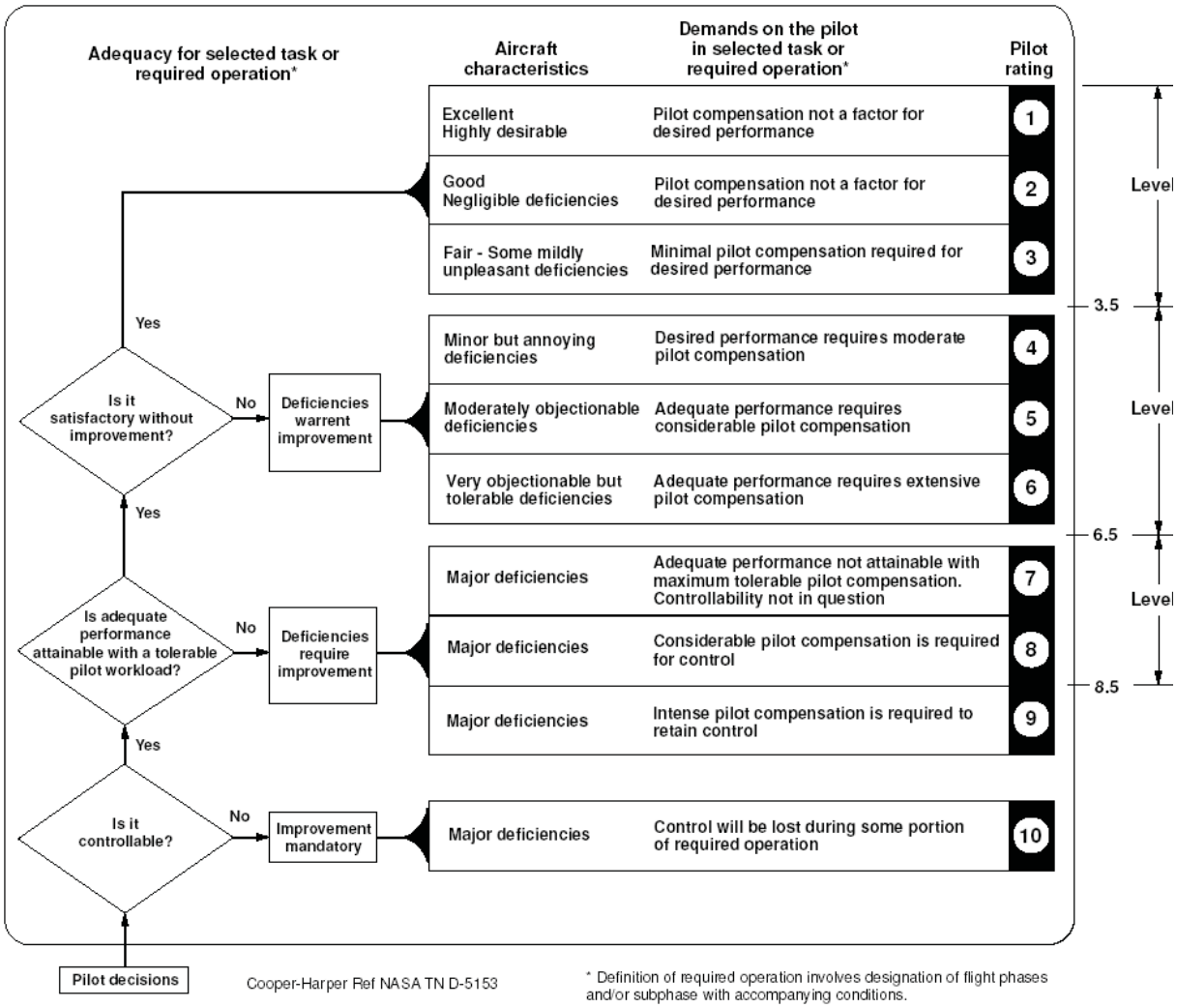

Figure 87. Cooper-Harper Handling Qualities Rating scale.

References

[1] Federal Aviation Administration: The Economic Impact of Civil Aviation on the U.S. Economy, Aug. 2011.

[2] Federal Aviation Administration: FAA Aerospace Forecast, Fiscal Years 2013–2033.

[3] Johnson, W.; Yamauchi, G.K.; and Watts, M.E.: NASA Heavy Lift Rotorcraft Systems Investigation. NASA/TP–2005-213467, Dec. 2005.

[4] Blake, M.; Smith, J.; Wright, K.; Mediavilla R.; Kirby, M.; Pfaender, H.; Clarke, J.-P.; Volovoi, V.; Dorbian, C.; Ashok, A.; Reynolds, T.; Waitz, I.; Hileman, J.; Arunachalam, S.; Hedrick, M.; Vempati, L.; Laroza, R.; denBraven, W.; and Henderson, J.: Advanced Vehicle Concepts and Implications for NextGen. NASA/CR-2010-216397, 2010.

[5] Wilkerson, J.B. and Smith, R.L.: Aircraft System Analysis of Technology Benefits to Civil Transport Rotorcraft. NASA/CR–2009-214594, 2009.

[6] Young, L.A.; Chung, W.W.; Paris, A.; Salvano, D.; Young, R.; Gao, H.; Wright, K.; and Cheng, V.: Civil Tiltrotor Aircraft Operations. 11th AIAA Aviation Technology, Integration, and Operations (ATIO) Conference, Virginia Beach, VA, Sept. 2011.

[7] Chung, W.W.; Paris, A.; Salvano, D.; Linse, D.; Trept, T.; Wood, T.; Young, R.; Gao, H.; Wright, K.; Miller, D.; and Cheng, V.: Modeling High-Speed Civil Tiltrotor Transports in the Next Generation Airspace. NASA/CR–2011-215960, Oct. 2011.

[8] Chung, W.W.; Salvano, D.; Rinehart, D.; Young, R.; Cheng, V.; and Lindsey, J.: An Assessment of Civil Tiltrotor Concept of Operations in the Next Generation Air Transportation System. NASA/CR–2012-215999, Jan. 2012.

[9] Acree C.W., Jr.; Yeo, H.; and Sinsay, J.D.: Performance Optimization of the NASA Large Civil Tiltrotor. NASA/TM–2008-215359, June 2008.

[10] Anon.: Handling Qualities Requirements for Military Rotorcraft, U.S. Army Aviation and Missile Command, ADS-33E-PRF, Mar. 21, 2000.

[11] Anon.: Aerospace - Flight Control Systems - Design, Installation and Test of Piloted Military Aircraft, General Specification for, SAE Aerospace Standard, AS94900, July 2007.

[12] Anon.: Detail Secification: Flight Control Systems - Design, Installation and Test of Piloted Aircraft, General Specification for, MIL-DTL-9490E, Apr. 22, 2008.

[13] Blanken, C.L.; Lusardi, J.A.; Ivler, C.M.; Tischler, M.B.; Hoefinger, M.T.; Decker, W.A.; Malpica, C.A.; Berger, T.; and Tucker, G.E.: An Investigation of Rotorcraft Stability–Phase Margin Requirements in Hover. Proc. American Helicopter Society 65th Annual Forum, Grapevine, TX, May 27–29, 2009.

[14] Malpica, C.A.; Decker, W.A.; Theodore, C.R.; Blanken, C.L.; and Berger, T.: An Investigation of Large Tilt-Rotor Short-term Attitude Response Handling Qualities Requirements in Hover. Proc. American Helicopter Society 66th Annual Forum, Phoenix, AZ, May 11–13, 2010.

[15] Malpica, C.A.; Decker, W.A.; Theodore, C.R.; Lindsey, J.E.; Lawrence, B.; and Blanken, C.L.: An Investigation of Large Tilt-Rotor Hover and Low Speed Handling Qualities Requirements. Proc. American Helicopter Society 67th Annual Forum, Virginia Beach, VA, May 3– 2011.

[16] Malpica, C.A.; Theodore, C.R.; Lawrence, B.; Lindsey, J.E.; and Blanken, C.L.: Handling Qualities of a Large Civil Tiltrotor in Hover Using Translational Rate Command. Proc. American Helicopter Society 68th Annual Forum, Fort Worth, TX, May 1–3, 2012.

[17] Howlett, J.J.: UH-60A Black Hawk Engineering Simulation Program. Volume I: Mathematical Model. NASA-CR-166309, Dec. 1, 1981.

[18] Tischler, M.B.; Ivler, C.M.; Mansur, M.H.; Cheung, K.K.; Berger, T.; and Berrios,M.: Handling-Qualities Optimization and Trade-offs in Rotorcraft Flight Control Design. American Helicoter Society Specialists' Meeting on Rotorcraft Handling-Qualities, Liverpool, U.K., Nov. 4–6, 2008.

[19] Blanken, C.L.; Hoh, R.H.; Mitchell, D.G.; and Key, D.L.: Test Guide for ADS-33E-PRF, July 2008.

[20] Johnson, W.: CAMRAD II, Comprehensive Analytical Model of Rotorcraft Aerodynamics and Dynamics. Johnson Aeronautics, Palo Alto, CA, 1992–2009.

[21] Johnson, W.: Technology Drivers in the Development of CAMRAD II. American Helicopter Society Aeromechanics Specialists' Meeting, San Francisco, CA, Jan. 1994.

[22] Lawrence, B.; Malpica, C.A.; and Theodore, C.R.: The Development of a Large Civil Tiltrotor Simulation for Hover and Low-Speed Handling Qualities Investigations, Proc. 36th European Rotorcraft Forum, Paris, France, Sept. 7–9, 2010.

[23] Zivan, L. and Tischler, M.B.: Development of a Full Flight Envelope Helicopter Simulation Using System Identification. J. American Helicopter Society, vol. 55, no. 2, Apr. 2010.

[24] Marcos, A. and Balas, G.J.: Development of Linear-Parameter-Varying Models for Aircraft. AIAA J. Guidance, Control, and Dynamics, vol. 27, no. 2, Mar.– Apr. 2004, pp. 218-228.

[25] Tischler, M.B.: Aerodynamic Model for Piloted V/STOL Simulation, Systems Technology Inc. (STI). Working Paper 1171-2, Mar. 1982.

[26] Aiken, E.W.: A Mathematical Representation of an Advanced Helicopter for Piloted Simulator Investigations of Control System and Display Variations. NASA-TM-81203, July 1980.

[27] Tischler, M.B. and Remple, R.K.: Aircraft and Rotorcraft System Identification: Engineering Methods and Flight Test Examples, 2nd ed., AIAA, 2012.

[28] DuVal, R.W.: A Real-Time Multi-Body Dynamics Architecture for Rotorcraft Simulation. The Challenge for Realistic Simulation, RAeS Conference, London, U.K., 2001.

[29] Lusardi, J.A.: Control Equivalent Turbulence Input Model for the UH-60 Helicopter. Ph.D. Dissertation, University of California, Davis, 2004.

[30] Lusardi, J.A.; von Gruenhagen, W.; and Seher-Weiss, S.: Parametric Turbulence Modeling for Rotorcraft Applications, Approach, Flight Tests and Verification. Proc. Rotorcraft Handling Qualities Conference, University of Liverpool, U.K., Nov. 2008.

[31] Aponso, B.L.; Tran, D.T.; and Schroeder, J.A.: Rotorcraft Research at the NASA Vertical Motion Simulator. Proc. American Helicopter Society 64th Annual Forum, Montreal, Canada, April 29–May 1, 2008.

[32] Blanken, C.L.; Arterburn, D.R.; and Cicolani, L.S: Evaluation of Aeronautical Design Standard-33 Using a UH-60A Black Hawk. Proc. American Helicopter Society 56th Annual Forum, Virginia Beach, VA, May 2–4, 2000.

[33] Fletcher, J.W.; Lusardi, J.; Mansur, M.H.; Moralez, E., III; Robinson, D.E.; Arterburn, D.R.; Cherepinsky, I.; Driscoll, J.; Morse, C.S.; and Kalinowski, K.F.: UH-60M Upgrade Fly-by-Wire Flight Control Risk Reduction Using the RASCAL JUH-60A In-Flight Simulator. Proc. American Helicopter Society 64th Annual Forum, Montreal, Canada, April 29–May 1, 2008.

[34] Cooper, G.E. and Harper, R.P.: The Use of Pilot Rating in the Evaluation of Aircraft Handling Qualities. NASA TN D-5153, Apr. 1969.

[35] Bellera, J. and Varra, G.: NH90 ADS33 Handling Qualities Level 1 Methodology of a Success. Rotorcraft Handling, Liverpool, U.K., Nov. 2008.

[36] Stiles, L.; Knaust, G.; and Wittmer, K.: The S-92 Goes Fly By Wire. Proc. American Helicopter Society 64th Annual Forum, Montreal, Canada, April 29–May 1, 2008.

[37] Mansur, M.H.; Lusardi, J.A.; Tischler, M.B.; and Berger, T.: Achieving the Best Compromise between Stability Margins and Disturbance Rejection Performance. American Helicopter Society 65th Annual Forum, Grapevine, TX, May 27–29, 2009.

[38] Franklin, G.F.; Powell, J.D.; and Emani-Naeini, A.: Feedback Control of Dynamic Systems, Addison-Wesley Publishing Co., 1994.

[39] Aviation Safety and Pilot Control – Understanding and Preventing Unfavorable Pilot-Vehicle Interactions, National Research Council, National Academy of Press, Washington, D.C., 1997.

[40] Einthoven, P.G.; Miller, D.G.; Irwin, J.G.; McCurdy, B.J.; Bender, J.; Blanken, C.L.; and Lawler, M.A.: Development of Control Laws for the Chinook Digital AFCS Program. American Helicopter Society 62nd Annual Forum, Phoenix, AZ, May 2006, pp. 9–11.

[41] Sahasrabudhe, V.; Faynberg, A.; Pozdin, M.; Cheng, R.; Tischler, M.; Stumm, A.; and Lavin, M.: Balancing CH-53K Handling Qualities and Stability Margin Requirements in the Presence of Heavy External Loads. Proc. American Helicopter Society 63rd Annual Forum, Virginia Beach, VA, May 2007.

[42] Blanken, C.L.; Hart, D.C.; and Hoh, R.H.: Helicopter Control Response Types for Hover and Low-Speed Near-Earth Tasks in Degraded Visual Conditions. Proc. American Helicopter Society 47th Annual Forum, Phoenix, AZ, May 1991.

[43] Irwin, J.G.; Einthoven, P.G.; Miller, D.G.; and Blanken, C.L.: ADS-33E Predicted and Assigned Low-speed Handling Qualities of the CH- 47F With Digital AFCS. Proc. American Helicopter Society 63rd Annual Forum, Virginia Beach, VA, May 1–3, 2007.

[44] Sahasrabudhe, V.; Kubik, S.; Faynberg, A.; Tonello, O.; Engel, D; and Renfrow, J.: CH-53K Control Laws: An Overview and Some Analytical Results. Proc. American Helicopter Society 66th Annual Forum, Phoenix, AZ, May 11–13, 2010.

[45] Brigadier, W.L.: Analysis of Control Actuator Authority Requirements for Attitude and Translational Rate Command Augmentation Systems for the XV-15 Tilt Rotor Research Aircraft, Dec. 1980.

[46] Tischler, M.B.; Colbourne, J.D.; Morel, M.R.; and Biezad, D.J.: A Multidisciplinary Flight Control Development Environment and Its Application to a Helicopter. IEEE Control Systems Magazine, vol. 19, no. 4, Aug. 1999, pp. 22–33.

[47] Blanken, C.L.; Tischler, M.B.; Lusardi, J.A.; and Ivler, C.M.: Aeronautical Design Standard - 33 (ADS-33) … Past, Present, and Future. AHS Rotorcraft Handling Qualities Specialists' Meeting, Huntsville, AL, Feb. 19–20, 2014.

[48] Mansur, M.H. and Tischler, M.B.: Flight Test Comparison of Alternate Strategies for Multi-Loop Control Law Optimization. Proc. American Helicopter Society 69th Annual Forum, Phoenix, AZ, May 21–13, 2013.

[49] Atencio, A. Jr.: Fidelity Assessment of a UH-60A Simulation on the NASA Ames Vertical Motion Simulator. NASA TM 104016, Sept. 1993.

[50] Duda, H.: Prediction of Pilot-in-the-Loop Oscillations due to Rate Saturation. J. Guidance, Navigation, and Control, vol. 20, no. 3, May–June 1997, pp. 581–587.

[51] McRuer, D.T. and Krendel, E.S.: Mathematical Models of Human Pilot Behavior. Jan. 1974.

[52] Hoh, R.G. and Mitchell, D.G.: Proposed Revisions to MIL-F-83300 V/STOL Flying Qualities Specification, Jan. 1986.

[53] Hoh, R.H. and Ashkenas, I.L.: Development of VTOL Flying Qualities Criteria for Low Speed and Hover, Dec.1979.

[54] Radford, R.C. and Andrisani, D., II: An Experimental Investigation of VTOL Flying Qualities Requirements in Shipboard Landings. AIAA J. Aircraft, vol. 21, no. 6, June 1984, pp. 371–379.

[55] Andrisani, D., II; Bourne, S.M.; and Gau, C.F.: Experimentally Determined Pilot Models Using Hovering VTOL Flight Data. AIAA 9th Atmospheric Flight Mechanics Conference, San Diego, CA, Aug. 9–11, 1982.

[56] Krekeler, G.C.; Ehlers, J.C.; and Wilson, D.J.: Simulation Studies of Translation Rate Command Systems for Hover and Low Speed Flight. AIAA Atmospheric Flight Mechanics Conference, Monterey, CA, Aug. 17–19, 1987.

[57] Carpenter, C.G. and Hodgkinson, J.: Equivalent System Analysis of Translation Rate Command Systems for Hover and Low Speed Flight. AIAA Atmospheric Flight Mechanics Conference, Albuquerque, NM, Aug. 19–21, 1981.

[58] Corliss, L..D. and Dugan, D.C.: A VTOL Translational Rate Control System Study on a Six Degrees of Freedom Motion Simulator, Oct. 1972.

[59] Merrick, V.K.: Study of the Application of an Implicit Model-Following Flight Controller to Lift-Fan VTOL Aircraft, Nov. 1977.

[60] Chung, W.Y.; Borchers, P.F.; and Franklin, J.A.: Moving Base Simulation of an ASTOVL Lift-Fan Aircraft, Aug. 1995.

[61] Franklin, J.A. and Stortz, M.W.: Moving Base Simulation Evaluation of Translational Rate Command Systems for STOVL Aircraft in Hover, June 1996.

[62] Juhasz, O.; Ivler, C.M.; Tischler, M.B.; and Celi, R.: Control of a Large Flexible Tiltrotor Aircraft in Hover. 2014 American Helicopter Society Handling Qualities Specialists' Meeting, Huntsville, AL, Feb. 19–20, 2014.

[63] Juhasz, O.; Celi, R.; Ivler, C.M.; Tischler, M.B.; and Berger, T.: Flight Dynamic Simulation Modeling of Large Flexible Tiltrotor Aircraft. Proc. American Helicopter Society 68th Annual Forum, Fort Worth, TX, May 2012.

[64] Lawrence, B.; Malpica, C.A.; Theodore, C.R.; Decker, W.A.; and Lindsey, J.E.: Flight Dynamics Aspects of a Large Civil Tiltrotor Simulation Using Translational Rate Command. Proc. American Helicopter Society 67th Annual Forum, Virginia Beach, VA, May 3–5, 2011.